Monitoring and controlling GABAergic interneuron subtypes during epileptiform activity

Alexandru Călin

Thesis submitted for the degree of

Doctor of Philosophy

St. John's College
University of Oxford
Trinity Term 2018

Abstract

Inhibitory synaptic transmission is of paramount importance for maintaining the delicate balance between excitation and inhibition in the brain. If this balance is perturbed in favour of excitation, epilepsy is likely to develop. Fast synaptic inhibition is mediated by type A γ-aminobutyric acid ionotropic receptors ($GABA_ARs$), which are primarily permeable to Cl^-. The strength of synaptic inhibition crucially depends on the release of GABA from different populations of presynaptic interneurons and the transmembrane electrochemical gradient for Cl^- in postsynaptic cells. $GABA_AR$-mediated inhibition has been shown to oppose epileptic seizures by establishing an inhibitory restraint against spreading excitation. Of the different subtypes of GABAergic interneurons, parvalbumin-expressing (PV) interneurons that target the somatic compartment of excitatory neurons have been strongly implicated in this process. In the context of an epileptic seizure, it is thought that the inhibitory restraint is overwhelmed by runaway excitation, and the seizure front is able to spread from the pathologic epileptic focus into adjacent healthy areas, referred to as the 'penumbra'.

In the first part of this thesis I assess the potential of using chemogenetic strategies to suppress epileptiform activity by boosting the synaptic output from three major interneuron populations in the rodent hippocampus: PV, somatostatin (SST) and vasoactive intestinal peptide (VIP) expressing interneurons. Electrophysiological recordings in an *in vitro* model of epilepsy reveal that the interneuron populations exhibit different effects on epileptiform events. Recruiting VIP interneurons does not change the total duration of epileptiform activity. By contrast, recruiting SST or PV interneurons produces robust suppression of epileptiform synchronisation. PV interneurons exhibit the strongest effect per cell, eliciting at least a five-fold greater reduction in epileptiform activity than the other cell types. Consistent with this, I find that *in vivo* chemogenetic recruitment of PV interneurons suppresses convulsive behaviours by more than 80%.

In the second part of the thesis I use a genetically-encoded reporter to investigate activity-dependent intracellular pH and Cl^- concentration transients in pyramidal neurons and PV, SST and VIP interneurons. I demonstrate that pyramidal neurons and interneurons have different pH and intracellular Cl^- concentration steady states, and exhibit distinct dynamics during epileptiform events. Compared to the other cell types, PV interneurons maintain a relatively stable intracellular Cl^- concentration, even when challenged with epileptiform activity. This suggests that PV interneurons may be more likely to maintain a balance in their excitatory and inhibitory synaptic inputs during seizures.

In the final part of the thesis I investigate the contribution of PV interneurons to inhibitory restraint in an *in vitro* model of the epileptic penumbra. Although PV interneurons are recruited in response to spreading excitation, they can be overwhelmed as they enter a state referred to as 'depolarising block', which is characterized by a decrease in action potential firing. To investigate the impact of this process, I use a light-activated optogenetic tool to induce brief hyperpolarisations of the PV interneuron membrane potential. This successfully reduces depolarising block in PV interneurons, enhances their action potential firing, and reduces the spread of epileptiform activity.

In conclusion, this thesis demonstrates that selective enhancement of inhibitory synaptic pathways offers potential as an anti-seizure strategy, providing valuable insights into the development of therapeutic interventions.

This thesis is dedicated to my parents, to whom I shall always be grateful.

Statement of originality

I declare that the work in this thesis is entirely my own and I clearly acknowledge where others have made contributions. Tatsiana Waseem constructed the floxed ClopHensorN vector that was used in chapter 4. Mihai Stancu worked under my supervision as a project student and conducted some of the *in vivo* experiments that are presented in **Figure 3.6** and **Figure 3.7**. This work has not been submitted for any qualification or degree at this or any other institution.

Acknowledgements

First and foremost I am grateful to my supervisor Colin, who guided and inspired me throughout my MSc and DPhil. With your positive, forward-thinking attitude and your confident and professional demeanour, you are a true leader. I have learnt a lot from you, and I owe you a great deal of respect and gratitude. Thank you John for being my co-supervisor and for sharing your expertise in epilepsy research. It was brilliant to have you both on board during my DPhil.

Thank you Debbie and Andy for your continuous support over the course of my integrated MSc + DPhil programme. I am also grateful to Trevor and Judith for supervision during my MSc, and to the 'Sharpies' for the pleasant atmosphere in the lab. I am most grateful to the Wellcome Trust for funding my research through my Wellcome Trust Doctoral Fellowship [102364/Z/13/Z].

I must thank Andrei, who introduced me to the patch-clamp technique and who closely supervised me during my MSc and DPhil. You have inspired me even before I arrived in Oxford and I am grateful we have established such a wonderful collaboration.

I would like to thank Tanya, who, during her time as a visiting fellow in the Akerman lab, constructed the floxed version of ClopHensorN that I used in this thesis.

The Akerman lab as a whole was a fantastic and intellectually stimulating environment. I would like to thank all my lab mates for the great time we have had together. Thank you Richard for proofreading this thesis. Thanks also go to the Emptage lab for being good neighbours, and to Prof. Peter Somogyi and Prof. Peter Magill for advice and for antibodies for immunolabelling interneurons.

I am grateful for the productive collaboration with the neuroscience lab in Bucharest led by Prof. Leon Zagrean and Prof. Ana-Maria Zagrean. It was great to be able to work with an enthusiastic team of medical students, and I am particularly appreciative of the contribution made by Mihai Stancu who helped to collect the *in vivo* experimental data in chapter 3 of this thesis. I must also thank Prof. Leon Zagrean and Prof. Mihai Moldovan, who first instilled into me and nurtured my passion for neuroscience.

I would like to thank St. John's College for support, and for introducing me to the wonderful fellows of the SCR during my time as a North Senior Scholar. I am grateful that the college sustains such a rich environment for fostering friendship and excellence in research.

A debt of gratitude goes to my beloved family, particularly to my parents, who through kindness, love and wisdom encouraged me to always strive for being the best version of myself.

Last, but by no means least, Alina, thank you for your love and for being so wonderful, understanding and supportive. I love you very much.

Data in chapter 3 of this thesis was made available first on the bioRxiv platform at https://doi.org/10.1101/291179, and was later published and made available open access at https://doi.org/10.3389/fncel.2018.00293.

Contents

List of figures

Chapter 1: General Introduction

1.1 Epilepsy and seizures

Epilepsy is currently the world's third most prevalent neurological disease (Vos et al., 2016) and it is estimated to affect more than 65 million people globally (Ngugi et al., 2010). This chronic and debilitating condition significantly impacts patients' quality of life and in some cases may even be lethal (Leestma et al., 1997; Fazel et al., 2013; Devinsky et al., 2016). It is also often associated with a substantial comorbidity burden, which further affects a patient's quality of life (Keezer et al., 2016).

Epilepsy is a condition of the brain that is characterised by an enduring predisposition to generate epileptic seizures (Fisher et al., 2014). Seizures are thought to be caused by excessive and/or synchronous neuronal activity in the brain. This aberrant neuronal activity can manifest in a variety of different ways, ranging from brief moments of loss of awareness, such as in the case of absence seizures, to complete loss of consciousness and uncontrolled jerking, such as during tonic-clonic seizures. Seizures can occur as a result of many types of insult that disrupt brain function, covering a range of aetiologies such as structural, genetic, metabolic, infectious or immunological (Scheffer et al., 2017). These include traumatic brain injury, stroke, brain tumours, drugs, genetic disorders and inflammation caused by infection or autoimmune diseases (Temkin, 1994; Tardy et al., 1995; Scheffer et al., 1995; Burn et al., 1997; O'Brien, 1998; Well et al., 2009; Singhi et al., 2000; Wang et al., 2005; Lowenstein, 2009; Lancaster et al., 2010; Lancaster and Dalmau, 2012;

Guerrini and Dobyns, 2014; Devinsky et al., 2018). Whilst epilepsy involves recurrent seizure events, isolated seizures may occur acutely without necessarily leading to the development of epilepsy. In fact, seizures are rather common and it is generally predicted that approximately one in ten people will experience a seizure at some point in their lifetime (Hauser and Beghi, 2008). In order for us to address the tremendous burden caused by epilepsy, we first need to better understand the underlying pathophysiology.

1.1.1 Terminology

In this thesis, the term 'epilepsy' refers to the symptomatic brain disorder defined by the propensity to develop recurring, unprovoked seizures. The term 'epileptogenesis' refers to the gradual process by which the normal brain develops epilepsy (Sloviter and Bumanglag, 2013). The term 'seizure' is used when referring to events characterised by neuronal hyperexcitability and hypersynchrony, which have a behavioural correlate, such as tonic (stiffening) and clonic (jerking) motor manifestations known as 'convulsions'. The term 'seizure' will also be used when making predictions about *in vivo* events based on *in vitro* data. The term 'epileptiform' refers to the *in vitro* electrographic equivalent of seizure events, and will be used throughout this thesis to strictly relate to *in vitro* experiments.

1.1.2 Animal models of epilepsy and seizures

As there are numerous challenges associated with investigating the mechanisms underlying epilepsy in patients, animal models have been developed to replicate the features of human epilepsy and seizures. The 'acute seizure models' involve triggering seizures in healthy animal subjects, such as in the case of the maximal

electroshock model, or chemical stimulation using proconvulsant substances such as kainic acid, pilocarpine or tetanus toxin (Toman et al., 1946; Mellanby et al., 1977; Ben-Ari and Lagowska, 1978; Ben-Ari et al., 1979; Turski et al., 1983). Acute models do not mimic the epileptogenic process that occurs in patients who acquire epilepsy, but are still useful for dissecting mechanisms involved in the generation and progression of seizure activity. By contrast, 'chronic seizure models' aim to replicate the process of epileptogenesis and involve certain manipulations, such as the induction of status epilepticus or genetic alterations, which reproduce structural and functional changes found in epileptic patients, and initiate the development of spontaneous seizures (Goddard, 1967; Jobe et al., 1973; van Luijtelaar and Coenen, 1986; Sloviter, 1987; Lothman et al., 1990; Tanaka et al., 1992; Mathern et al., 1993; Morimoto et al., 2004).

The main advantage of these animal models is that they provide a platform on which to study the mechanisms underlying epilepsy and seizures. This is important as it provides valuable insights into potential treatment options for the human disorder. For example, the discovery of novel anti-seizure drugs has relied on the use of rodent models of seizures and epilepsy (Löscher, 2017). Ever since the first use of animal models for anti-seizure drug screening in the 1930s, a plethora of compounds have been identified as having anti-seizure effects and were later clinically tested and approved for widespread medical use, starting with phenytoin (Merritt and Putnam, 1938). However, a third of patients suffering from epilepsy do not respond to currently available medication (Kwan and Brodie, 2009). Animal models that demonstrate such drug resistance may therefore be particularly

useful in identifying novel therapeutic strategies against this common ‘intractable’ form of epilepsy.

1.2 A circuit perspective on seizure activity

Typical *in vitro* models that lend themselves more readily to experimental manipulation include the use of cortical or hippocampal tissue sections from mice or rats (Trevelyan et al., 2006, 2007; Losi et al., 2010, 2016). These models have provided valuable insight into the cellular mechanisms that are likely to underly epilepsy and seizures. I will use this section of my introduction to outline specific cellular mechanisms, with an emphasis on ion homeostasis perturbations involved in the pathophysiology of epilepsy and seizures.

1.2.1 Excitation-inhibition balance is key to normal brain function

Generally, the two cellular components of the brain that generate synaptic excitation and inhibition are projecting principal neurons and local inhibitory interneurons, respectively (Stackman, 2005).

Principal neurons send axonal projections that form excitatory synapses onto target neurons over large distances. At the level of these synapses, principal neurons release the excitatory neurotransmitter glutamate that then binds to glutamatergic receptors on the postsynaptic site. There are two classes of glutamate receptors: ionotropic receptors and metabotropic receptors (Nakanishi and Masu, 1994). The ionotropic receptors are cation-permeable ion channels subdivided in three groups: N-methyl-D-aspartate (NMDA), α-amino-3-hydroxy-5-methyl-4-isoxazolepropionate (AMPA) and kainate receptors (Johnson, 1978; Watkins and

Evans, 1981). Rapid glutamatergic excitatory neurotransmission is mediated by the ionotropic receptors. When glutamate binds to an ionotropic receptor, the ion channel opens, allowing Na^+, K^+ and, in most cases also Ca^{2+}, to flow according to their electrochemical gradient. These ion fluxes generate a net depolarising effect, pushing the membrane potential of the postsynaptic neuron towards the threshold for action potential generation. By contrast, the metabotropic receptors are G protein-coupled receptors that comprise several subtypes and mediate relatively slow responses by modulating multiple intracellular signalling pathways and ion channels (Sladeczek et al., 1985; Nakanishi, 1994).

Interneurons form inhibitory connections that are generally confined to local circuitry. Interneuron synapses primarily involve the release of γ-aminobutyric acid (GABA) that then acts on GABA receptors on the postsynaptic site. GABA receptors comprise multiple subtypes of both ionotropic and metabotropic receptors (Hill and Bowery, 1981; Bormann, 2000). The principal ionotropic GABA receptors are the type A GABA receptors ($GABA_ARs$) (Sigel et al., 1982). Type C GABA receptors ($GABA_CRs$) have also been described, although whether these receptors should be considered a separate group is debatable (Qian, 1995; Olsen and Sieghart, 2008). $GABA_CRs$ seem to be topographically more restricted, have been more recently discovered and are less well understood (Bormann and Feigenspan, 1995). $GABA_ARs$ are ion channels that mediate fast GABAergic inhibitory neurotransmission and are mainly permeable to Cl^- ions. When GABA binds to the receptor, the ion channel opens and Cl^- flows down its electrochemical gradient, normally generating an influx. This typically results in hyperpolarisation

of the membrane potential in postsynaptic mature neurons, and keeps the membrane voltage away from the threshold for action potential generation. By contrast, type B GABA receptors ($GABA_BRs$) are associated with slow, metabotropic responses. The $GABA_BRs$ are G protein-coupled receptors that mediate the increase of K^+ conductances and the decrease of Ca^{2+} conductances (Hill and Bowery, 1981).

Excitatory and inhibitory neurons are coupled together at the circuit level, where they are involved in a range of mutual interactions. What has emerged from studies in different brain regions and species is a number of different inhibitory circuit motifs (Roux and Buzsáki, 2015). A particularly important motif is referred to as 'feedforward inhibition'. In this motif, long-range excitatory afferents originating from a brain structure or area, typically innervate a different region or area and synapse onto both excitatory and neighbouring inhibitory neurons, with the inhibitory neurons then connecting to the local excitatory neurons (Alger and Nicoll, 1982; Buzsáki, 1984). Under physiological conditions, this circuit generates a disynaptic feedforward inhibition that arrives within a few milliseconds of the direct excitation of the principal neurons. Such a mechanism can reduce the output of excitatory neurons, modulate the gain of the network (Atallah et al., 2012) and is capable of enhancing the temporal fidelity of principal neuron spiking (Pouille and Scanziani, 2001). A second common inhibitory motif involves feedback control, operating typically within the same brain region. In this circuit, excitatory neurons provide drive to local inhibitory neurons that then form synapses back to the original excitatory population (Miles, 1990). Such reciprocal connections that shape local excitability have been found throughout the brain (Csicsvari et al., 1998;

Thomson et al., 2002; Ko et al., 2011). The interplay of feedforward and feedback inhibition has been implicated in information processing by division and subtraction of input (Wilson et al., 2012). A related inhibitory microcircuit motif, often considered an extension of the feedback inhibition motif, is lateral inhibition, where, within the same area, the local interneurons inhibit principal cells that are different to the ones that initially excited them (Hartline et al., 1956; Isaacson and Scanziani, 2011). Another form of inhibition involves long-range GABAergic projections, which provide direct inhibition to different structures of the brain (Alonso and Köhler, 1982; Bolam et al., 2000; Higo et al., 2007). And finally, inhibitory neurons can also establish connections with one another. This reciprocal inhibition has been suggested to contribute to network synchronicity (Van Vreeswijk et al., 1994), to generate disinhibitory actions, or to regulate excitability across the somatodendritic axis of principal neurons (Letzkus et al., 2011; Lovett-Barron et al., 2012; Pi et al., 2013).

Synaptic inhibition can have a dual effect on the postsynaptic neuron. Firstly, the opening of the $GABA_AR$-associated ion channels will generate a 'short-circuit' or 'shunt' effect on adjacent currents because the input resistance of the neuronal membrane decreases. Given Ohm's law, the gain of the neuron's response will change as the slope of the input-output function will be reduced. This represents a divisive operation performed by synaptic inhibition, which is very localised and temporally locked to the opening of the transmembrane conductances (Blomfield, 1974; Cardin et al., 2008; Silver, 2010). Secondly, the ion fluxes generated by the opening of the $GABA_AR$-associated ion channels will induce transient changes in

membrane potential. The effect is typically hyperpolarising, which results in moving the resting potential away from the action potential threshold. Consequently, a stronger input will be required to reach the spiking threshold. The input-output curve of the neuron will therefore be offset to the right (Tamás et al., 2002; Pouille et al., 2013). This represents a subtractive operation performed by synaptic inhibition. The duration of the hyperpolarising effect will depend on the membrane time constant, therefore it will not be as temporally precise as the shunt effect.

The interplay between different neurons through these circuit motifs enables the normal brain to maintain a dynamic balance between excitation and inhibition. This balance is continuously controlled over a large dynamic range of network states, from resting conditions characterised by low levels of spontaneous activity, to stimulus-driven intense network recruitment (Haider et al., 2006; Okun and Lampl, 2008). Importantly, in order for this balance to be maintained, the output of both excitatory and inhibitory neurons are scaled proportionally in response to increasing stimulus intensity (Wilent and Contreras, 2004). These observations suggest that continuously maintaining the balance between excitation and inhibition is key to normal brain function (Isaacson and Scanziani, 2011).

The importance of the dynamic balance between excitation and inhibition is emphasised by results from acute experimental manipulations of neuronal synaptic transmission. For example, pharmacologically blocking fast synaptic inhibition with $GABA_AR$ antagonists generates seizures (Dichter and Ayala, 1987). By contrast, anti-seizure medication that enhances GABAergic transmission, such as

benzodiazepines, terminates seizure activity (Gale, 1992). Taken together, these observations helped form the concept that seizure activity is caused by a perturbed balance between excitation and inhibition (Olsen and Avoli, 1997; Fritschy, 2008). This idea was further strengthened by the discovery that glutamate agonists, such as kainic acid, can promote excessive excitation and provoke seizure activity (Ben-Ari et al., 1980).

Various structural and morphological cellular changes that occur in the context of epileptogenesis are also consistent with this concept. These include aberrant excitatory axonal sprouting, loss of inhibitory neurons and sclerosis (Bouchet and Cazauvieilh, 1825; Sommer, 1880; Devinsky et al., 2018). The mossy fibre sprouting revealed in temporal lobe epilepsy patients (Scheibel et al., 1974) creates an aberrant, recurrent, excitatory circuit (Buckmaster, 2012). This is thought to lead to a positive feedback mechanism resulting in increased excitatory synaptic input to granule cells, and increased probability of seizures (Wuarin and Dudek, 2001; Sutula and Dudek, 2007). By contrast, it has been suggested that aberrant mossy fibres preferentially innervate GABAergic interneurons in an attempt to restore the excitation-inhibition balance in epilepsy and suppress seizures (Sloviter et al., 2006). Despite these conflicting hypotheses, it is evident that the axonal sprouting and hyperexcitability that are prevalent in an epileptic network are not only restricted to granule cells, but seem to involve other excitatory neurons both in the hippocampus and in cortex (Salin et al., 1995; Perez et al., 1996; McKinney et al., 1997; Lehmann et al., 2001). However, mossy fibres have also been shown to release GABA, although the role of this GABAergic signalling is unclear

(Walker et al., 2002). Interestingly, suppression of mossy fibre sprouting by rapamycin was found not to change the frequency of seizures, suggesting that this aberrant sprouting might not be required for epileptogenesis (Buckmaster and Lew, 2011).

Apart from mossy fibre sprouting, other mechanisms might contribute to epileptogenesis, such as synaptic plasticity, changes in ion homeostasis (discussed later in this chapter) or intrinsic excitability, for example due to upregulation of T-type Ca^{2+} channels (Su et al., 2002), combined with mutual excitation between hippocampal neurons (Traub and Wong, 1982). The excitatory-inhibitory balance is thought to be further disrupted in epilepsy by the loss of subpopulations of GABAergic interneurons (Cossart et al., 2001; Kumar and Buckmaster, 2006).

1.2.2 GABAergic interneuron subtypes

The last 30 years of studies into the circuit alterations in epilepsy, has generated a desire to understand the contribution of defined cell types. Particular attention has been focused on GABA-releasing interneurons. One of the reasons for this is that, although they represent only 10-20% of the neurons in the mammalian brain, there is a great diversity amongst GABAergic interneurons (Markram et al., 2004; Klausberger and Somogyi, 2008). This diversity was first revealed by investigating the morphology of neurons by Golgi staining (Cajal, 1893, 2002). The development of new techniques has since enabled us to describe interneurons in greater detail (Yuste, 2005; Somogyi et al., 2014). For example, with the advent of electron microscopy, information emerged about the synaptic targets of the various GABAergic cell types. This revealed that some interneuron subtypes are very

specific in terms of the subcellular compartment that they target on the postsynaptic neuron (Somogyi et al., 1982). Furthermore, specific molecular markers have been identified to be expressed by distinct subtypes of GABAergic neurons, including neuropeptides and calcium-binding proteins (DeFelipe, 1993). The development of antibodies against these markers has made it possible to reliably identify different interneuron subtypes (Somogyi et al., 1984). Electrophysiology has also played a significant role in the study of GABAergic cells. Intracellular recordings of interneurons have helped differentiate them from the pyramidal cell counterparts. For example, interneurons typically have a firing pattern that is fast spiking, without spike frequency adaptation, compared to principal cells, which display a regular spiking pattern with marked spike frequency adaptation. Furthermore, specific spike timings have been identified in relation to network oscillations and/or state (Sik et al., 1995; Klausberger and Somogyi, 2008). Developmental studies have also contributed to our understanding of GABAergic interneurons by discovering that they originate in different regions of the ganglionic eminence and migrate to the cortical plate (Anderson et al., 1997).

We have learned a lot about the GABAergic interneuron subtypes from one of the most intensely studied neuronal systems, the hippocampus (Freund and Buzsáki, 1996). Seminal work has contributed to describing 21 different interneuron subtypes in the hippocampus (Klausberger and Somogyi, 2008). For example, axo-axonic cells, also called chandelier cells (**Figure 1.1***A*, type 1) have been shown to exclusively target the axon initial segment of pyramidal

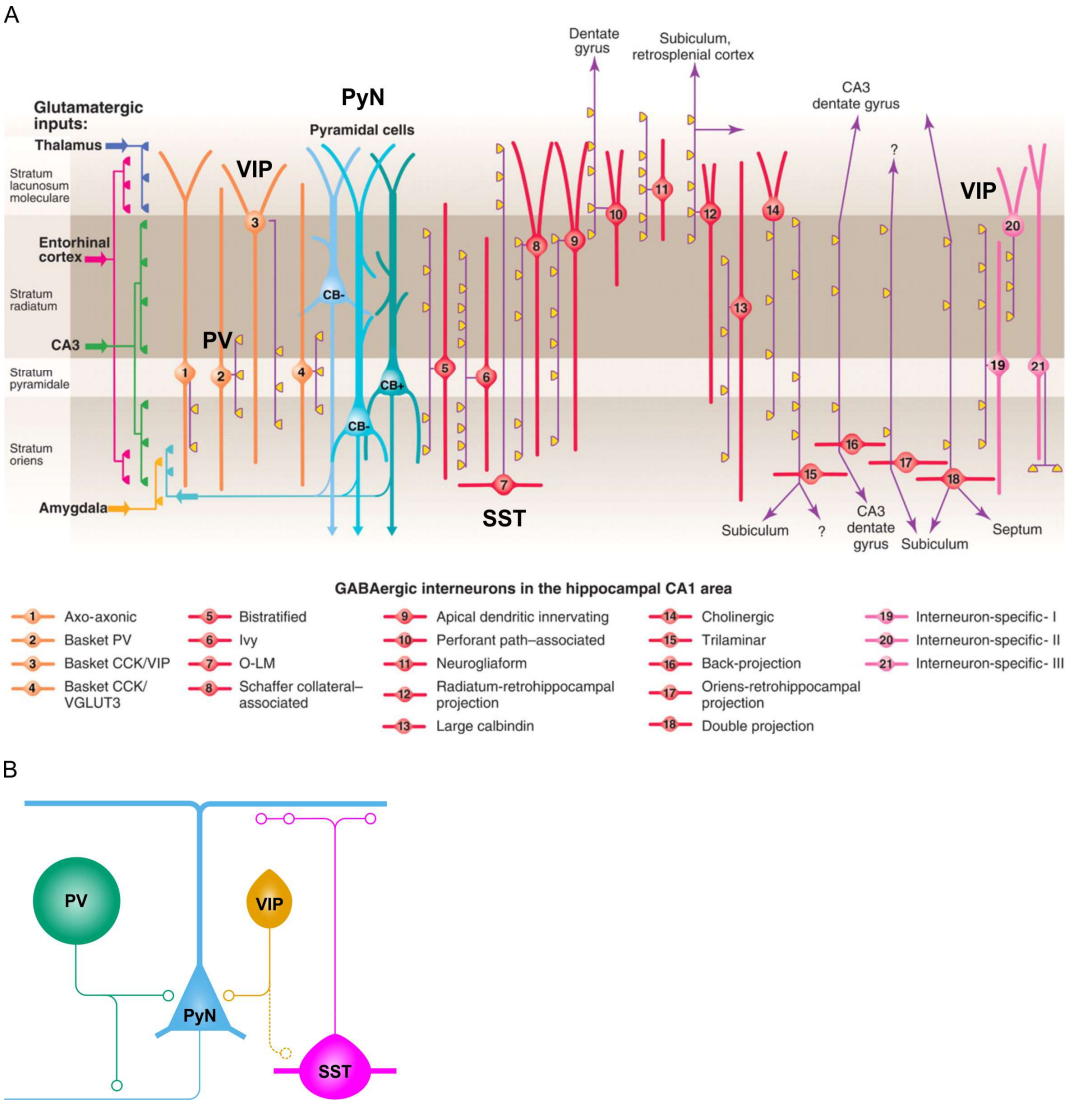

Figure 1.1. Interneurons of the hippocampus. (A) More than 21 interneuron subtypes have been identified in the CA1 region of the rodent hippocampus. The glutamatergic inputs to the CA1 area are indicated on the left. Pyramidal neurons (PyN) are shown in blue. Interneurons targeting mainly principal cells are shown in orange and interneurons mainly targeting other interneurons are shown in pink. Axons are purple and synaptic connections are yellow. CCK, cholecystokinin; VGLUT, vesicular glutamate transporter; O-LM, oriens lacunosum moleculare. Modified from Klausberger and Somogyi (2008). **(B)** A simplified circuit illustrating the main interneuron subtypes investigated in this thesis. PV interneurons mainly target the somatic compartment and axons of pyramidal neurons. SST interneurons mainly inhibit the apical dendrites of principal cells. VIP interneurons are a mixed population of neurons targeting either pyramidal neurons or SST interneurons.

neurons (Somogyi, 1977; Somogyi et al., 1982). These interneurons mostly fire action potentials during the hippocampal theta oscillation peak, when excitatory neurons are least active. These axo-axonic cells have been shown to express parvalbumin (PV), which is a calcium-binding protein, but PV is not restricted to this cell population. Other interneuron subtypes have been shown to contain PV, such as the PV-expressing basket cells (Kawaguchi et al., 1987). These interneurons target the soma of principal neurons (**Figure 1.1***A*, type 2), have a fast firing pattern and elicit action potentials during the descending phase of the theta rhythm (Varga et al., 2012). Basket cells also comprise interneurons expressing cholecystokinin (CCK). CCK cells synapse on the soma of pyramidal neurons (**Figure 1.1***A*, types 3 and 4), but they also target the apical dendrites (Cope et al., 2002). They have a regular spiking pattern and fire action potentials during the ascending phase of the theta oscillation (Klausberger et al., 2005). Axo-axonic cells, together with the PV and CCK basket cells, collectively target the perisomatic region of pyramidal neurons and act cooperatively to suppress pyramidal neuron firing at the peak of the theta oscillations. Other interneuron subtypes target the dendritic compartment of principal cells. These include the bistratified and ivy cells (**Figure 1.1***A*, types 5 and 6) that synapse on both the apical and basal dendrites of pyramidal neurons (Halasy et al., 1996; Fuentealba et al., 2008). Bistratified interneurons contain a combination of PV, somatostatin (SST) and neuropeptide Y (NPY), whilst ivy cells express nitric oxide synthase and NPY (Klausberger et al., 2004; Fuentealba et al., 2008). Distal or apical dendrites of pyramidal neurons are preferentially innervated by oriens-lacunosum moleculare (O-LM) and neurogliaform cells (**Figure 1.1***A*,

types 7 and 11). O-LM interneurons express SST, whilst neurogliaform cells contain NPY and α-actinin-2 (McBain et al., 1994; Sik et al., 1995; Price et al., 2005; Klausberger, 2009). O-LM interneurons fire action potentials in phase with pyramidal neurons during theta oscillations. However, neurogliaform cells spike during the peak of theta, concurrently with the axo-axonic cells, when pyramidal neuron activity is the lowest (Klausberger et al., 2003; Fuentealba et al., 2010; Varga et al., 2012). A unique feature of both neurogliaform and ivy cells is their remarkably dense axonal arbour. The apical dendrites of principal neurons are also innervated by several additional subtypes of CCK-expressing interneurons (**Figure 1.1***A*, types 8, 9 and 10). Long-range projection interneurons have been shown to project their axons to neighbouring regions or to other structures such as the medial septum (**Figure 1.1***A*, types 12, 15-18) (Klausberger, 2009). Finally, interneuron-selective interneurons that express vasoactive intestinal polypeptide-expressing (VIP) or calretinin have also been discovered (**Figure 1.1***A*, types 19-21) (Acsády et al., 1996; Gulyás et al., 1996). These neurons are believed to provide disinhibitory mechanisms (Chamberland et al., 2010; Chamberland and Topolnik, 2012; Tyan et al., 2014).

This extensive heterogeneity amongst GABAergic interneuron populations presents challenges when studying the function of specific cell types. However, the recent development of genetic approaches has enabled the generation of tools, such as transgenic knockin mouse ‘driver lines’, which express cre recombinase under the control of specific genetic promoter sequences. This has afforded unprecedented access to distinct genetically-defined populations of interneurons (Taniguchi et al.,

2011). To date, the best characterised driver lines have afforded access to PV-, SST- and VIP-expressing interneurons. These tools are not without limitations. These molecular-genetic markers are not strictly restricted to morpho-functional interneuron subtypes, as outlined above. At the same time, however, these tools offer the opportunity to both measure and manipulate restricted sets of GABAergic cell types (**Figure 1.1***B*), which are thought to vary in terms of their inhibitory capacity (Klausberger et al., 2003). For example, PV interneurons have been considered particularly effective at inhibiting principal neurons (Cobb et al., 1995; Freund and Buzsáki, 1996; Miles et al., 1996) and at restricting the propagation of network activity (Trevelyan et al., 2006; Cammarota et al., 2013). This is a result of their intrinsic properties and perisomatic targeting of multiple postsynaptic pyramidal neurons. Meanwhile, SST interneurons have been associated with the regulation of dendritic excitability (Miles et al., 1996; Paz and Huguenard, 2015a), which can then affect the spiking output of principal neurons (Lovett-Barron et al., 2012). This feature of SST cells is a result of their preference for targeting apical pyramidal neuron dendrites. And finally, VIP interneurons can mediate both inhibitory and disinhibitory effects, apparently because many of their postsynaptic targets are interneurons (Acsády et al., 1996; Chamberland et al., 2010).

The increasing awareness of the different cell types in key regions of the mammalian brain have led to examinations of how these cell types are affected in epilepsy. For example, in chronic epilepsy, certain subtypes of GABAergic interneurons have been shown to become depleted. Indeed, a loss of SST interneurons has been reported both in animal models of epilepsy (Cossart et al.,

2001) and in patients suffering from temporal lobe epilepsy (Robbins et al., 1991). By contrast, other populations of interneurons appear to be more resistant, in the sense that they maintain their cell numbers. Notably, the PV interneurons have been shown to survive both in epileptic animals (Sloviter, 1991; Sloviter et al., 2003) and in epilepsy patients (Sloviter et al., 1991). Although there are conflicting reports regarding which specific interneuron subtypes are more vulnerable in epilepsy (de Lanerolle et al., 1989; Mathern et al., 1995; Andrioli et al., 2007; Marx et al., 2013), in most studies, perisomatic inhibition seems to be relatively more preserved compared to dendritic inhibition (Sundstrom et al., 2001; Wittner et al., 2001; Maglóczky and Freund, 2005; Tóth and Maglóczky, 2014). Furthermore, GABA cell type-specific developmental deficits can also cause epilepsy (Powell et al., 2003; Cobos et al., 2005). This has led to the idea that restoring the numbers and function of interneuron populations may re-establish the balance between excitation and inhibition and provide insights into potential therapies for epilepsy (Howard et al., 2014; Hunt and Baraban, 2015).

1.3 Tools for cell-specific control of seizure activity

As data has accumulated on the differences between the various neuronal types, there has been increasing interest to study the effects of selectively controlling their individual function within the network. Within the context of experimental epilepsy, this field has benefited enormously from the advent of genetically-targeted tools, which enable selective manipulation of defined populations of cells. This has simultaneously offered new strategies for disrupting seizure activity, as well as new insights into the roles played by particular cell populations in seizure

initiation and maintenance (Cammarota et al., 2013; Krook-Magnuson et al., 2013; Ellender et al., 2014; Sessolo et al., 2015; Yekhlef et al., 2015; Wykes et al., 2016; Khoshkhoo et al., 2017). I will use this section to briefly introduce the various tools available for manipulating the activity of genetically-defined neuronal populations and how these have been applied in the context of epilepsy and seizure research.

Optogenetics was the first technology to allow parsing of neural circuits through the manipulation of specific neuron types in a temporally precise manner (Zemelman et al., 2002; Nagel et al., 2003; Banghart et al., 2004; Boyden et al., 2005; Deisseroth, 2010). This technique uses light-sensitive proteins, called opsins. The first optogenetic tool that was used in mammalian neurons was a photoreceptor coupled to a signalling cascade, which allowed transmembrane ion fluxes to be triggered by light (Zemelman et al., 2002). The currents generated were slow because of the multiple proteins involved in the signalling. Later, channelrhodopsin-2 (ChR2, **Figure 1.2**), a light-driven inward cation channel was isolated from green algae and used to excite mammalian neurons with high temporal precision (Nagel et al., 2003; Boyden et al., 2005). Inhibitory opsins that generate hyperpolarisation of the membrane were later derived from archaeal prokaryote species, and include light-driven inward Cl^- pumps, such as halorhodopsins (**Figure 1.2**) (Han and Boyden, 2007; Zhang et al., 2007), or light-driven outward proton pumps, such as archaerhodopsins (**Figure 1.2**) (Chow et al., 2010; Han et al., 2011). Another type of inhibitory opsin is the Cl^--conducting channelrhodopsin-2 (Cl^-ChR2, **Figure 1.2**), which was developed by modifying

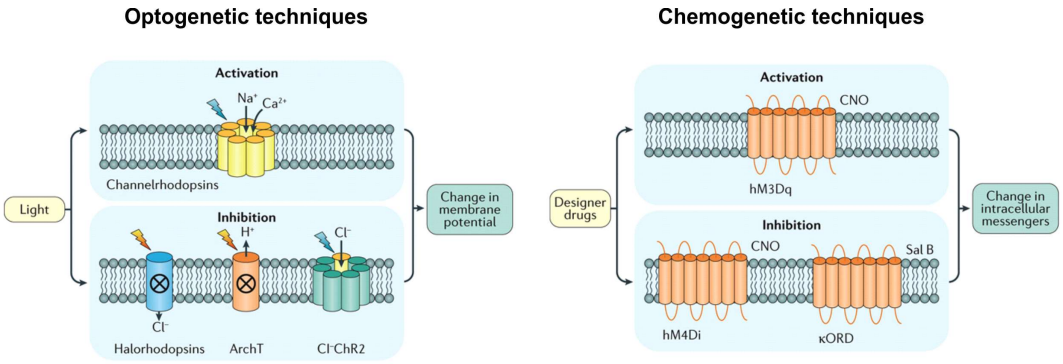

Figure 1.2. Optogenetic and chemogenetic tools for cell-specific excitation or inhibition of activity. Optogenetic tools (left) comprise excitatory opsins represented by channelrhodopsins and inhibitory opsins that include halorhodopsins, one type of archaerhodopsin with improved light sensitivity (ArchT) and Cl^-ChR2. Chemogenetic tools comprise excitatory DREADDs (hM_3D_q) and inhibitory DREADDs that include hM_4D_i and κORD. The stimulus is shown on the left (yellow box) and the cellular action is mentioned on the right (green box) for each tool. Adapted from Boesmans et al. (2018).

channelrhodopsin to have negligible cation conductance and show preferential permeability to Cl^- (Wietek et al., 2014).

Despite the potential for temporally precise optogenetic manipulations of neuronal circuits in epilepsy, a significant challenge in using this technology is the necessity to detect seizure activity in real-time. This implies that the electrical activity of the brain needs to be continuously monitored such that the onset of seizure activity can be detected and then the appropriate light stimulation provided. Such ‘closed-loop’ systems have been successfully implemented and used in multiple brain regions to interrupt seizure activity (Armstrong et al., 2013; Krook-Magnuson et al., 2013; Paz et al., 2013; Paz and Huguenard, 2015b).

Optogenetic techniques have provided promising strategies to study seizures and have proposed new therapeutic approaches. The earliest seizure experiments successfully expressed and activated silencing opsins in excitatory neurons in order to generate anti-seizure effects (Tønnesen et al., 2009; Wykes et al., 2012; Krook-Magnuson et al., 2013; Sukhotinsky et al., 2013). This work demonstrated an important proof of principle and prompted further questions, such as what are other neuron types contributing to seizure activity, and could these be targeted to disrupt seizures. Later work has therefore aimed to increase the output from interneurons (Krook-Magnuson et al., 2013; Ledri et al., 2014). As a strategy, targeting interneurons gained support from evidence that drugs that enhance GABA-mediated synaptic inhibition can be potent anticonvulsants (Czapiński et al., 2005). However, because of their system-wide actions, these drugs exhibit multiple deleterious side-effects (Snodgrass, 1992; Mula, 2011). Whilst GABAergic signalling can become altered in cells within the epileptic focus (Cohen et al., 2002; Huberfeld et al., 2007), inhibitory mechanisms are thought to remain effective within the 'penumbra' surrounding the epileptic focus and are able to oppose seizure spread (Trevelyan et al., 2006, 2007; Schevon et al., 2012; Cammarota et al., 2013). Selectively enhancing these endogenous inhibitory mechanisms therefore offers the potential to disrupt the propagation of seizures.

Previous studies using optogenetic strategies to increase interneuron activity have reported promising results in terms of reducing seizure activity (Krook-Magnuson et al., 2013; Ledri et al., 2014). Furthermore, it has emerged that interneuron subtypes can exert differential effects upon seizure generation and

progression (Cammarota et al., 2013; Krook-Magnuson et al., 2013; Sessolo et al., 2015; Khoshkhoo et al., 2017). However, the temporally-synchronous nature of optical activation can also generate counterintuitive effects. Notably, the simultaneous recruitment of interneurons can enhance network synchronisation and actually initiate epileptiform activity (Sessolo et al., 2015; Yekhlef et al., 2015; Chang et al., 2018a). Other challenges associated with the optogenetic strategy include the need to deliver the genetic constructs by means of viral vectors, the requirement of an implantable device for light delivery, the limited penetrance of light through neuronal tissue, and potential damage due to overheating (Aravanis et al., 2007; Huber et al., 2008; Yizhar et al., 2011; Williams and Denison, 2013; Zhao et al., 2015).

An alternative strategy is afforded by chemogenetic tools such as Designer Receptors Exclusively Activated by Designer Drugs (DREADDs). These tools use pharmacological agents to enhance or inhibit the activity of defined cell populations (Armbruster et al., 2007; Alexander et al., 2009). DREADDs are mutated human receptors that can be expressed in a cell-specific manner. These receptors are not activated by endogenous ligands, but instead require exogenous agents, such as clozapine N-oxide (CNO) and related metabolites (Gomez et al., 2017). Inhibitory DREADDs were first described (Armbruster et al., 2007). These include the human type-4 muscarinic designer receptor coupled with the G_i protein (hM_4D_i receptor, **Figure 1.2**) and the kappa-opioid designer receptor (κORD, **Figure 1.2**). The specific ligand for hM_4D_i receptors is CNO, and the ligand for κORD receptors is salvinorin B (SALB). Activating these receptors leads to opening of K^+ channels

that hyperpolarise the cell (Armbruster et al., 2007; Vardy et al., 2015). Alternatively, activating excitatory DREADDs, such as the human type-3 muscarinic designer receptor coupled with the G_q protein (hM_3D_q receptor, **Figure 1.2**), is thought to enhance neuronal excitability by downregulating ion channels that hyperpolarise the membrane (Alexander et al., 2009). A potential caveat of using the DREADD technology is the fact that CNO has been shown to be converted to clozapine *in vivo* (Gomez et al., 2017; Manvich et al., 2018). Although clozapine activates DREADD receptors with high affinity, it may also act as an antipsychotic by activating several types of endogenous receptors in the brain. Nevertheless, given its good brain permeability and high affinity for DREADD receptors, 'sub-threshold' levels of clozapine may represent an alternative to CNO *in vivo* for potential therapeutic interventions (Gomez et al., 2017).

Compared to optogenetic tools, chemogenetic methods do not afford spike-level temporal resolution. However, in the context of epilepsy, this could be an advantage because the long-lasting DREADD effects eliminate the need for real-time seizure detection. As optogenetic strategies rely on light delivery, chemogenetic tools rely on the intracellular signal transduction machinery. This may also be an advantage, since chemogenetic strategies use the endogenous intracellular signalling pathways, which could avoid the artificial synchronisation of manipulated neurons. Moreover, DREADDs offer broad spatial coverage compared to optogenetics due to the fact that chemogenetic ligands can be delivered systemically. This can practically circumvent all issues associated with implanted

devices and light delivery, which are associated with optogenetic strategies (Forcelli, 2017).

Excitatory hM_3D_q DREADDs have been used to activate interneurons in several brain regions (Hamm and Yuste, 2016; Chen et al., 2017; Wang et al., 2017). However, it remains unclear to what extent different subtypes of GABAergic interneurons can be modulated via DREADDs, and whether chemogenetic control of different interneurons is a viable strategy to reduce seizure activity. Targeting interneurons may offer advantages over inhibiting principal cells, which may induce undesired effects on cognitive function (Wang et al., 2018). Furthermore, boosting the endogenous inhibitory mechanisms is an attractive approach since interneurons can exert widespread control over the neuronal network due to their large axonal arborisations (Freund and Buzsáki, 1996) and inhibitory circuits are recruited as excitatory network activity intensifies (Trevelyan et al., 2006; Derchansky et al., 2008; Schevon et al., 2012; Cammarota et al., 2013). However, particularly given their large diversity, it is important to establish which interneuron subtypes may be optimal for targeting. It is also important to understand and compare the potential benefits for targeting different interneuron subtypes. **To investigate this, chapter 3 of this thesis will explore the potential of chemogenetically recruiting distinct interneuron subtypes, and will examine the effects on epileptiform events *in vitro* and on seizure activity *in vivo*.**

1.4 Changes in cellular physiology underlying seizure activity

In addition to examining the contribution of different cell types to seizures, there is a long history in the use of animal models to examine the underlying cellular mechanisms that operate around different phases of seizure activity. The motivation behind this interest is the hypothesis that understanding these cellular mechanisms may allow for novel strategies to manipulate them in order to restore the balance between excitation and inhibition, which could ultimately provide insight into the development of new anti-seizure therapies. This has led to a variety of ideas about how changes in cellular physiology and synaptic transmission contribute to the onset and progression of seizure activity. Given the experimental focus of this thesis, my review of these physiological mechanisms will concentrate on why inhibitory synaptic mechanisms may fail to match the excitatory synaptic mechanisms in the circuit.

1.4.1 Presynaptic mechanisms that could reduce the efficacy of inhibition

The study of focal seizure activity in animal models has revealed that it is associated with intense inhibitory barrages in the surrounding territories (Trevelyan and Schevon, 2013; Trevelyan, 2016). This work showed that the pathologic ‘epileptic focus’ projects excitatory signals onto adjacent neurons of the ‘penumbra’ via glutamatergic synaptic release. The penumbra, however, is not immediately recruited to the seizure activity. Instead, endogenous feedforward inhibitory mechanisms oppose seizure spread by establishing a powerful inhibitory restraint, which restricts epileptiform recruitment (Trevelyan et al., 2006, 2007). This

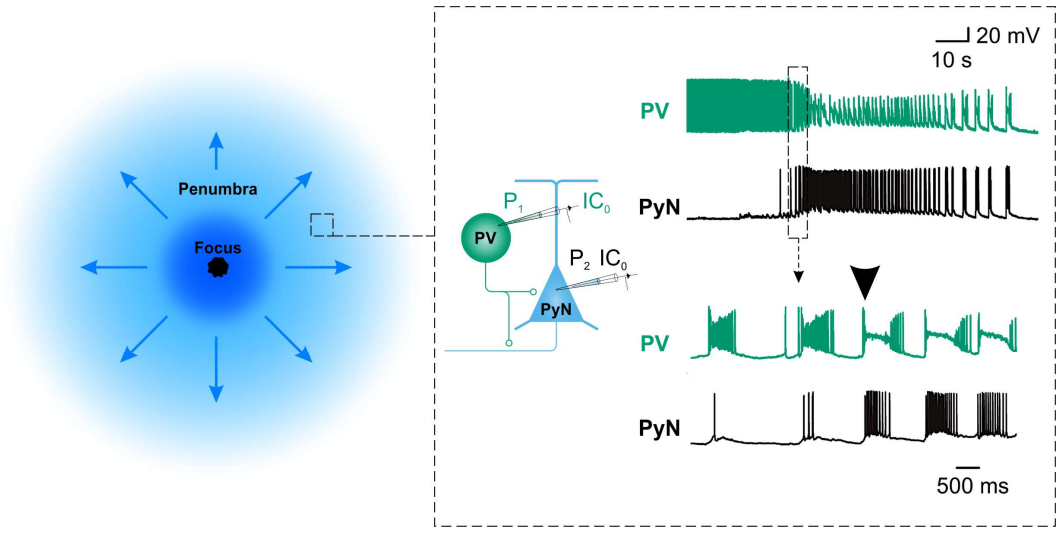

Figure 1.3. Inhibitory restraint and depolarising block of PV interneurons around the onset of epileptiform events. A schematic illustration (left) of an epileptiform event initiated from a focus of damaged tissue (black area in the centre) and the recruitment of the surrounding healthy tissue or 'penumbra' (blue). As the epileptiform event spreads, the inhibitory restraint mechanisms of the penumbra are recruited. A dual intracellular current-clamp recording of a pyramidal neuron and an adjacent PV interneuron are shown on the right. PV interneurons contribute to the inhibitory restraint by generating high frequency action potentials opposing the spreading excitation (right top trace). If the inhibitory restraint is not sufficient to prevent the spread of excitation, pyramidal neurons are recruited to the epileptiform event at the same time that PV interneurons experience depolarisation block (black arrowhead on expanded traces at the bottom of the box). IC_0, current-clamp. Modified from Cammarota et al. (2013).

phenomenon has also been demonstrated in humans (Schevon et al., 2012). The PV interneurons appear to be a principal mediator of this inhibitory restraint that counters the propagation of seizure activity (Cammarota et al., 2013; Sessolo et al., 2015). However, when the inhibitory restraint fails, seizure activity is allowed to propagate freely within the brain (**Figure 1.3**).

As alluded to above, an important question in the field is why does synaptic inhibition fail at seizure onset? A number of possible presynaptic mechanisms have been hypothesised. For example, a frequency-dependent depression at the synapse between basket cells and pyramidal neurons in the hippocampus has been described, which could cause failure of inhibition at seizure onset (Kraushaar and Jonas, 2000). It was postulated that underlying this synaptic depression could be processes that precede presynaptic vesicular release of GABA, including the decreased probability of successful action potential conductance (Lüscher and Shiner, 1990), possible inactivation of voltage-gated Ca^{2+} channels at presynaptic terminals (Patil et al., 1998), or a reduction in release probability caused by desensitisation of the Ca^{2+}-sensitive proteins involved in neurotransmitter release (Südhof, 2012).

Zhang et al. (2012), however, suggested that the releasable pool of GABA-containing synaptic vesicles actually becomes depleted, and proposed that seizure onset may be triggered by exhausted presynaptic GABA release. Zhang et al. (2012) monitored inhibitory postsynaptic currents generated by osmotically-triggered neurotransmitter release. The result was that presynaptic GABA release diminished

in the period immediately prior to the onset of epileptiform activity, even though postsynaptic $GABA_A$ receptor responses to muscimol were maintained.

Others meanwhile have shown that, concurrently with the failure of inhibitory restraint and the onset of epileptiform activity, PV interneurons can enter a state of depolarisation block (DB) that impairs their spiking output (**Figure 1.3**) (Cammarota et al., 2013). DB can occur as a result of the incomplete return of voltage-gated Na^+ channels to a fully deinactivated state between action potentials (Bianchi et al., 2012). If K^+ currents are not able to repolarise the neuronal membrane, spiking is impaired due to a reduced availability of voltage-gated Na^+ channels. However, no studies have so far investigated the functional significance of DB in PV interneurons and whether this phenomenon indeed contributes to the failure of inhibitory restraint, or if it is effectively irrelevant due to the depletion of GABA-containing vesicles. **To address these unknowns, chapter 5 of this thesis will investigate the phenomena of inhibitory restraint and DB in PV interneurons.**

1.4.2 Postsynaptic ion changes related to seizure activity

In addition to mechanisms associated with presynaptic GABAergic transmission, altered ion homeostasis has emerged as an important factor that can increase the propensity for seizure generation (Raimondo et al., 2015). I will use this section to outline perturbations in ion homeostasis associated with seizure activity.

Ion channels are key for regulating neuronal excitability, and their function depends on the state of the transmembrane ion gradients. These gradients enable

ion channels to mediate ion fluxes, which stand as a fundamental process underpinning electrical signalling between neurons in the brain (Hille, 1978). Alteration of these ion concentration gradients across the neuronal membrane can disrupt normal excitability and lead to positive feedback loops, promoting pathologic states, including seizure activity (Somjen, 2002).

One of the earliest established associations between ion concentration changes and seizure activity involves K^+ ions. It was observed that raising the intracerebral K^+ concentration can generate seizure activity (Feldberg and Sherwood, 1957). At the same time, neuronal activity has been shown to generate elevations in extracellular K^+ levels (Orkand, 1980; Amzica and Steriade, 2000). Consistent with this, significant extracellular K^+ accumulation has been revealed during epileptiform events (**Figure 1.4**) (Meyer et al., 1961; Pumain et al., 1985; Yaari et al., 1986; Avoli et al., 1987). Under normal conditions, K^+ ions are approximately 25 times more concentrated inside neurons, and the extracellular concentration is typically low, around 4 mM (Raimondo et al., 2015). Under resting conditions, K^+ currents are an important contributor to the leak conductance, which is a principal determinant of neuronal excitability (Lesage, 2003). Therefore, small alterations in extracellular K^+ concentration can determine important changes in the reversal potential of K^+ ions, which, in turn, can affect the leak current and depolarise the neurons (Fröhlich et al., 2008).

During network activity, K^+ efflux from neurons occurs via several mechanisms. For example, spiking activity depends on voltage-gated K^+ channels

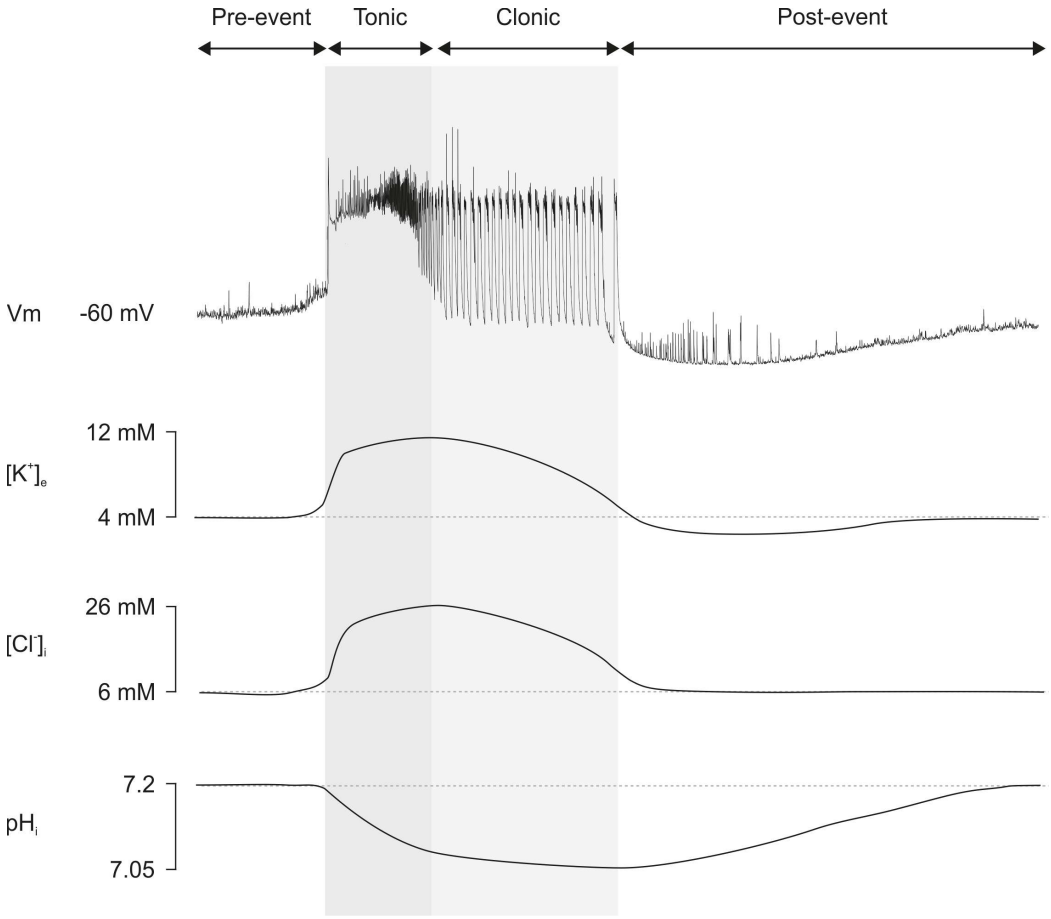

Figure 1.4. Ion dynamics during epileptiform activity. An intracellular current-clamp recording of a CA3 principal neuron in an *in vitro* preparation shows the typical membrane potential changes during an epileptiform event triggered by removing Mg^{2+} from the extracellular solution (top). A 'pre-event' period precedes the onset of epileptiform activity, which comprises a 'tonic' or 'discharge' phase (grey region) of sustained depolarisation accompanied by high frequency, low-amplitude oscillations in the membrane voltage, and a 'clonic' or 'after-discharge' phase (light grey region) characterised by rhythmic bursting occurring from a more hyperpolarised membrane potential relative to the tonic phase. Finally, during the 'post-event' phase, the membrane potential further hyperpolarises before ultimately recovering to pre-event levels. Traces below illustrate the approximation of different ion dynamics during the epileptiform event. Both extracellular K^+ ($[K^+]_e$) and intracellular Cl^- ($[Cl^-]_i$) are thought to peak towards the end of the tonic phase, whilst intracellular acidification (pH_i) reaches its maximal extent at the end of the clonic phase. Figure modified from Raimondo et al. (2015).

that are essential for action potential generation (Lodish et al., 2000). Ca^{2+}-activated K^+ channels also contribute to K^+ effluxes if cytoplasmic Ca^{2+} levels increase (Faber and Sah, 2003), which occurs as a result of spiking activity or via glutamatergic ionotropic receptors (Shih et al., 2013). These effects are further exacerbated if neurons are depolarised, because the driving force for K^+ extrusion from neurons increases. A number of mechanisms oppose the extracellular accumulation of K^+, including passive diffusion, transmembrane transport and cellular mechanisms (Kofuji and Newman, 2004). The Na^+/K^+ ATPase is an important contributor to recovering K^+ gradients. This primary transporter moves Na^+ ions out and K^+ ions into the neuron, and is fuelled by the catalysis of ATP (Skou and Esmann, 1992). Other transmembrane transport mechanisms that help to clear extracellular K^+ include co-transporters such as NKCC1 in neurons and inwardly rectifying K^+ channels in glia (Butt and Kalsi, 2006). The discovery of the latter process led to the idea that the glial syncytium may be contributing to a 'spatial buffering' by which K^+ is shunted between areas with different K^+ concentrations to prevent local accumulation (Amzica et al., 2002; Kofuji and Newman, 2004). In this context, it is interesting that hippocampal astrocytes from patients suffering from temporal lobe epilepsy were found to have dysfunctional K^+ conductances (Hinterkeuser et al., 2000).

One would predict that changes in extracellular K^+ concentration will affect both excitatory and inhibitory neurons alike. By contrast, seizure-related changes in another key ion, Cl^-, have attracted interest because these are predicted to impact the efficacy of inhibition by specifically affecting GABAergic transmission.

Recordings from epileptic tissue resected from patients suffering from medically intractable temporal lobe epilepsy has revealed that GABAergic signalling is excitatory (Cohen et al., 2002). This led to the hypothesis that Cl^- homeostasis may be perturbed in this epileptic tissue. Subsequently, there has been a growing interest into investigating the mechanisms by which Cl^- regulation may be disrupted. For example, Muñoz et al. (2007) studied the expression of co-transporters that mediate physiologic Cl^- accumulation in neurons, such as NKCC1, relative to co-transporters that facilitate Cl^- extrusion, such as KCC2. Interestingly, in the sclerotic area corresponding to the epileptic focus, KCC2 expression was reduced and NKCC1 expression was increased. This observation is in line with previous measurements of mRNA for these transporters in tissue from human epileptic patients (Palma et al., 2006). And blocking NKCC1 with bumetanide was able to recover the anomalous GABAergic signalling in human tissue (Huberfeld et al., 2007). These observations argue that changes in postsynaptic ion homeostasis are important (Miles et al., 2012). Seizure-induced NKCC1-mediated neuronal Cl^- accumulation has been hypothesised as a potential mechanism by which excitatory-inhibitory balance is disrupted in epilepsy (Dzhala et al., 2010). Indeed, Cl^- accumulation in excitatory neurons can, under certain conditions, determine a network to generate epileptiform activity (Alfonsa et al., 2015).

The fact that Cl^- changes can compromise postsynaptic inhibition is therefore relevant to the question of why inhibition might fail at seizure onset. To understand the role of disrupted Cl^- dynamics in the development of seizures, one needs to first consider the synaptic mechanisms in which they are involved. Fast

synaptic inhibition is mediated by $GABA_A$Rs that are mainly permeable to Cl^- (Kaila and Voipio, 1987). Thus, the electrochemical gradient of Cl^- ions is a determining factor for GABAergic transmission. As typical reversal potentials for the $GABA_A$R conductance (around -70 mV) are relatively close to the resting membrane potential of neurons, small changes in the Cl^- gradient or in the membrane voltage can strongly influence the strength and direction of the ionic flow (Raimondo et al., 2012c). Consistent with this idea, inhibitory synapses have been found to be particularly prone to a process termed 'short-term ionic plasticity' (Rivera et al., 2004; Raimondo et al., 2012c; Kaila et al., 2014), whereby GABAergic activity can lead to Cl^- accumulation in the postsynaptic neuron (Kaila and Voipio, 1987; Staley et al., 1995; Staley and Proctor, 1999). This process is further exacerbated by membrane depolarisation of the postsynaptic neuron, such as occurs during seizure events, because the driving force for Cl^- influx increases if neurons are depolarised. Indeed, intracellular Cl^- accumulation in excitatory neurons has been revealed during epileptiform activity (**Figure 1.4**) (Ilie et al., 2012; Raimondo et al., 2013; Ellender et al., 2014). When Cl^- inflow exceeds the capacity of Cl^--extruding mechanisms such as KCC2, the collapsing Cl^- gradient reduces the strength of fast GABAergic inhibition, and GABAergic signalling can become facilitatory and even excitatory (Ilie et al., 2012; Raimondo et al., 2012c; Ellender et al., 2014). In agreement with these ideas, it has been shown in a variety of models that Cl^- increases during seizure/epileptiform activity (Raimondo et al., 2013; Sato et al., 2017).

The vast majority of work has focused on Cl^- homeostasis and dynamics in principal neurons. By contrast, not much is known about Cl^- homeostasis in GABAergic interneurons, although there is some evidence that Cl^- may be regulated differently in interneurons. For example, at the same time that GABAergic synaptic transmission changes from depolarising to hyperpolarising in developing pyramidal cells, GABAergic transmission in interneurons has been shown to remain shunting (Banke and McBain, 2006). Other work has suggested that the level and regulation of intracellular Cl^- in interneurons may play an important role in maintaining stable network dynamics (Vida et al., 2006). As a consequence, there are a series of unanswered questions regarding Cl^- regulation in interneurons. For example, it is not clear if inhibitory neurons experience a collapse in the transmembrane Cl^- gradient during seizure events. Are there any differences in activity-dependent Cl^- dynamics experienced by distinct interneuron subtypes during epileptiform events? **To address these questions, chapter 4 of this thesis will investigate Cl^- levels in genetically-defined interneuron subtypes using a novel fluorescent reporter, under baseline conditions and during epileptiform events.**

GABAergic signalling is intricately linked to the regulation of another key ion, H^+, which has also been implicated in seizure activity. In addition to Cl^-, the ionotropic $GABA_AR$ is also permeable to HCO_3^-, which can influence intracellular H^+ ions as a result of its central role in intracellular pH buffering mechanisms (Kaila and Voipio, 1987). The pH level has been shown to regulate synaptic transmission and neuronal excitability in a variety of ways (Drapeau and Nachshen, 1988). The

gradient of H^+, for example, is fundamental for neurotransmitter uptake into synaptic vesicles (Forgac, 2007). Moreover, multiple transmembrane channel proteins (Tombaugh and Somjen, 1996, 1997) and receptors, including glutamate receptors, are modulated by pH (Giffard et al., 1990; McDonald et al., 1998; Ruffin et al., 2014). Generally, a low pH has been associated with reduced excitability, whilst a high pH has been associated with elevated neuronal activity (Schuchmann et al., 2006; Sinning and Hübner, 2013). Therefore, the control of pH is important for maintaining a stable excitatory-inhibitory balance in the brain. Endogenous buffering and transport mechanisms exist to control pH levels in the brain. Most notably, the bicarbonate buffering system relies on carbonic anhydrases to catalyse the reversible reaction between CO_2 and H_2O to HCO_3^- and H^+ (Supuran, 2008; Raimondo et al., 2015). Under experimental conditions, however, the CO_2 concentration is typically clamped in the extracellular space. Given CO_2 readily permeates the neuronal membranes following production, clamping the extracellular CO_2 will prevent changes in pH caused by fluctuating CO_2 levels. As with K^+, under physiological conditions, the link between pH and neuronal activity can be considered as bidirectional, in the sense that neuronal activity is capable of inducing transient changes in H^+ concentration, in spite of pH buffering mechanisms (Chesler, 2003). With regards to seizures, excitatory neurons have been shown to acidify as a result of intense network activity (**Figure 1.4**) (Xiong et al., 2000; Raimondo et al., 2012a). At the same time, manipulation of intracellular pH has been demonstrated to impact epileptiform activity. This suggests that intraneuronal acidification may play an important role in seizure termination

(Xiong et al., 2000). Although pH dynamics have been studied in the extracellular compartment and in excitatory neurons, pH regulation and seizure-related dynamics have not been investigated in inhibitory interneurons. This raises a series of questions, such as whether GABAergic interneurons experience pH changes during seizure activity, and whether all interneuron subtypes regulate their pH homeostasis in a similar fashion. **To try to answer these questions, chapter 4 of this thesis will explore pH levels in genetically-defined GABAergic interneurons under resting conditions and during epileptiform events.**

1.4.3 Interacting ion dynamics

An important theme that has emerged from studies into ion dynamics is that there are many opportunities for interaction, or 'crosstalk', through ion regulatory mechanisms. For example, the extracellular accumulation of K^+ can reduce fast GABAergic transmission by depolarising the reversal potential of $GABA_A$Rs (Thompson and Gähwiler, 1989). This is caused by a reduction in Cl^- extrusion by KCC2, because of the diminished K^+ gradient. Furthermore, if intracellular levels of Cl^- are low and extracellular K^+ is high, KCC2 can switch transport direction and facilitate K^+ and Cl^- influx (Staley and Proctor, 1999). Another example involves the interplay of pH and Cl^- via $GABA_A$Rs. As $GABA_A$Rs are permeable to both HCO_3^- and Cl^-, intracellular pH and Cl^- regulatory mechanisms can have either synergistic or opposing effects on E_{GABA_A} (Raimondo et al., 2015).

These sorts of interactions can generate significant challenges for experimentally measuring both resting and dynamic ion concentrations. The field of Cl^- imaging, for example, has suffered from methods where different ions can

confound independent quantification. The application of genetically-encoded Cl^- reporters such as 'Clomeleon' (Kuner and Augustine, 2000; Dzhala et al., 2010; Grimley et al., 2013; Glykys et al., 2014) and 'Cl-sensor' (Markova et al., 2008) has been limited by the sensitivity that these reporters also have for pH. The inherent problem is that the cells' pH, and any changes in pH, will confound all estimates of Cl^-. Importantly, the development of ClopHensor (Arosio et al., 2010) and of its optimised version for expression in neuronal tissue, ClopHensorN (Raimondo et al., 2013), has enabled simultaneous readout of absolute pH and Cl^- concentration and, for the first time, has afforded the functional dissociation of the two ions in neurons. These inter-dependences of ion species emphasise the importance of using experimental tools that are able to distinguish between the separate ion dynamics, especially during periods of intense transmembrane fluxes, such as occurring during seizure events. For this reason, the pH and Cl^- reporter used in chapter 4 of this thesis, is well-suited for differentiating between H^+ and Cl^- ion transients during epileptiform activity.

1.5 The hippocampal formation

The experimental work in this thesis was performed on the mouse hippocampal formation. I will therefore use this section to briefly introduce this brain structure, and its relevance to epilepsy. The hippocampus has been shown to have a particularly high seizure susceptibility (Burnham, 2002) and it is the region of the brain that often contains the epileptic focus in temporal lobe epilepsy patients. To understand why the hippocampus is prone to generating seizures, we first need to consider its circuitry.

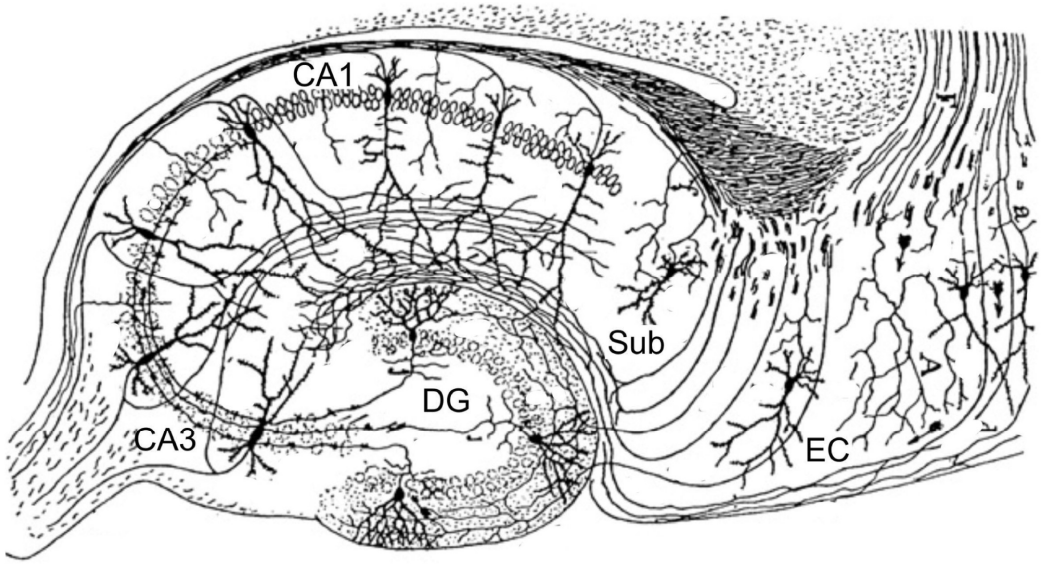

Figure 1.5. Architecture of the hippocampus. A coronal section of the hippocampal formation illustrates its main subdivisions: DG, dentate gyrus; CA3, Cornu Ammonis area 3; CA1, Cornu Ammonis area 1; Sub, subiculum; EC, entorhinal cortex. Modified from Cajal, 2002.

The hippocampal formation is part of the limbic system located in the medial part of the temporal lobe of the cerebrum. The hippocampus has been extensively studied since the report on patient H.M., who suffered a severe impairment in forming new memories as a result of bilateral neurosurgical resection of the hippocampus, which was performed in an attempt to treat the patient's refractory epilepsy (Scoville and Milner, 1957). Accumulating evidence suggested that this is a critical structure for storing and retrieving memories. At present, it is thought that the hippocampus provides a spatio-temporal framework that enables the different elements of sentience to be interlaced and stored in a way that allows for future retrieval of experiences (Knierim, 2015).

The hippocampal formation consists of the dentate gyrus (DG), the subiculum, the entorhinal cortex and the hippocampus proper. Furthermore, within the hippocampus proper there are three major subdivisions, namely the Cornu Ammonis (CA) subfields CA1 to CA3 (Schultz and Engelhardt, 2014). At a synaptic level, the classically described 'trisynaptic circuit' is thought to convey information unidirectionally via a loop starting from the entorhinal cortex, through the hippocampus and ending back to the entorhinal cortex (**Figure 1.5**). Principal neurons from the entorhinal cortex project through the perforant path to the DG, forming the first synapse. The DG then sends axons via mossy cell fibres to the CA3 region, establishing the second synapse. The CA3 then projects to CA1 through the Schaffer Collateral pathway, creating the third synapse. Finally, CA1 relays the information back to the entorhinal cortex to complete the circular circuit. In addition to this, CA3 pyramidal neurons send collaterals to other CA3 neurons. This recurrent connectivity within CA3 has been suggested to underly important neural processes, such as the formation of sparsely encoded associative memory (Bennett et al., 1994).

This recurrent connectivity within the hippocampus could explain why it is so prone to seizures. Several specific features of CA3 pyramidal neurons are likely to contribute to the role that the hippocampus plays in seizures and epilepsy (Schwartzkroin, 1994). Among the numerous voltage-gated membrane conductances, pyramidal neurons express high threshold Ca^{2+} channels across their entire somatodendritic axis (Wong et al., 1979; Fisher et al., 1990). These channels enable the pyramidal neurons to sustain physiological bursts of activity, which are

similar to paroxysmal discharges that are characteristic to seizure events. However, the difference is that in seizures, this activity is synchronised across large ensembles of pyramidal neurons. And this synchronisation is particularly pronounced in the CA3 region because of the recurrent connectivity that is characteristic of this brain area. Under normal conditions, synaptic inhibition prevents hippocampal activity from evolving into runaway excitation. Indeed, loss of inhibitory control has been shown to lead to synchronous firing of large groups of hippocampal neurons through recurrent pathways (Miles and Wong, 1987). Moreover, the sustained neuronal depolarisation can release the Mg^{2+} block of NMDA channels, which may further promote excitability (Kampa et al., 2004).

Despite these characteristics that promote excitability, activity in the hippocampus is normally contained by a variety of powerful intrinsic inhibitory circuits. This inhibitory system contributes to the 'dentate gateway' that is thought to filter the excitatory afferents to the hippocampus (Heinemann et al., 1992; Lothman et al., 1992). As I have discussed above (section 1.2.2), the rodent hippocampus has been the 'powerhouse' for discovering and characterising different classes of GABAergic interneurons and inhibitory circuit motifs. In fact, as well as being an important structure in epilepsy, the hippocampus has long been the brain region of choice for anatomical and electrophysiology experiments (Bliss and Gardner-Medwin, 1973; Bliss and Lomo, 1973). Given its propensity for seizure generation, in vitro slice preparations of hippocampus have been used as a model of seizures or epilepsy. Organotypic hippocampal brain slices for example, have been shown to replicate several features of human epilepsy, such as

denervation, synaptic reorganisation leading to formation of excitatory recurrent connections, mossy fibre sprouting and the development of spontaneous epileptiform events (Dyhrfjeld-Johnsen et al., 2010). This model will be used in this thesis to study epileptiform activity and the inhibitory system of the hippocampus.

1.6 Thesis aims

The overall objective of this thesis was to study the role played by different populations of GABAergic interneurons of the rodent hippocampus in the mechanisms underlying seizure/epileptiform activity. To achieve this, I set out to complete the following experimental aims:

The first aim of this thesis was to examine the potential to enhance inhibitory synaptic mechanisms using chemogenetic recruitment of GABAergic interneurons in the hippocampus. Given their heterogeneity, it is predicted that the choice of interneuron subtype will be important. I will therefore first establish whether different, genetically-defined interneuron subtypes are compatible with chemogenetic recruitment, and then compare these subtypes in terms of their ability to disrupt epileptiform activity (chapter 3).

The second aim of this thesis was to examine how pH and Cl^- ion dynamics differ across different neuronal populations of the hippocampus and how this might relate to the onset and maintenance of epileptiform activity. Previous work has focused almost exclusively on pyramidal neurons, and there is a paucity of information on ion dynamics in interneuron populations. To address this issue, I will target a genetically-encoded fluorescent reporter to defined neuronal

populations, which will include pyramidal neurons and a series of major interneuron subtypes. Ion concentrations will be compared quantitatively across the different cell populations under resting conditions and during epileptiform activity (chapter 4).

The third aim of this thesis was to examine mechanisms underlying the failure of synaptic inhibition around the onset of epileptiform activity. More specifically, I will focus on the impact of DB in attenuating the inhibitory output from PV-expressing interneurons. I will examine whether this process is associated with the loss of inhibitory restraint at seizure onset, and whether targeted optogenetic strategies can be used to reverse these events (chapter 5).

Chapter 2: Materials and Methods

2.1 Preparation and viral transduction of organotypic hippocampal brain slices

All animal work relating to *in vitro* preparations was carried out in accordance with the Animals (Scientific Procedures) Act, 1986 (UK) and under project and personal licenses approved by the Home Office (UK). Organotypic hippocampal brain slice cultures, from here onwards referred to as 'brain slices' or 'slices', were prepared from 5-7 day-old male and female transgenic mice, as described by Stoppini et al., 1991. These mice were either heterozygous or homozygous PV-cre mice (B6;129P2-Pvalb$^{tm1(cre)Arbr}$/J), SST-IRES-cre mice (Sst$^{tm2.1(cre)Zjh}$/J), VIP-IRES-cre mice (Vip$^{tm1(cre)Zjh}$/J), or CamK2a-cre mice (Tg(Camk2a-cre)T29-1Stl/J). Heterozygous mice were produced by crossing homozygous animals of the above cre-expressing lines with C57BL/6J mice. All mice were purchased from The Jackson Laboratory (USA), and were maintained in rooms with controlled light, temperature, and humidity, where they had *ad libitum* access to water and food. All reagents were purchased from Sigma-Aldrich (USA), unless stated otherwise. The whole brain was extracted and transferred into cold (4°C) dissection media containing Earle's Balanced Salt Solution with $CaCl_2$ and $MgSO_4$ (Thermo Fisher Scientific, UK), supplemented with 25.5 mM HEPES, 36.5 mM D-glucose and 5 mM NaOH. The hemispheres were separated, and the individual hippocampi were dissected and immediately sectioned into 400-µm-thick slices on a McIlwain tissue chopper (Mickle, UK). Cold dissection media was then used to rinse slices before placing the onto sterile, porous Millicell-CM membranes. Slices were maintained

in culture for 2-8 weeks in media containing 78.8% (vol/vol) Minimum Essential Media with GlutaMAX-I (Thermo Fisher Scientific), 20% (vol/vol) heat-inactivated horse serum (Thermo Fisher Scientific), 1% (vol/vol) B27 (Thermo Fisher Scientific), 30 mM HEPES, 26 mM D-glucose, 5.8 mM $NaHCO_3$, 1 mM $CaCl_2$, 2 mM $MgSO_4 \cdot 7H_2O$. Brain slices were incubated at 35.5-36°C in a 5% CO_2 humidified incubator.

After 3-5 days in culture, brain slices were transduced with adeno-associated virus (AAV, serotype 8) containing loxP-flanked, inverted DNA sequences under the control of the human Synapsin 1 promoter (University of North Carolina Gene Therapy Center Vector Core and Addgene, USA). Viral DNA contained the double-floxed sequence for hM_3D_q-mCherry (Addgene #44361), which was used to target the excitatory DREADDs to specific cre-expressing populations. In control and interneuron expression profiling experiments, viral DNA contained the double-floxed sequence for the enhanced green fluorescent protein (EGFP, Addgene #50457). For pH and Cl^- imaging experiments, viral DNA contained the double-floxed sequence for ClopHensorN. Transduction was achieved by injecting viral particles (mixed with 1% wt/vol fast-green for visualisation) into 5-to-10 locations along the pyramidal cell layer of the hippocampus in each brain slice. Injection pipettes were pulled from glass capillaries (1.2 mm outer diameter, 0.69 mm inner diameter; Warner Instruments) using a horizontal puller (Sutter P-97, USA). Pipettes were mounted on a manual manipulator (Narishige, Japan) and monitored under a microscope (Leica S6E, Germany) coupled with an external fibre optic light source (Photonic Leica CLS

100X, Germany). A Picospritzer II system (General Valve, Germany) delivered controlled pressure pulses (5-to-10 psi for 1 s) to facilitate gradual diffusion of the viral solution into the tissue. Typical titres were ~10^{12} IU/ml and injection volumes were ~250 nL per slice. Feeding media was supplemented with 1% (vol/vol) antibiotic and antimycotic solution (with 10,000 units penicillin, 10 mg streptomycin and 25 µg amphotericin B per mL) for up to two feeding sessions after injection and brain slices were allowed at least two weeks for expression before being used.

2.2 Electrophysiological recordings *in vitro*

Brain slices were transferred to a submerged recording chamber and maintained at 28°C. The chamber was continuously superfused with artificial cerebrospinal fluid (aCSF) containing (in mM): NaCl (120), KCl (3), $MgCl_2$ (0.5-to-1.5), $CaCl_2$ (2-to-3), NaH_2PO_4 (1.2), $NaHCO_3$ (23), D-glucose (11) and ascorbic acid (0.2). Osmolarity was adjusted to 290 mOsm and pH was adjusted to 7.36 with NaOH. Oxygen and pH levels were stabilised by bubbling the aCSF with 95% O_2 and 5% CO_2. Neurons within the hippocampal formation were visualised with 10x and 60x water-immersion microscope objectives (Olympus BX51WI, Japan) and targeted for single or dual-patch whole-cell recordings. Patch pipettes of 4-9 MΩ tip resistance were pulled from filamental borosilicate glass capillaries with an outer diameter of 1.2 mm and an inner diameter of 0.69 mm (Warner Instruments, USA), using a horizontal puller (Sutter P-97, USA). For current-clamp recordings, pipettes were filled with a K-gluconate internal solution (134 mM K-gluconate, 2 mM NaCl, 10 mM HEPES, 2 mM Na_2ATP, 0.3 mM NaGTP, 2 mM MgATP), which had been

prepared to a pH of 7.36 using KOH, and an osmolarity of 290 mOsm. For voltage-clamp recordings, pipettes were filled with a caesium-gluconate internal solution (120 mM Cs-gluconate, 4 mM NaCl, 40 mM HEPES, 2 mM MgATP, 0.3 mM NaGTP and 0.2 mM QX-314). Before use, internal solutions were filtered with a 0.22 μm syringe filter (Merck Millipore, USA). Pipettes were mounted to a headstage (CV-7b, Molecular Devices, USA) and controlled via a Multiclamp 700B amplifier (Molecular Devices, USA). Following entry into whole-cell configuration, access resistance (R_a) was monitored every 2 min and experiments were only included if R_a remained stable (less than 25% change) and below 25 MΩ. For a subset of voltage-clamp recordings (**Figure 5.1***B*), pipettes were filled with the K-gluconate internal solution, and neurons were clamped at -60 mV to allow the detection of both excitatory and inhibitory synaptic currents. Recordings were low-pass filtered online at 2 kHz (8-pole Bessel), acquired using Clampex software (pClamp 10, Molecular Devices, USA), and exported into Matlab (R2017a, Mathworks, USA) for off-line analysis using custom-made scripts.

To examine the direct effects of activating excitatory DREADDs upon interneuron excitability, current-clamp recordings were conducted in aCSF containing kynurenic acid (3 mM) and hM_3D_q receptors were activated by bath application of CNO (10-20 μM, Bio-Techne, USA). Spontaneous action potential firing rate of each interneuron was recorded 5 min before and 8 min after CNO application. This included a 3-min delay to allow for CNO to fully perfuse the recording chamber. Voltage-clamp recordings were performed to measure the postsynaptic GABAergic currents induced by activating hM_3D_q receptors in

specific interneuron populations. Here, CA1 and CA3 pyramidal neurons were clamped at the reversal potential for glutamatergic current (E_{GLUT}) in the presence of kynurenic acid. Once recordings had stabilised, the amplitude of postsynaptic inhibitory conductances were compared across 2-min periods recorded under baseline conditions, after bath application of CNO and then after co-administration of CNO and the sodium channel blocker tetrodotoxin (TTX, 1-2 μM).

2.3 Quantification of epileptiform discharges *in vitro*

The *in vitro* electrographic equivalent of seizures is referred to as 'epileptiform discharges' (EDs). A semi-automated detection algorithm was used to identify the start and end of individual EDs *in vitro*. Current-clamp traces were down-sampled to 1 kHz and then band-pass filtered (typically 0.05-to-0.2 Hz) using a Bessel filter (2^{nd} order). The signal was corrected for the rise time of the filter and then rectified, thresholded and binarised. This merged events that were close in time (typically under 60 s apart) while ignoring events shorter than 5 s. Experiments measuring the effects of a specific drug (e.g. CNO) consisted of a 15-min baseline period, a three-min period to allow the drug to reach the recording chamber, and finally a 15-min period in which the brain slice was continuously superfused with drug-containing aCSF. The 15-min time periods ('baseline' and 'drug') were assessed using the same ED detection settings. Total ED activity was defined as the sum of time that the brain slice displayed ED activity during a 15-min period. ED frequency was calculated from the number of EDs that were initiated during a 15-min period and ED length was the mean duration of individual EDs that were completely contained within a 15-min period.

2.4 NMDA-evoked experimental seizure model

To induce EDs, local 'puffs' of 1 mM N-methyl-D-aspartate (NMDA) in aCSF were delivered by a Picospritzer III system (General Valve, USA) connected to a patch pipette positioned over the CA3 region using a micromanipulator (MP225, Sutter Instrument, USA). The amount and temporal spacing of puffed NMDA were adjusted until a brain slice-dependent threshold for reliably triggering EDs was reached. During the pre-ED phase, action potentials from cell-attached recordings were automatically detected as peaks with an amplitude of more than 3 mV following filtering of the electrophysiological trace with a high-pass 0-phase, 1st order Butterworth filter at 100 Hz.

2.5 Optogenetic manipulation

Photoactivation of archaerhodopsin was achieved by illuminating the entire brain slice using a widefield, green light-emitting diode (LED, 530 nm peak, Luxeon) placed directly under the slice chamber. Light pulses were 5 ms long and were delivered at 50 Hz using an external electrical stimulator (Grass S48, Grass Medical Instruments, USA) coupled to an LED controller. Current-induced DB was elicited in single PV interneurons by 1 s long positive current steps delivered in 50 pA increments until an impairment in action potential firing was observed. The DB threshold was defined as the first current step at which the PV interneuron stopped firing action potentials during the step.

2.6 Viral transduction of hippocampal interneurons *in vivo*

All animal procedures relating to *in vivo* experiments were carried out with the approval of the local ethics committee for animal research in Bucharest and in

accordance with European Union Directive 2010/63/EU on the protection of animals used for scientific purposes. For viral injections, adult animals of either sex were anaesthetised with isoflurane (maintained at 1.5-2%, 0.4 L/min) and mounted on a stereotaxic instrument (Kopf, RWD Life Science, USA). The level of anaesthesia was continuously monitored, eye drops (Corneregel, Bausch & Lomb, USA) were applied to avoid corneal desiccation and a heat pad system (DC Temperature Controller, FHC, USA) was used to maintain the body temperature in the physiological range. Wiretrol II glass capillaries (Drummond Scientific, USA) were pulled using a vertical puller (Narishige PC-10, Japan) and connected to the Hamilton syringe via compression fittings (RN 1 mm, Hamilton, USA). Small craniotomies were generated with a precision drill (FBS 240/E, Proxxon Micromot, Luxemburg) and hippocampal bilateral injections were performed both dorsally (-2.18 anteroposterior (AP), 2.3 mediolateral (ML), 2.4-1.85 dorsoventral (DV), relative to bregma) and ventrally (-2.7 AP, 2.9 ML, 3.1-2.25 DV, relative to bregma) at a rate of 1.66 nL/s, slowly retreating the injection pipette (0.91 µm/s) to maximise delivery throughout the hippocampus. The injection was controlled via a micromanipulator (NeuroCraft MCM, FHC, USA) attached to a syringe (705RN, 50 µL, Hamilton, USA). Each of four injection tracks was infused with 1350 nL of virus (Addgene, USA), of which 170 nL were delivered at each end of the track. After infusing the target volume of viral solution, a time window of 5 min allowed the virus solution to spread through the hippocampal tissue before the injection pipette was completely retracted. After allowing 2 to 6 months for expression, and at least 3 days before commencing seizure experiments, mice were anaesthetised

and implanted with an infusion cannula (C315GS-5 guide cannula, Plastics One, USA) directly over the viral injection site in the right dorsal hippocampus. The cannula was secured to the skull via bone cement (Refobacin R40, Zimmer Biomet, UK).

2.7 Quantification of seizure behaviour *in vivo*

For each seizure experiment, mice were briefly anaesthetised with isoflurane to allow insertion of the infusion cannula into the guide cannula, such that the tip of the infusion cannula was located within the hippocampus at -2.18 AP, 2.3 ML, 2.2 DV, relative to bregma. At this point, an intraperitoneal (i.p.) bolus of solution containing CNO (4 mg/kg with 4% dimethyl sulfoxide (DMSO) in saline) or vehicle (4% DMSO in saline) was administered and the mouse was allowed to fully recover from anaesthesia for 15 min before starting experiments. To monitor behaviour, the mouse was placed in a square arena (400 mm by 400 mm) in which it was able to move freely virtue of a connector assembly (C313C, Plastics One, USA) and swivel system (375/22PS blue, 22 gauge, Instech, USA), which connected the infusion tubing to a 1 µL syringe (7101, Hamilton, USA) controlled by an infusion pump (IVAC P6000, Cardinal Health, USA). Following a 20-min baseline period, 4-aminopyridine (4-AP) was infused directly into the hippocampus according to a spaced delivery protocol (three 4-AP infusions, each separated by 12 min and consisting of a 200 nL injection of 2 mM 4-AP over 2 min). Infusions were terminated immediately if the mouse reached the stage of generalised motor convulsions. Throughout each experiment video recordings were performed using two high speed, high definition cameras located at a right angle from each other

(Hero 3+ Silver, GoPro, USA) at 60 frames per second, 1920×1080 pixels per frame. Polarised filters were used to reduce glare from the arena walls. A third camera captured the animals' movements directly from above, allowing to track the location and locomotor activity of the mouse at any given time point. Seizure behaviour scoring was done blindly using the Racine scale. The Racine scale was adapted to reflect the observed natural progression of seizure behaviour induced by 4-AP – orofacial clonic activity associated with rearing was included in stage 4, and jumping behaviour was included in stage 5. Individual behaviours were considered as binary point events across time at a sampling frequency of 1 Hz. Racine 1 and 2 behaviours were classified as 'non-convulsive' events, and Racine 3, 4 and 5 behaviours were considered 'convulsive' events (Bergstrom et al., 2013; Tse et al., 2014; Sharma et al., 2018). For the cumulative convulsive Racine index, convulsive events were weighted according to the Racine classification of the behaviour: (1) limb clonic activity (Racine 3), (2) retreating/rearing with orofacial clonic activity (Racine 4), (3) rearing and falling and/or jumping (Racine 5 – full motor convulsions).

2.8 Immunohistochemistry and quantification of interneuron distribution

For *in vitro* studies, brain slices expressing hM_3D_q-mCherry or EGFP in specific interneuron populations were fixed overnight at 4°C in 4% paraformaldehyde with 4% sucrose, in 0.01 M phosphate buffer solution (PBS), pH 7.4. The slices used for immunofluorescence were washed and embedded in 3% agar, and re-sectioned at 50 μm on a vibrating microtome (Microm HM 650V, Thermo Fisher Scientific).

For *in vivo* studies, mice expressing hM_3D_q-mCherry were transcardially perfused and the brains sectioned at 50 μm. PV expression was visualised by incubating sections in 1:500 guinea pig primary antibody (cat. no. 195 004, Synaptic Systems) in PBS with 0.3% Triton-X (PBST) with 1% normal goat serum (NGS, Thermo Fisher Scientific, UK) overnight at 4°C, followed by 1:500 Alexa 488 goat anti-guinea pig secondary antibody (Thermo Fisher Scientific, UK) in PBST with 1% NGS overnight at 4°C. For SST immunolabelling, the tissue was processed with a basic antigen retrieval kit at 95°C for 10 min (R&D Systems, USA). All sections were pre-incubated in 10% NGS in PBST for at least 2 hr at room temperature. SST expression was visualised by incubating sections in 1:250 rat primary antibody (MAB 354, Millipore, USA) in PBST with 1% NGS for 11 days at 4°C, followed by 1:500 Alexa 488 goat anti-rat secondary antibody (Thermo Fisher Scientific, UK) in PBST with 1% NGS for 2 days at 4°C. VIP expression was visualised by incubating sections in 1:5000 rabbit primary antibody (donation from Professor Peter P. Somogyi) in PBST with 1% NGS for 2 days at 4°C, followed by 1:500 Alexa 488 goat anti-rabbit secondary antibody (Thermo Fisher Scientific, UK) in PBST with 1% NGS overnight at 4°C. Finally, all sections were mounted in Vectashield (Vector Laboratories, UK) and images were captured with an LSM 880 confocal microscope equipped with 488 nm and 561 nm lasers, a 20x water-immersion objective (W Plan-Apochromat, NA 1.0) and controlled via the ZEN black software (Zeiss, Germany).

To determine the number and distribution of soma and processes associated with each interneuron subtype, quantitative image analysis was performed on brain

slices from PV-cre, SST-cre and VIP-cre mice that had been injected with floxed AAVs. Slices were subjected to confocal microscopy and, in the resulting images, the CA areas were linearised along the pyramidal layer and the soma of fluorescent neurons were automatically detected via a custom-made, two-pass algorithm extracting maximally stable extremal region features using Matlab (Matas et al., 2004; Nistér and Stewénius, 2008). The number of virally-transduced interneurons was derived directly from the number of fluorescent soma per optical section. Meanwhile, to describe the distribution of processes associated with each interneuron subtype, soma were digitally removed from the linearised images to generate a transverse expression profile of fluorescent processes relative to the pyramidal cell layer. To compare across multiple interneuron populations, these expression profiles were normalised by the area under each curve.

2.9 Subcloning of the floxed ClopHensorN

Subcloning of the floxed version of ClopHensorN was performed by Tatsiana Waseem by inserting the inverted sequence of ClopHensorN into a backbone from another double floxed plasmid (Addgene #20298). The newly resulted construct included an elongation factor 1α (EF-1α) promoter, the Woodchuck hepatitis virus posttranscriptional regulatory element (WPRE), a polyadenylation termination sequence (polyA), an inverted terminal repeat sequence (ITR), and the ampicillin resistance (AmpR) gene. The 22 aminoacid linker from the original ClopHensor construct was maintained (Arosio et al., 2010). High titre virus ($\sim 10^{12}$ IU/ml) has been made by packaging the floxed ClopHensorN construct into AAV serotype 8 at the University of North Carolina Gene Therapy Center Vector Core (USA).

2.10 ClopHensorN imaging of intracellular pH and Cl^-

All ClopHensorN imaging and calibration experiments were performed using the same Zeiss LSM 880 optical system described above. ClopHensorN was used as a ratiometric probe and was excited at 561 nm using a diode-pumped solid-state laser, and at 458 nm and 488 nm using an argon laser. Emitted fluorescence was collected by one photomultiplier tube (PMT) in the 635-700 nm range when ClopHensorN was excited at 561 nm, and by a different PMT in the 500-550 nm range during 458 nm and 488 nm excitation. ClopHensorN is a fusion protein comprising the pH and Cl^- sensitive E^2GFP linked to tdTomato, which is insensitive to both pH and Cl^-. The excitation spectrum of E^2GFP displays a particular wavelength at which emission is stable regardless of pH. This is called the pH isosbestic point and the corresponding wavelength is 458 nm (Arosio et al., 2010). Thus, the ratio of emitted fluorescence during excitation at 458 nm and 561 nm was converted into Cl^- , and the ratio of emitted fluorescence during excitation at 488 nm and 458 nm was converted into pH, using the calibration curves described in thesis section 2.11. Fluorescence was always collected over the cell body and background fluorescence was subtracted. Data was then exported and processed using custom-made Matlab scripts. Under- and over-exposure thresholds were used to exclude regions of interest that had low signal-to-noise ratio or were overexposed. For recordings during seizure activity, bleaching correction was separately performed for all three wavelengths. The reason for performing bleaching correction separately – even for signals recorded from the same fluorophore, such as for pH measurements – was that, when excited at different wavelengths, bleaching of the background

fluorescence might contribute differentially to the collected emission signal. EDs were first detected and fluorescence data during epileptiform events was excluded before fitting exponential decay or polynomial functions to approximate the bleaching rate and to stabilise the optical signals. Following bleaching correction, the pH (F_{488}/F_{458}) and Cl^- (F_{458}/F_{561}) ratios were calculated and used to infer the pH and Cl^- concentration according to determined calibration curves. If pH ratios were not within the pH calibration curve range, they were not considered for inferring pH. Cl^- ratios were excluded if they were lower than the minimum ratio of the Cl^- calibration curve range for the corresponding inferred pH. Resting Cl^- concentration values and Cl^- concentration peak changes during EDs that were more than two interquartile ranges (IQRs) below the first quartile or above the third quartile of the respective population were excluded as outliers. Cl^- values above 200 mM were considered artefacts and excluded from analysis. Only experiments in which Cl^- values recovered within 40 mM of the baseline values after ED were included for analysing ED-induced Cl^- dynamics.

2.11 ClopHensorN calibration

ClopHensorN calibration was performed as previously described (Raimondo et al., 2013). HEK239 cells were transduced by Tatsiana Waseem with lentivirus containing the ClopHensorN construct. Intra- and extracellular pH and Cl^- concentration were equilibrated by using the K^+/H^+ exchanger nigericin (20 μM), the Cl^-/OH^- exchanger tributyltin chloride (40 μM) and the Cl^- ionophore I (1 μM) in high-K^+ buffer solution containing (in mM) K-gluconate (123), HEPES (23), D-glucose (11), NaH_2PO_4 (1.2), $MgSO_4$ (2) and Ca-gluconate (2). This method has

been previously described and used to calibrate fluorescent reporters or dyes (Boyarsky et al., 1988; Arosio et al., 2010; Raimondo et al., 2013). Separate calibration curves were obtained by monitoring the pH and Cl^- ratios while systematically changing the extracellular pH or Cl^- concentration.

2.11.1 pH calibration

The intracellular pH was controlled by titrating KOH or HNO_3 to the HEPES-based buffer solution containing the ionophore cocktail described above. Following each pH adjustment, the intra- and extracellular compartments were left to equilibrate at least 15 min before the pH ratio was measured by imaging ClopHensorN. According to the Grynkiewicz equation (Grynkiewicz et al., 1985), the formation of a 1:1 proton:ClopHensorN complex would lead to the following relationship:

$$pH_i = pK_a + \log\left(\frac{R_{pH} - R_A}{R_B - R_{pH}}\right) + \log\left(\frac{F_{458,A}}{F_{458,B}}\right)$$

In this equation, pH_i is intracellular pH, pK_a is acid dissociation constant of ClopHensorN, R_{pH} is the pH ratio, R_A and R_B are the pH ratios for ClopHensorN in the most acidic and basic conditions, respectively, and $F_{458,A}$ and $F_{458,B}$ represent the fluorescence of ClopHensorN when excited at 458 nm in its most acidic and basic form, respectively. Given that the fluorescence of E^2GFP does not change with pH when the fluorophore is excited at 458 nm, the equation above can be simplified as shown below:

$$pH_i = pK_a + \log\left(\frac{R_{pH} - R_A}{R_B - R_{pH}}\right)$$

The calibration data were then fitted using this rearranged equation:

$$R_{pH} = \frac{R_B \times 10^{pH-pK_a} + R_A}{1 + 10^{pH-pK_a}}$$

For fitting this equation, the pH ratio data within one standard deviation of the mode for each pH value was used. This allowed for pK_a, R_A and R_B to be calculated.

2.11.2 Cl^- calibration

The intracellular Cl^- concentration was controlled by systematically adjusting the extracellular pH and Cl^- concentration, which was changed by replacing determined amounts of potassium gluconate from the HEPES-based buffer solution containing the ionophore cocktail with KCl. Following each adjustment of pH and/or Cl^- concentration, the intra- and extracellular compartments were left to equilibrate for at least 15 min before the Cl^- ratio was measured by imaging ClopHensorN. According to the Grynkiewicz equation, the formation of a 1:1 Cl^--ClopHensorN complex would result in the following relationship:

$$[Cl^-]_i = K_d^{Cl^-}[pH_i] \times \left(\frac{R_{Cl^-} - R_{free}}{R_{bound}[pH_i] - R_{Cl^-}}\right) \times \left(\frac{F_{561,free}}{F_{561,bound}}\right)$$

In this equation, $[Cl^-]_i$ is the intracellular Cl^- concentration, $K_d^{Cl^-}[pH_i]$ is the Cl^- dissociation constant that depends on pH, R_{Cl^-} is the Cl^- ratio, R_{free} is the Cl^- ratio of ClopHensorN in its Cl^--free form, $R_{bound}[pH_i]$ is the Cl^- ratio of ClopHensorN in its Cl^--bound form and $F_{561,free}$ and $F_{561,bound}$ represent the fluorescence of ClopHensorN when excited at 561 nm in its Cl^--free and Cl^--bound form,

respectively. Given the fluorescence of tdTomato does not change with pH or Cl^- when the fluorophore is excited at 561 nm, the equation above can be simplified as:

$$[Cl^-]_i = K_d^{Cl^-}[pH_i] \times \left(\frac{R_{Cl^-} - R_{free}}{R_{bound}[pH_i] - R_{Cl^-}}\right)$$

The calibration data were then fitted using the following rearranged equation:

$$R_{Cl^-} = \frac{[Cl^-]_i \times R_{bound}[pH_i] + K_d^{Cl^-}[pH_i] \times R_{free}}{K_d^{Cl^-}[pH_i] + [Cl^-]_i}$$

Separate Cl^- calibrations were performed at different pH values, which allowed the calculation of $K_d^{Cl^-}[pH_i]$, R_{free} and $R_{bound}[pH_i]$. $R_{bound}[pH_i]$ was assumed to relate linearly with pH, and $K_d^{Cl^-}[pH_i]$ relates with pH according to the relationship shown below:

$$K_d^{Cl^-}[pH_i] = {}^1K_d^{Cl^-} \times \left(\frac{1 + 10^{pK_a - pH_i}}{10^{pK_a - pH_i}}\right)$$

${}^1K_d^{Cl^-}$ represents the dissociation constant for Cl^- in the fully protonated form of ClopHensorN.

2.12 Data analysis

Digital signal processing and presentation were performed using custom-made programs in the Matlab environment (R2017b, Mathworks, USA). Figures were built using vector-based graphic design in CorelDraw (X6, Corel Corporation, USA) and the statistical software GraphPad Prism (v6.01, GraphPad Software, USA). Video data processing for tracking locomotor activity of animals was performed using the open-source software Bonsai v2.3 (Lopes et al., 2015). Data

are presented as mean ± standard error of mean, and the statistical tests are reported at the relevant points in the text (GraphPad Prism; Matlab). Non-parametric tests were used when a normal distribution of data could not be ascertained. Appropriate post-hoc tests were used when ANOVA tests confirmed a statistically significant effect. The choice of post-hoc tests was guided by recommendations of the software in order to reduce the probability of type II error.

Chapter 3: Chemogenetic recruitment of specific interneurons suppresses seizure activity

3.1 Introduction

In the introduction to this thesis I described how different mechanisms can account for the generation and propagation of seizure activity. In focal epilepsy, the 'epileptic focus' refers to a region of brain which is able to generate recurrent, spontaneous (or unprovoked) seizures, and typically contains neurons characterised by an abnormal functional organisation. Seizures are characterised by hypersynchronous, hyperexcitable neuronal activity. These pathologic events are thought to occur when a large enough ensemble of excitatory neurons become synchronised by abrupt paroxysmal depolarising shifts (PDS) that then lead to high frequency bursts of action potentials (Jefferys, 1990). The generation of the PDS relies on two key factors: the main excitatory neurotransmitter in the brain, glutamate and the intrinsic depolarising conductances of the pyramidal neurons recruited into these synchronous discharges. Under physiologic conditions this excessive excitation and synchronisation is prevented by local GABAergic interneurons. However, if a critical mass of inter-connected excitatory neurons constituting the 'epileptic core' are involved in the paroxysmal electrical discharges, GABAergic inhibition can become ineffective, allowing for a seizure to develop. Furthermore, in some cases, seizure activity is able to extend by overriding the intact inhibitory mechanisms in the surrounding tissue, referred to as 'penumbra'. This permits for more neurons to be recruited and allows the seizure to propagate.

Drugs that enhance GABA-mediated synaptic inhibition can be potent anticonvulsants (Czapiński et al., 2005). However, because of their system-wide actions, these drugs exhibit multiple deleterious side-effects, such as cognitive impairment or acute respiratory failure (Snodgrass, 1992; Mula, 2011). Whilst GABAergic signalling can become altered in the dysfunctional cells within the epileptic focus (Cohen et al., 2002; Huberfeld et al., 2007), inhibitory mechanisms are thought to remain effective in the neighbouring healthy tissue of the core and the surrounding penumbra, and are able to oppose seizure spread (Trevelyan et al., 2006, 2007; Schevon et al., 2012; Cammarota et al., 2013). Therefore, selectively enhancing these endogenous inhibitory mechanisms may offer the potential to disrupt the initiation and propagation of epileptic seizure activity.

The first aim of this chapter was to investigate whether GABAergic interneurons, specifically PV interneurons, can be manipulated using the novel chemogenetic tool – hM_3D_q receptors – described in the introduction to this thesis. To achieve expression of hM_3D_q receptors in different neuronal populations, I combined promoter-specific cre recombinase mice with viral-mediated delivery of chemogenetic constructs. The second aim of this chapter was to use chemogenetics to assess the potential of suppressing epileptiform activity by enhancing the synaptic output from three major interneuron populations in the mouse hippocampus: PV, SST and VIP expressing interneurons. To this end, I performed targeted electrophysiological recordings in an *in vitro* model of chronic, drug-resistant temporal lobe epilepsy. Finally, the third aim of this chapter was to test the

potential of this chemogenetic strategy to reduce seizure activity *in vivo*. To achieve this, I performed behavioural video-scoring in an *in vivo* model of acute seizures.

3.2 Recruiting distinct hippocampal GABA-releasing interneuron populations with excitatory DREADDs

To examine the potential of enhancing the synaptic output of hippocampal interneurons chemogenetically, I used mouse organotypic hippocampal brain slices, referred to in this thesis as 'brain slices'. This system enabled me to perform targeted patch-clamp recordings to determine the presynaptic and postsynaptic efficacy of DREADDs, as well as the opportunity to examine the impact of interneuron recruitment upon spontaneously generated epileptiform activity. Organotypic slices can be used as a model of temporal lobe epilepsy because when kept in culture beyond 2 weeks, they develop spontaneous EDs without any pharmacological treatment, analogous to epileptogenesis in post-traumatic epilepsy (Dyhrfjeld-Johnsen et al., 2010; Lillis et al., 2015).

As shown in previous work (Trevelyan et al., 2006; Sessolo et al., 2015), my recordings from excitatory pyramidal neurons within the CA areas revealed reproducible spontaneous EDs that exhibited a sustained duration (mean duration 48.3±8 s) and stable event frequency (**Figure 3.1***A,B*). Consistent with epileptiform activity in many systems (Trevelyan et al., 2006; Sessolo et al., 2015), these spontaneous EDs recruited both excitatory and inhibitory neurons within the network. Paired recordings revealed that during each ED, pyramidal neurons received intense barrages of both glutamatergic and GABAergic postsynaptic

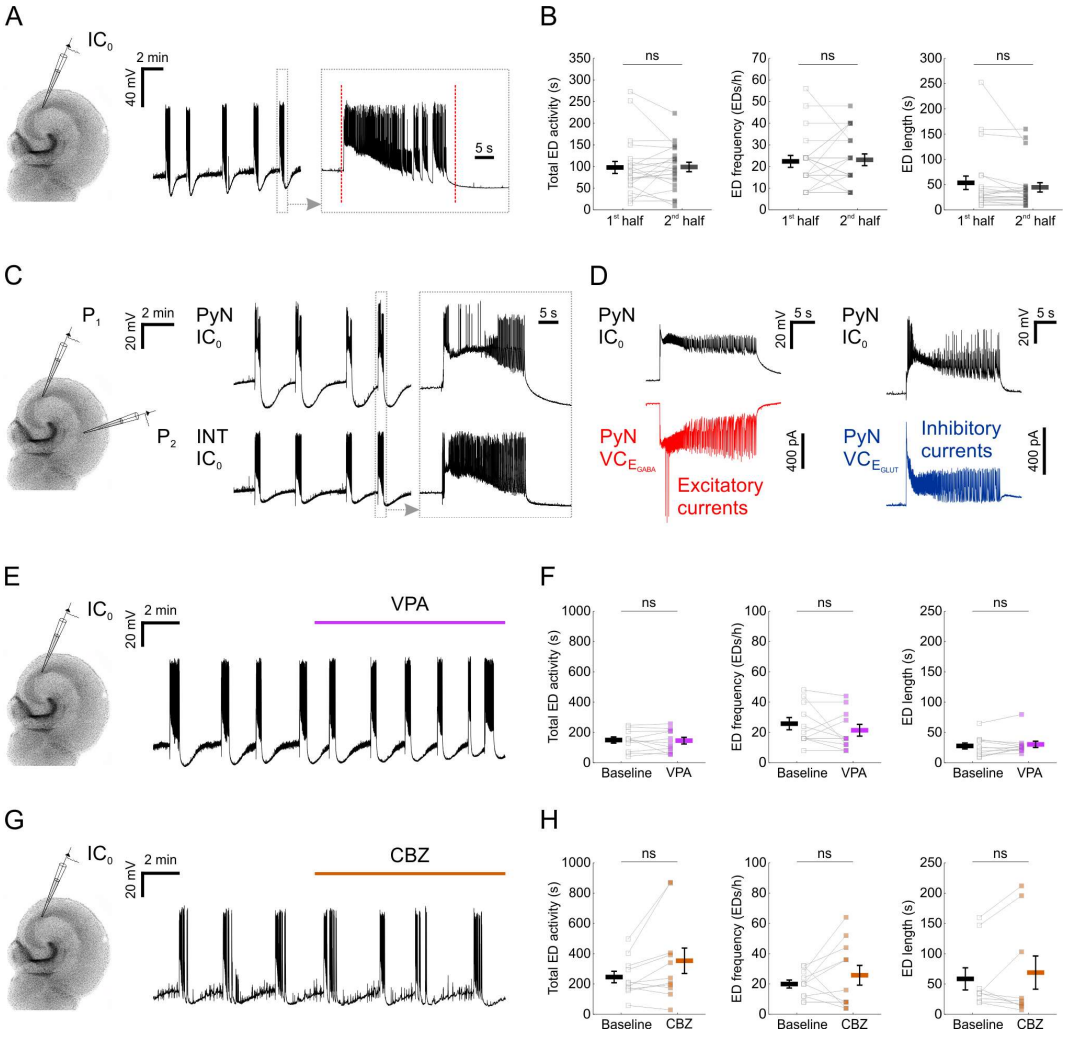

Figure 3.1. Epileptiform activity in mouse organotypic hippocampal brain slices is resistant to first-line anti-seizure drugs.(A) Current-clamp recording of a CA3 pyramidal neuron from a mouse brain slice reveals repeated EDs. The vertical red dotted lines in the expanded trace mark the onset and the termination of the underlying ED, as determined by an automated detection algorithm. **(B)** A 15-min time window was used to assess the stability of the epileptiform activity. Total ED activity, defined as the cumulative duration of ED activity (left, 96.8±13.9 s during 1st half, 97.9±10.9 s during 2nd half; N=22 slices, $W_{(21)}$=110.5, p=0.8715, two-tailed Wilcoxon signed-rank test), ED frequency (middle, 22.2±2.7 EDs/h during 1st half, 22.9±2.7 EDs/h during 2nd half; N=22 slices, $W_{(12)}$=34, p=0.7153, two-tailed Wilcoxon signed-rank test) and individual ED length (right, 52.8±13.4 s during 1st half, 43.9±9.2 s during 2nd half; N=22 slices, $W_{(21)}$=71, p=0.1281, two-tailed Wilcoxon signed-rank test) were stable across the 15-min time window. **(C)** A dual current-clamp (IC_0) electrophysiological recording of a CA3 pyramidal neuron (PyN) and a GABAergic interneuron (INT) reveal spontaneous EDs in a mouse brain slice (left). Expanded traces (right) show that both excitatory and

(figure legend continued on facing page) ——————►

currents (**Figure 3.1***C,D*). The brief negative voltage transients preceding the onset of EDs likely resulted from the particularly intense inhibitory currents occurring around the onset of EDs, as illustrated in **Figure 3.1***D*. The few large negative current transients during the recording of excitatory currents in **Figure 3.1***D* could represent dendritic Ca^{2+} spikes, as it is unlikely these were action potentials since the internal solution contained QX-314. To further characterise EDs, I tested the effect of first-line anti-seizure drugs, valproate (**Figure 3.1***E*) and carbamazepine (**Figure 3.1***G*). At therapeutically-relevant doses, both drugs were ineffective at suppressing EDs (**Figure 3.1***F,H*), consistent with the idea that organotypic slices represent a model of drug-resistant temporal lobe epilepsy (Albus et al., 2008; Avaliani et al., 2016). By combining promoter-specific cre recombinase mice with

---

inhibitory neurons are recruited during the EDs. **(D)** Simultaneous current-clamp and voltage-clamp (VC) recordings from pairs of pyramidal neurons demonstrate that strong barrages of excitatory (bottom-left, red) and inhibitory (bottom-right, blue) postsynaptic currents occur throughout the EDs, as monitored by current-clamp recordings from a neighbouring pyramidal neuron (top). E_{GABA}, reversal potential for GABAergic current; E_{GLUT}, reversal potential for glutamatergic current. **(E)** A representative recording showing that 1.5 mM valproic acid (VPA) did not disrupt the spontaneous EDs. **(F)** No effect could be detected of VPA on the total ED activity (left, 146.6±20.4 s during baseline and 142.6±22 s during VPA; N=11, $t_{(10)}$=0.31, p=0.7643, two-tailed paired t-test), frequency (middle, 25.5±4 EDs/h during baseline and 21.1±3.9 EDs/h during VPA; N=11, $t_{(10)}$=1.17, p=0.2674, two-tailed paired t-test) or individual ED length (right, 27±5 s during baseline and 29.5±5.2 s during VPA; N=11, $W_{(11)}$=22, p=0.3652, two-tailed Wilcoxon signed-rank test). **(G)** A representative recording showing that 50 μM carbamazepine (CBZ) did not disrupt the spontaneous EDs. **(H)** No effect could be detected of CBZ on the total ED activity (left, 242.7±37.8 s during baseline and 350.3±84.2 s during CBZ; N=11, $t_{(10)}$=2.136, p=0.0584, two-tailed paired t-test), frequency (middle, 19.6±2.7 EDs/h during baseline and 25.5±6.5 EDs/h during CBZ; N=11, $t_{(10)}$=1.03, p=0.3266, two-tailed paired t-test) or individual ED length (right, 57.8±18.3 s during baseline and 68.1±27.4 s during CBZ; N=9, $W_{(9)}$=21, p=0.9102, two-tailed Wilcoxon signed-rank test). VPA and CBZ drug concentrations were equivalent to effective doses *in vivo* (Albus et al., 2008).

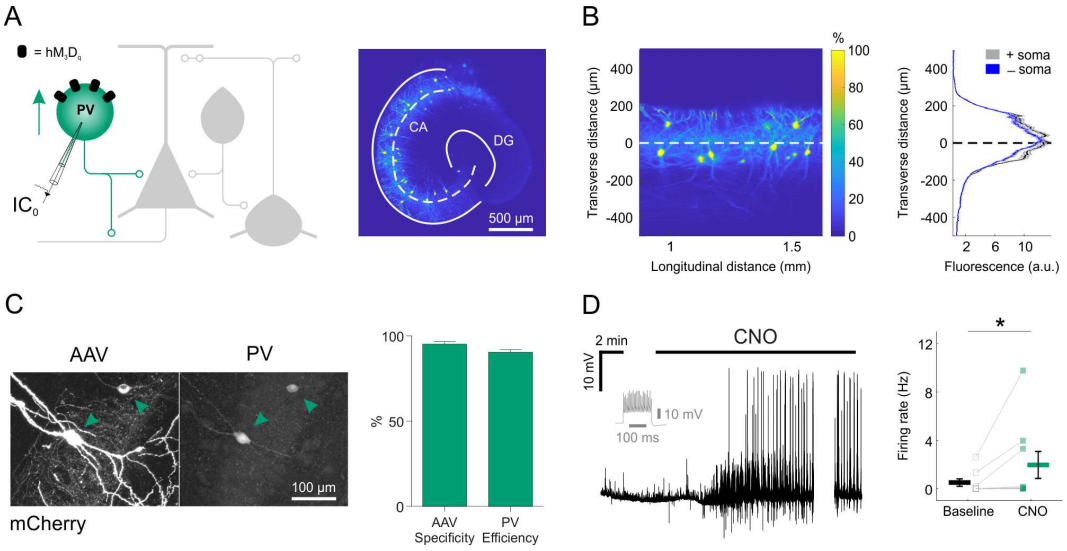

Figure 3.2. Chemogenetic recruitment of hippocampal PV interneurons. (A) Cartoon of hippocampal circuitry (left) showing the targeting of the hM_3D_q receptor to PV interneurons. Confocal image (right) of a brain slice from a PV-cre mouse illustrates the distribution of fluorescence of virally-transduced PV interneurons. The superimposed white dashed line marks the centre of the pyramidal cell layer. Continuous white lines indicate the DG and the outline of the CA areas. **(B)** The confocal image was linearised (left) to facilitate the quantification of the transverse expression profile for PV interneurons, relative to the pyramidal cell layer (dashed line at zero). This confirmed that PV interneurons (+ soma) as well as their processes (- soma) were restricted to the pyramidal cell layer (right). **(C)** The immunohistochemical characterisation of PV interneurons transduced with AAV_8-hSyn-DIO-hM_3D_q-mCherry demonstrates high targeting specificity and efficiency (N=14 sections from 6 slices). **(D)** An example current-clamp recording of a PV interneuron expressing hM_3D_q receptors shows that CNO promotes action potential firing (left). The firing pattern of the neuron in response to a 500 pA square wave current pulse is shown in grey. The break in the recording reflects a period during which the intrinsic properties of the neuron were monitored. Recordings were conducted in kynurenic acid to isolate the direct effects of hM_3D_q receptor activation, and to prevent the occurrence of EDs. Population data shows a significant increase in firing rate following CNO (right; N=9 slices, $W_{(7)}=0$, $p=0.0156$, two-tailed Wilcoxon signed-rank test).

floxed chemogenetic constructs, I was then able to investigate the cellular and network effects of delivering DREADDs to specific interneuron populations.

PV interneurons, a principal GABAergic population, reside primarily within the pyramidal layer of CA areas, and their axons target the somatic compartment of pyramidal neurons (Pawelzik et al., 2002; Bartos and Elgueta, 2012). Consistent with this, injection of AAV containing floxed constructs into brain slices from PV-cre mice resulted in somatic and process expression that was restricted to the pyramidal cell layer (**Figure 3.2***A,B*). Immunohistochemical experiments confirmed that the PV interneurons could be efficiently and specifically targeted with the excitatory DREADD receptor, hM_3D_q. Two-to-four weeks after viral transduction with AAV_8-hSyn-DIO-hM_3D_q-mCherry, the majority of expressing neurons were immunopositive for PV (95.2±1.5% 'specificity') and the majority of all PV immunopositive neurons were expressing hM_3D_q-mCherry (90.5±1.4% 'efficiency'; **Figure 3.2***C*). To assess whether activating hM_3D_q receptors could increase the output of the PV interneuron population, current-clamp recordings were targeted to hM_3D_q-mCherry positive neurons. The addition of the hM_3D_q ligand, CNO, led to a significant increase in the firing rate of PV interneurons, from 0.5±0.3 Hz during baseline, to 1.9±1.1 Hz in the presence of CNO (**Figure 3.2***D*).

I performed similar experiments in slices generated from SST-cre mice and VIP-cre mice (**Figure 3.3**). Here, I found that the soma and processes of SST interneurons were located within stratum oriens and lacunosum-moleculare, and tended to avoid the pyramidal cell layers (**Figure 3.3***A,B*). This is consistent with

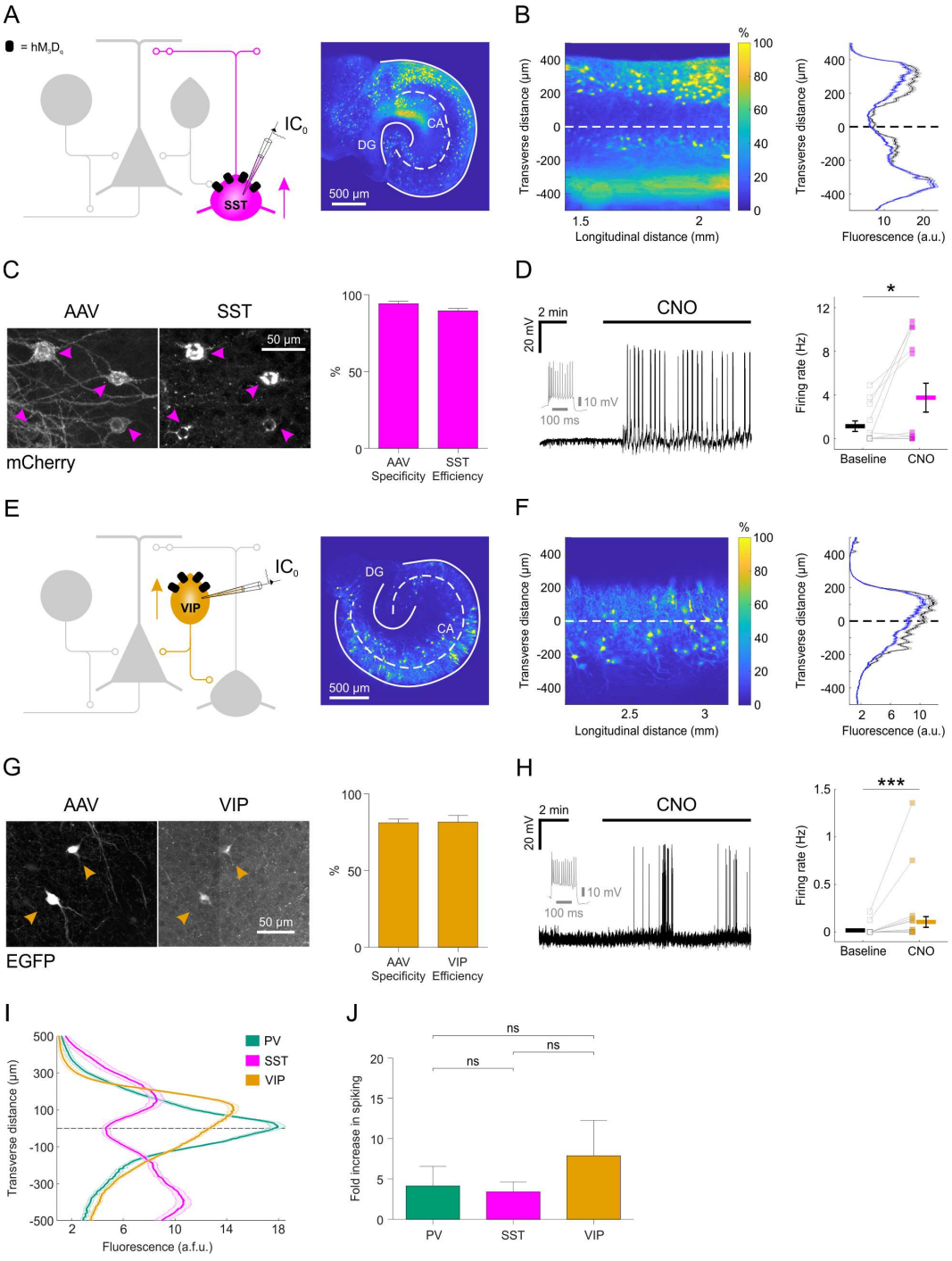

Figure 3.3. Distinct subtypes of hippocampal GABAergic interneurons can be recruited via excitatory DREADDs. (A) Cartoon (left) showing the targeting of hM_3D_q receptors to SST hippocampal interneurons. A confocal image of a SST-cre mouse slice (right) illustrates the fluorescence distribution profile of virally-transduced SST interneurons. Continuous white lines outline the DG and CA areas. **(B)** The confocal image was linearised (left) to facilitate quantification of the

(figure legend continued on facing page) ⟶

previous evidence that SST interneurons target the dendritic compartments of hippocampal principal neurons (Katona et al., 1999; Lovett-Barron et al., 2012). Immunohistochemistry confirmed that the SST interneurons were efficiently (89.6±1.5%) and specifically (94.1±1.6%; **Figure 3.3***C*) targeted with hM_3D_q receptors. Consistent with the results in PV interneurons, CNO significantly

---

transverse expression profile for SST interneurons, relative to the pyramidal cell layer (dashed white line at zero). This confirmed that SST interneurons (+ soma) as well as their processes (- soma) were associated with stratum oriens and lacunosum-moleculare (right). **(C)** Immunohistochemical characterisation of SST interneurons transduced with AAV_8-hSyn-DIO-hM_3D_q-mCherry demonstrates high targeting specificity and efficiency (N=16 sections from 6 slices). **(D)** Current-clamp recording from a SST interneuron expressing hM_3D_q in the presence of kynurenic acid, showing that CNO promotes action potential firing (left). The firing pattern of the neuron in response to a 500 pA square wave current pulse is shown in grey. Population data shows a significant increase in firing rate in the presence of CNO (right, N=13 slices, $W_{(9)}$=4, p=0.0273, two-tailed Wilcoxon signed-rank test). **(E)** Cartoon (left) shows the targeting of hM_3D_q receptors to VIP interneurons and confocal image (right) illustrates the fluorescence distribution profile of virally-transduced interneurons in a VIP-cre slice. **(F)** Linearising the confocal image (left) confirmed that the expression profile for VIP interneurons (+ soma) and their processes (- soma) was associated with stratum radiatum/lacunosum-moleculare, pyramidale and oriens (right). **(G)** Immunohistochemical characterisation of VIP interneurons transduced with AAV_8-hSyn-DIO-hM_3D_q-mCherry demonstrates high targeting specificity and efficiency (N=4 sections from 2 slices). **(H)** Example current-clamp recording from a VIP interneuron expressing hM_3D_q in kynurenic acid, showing that CNO promotes action potential firing (left). The firing pattern of the neuron in response to a 500 pA square wave current pulse is shown in grey. Population data (right) shows a significant increase in firing rate in the presence of CNO (N=27 slices, $W_{(13)}$=1, p=0.0005, two-tailed Wilcoxon signed-rank test). **(I)** Comparison of the fluorescence distribution profiles following viral-transduction of the three interneuron populations (PV, N=38 slices; SST, N=37 slices; VIP, N=57 slices). Each distribution was normalised by the area under the profile curve and shown to be significantly different between the cell types (interaction between cell type and location: $F_{(8,516)}$=58.81; p<0.0001, repeated measures two-way ANOVA). **(J)** There was no difference in the CNO-induced fold-increase in spiking rate (normalised to baseline) between the three interneuron populations ($\chi^2_{(2)}$=0.9136, p=0.6333, Kruskal-Wallis test). There was also no difference in absolute changes in spiking rate (1.5±0.8 Hz for PV; 2.6±1.1 for SST; 0.1±0.1 for VIP; $\chi^2_{(2)}$=4.343, p=0.114, Kruskal-Wallis test).

increased the firing rate of SST interneurons, from 1.1±0.5 Hz during baseline, to 3.7±1.3 Hz (**Figure 3.3***D*).

Consistent with previous evidence that distinct VIP interneuron subtypes target oriens lacunosum-moleculare interneurons and the perisomatic regions or proximal dendrites of pyramidal neurons (Léránth et al., 1984; Acsády et al., 1996; Chamberland et al., 2010; Tyan et al., 2014) (**Figure 3.3***E*), I found that the soma and processes of virally-transduced VIP interneurons were located within stratum radiatum/lacunosum-moleculare, pyramidale and oriens in slices from the VIP-cre mice (Köhler, 1982; Taniguchi et al., 2011) (**Figure 3.3***F*). The majority of expressing neurons were immunopositive for VIP (81.2±2.4% specificity) and the majority of VIP immunopositive neurons expressed the floxed construct (81.6±4.4% efficiency; **Figure 3.3***G*). Finally, CNO increased the firing rate from 0.01±0.01 Hz during baseline, to 0.1±0.1 Hz (**Figure 3.3***H*).

A summary plot for the three interneuron populations confirmed that the expression profiles of PV, SST and VIP interneurons were significantly different from one another (**Figure 3.3***I*) and were consistent with data from acute preparations of mouse hippocampus (Taniguchi et al., 2011; Lovett-Barron et al., 2012). These results are in accordance with previous observations that organotypic slices retain fundamental features of the circuit, including the subcellular targeting of perisomatic and dendritic domains of pyramidal neurons by distinct interneuron populations (Streit et al., 1989; De Simoni et al., 2003; Cristo et al., 2004). Meanwhile, CNO-mediated activation of hM_3D_q receptors resulted in comparable fold-increases in spiking activity across the three interneuron populations: PV

interneurons showed a 4.1±2.4 fold increase in their firing rate, SST interneurons showed a 3.4±1.2 fold increase and VIP interneurons showed a 7.9±4.4 fold increase (**Figure 3.3***J*).

3.3 Chemogenetic enhancement of GABAergic interneuron populations can attenuate epileptiform activity *in vitro*

Having shown that different interneuron subtypes can be chemogenetically manipulated, I next tested the effects of enhancing the activity of each interneuron population on EDs. Spontaneous EDs were recorded from pyramidal neurons before and after CNO-mediated activation of the relevant interneuron population. I quantified total ED activity, ED frequency and individual ED duration. In PV-targeted slices (**Figure 3.4***A*), CNO-mediated activation of hM_3D_q receptors significantly reduced the total ED activity (from 247.5±47.8 s during baseline to 116.5±47.4 s during CNO), which resulted from a significant decrease in ED frequency (from 17.6±5.3 EDs/h during baseline to 8.4±3.3 EDs/h during CNO), without affecting the duration of individual EDs (65.8±15.7 s during baseline and 77.5±27.4 s during CNO) (**Figure 3.4***B*). In SST-targeted slices (**Figure 3.4***C*), CNO also significantly reduced total ED activity (from 263.2±41.4 s during baseline to 133.3±40.2 s during CNO), which involved a decrease in ED frequency (from 26±6.8 EDs/h during baseline to 13.3±3.5 EDs/h during CNO), without significantly affecting individual ED length (72±21.7 s during baseline and 47.6±14.5 s during CNO) (**Figure 3.4***D*). In VIP-targeted slices (**Figure 3.4***E*), CNO did not decrease the total ED activity (234.3±40.6 s during baseline and

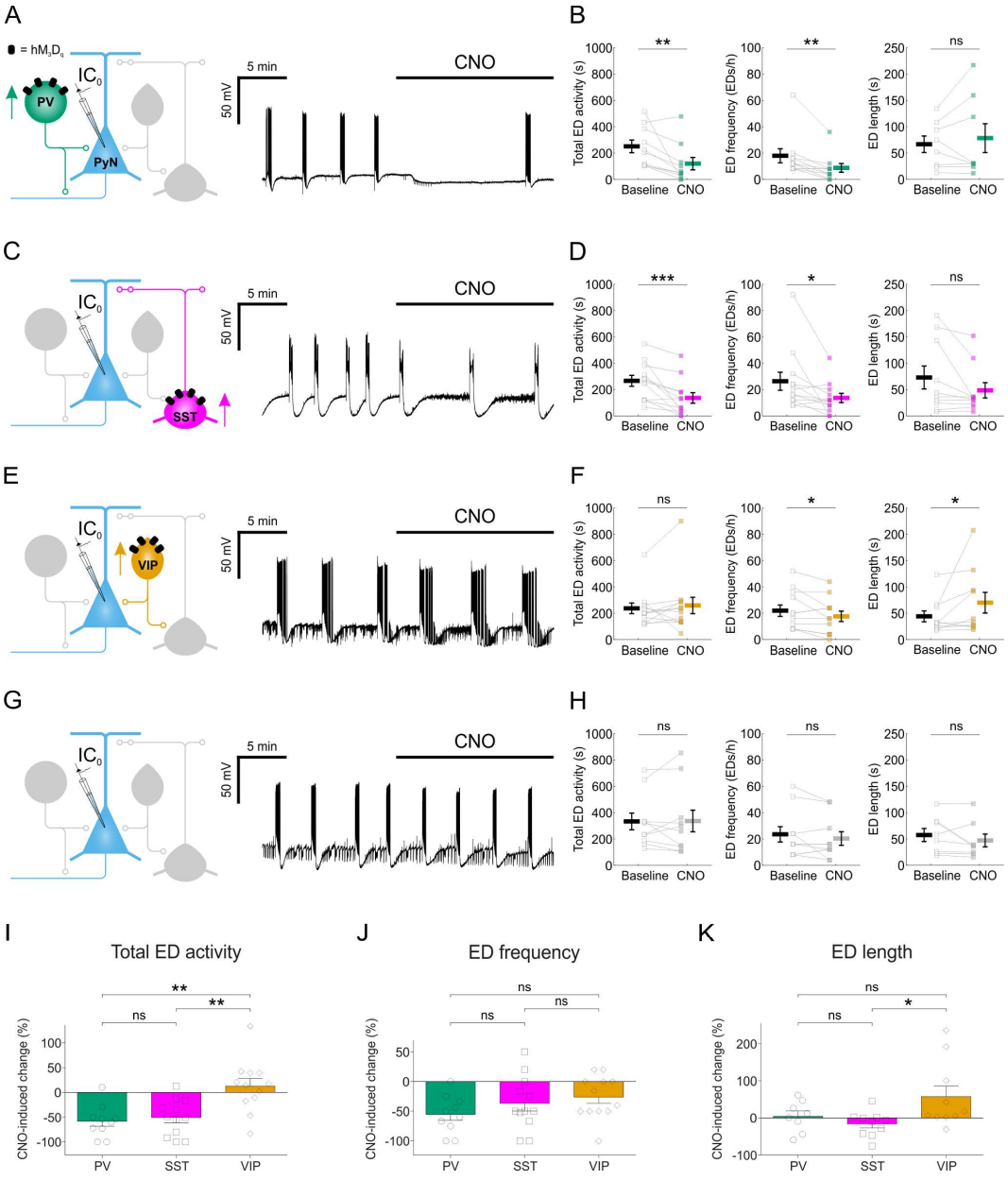

Figure 3.4. Chemogenetic enhancement of specific GABAergic interneuron populations attenuates hippocampal EDs. (A) PV-cre mice and floxed viral constructs were used to target hM_3D_q receptors to PV interneurons in brain slices. The effects of CNO upon spontaneous EDs were monitored by current-clamp recordings from CA1 or CA3 pyramidal neurons. **(B)** Population data from experiments targeting PV interneurons (N=10 slices) showed a reduction in total ED activity (left, $W_{(10)}=1$, p=0.0039, two-tailed Wilcoxon signed-rank test), a decrease in ED frequency (middle, $W_{(9)}=0$, p=0.0039, two-tailed Wilcoxon signed-rank test), and no change in ED length (right, $W_{(8)}=12$, p=0.4609, two-tailed Wilcoxon signed-rank test) following addition of CNO. **(C)** SST-cre mice were

(figure legend continued on facing page)

256.3±62.7 s during CNO). Whilst enhancing VIP interneuron output led to a decrease in ED frequency (from 21.7±4.3 EDs/h during baseline to 17.3±4 EDs/h during CNO), there was a simultaneous increase in the duration of individual EDs (from 43.5±10.3 s during baseline to 69.4±19.6 s during CNO) (**Figure 3.4***F*). Finally, to assess potential off-target effects of CNO, the drug was bath-applied during the recording of spontaneous EDs in control slices virally-transduced with the same AAV type expressing EGFP in a cre-dependent manner, and not hM_3D_q

---

used to target hM_3D_q receptors to SST interneurons. **(D)** Population data from experiments targeting SST interneurons (N=12 slices) showed a reduction in total ED activity (left, $W_{(12)}$=1, p=0.001, two-tailed Wilcoxon signed-rank test), a decrease in ED frequency (middle, $W_{(12)}$=6, p=0.0166, two-tailed Wilcoxon signed-rank test), and no change in ED length (right, $W_{(10)}$=10, p=0.0840, two-tailed Wilcoxon signed-rank test) following addition of CNO. **(E)** VIP-cre mice were used to target hM_3D_q receptors to VIP interneurons. **(F)** Population data from experiments targeting VIP interneurons (N=12 slices) showed no change in total ED activity (left, $W_{(12)}$=25, p=0.3013, two-tailed Wilcoxon signed-rank test), a reduction in ED frequency (middle, $t_{(11)}$=2.24, p=0.0468, two-tailed paired t-test), and an increase in ED length (right, $W_{(10)}$=6, p=0.0273, two-tailed Wilcoxon signed-rank test) following addition of CNO. **(G)** Control experiments were conducted on slices that had not received floxed DREADD constructs. **(H)** Population data (N=10 slices) demonstrated no change in total ED activity (left, $t_{(9)}$=-0.08, p=0.9337, two-tailed paired t-test), ED frequency (middle, $t_{(9)}$=1.31, p=0.2229, two-tailed paired t-test), or ED length (right, $W_{(8)}$=6, p=0.1094, two-tailed Wilcoxon signed-rank test) following the addition of CNO to control slices. **(I)** Total ED activity was significantly reduced by chemogenetically enhancing either PV or SST interneurons, compared to enhancing VIP interneurons ($F_{(2,31)}$=9.747, p=0.0005, one-way ANOVA, followed by Tukey's post-hoc multiple comparison tests; VIP vs PV, p=0.0013; VIP vs SST, p=0.0025). **(J)** The frequency of EDs was reduced when PV interneurons, SST interneurons or VIP interneurons were targeted. No significant difference in the reduction in ED frequency was detected across the three interneurons ($F_{(2,31)}$=1.583, p=0.2215, one-way ANOVA). **(K)** Individual EDs became significantly longer when VIP interneurons were recruited, compared to SST interneurons ($F_{(2,25)}$=3.772, p=0.037, one-way ANOVA, followed by Tukey's post-hoc multiple comparison tests; VIP vs SST, p=0.0337). * indicates p<0.05, ** indicates p<0.01.

(**Figure 3.4***G*). In these experiments, no changes were detected for total ED activity, ED frequency, or individual ED length (**Figure 3.4***H*).

Total ED activity changes were different across the four groups – including the control group ($F_{(3,40)}$=8.275, p=0.0002, one-way ANOVA). Compared to the change in total ED activity in control experiments, Dunnett's post-hoc multiple comparison tests confirmed that total ED activity reduction was greater following activation of either PV interneurons (down 54.6±18.1%; p=0.0121) or SST interneurons (down 47.1±17.3%; p=0.0255), but not of VIP interneurons (up 16.3±17.3%; p=0.6695). ED frequency changes were not different across the four groups, likely because of lack of statistical power for this comparison ($F_{(3,40)}$=2.702, p=0.0583, one-way ANOVA). Nevertheless, ED frequency reduction tended to be greater relative to control following activation of either PV interneurons (down 48.4±17.5%), SST interneurons (down 29.8±16.7%), or VIP interneurons (down 19.4±16.7%). Meanwhile, ED length changes were different across the four groups ($F_{(3,32)}$=3.629, p=0.0232, one-way ANOVA). Compared to control experiments, Dunnett's post-hoc multiple comparison tests confirmed that ED length increase was greater following activation of VIP interneurons (up 72±26.7%; p=0.0293), but not following the activation of either PV interneurons (up 18.9±28.1%; p=0.8412) or SST interneurons (down 1.6±26.7%; p=0.9999).

Comparisons across the different interneuron populations confirmed subtype-specific effects. Total ED activity was reduced by more than half following activation of either PV interneurons (down 58.2±10.3%) or SST interneurons (down 50.8±10.5%), and both of these reductions were significantly greater than

the change in total ED activity induced by recruiting VIP interneurons (up 12.7±15.4%) (**Figure 3.4***I*). Each of the interneuron populations was able to decrease ED frequency: PV interneurons by 55.4±10.1%, SST interneurons by 36.7±13% and VIP interneurons by 26.3±10.4% (**Figure 3.4***J*). Meanwhile, only the VIP population increased individual ED length by 57.5±28.4% (**Figure 3.4***K*). In summary, chemogenetically enhancing the output of interneuron populations can generate effective suppression of epileptiform synchronisation, but the effectiveness of this approach varied by interneuron subtype.

3.4 Chemogenetically-enhanced interneuron subtypes differ in their postsynaptic inhibition of pyramidal neurons

To examine the cellular basis of these effects, I performed voltage-clamp recordings to compare how chemogenetic recruitment affects the postsynaptic inhibition converging upon pyramidal neurons. Inhibitory postsynaptic currents were isolated at the reversal potential for glutamatergic current (E_{GLUT}) (**Figure 3.5***A,C,E*). For each of the three interneuron populations, CNO-activation of hM_3D_q receptors resulted in a significant increase in postsynaptic inhibitory input (**Figure 3.5***A,C,E*), which was abolished by bath application of TTX (1-2 μM; **Figure 3.5***A,C,E*), confirming that it was mediated by action potential-evoked GABA release. Total inhibitory postsynaptic input to pyramidal neurons increased from 11±4.2 pA to 34±6.1 pA when PV neurons were recruited, from 9.3±2.6 pA to 126.6±14.6 pA for SST interneurons and from 5.7±1.1 pA to 16.2±2.4 pA for VIP interneurons (**Figure 3.5***B,D,F*). At the population level, the overall increase in postsynaptic

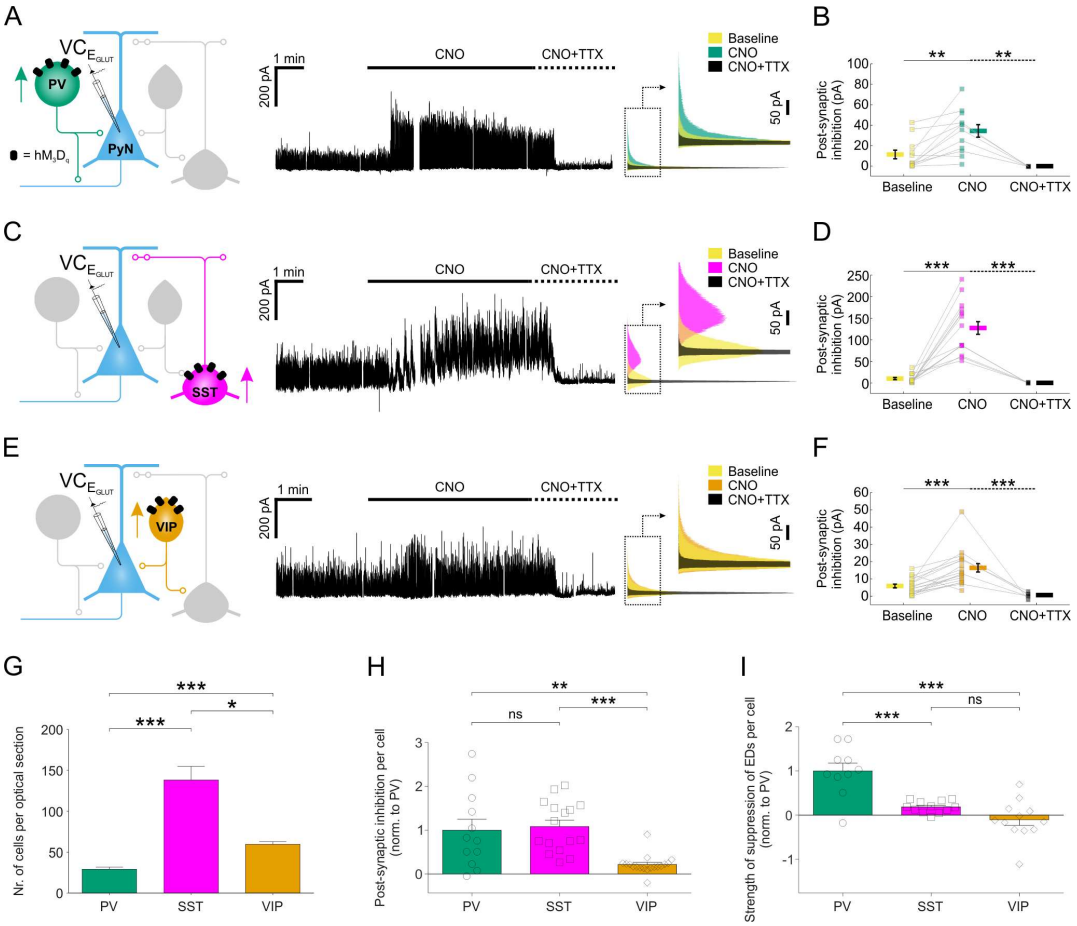

Figure 3.5. Chemogenetic recruitment of interneuron populations generates different amounts of postsynaptic inhibition in pyramidal neurons. (A) hM_3D_q receptors were targeted to PV interneurons and voltage-clamp recordings (at E_{GLUT}) were performed from pyramidal neurons (left). CNO application elicited a pronounced increase in inhibitory postsynaptic currents converging upon the pyramidal neuron (middle). This increase was associated with spiking activity as it was abolished by bath application of TTX. Overlapping histograms (right) illustrate the probability distribution functions for the inhibitory postsynaptic currents during baseline, CNO, and co-administration of CNO plus TTX. **(B)** PV recruitment resulted in a significant change in total postsynaptic inhibitory charge converging onto pyramidal neurons ($F_{(2,26)}$=9.541, p=0.0008, one-way ANOVA, followed by post-hoc Sidak's multiple comparisons tests; baseline vs. CNO, N=12, p=0.0047; CNO vs. CNO plus TTX, N=5, p=0.0013). **(C)** hM_3D_q receptors were targeted to SST interneurons and all conventions are the same as in 'A'. **(D)** SST recruitment resulted in a significant change in total postsynaptic inhibitory charge converging onto pyramidal neurons ($\chi^2_{(2)}$=29.77, p<0.0001, Kruskal-Wallis test, followed by post-hoc Dunn's multiple comparisons tests; baseline vs. CNO, N=16, p<0.0001; CNO vs. co-administration of CNO plus TTX, N=5, p<0.0001). **(E)** hM_3D_q receptors were targeted to VIP interneurons and all conventions are the same

(figure legend continued on facing page) ⟶

inhibitory input resulting from CNO-mediated activation of hM_3D_q receptors was highest for the SST interneuron population (increase of 116.7±15.5 pA), then the PV interneuron population (increase of 22.6±5.7 pA), followed by the VIP interneuron population (increase of 10.3±2.3 pA).

Next, I aimed to compare measurements of inhibitory efficacy across different individual interneuron subtypes. First, the CNO-induced increase in postsynaptic inhibitory input was normalised by the number of hM_3D_q-expressing cells, as determined from stereological cell counts (**Figure 3.5***G*; see Materials and Methods, thesis section 2.8). The increase in inhibitory postsynaptic input was similar for an individual PV interneuron (1.0±0.3 fold, relative to a PV interneuron) and an SST interneuron (1.1±0.1 fold, relative to a PV interneuron), both of which

---

as in 'A'. **(F)** VIP recruitment resulted in a significant change in total postsynaptic inhibitory charge converging onto pyramidal neurons ($F_{(2,39)}$=14.09, p<0.0001 by one-way ANOVA, followed by post-hoc Sidak's multiple comparisons tests; baseline vs. CNO, N=18, p=0.0003; CNO vs. co-administration of CNO plus TTX, N=6, p=0.0001). **(G)** The average number of hM_3D_q expressing interneurons (per 24 μm optical section) differs significantly between the three interneuron populations, with an average of 29.1±2.7 PV cells, 138.1±16.8 SST interneurons, and 59.7±3.2 VIP cells ($\chi^2_{(2)}$=54.44, p<0.0001, Kruskal-Wallis test, followed by Dunn's multiple post-hoc comparisons; PV vs SST, p<0.0001; PV vs VIP, p<0.0001; SST vs VIP, p=0.0118). **(H)** Normalising by the size of each interneuron population (i.e. number of hM_3D_q-expressing cells per slice), PV and SST interneurons were associated with similar amounts of postsynaptic inhibition, and both were significantly greater than that associated with VIP interneurons ($\chi^2_{(2)}$=20.46, p<0.0001, Kruskal-Wallis test, followed by Dunn's multiple post-hoc comparisons; PV vs SST, p>0.9999; PV vs VIP, p=0.0064; SST vs VIP, p<0.0001). **(I)** Normalising by the size of each interneuron population, PV interneurons had the greatest effect upon the total ED activity (shown in **Figure 3.4***I*) ($F_{(2,31)}$=21.03, p<0.0001, one-way ANOVA, followed by post-hoc Bonferroni's multiple comparisons tests; PV vs SST, p=0.0002; PV vs VIP, p<0.0001; SST vs VIP, p=0.2808). * indicates p<0.05, ** indicates p<0.01, *** indicates p<0.001.

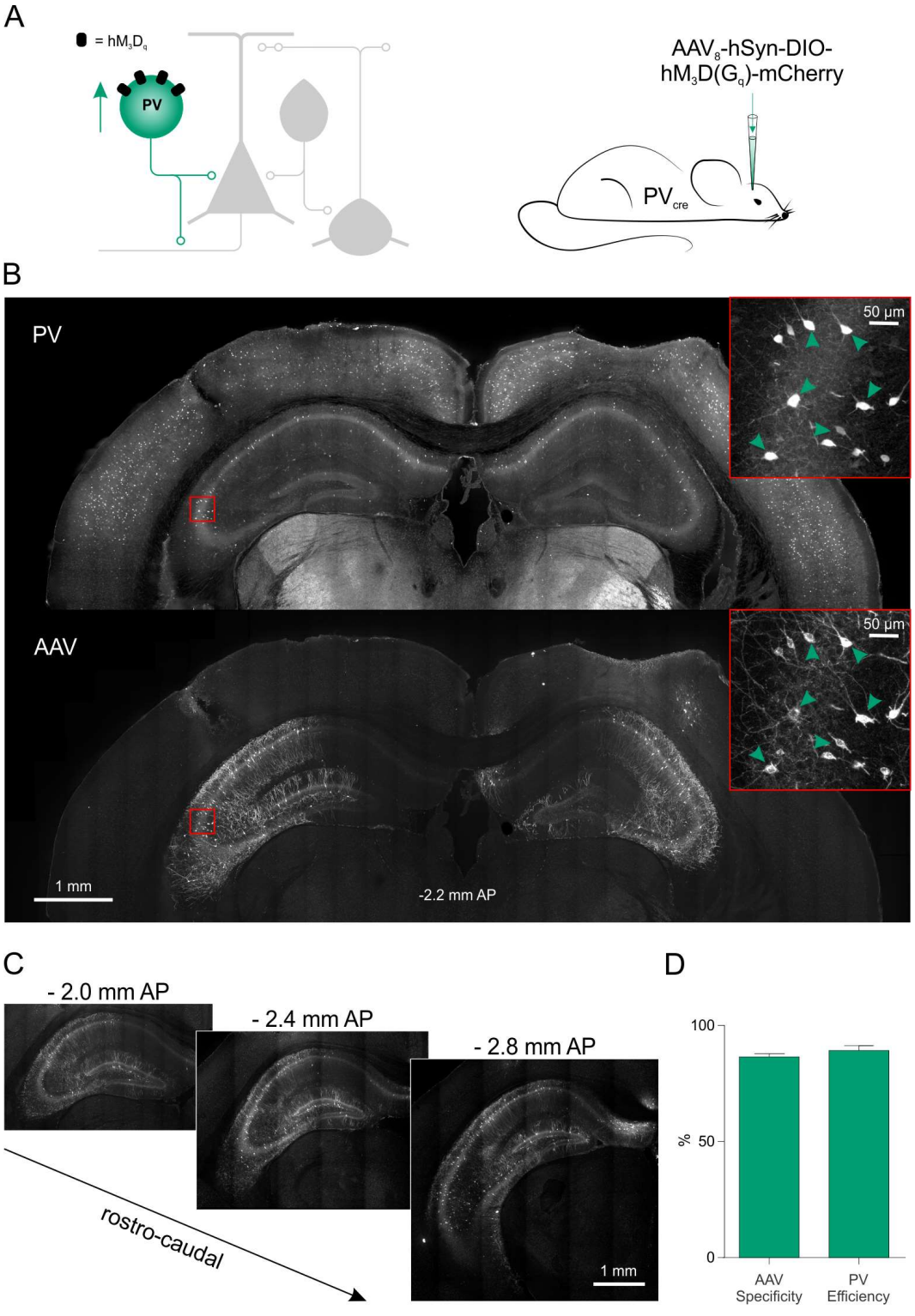

Figure 3.6. Excitatory DREADDs can be specifically and efficiently targeted to hippocampal PV interneurons *in vivo*. (A) To deliver hM_3D_q receptors to PV

(figure legend continued on facing page)

were five times greater than for an individual VIP interneuron (0.2±0.1 fold, relative to a PV interneuron; **Figure 3.5***H*). Second, I normalised the effects upon total ED activity by the number of hM_3D_q-expressing cells. Individual PV interneurons were associated with the greatest reduction in epileptiform activity (1.0±0.2 fold, relative to a PV interneuron), which was at least five times more than an individual SST interneuron (0.2±0.04 fold, relative to a PV interneuron) or VIP interneuron (-0.1±0.1 fold, relative to a PV interneuron; **Figure 3.5***I*). These observations are consistent with previous evidence showing that individual PV interneurons can mediate effective inhibition of pyramidal neurons due to their peri-somatic targeting and extensive axonal arbours (Freund and Buzsáki, 1996; Miles et al., 1996).

3.5 Chemogenetic recruitment of PV interneurons attenuates seizure activity *in vivo*

I next assessed the potential of this chemogenetic strategy to reduce seizure activity *in vivo*. Given my findings *in vitro*, the PV interneurons were selected as an effective cell population to target. The hM_3D_q receptor was delivered to PV hippocampal interneurons by bilateral injections of AAV_8-hSyn-DIO-hM_3D_q-

---

interneurons *in vivo* (left), PV-cre mice received bilaterally injections of AAV_8-hSyn-DIO-hM_3D_q-mCherry into the ventral and dorsal hippocampus (right). **(B)** Immunohistochemical characterisation confirmed that hippocampal PV interneurons ('PV', top) were efficiently transduced with hM_3D_q-mCherry ('AAV', bottom). Insets in red squares indicate cells co-expressing PV and hM_3D_q-mCherry (arrow heads). **(C)** Serial sections illustrate extensive AAV spread and hM_3D_q-mCherry expression throughout the hippocampus. AP, anteroposterior. **(D)** Population data showing high targeting specificity and efficiency of the hM_3D_q-mCherry expression in PV interneurons (N=7 animals).

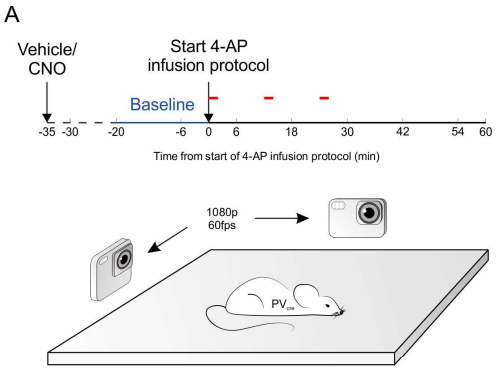

B

Racine stage	Behaviours
1	Orofacial clonic activity
2	Head nodding
3	Limb clonic activity
4	Retreating/rearing with orofacial clonic activity
5	Rearing and falling and/or jumping

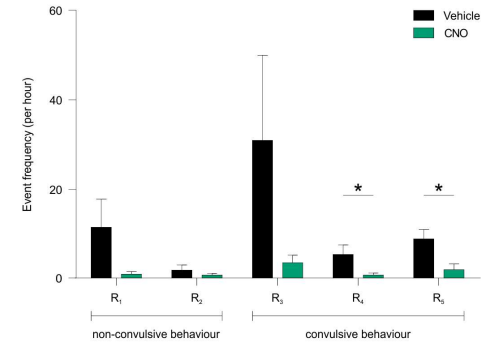

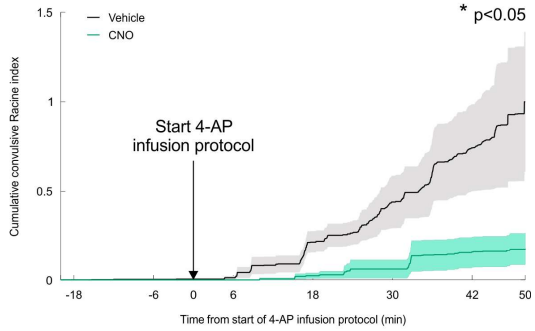

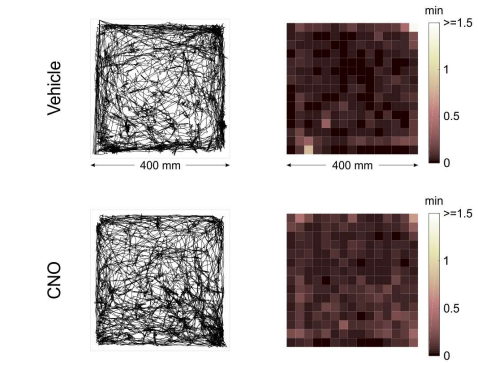

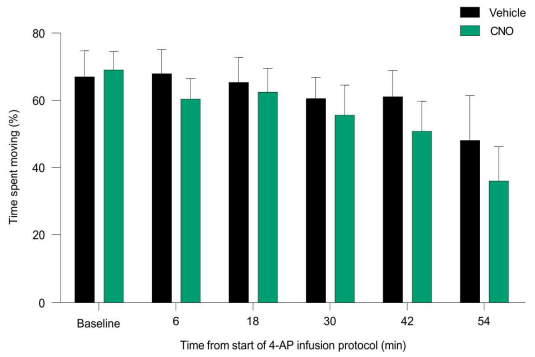

Figure 3.7. Chemogenetic recruitment of hippocampal PV interneurons suppresses convulsive behaviours *in vivo*. (A) Cartoon showing experimental design for assessing seizure activity in animals expressing the hM_3D_q receptor in hippocampal PV interneurons. Fifteen min before behavioural monitoring, each animal received an i.p. injection of either vehicle control or CNO. Baseline behaviour was then monitored for 20 min (blue period), after which the intra-hippocampal 4-AP infusion protocol was started and monitoring continued for a period of 60 min (red bars indicate the timing of each infusion). Behaviour was recorded by two high-speed, high-definition cameras oriented at right angles to one another, while a third camera tracked the animal from above. **(B)** Table describing

(figure legend continued on facing page) ⟶

mCherry in the hippocampus of 4-to-14-month-old PV-cre mice (**Figure 3.6***A*). The virus was delivered at multiple depths in the ventral and dorsal hippocampus, which resulted in extensive expression of the hM_3D_q receptor across the rostro-caudal axis (**Figure 3.6***B,C*). The majority of all virally-transduced neurons were immunopositive for PV (86.42±1.43% specificity) and the majority of PV immunopositive neurons expressed hM_3D_q-mCherry (89.17±2.12% efficiency; **Figure 3.6***D*).

The final aim of this chapter was to investigate the effect of activating PV interneurons on seizure activity *in vivo*. Here, I triggered acute seizures by local application of the potassium channel blocker 4-AP to one of the hippocampi, which allows for a controlled focal induction of seizure activity (Salam et al., 2017). Local application of 4-AP likely disrupted the activity of both pyramidal cells and

---

the Racine scale used to score the animal's seizure behaviour from video analysis offline. **(C)** There was a general tendency for seizure behaviours to be supressed by CNO across the Racine categories. The frequency of Racine 4 and 5 convulsive events was significantly reduced when CNO was administered compared to vehicle (N=12 vehicle and 10 CNO experiments; Racine 1: $U_{(12,10)}$=34, p=0.0571; Racine 2: $U_{(12,10)}$=59.5, p>0.9999; Racine 3: $U_{(12,10)}$=37, p=0.1335; Racine 4: $U_{(12,10)}$=31, p=0.0372; Racine 5: $U_{(12,10)}$=24.5, p=0.0127, two-tailed Mann–Whitney tests). **(D)** Convulsive behaviour, plotted as a normalised cumulative score was significantly lower following administration of CNO compared to vehicle (N=12 vehicle and 10 CNO experiments, $U_{(12,10)}$=29.5, p=0.0411, two-tailed Mann–Whitney test). **(E)** For mice expressing the hM_3D_q receptor in hippocampal PV interneurons, plots illustrate tracking data and corresponding spatial distribution of time spent across the behavioural arena (400 mm x 400 mm). Representative data are shown for an animal receiving an i.p. injection of vehicle (top) or CNO (bottom). In each case, data is shown for a 20-min period following the start of the 4-AP infusion protocol. **(F)** There was no difference between the vehicle and CNO groups in terms of the percentage of time spent moving (N=10 vehicle and 11 CNO experiments, treatment: $F_{(1,104)}$=1.686, p=0.197, two-way ANOVA).

interneurons in a limited brain area and thus generated focal seizures at the injection site, which then spread leading to generalised convulsions. This resembles the clinical situation where focal seizures are initiated in an area of limited abnormal brain tissue from where they propagate through normal brain networks. Such models of acutely triggered focal seizures have been important in the development of anti-seizure drugs (Kupferberg, 2001) and allow for investigating seizure spread regardless of the initial cause of seizure initiation. Animals were randomised to receive an i.p. injection of either CNO or vehicle in their first experiment, and then alternated between CNO and vehicle for subsequent experiments. Each i.p. injection was delivered 15 min before the animal was placed in an arena, and their freely moving behaviour was monitored for a period of 80 min using high-speed, high-definition cameras (**Figure 3.7***A*). Following a 20-min baseline period, 4-AP was infused directly into the hippocampus according to a spaced delivery protocol (three 4-AP infusions, each separated by 12 min; see Materials and Methods).

To provide a detailed description of seizure activity and seizure spread, each animal's behaviour was scored blindly using the five-point Racine scale (**Figure 3.7***B*), at a sampling frequency of 1 Hz across at least 70 min per experiment (see Materials and Methods). These analyses revealed that CNO-mediated recruitment of hippocampal PV interneurons caused a reduction in the frequency of convulsive behaviours across the Racine 4 and 5 categories (**Figure 3.7***C*). To characterise the temporal nature of these effects, the Racine scoring scale was used to generate an integrated measure of convulsive behaviour that could be tracked over time (see Materials and Methods, thesis section 2.7). This integrated measure revealed that

CNO-mediated recruitment of hippocampal PV interneurons reduced the occurrence of all convulsive behaviours by more than 80% compared to controls (**Figure 3.7***D*). By contrast, CNO did not have any effect on non-convulsive focal seizure activity (Racine 1-3). Taken together, these results are consistent with the idea that increasing PV activity beyond the area affected by 4-AP reduced seizure spread and propagation. CNO has been shown to metabolise to clozapine, which passes the blood-brain-barrier *in vivo* (Gomez et al., 2017; Manvich et al., 2018), and locomotor activity has been shown to be affected by clozapine (McOmish et al., 2012; Ilg et al., 2018). To assess whether the reduction in convulsive seizures was associated with non-specific effects upon behaviour possibly mediated by clozapine, I monitored the animals' locomotor activity throughout the experiment. The distribution of time spent throughout the arena was indistinguishable between the vehicle and CNO-treated groups (**Figure 3.7***E,F*), supporting the conclusion that the CNO-mediated reduction in convulsive seizures was not associated with a non-specific effect upon locomotor activity. In summary, my results suggest that chemogenetic recruitment of PV interneurons is effective at supressing the spread of convulsive seizure activity *in vivo*.

3.6 Discussion

In this chapter I have used a combination of *in vitro* and *in vivo* studies in rodent models to demonstrate that chemogenetic enhancement of distinct populations of GABAergic interneurons can robustly reduce seizure activity. Targeted whole-cell recordings from both presynaptic interneurons and postsynaptic principal neurons revealed that PV, SST and VIP interneuron populations all increased their firing

rate and synaptic output following CNO-mediated activation of hM_3D_q DREADD receptors. Chemogenetic enhancement of either the PV or SST interneurons decreased drug-resistant synchronised epileptiform activity *in vitro*, through a reduction in the frequency of EDs. By contrast, enhancing VIP interneuron activity did not reduce total epileptiform activity. When accounting for the relative density of cells, PV interneurons generated the strongest effect per cell in terms of their ability to suppress EDs. Finally, to confirm the potential of such an intervention strategy, chemogenetic activation of PV interneurons was shown to produce a five-fold reduction in convulsive behaviours in an *in vivo* model of temporal lobe seizures.

$GABA_AR$ positive allosteric modulators such as benzodiazepines and phenobarbital have previously been shown to be ineffective in suppressing EDs in organotypic slices, while $GABA_A$ agonists demonstrated mixed efficiency against EDs (Albus et al., 2008; Wahab et al., 2009). Investigating the effect of GABAergic drugs is important in determining the efficacy of enhancing the overall GABAergic activity. However, given the non-specific action of such drugs, for example also inhibiting interneurons that express $GABA_ARs$, my study focused on exploring the potential to selectively enhance synaptic inhibition from specific interneuron subtypes.

Previous work has shown that targeting pyramidal neurons with inhibitory DREADDs can mitigate seizure activity (Kätzel et al., 2014; Avaliani et al., 2016). My study extends this by demonstrating that, although they make up a relatively small proportion of the network, chemogenetically recruiting GABAergic

populations can mediate robust anti-seizure effects. Enhancing such endogenous inhibitory mechanisms may represent an attractive intervention strategy, as interneurons can exert widespread effects on the tissue and inhibitory circuits are recruited as excitatory network activity intensifies (Trevelyan et al., 2006; Derchansky et al., 2008; Schevon et al., 2012; Cammarota et al., 2013). However, given their diversity, the particular interneuron population that is targeted is likely to be important. In line with this prediction, my data show that chemogenetic enhancement of VIP interneurons did not reduce overall ED activity, and in fact increased the duration of individual EDs. This is in accordance with observations that the preferential postsynaptic targets of VIP interneurons are other GABAergic interneurons (Acsády et al., 1996), and that activating VIP interneurons may prevent downstream GABAergic interneurons from counteracting seizure-related excitation, since VIP interneurons specialise in disinhibitory control (Lee et al., 2013; Pi et al., 2013). In addition, it is possible that the activation of VIP interneurons leads to direct VIP release, which could increase excitability by enhancing NMDA receptor responses and excitatory transmission (Cunha-Reis et al., 2005; Yang et al., 2009). Consistent with these ideas, optically inhibiting VIP interneuron activity has been shown to generate anti-seizure effects (Khoshkhoo et al., 2017). In the context of structural changes that occur as a result of seizure activity, VIP interneurons of the hippocampus were reported to survive in experimental epilepsy (Sloviter, 1987). Future studies could investigate VIP interneuron function in chronic epilepsy, and test whether targeting VIP interneurons with inhibitory DREADDs can attenuate epileptiform activity.

By comparison, PV and SST interneurons have been shown to preferentially target principal neurons. PV interneurons comprise mainly basket cells and axo-axonic cells, which synapse on the soma and axon-initial segment of pyramidal neurons (Klausberger et al., 2003). The dense axonal branching of PV interneurons is therefore restricted to the pyramidal layer, but exhibits a broad transverse extent (~1 mm in rodent hippocampus). This can generate widespread synaptic inhibition, with each cell targeting around 1500-2000 pyramidal neurons (Freund and Buzsáki, 1996). SST interneurons meanwhile, mainly synapse on the dendrites of pyramidal neurons (Katona et al., 1999), where they regulate dendritic activation (Miles et al., 1996) and may account for as much as half of the firing rate increase following complete removal of inhibition (Lovett-Barron et al., 2012). In addition, SST interneurons can directly release SST when activated, which in turn can reduce neuronal excitability by acting via G-protein coupled receptors (Tallent and Qiu, 2008).

Activating hM_3D_q receptors at single cell level resulted in increased spiking activity, in the absence of pronounced somatic depolarisation (**Figure 3.2***D*, **Figure 3.3***D,H*). The mechanism of action for hM_3D_q receptors was proposed to be downregulation of the function of K^+ channels involved in generating the M-current (Alexander et al., 2009). These K^+ channels are concentrated at the axon initial segment (Pan et al., 2006). It is therefore likely that the increase in spiking observed at single cell level in my preparation was caused by antidromically propagated action potentials from the axon initial segment. This spiking behaviour could not be caused by excitatory input to interneurons, since brain slices were bathed in

aCSF containing kynurenic acid, to avoid ED activity. The enhanced subthreshold membrane potential noise detected after CNO application in the current-clamp recordings investigating the hM_3D_q-mediated cellular effects (**Figure 3.2***D*, **Figure 3.3***D,H*) may have been contributed to by inhibitory input from other activated interneurons, especially since interneurons are known to establish reciprocal connections. This could also potentially explain the lack of somatic depolarisation. The putative augment in inhibitory synaptic inputs, coupled with the possibility that intracellular mediators were dialysed by whole-cell patching, may account for the subtle increase in spiking activity recorded at single cell level in interneurons, compared to the robust increase in postsynaptic inhibitory currents measured in pyramidal neurons (**Figure 3.5**). Cell-attached recordings with blockers of both GABAergic and glutamatergic transmission may constitute a better experimental strategy to record the hM_3D_q-mediated cellular effects on spiking activity.

In my experiments, DREADD activation of either PV or SST interneurons resulted in pronounced increases in spike-evoked, postsynaptic inhibitory currents in pyramidal neurons and strong attenuation of spontaneous EDs. For both cell types, I observed a ~50% reduction in the total ED activity, which was driven by a decrease in the probability of ED initiation. It has been shown that relevant concentrations of CNO can lead to competitive binding of some endogenous receptors (Gomez et al., 2017). However, my control experiments show that CNO did not affect epileptiform activity in the absence of DREADD expression. Therefore, my data supports the conclusion that the anti-seizure effects are mediated by the chemogenetic activation of the interneurons and are not an artefact

of CNO off-target activity. Potential long-term drifts in network activity might influence ED measurements, but ED activity appeared to be stable in my preparation (**Figure 3.1***A,B*). An additional way to account for possible drifts in network activity would be to randomise experiments to begin with either a control or drug temporal window. However, hM_3D_q receptor activation results in long-lasting effects *in vivo* even after CNO or clozapine are removed from plasma (Alexander et al., 2009). Indeed, in a subset of voltage-clamp experiments in which I investigated the postsynaptic effects of activating hM_3D_q receptors (**Figure 3.5**), the CNO-triggered effect persisted even after 30 min following the wash out of CNO. Therefore, examining network activity during CNO wash out would be complicated by the timing of the offset of hM_3D_q receptor activation.

At the population level, enhancing SST interneurons generated the largest postsynaptic inhibitory currents in pyramidal neurons. Although when adjusted for cell numbers, I estimated that individual PV interneurons elicited equivalent postsynaptic inhibitory currents and a five-fold greater attenuation of ED activity. These observations are consistent with evidence that GABAergic inputs to the axo-somatic region can exert particularly powerful inhibitory effects (Cobb et al., 1995) and that PV interneurons contribute significantly to a synaptic restraint that can oppose the initiation and propagation of seizure activity (Cammarota et al., 2013; Paz and Huguenard, 2015a). In the context of epilepsy, the targeting of PV interneurons may also be more preferable because there are reports that SST interneurons become depleted (Robbins et al., 1991), whereas PV interneurons

survive in epileptic animals (Sloviter, 1991; Sloviter et al., 2003) and epilepsy patients (Sloviter et al., 1991).

In agreement with these ideas and my *in vitro* results, I demonstrate that excitatory DREADDs in PV interneurons can generate potent anticonvulsant effects *in vivo*. Direct application of 4-AP to one hippocampus likely generated initial focal seizure activity by blocking K^+ conductances and altering the activity of both pyramidal and inhibitory neurons within local networks (Gustafsson et al., 1982; Segal, 1987; Storm, 1988; Martina et al., 1998). Under control conditions, these focal seizures spread and progressed to full convulsions (Racine 5). However, chemogenetically increasing the activity of PV interneurons prevented the propagation, as reflected by an 80% reduction in convulsive behaviour. It has recently been shown that CNO does not cross the blood brain barrier in naive rats, but is rather metabolised to clozapine that can cross the blood brain barrier and activate DREADDs directly (Gomez et al., 2017). It therefore seems likely that the CNO-mediated effects in my *in vivo* studies involved the metabolism of CNO to clozapine, although seizure-related activity could influence the permeability of the blood brain barrier and the relative contribution of CNO (Vliet et al., 2007). Although unlikely, there is a possibility that seizure activity can be affected directly by CNO or clozapine. To test this, future experiments could assess the effect of administering CNO or clozapine to mice that do not express hM_3D_q receptors. Clozapine is known to affect locomotion (McOmish et al., 2012). However, I did not detect any change in locomotor activity, potentially due to low levels of *in vivo* metabolism of CNO to clozapine. The hippocampus is known to support learning

and memory (Teyler and DiScenna, 1985; Bennett et al., 1994). Therefore, it would be interesting to assess if the CNO-mediated manipulation of PV interneurons in the hippocampus has any impact on working memory. Future studies could also test the potential to enhance DREADD activity in interneurons by direct clozapine administration. Indeed, clozapine is already approved as a drug for use in humans and DREADD activation requires very low concentrations of clozapine (Gomez et al., 2017), which may make it an attractive option for translational studies.

At the time of submission of my thesis, a report was just published that showed that PV interneuron chemogenetic activation in a chronic model of epilepsy was also effective (Wang et al., 2018). The same study shows that chemogenetic inactivation of excitatory neurons resulted in impaired cognitive function. This indicates that chronic enhancement of interneuron activity would seem to be the more promising strategy for controlling seizure activity compared to direct silencing of excitatory neurons, which might have more serious side effects, for example on memory processes. The suppression of focally-evoked seizures *in vivo* in the current study complements my results from the *in vitro* drug-resistant model of epilepsy, demonstrating efficacy across both acute and chronic models of seizure activity. More generally, my data confirms that chemogenetically enhancing a specific interneuron population can produce effective suppression of epileptiform activity.

Chapter 4: Monitoring pH and Cl^- concentration dynamics in specific GABAergic interneuron subtypes

4.1 Introduction

In the previous chapter I described the potential of recruiting different interneuron subtypes via excitatory DREADDs. In this chapter, using the same *in vitro* model of temporal lobe epilepsy, I will investigate the ionic changes that transiently occur in different cell types during epileptiform events, specifically changes in intracellular pH and Cl^-.

Protons are essential for cell function since pH fundamentally controls the stability of many cellular processes, including protein structure and function, enzymatic processes, transmembrane conductances, migration and proliferation. In addition, protons play an essential role in cell metabolism, specifically in the synthesis of adenosine triphosphate (ATP), the so-called 'molecular currency' of intracellular energy transfer (Drapeau and Nachshen, 1988; Denker and Barber, 2002; Putney and Barber, 2003; Abad et al., 2004; Srivastava et al., 2007). At the same time, Cl^- ions are also crucial for optimal neuronal function by controlling a variety of processes. These include fast synaptic inhibition via the Cl^--permeable $GABA_A$Rs, synaptic vesicle filling, neurotransmitter uptake and neurite growth (Kaila and Voipio, 1987; Chen et al., 2004; Faundez and Hartzell, 2004; Nakajima and Marunaka, 2016; Chang et al., 2018b).

Pyramidal neurons have been previously reported to acidify and load Cl^- during epileptiform events (Raimondo et al., 2013). However, these ionic states

have not yet been studied in the various GABAergic interneuron populations. Intracellular H^+ and Cl^- concentrations were identified to influence neuronal excitability and synaptic transmission (Drapeau and Nachshen, 1988; Tabb et al., 1992; Rivera et al., 2004; Kaila et al., 2014). In the context of epileptiform events, both pH and Cl^- dynamics have been shown to play a role in the development of this aberrant network activity within pyramidal cells (Xiong et al., 2000; Alfonsa et al., 2015). However, it is unknown how these ion dynamics influence the role GABAergic interneurons play during hypersynchronous hyperexcitable network states.

The first aim of this chapter was to construct a genetically-encoded probe that can be targeted to specific neuronal populations and report absolute intracellular pH and Cl^- concentration. To this end, a new plasmid containing a fluorescent reporter was generated. This reporter is a floxed version of ClopHensorN (Raimondo et al., 2013), which enables the targeting of genetically-defined cell types in a cre-dependent manner. The second aim of this chapter was to investigate the resting states of intracellular pH and Cl^- concentration in pyramidal neurons and PV, SST and VIP interneurons of the hippocampus. To this end, the probe was first calibrated under controlled pH and Cl^- concentration conditions. To measure the absolute intracellular pH and Cl^- concentration in distinct neuronal populations, the floxed ClopHensorN was delivered to hippocampi from mice expressing cre recombinase in specific cell types. The third and final aim of this chapter was to study the temporal dynamics of the intracellular pH and Cl^- concentration in pyramidal neurons and PV, SST and VIP interneurons

during EDs. To this end, the membrane potential of pyramidal neurons was first shown to faithfully reflect network activity and the recruitment of each interneuron subtype during EDs. This permitted the imaging of specific cell types expressing ClopHensorN, while the electrical activity of the network was concurrently monitored from nearby pyramidal neurons. Confocal and electrophysiological data were synchronised and EDs were quantified to study the relationship between these ion dynamics and various properties of EDs.

4.2 A cre recombinase dependent ClopHensorN can be used to target genetically-defined cell types

Multiple proton- or Cl^--sensitive dyes and genetic biosensors are available to measure changes in pH and Cl^- optically. Genetically encoded Cl^- reporters such as 'Clomeleon' (Kuner and Augustine, 2000; Grimley et al., 2013) and 'Cl-sensor' (Markova et al., 2008) are fusion proteins containing the yellow fluorescent protein (YFP), combined with the relatively Cl^--insensitive cyan fluorescent protein (CFP). In contrast to CFP, YFP is quenched by Cl^-, which allows the linked YFP-CFP protein to be used as a ratiometric indicator. However, such fluorescent reporters are also sensitive to pH, such that any changes or cell differences in pH can be mistakenly interpreted as changes or differences in Cl^-.

The development of ClopHensor (Arosio et al., 2010) enabled simultaneous ratiometric pH and Cl^- measurements. ClopHensor is a fusion of the pH and Cl^- sensitive E^2GFP with DsRed, which is insensitive to both pH and Cl^-. By taking advantage of the pH isosbestic point in the excitation spectrum of E^2GFP, the proton concentration can be measured independently of Cl^-. However, ClopHensor has

been reported to form aggregates when expressed in mammalian neurons (Raimondo et al., 2013), which has precluded its use as a ratiometric reporter in the nervous system. Raimondo et al. (2013) recently resolved this problem by developing ClopHensorN: a new fusion protein linking E^2GFP to tandem dimer tomato (tdTomato), which is effectively expressed in mammalian neurons and has afforded the functional dissociation of intracellular pH and Cl^- concentration measurements in neurons (Raimondo et al., 2013; Martineau et al., 2017).

To selectively express ClopHensorN within genetically-defined neuronal populations, I made use of the cre-lox system to design a floxed version of ClopHensorN (**Figure 4.1***A*). The novel construct expresses under the control of the EF-1α promoter, and employs the WPRE and a polyA sequence (**Figure 4.1***A*). The floxed ClopHensorN sequence is inverted in the presence of the enzyme cre recombinase, allowing the expression of the ratiometric probe. This enabled me to target ClopHensorN to distinct neuronal populations of the hippocampus via AAV viral vectors by delivering AAV8-EF-1α-FLEX-ClopHensorN-WPRE into brain slices expressing cre recombinase under the control of different promoters. After 1-4 weeks post viral transduction, expressing neurons were visualised under a confocal laser scanning microscope, while the electrical activity of the neuronal network was continuously monitored using whole-cell current-clamp recordings (**Figure 4.1***B*).

Pyramidal neurons were targeted by transducing brain slices from CamK2a-cre mice, resulting in a pattern of ClopHensorN expression typical for excitatory neurons along the pyramidal layer of the hippocampus (**Figure 4.1***C*). Neurons

showed robust expression, and both tdTomato and E^2GFP expression was detected (**Figure 4.1***D*). PV interneurons were targeted by transducing brain slices from PV-cre mice, resulting in ClopHensorN expression within soma and processes restricted to the pyramidal cell layer (**Figure 4.1***E,F*). SST interneurons were targeted by transducing brain slices from SST-cre mice, generating ClopHensorN expression in the soma and processes located within stratum oriens and lacunosum-moleculare (**Figure 4.1***G,H*). VIP interneurons were targeted by transducing brain slices from VIP-cre mice, resulting in ClopHensorN expression within the soma and processes located in stratum radiatum, lacunosum-moleculare, pyramidale and oriens (**Figure 4.1***I,J*).

4.3 Calibrating the floxed ClopHensorN enables imaging of intracellular pH and Cl^- concentration

ClopHensorN showed robust expression in hippocampal neurons following viral transduction, as demonstrated in **Figure 4.1**, and was used as a ratiometric indicator of pH and Cl^- concentration. To this end, ClopHensorN was excited sequentially at 561 nm, 458 nm and 488 nm using a confocal laser scanning microscope. Emitted fluorescence was collected by one PMT in the 635-700 nm range during excitation at 561 nm, and by a different PMT in the 500-550 nm range during 458 nm and 488 nm excitation. Calibration was achieved by systematically changing the pH and Cl^- concentration in the extracellular environment, in the presence of the proton and Cl^- permeable ionophores (nigericin, tributyltin chloride and chloride ionophore 1) that collapsed the transmembrane concentration gradients for the two ion species (see Materials and Methods, thesis section 2.11). The pH ratio – the ratio of emitted

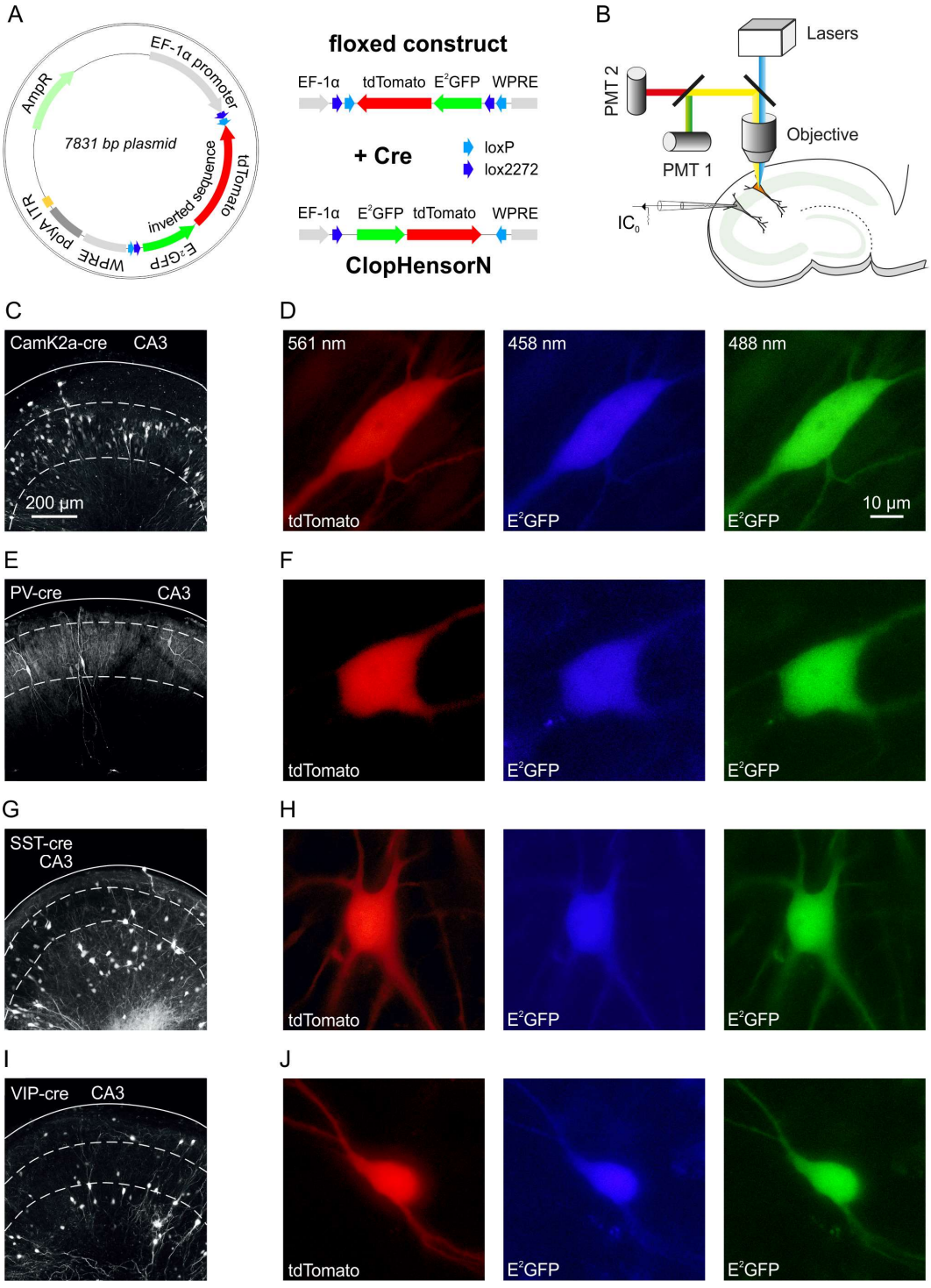

Figure 4.1. A novel pH and Cl⁻ genetically-encoded fluorescent reporter can be targeted to specific GABAergic interneuron populations. (A) A map of the ClopHensorN plasmid containing the inverted genetic sequence for the E²GFP-tdTomato fusion protein flanked by loxP and lox2272 sites. The construct includes

(figure legend continued on facing page) ——————►

fluorescence from the E^2GFP protein when excited sequentially at 458 nm and 488 nm (F_{488}/F_{458}) – was found to depend on intracellular pH with a pK_a of 7.14 (**Figure 4.2***A*). The fluorescence of the tdTomato protein is insensitive to pH or Cl^- concentration variations. By contrast, when excited at 458 nm – the pH isosbestic point in the excitation spectrum of E^2GFP – the emitted fluorescence from E^2GFP is insensitive to pH, but depends on the Cl^- concentration. Thus, the Cl^- ratio – the ratio of emitted fluorescence from the tdTomato and E^2GFP proteins when excited sequentially at 561 nm and 458 nm, respectively (F_{458}/F_{561}) – was

---

an elongation factor 1α (EF-1α) promoter, WPRE, polyA, ITR and the AmpR gene. The cre recombinase enzyme catalyses the recombination of the floxed ClopHensorN sequence, which allows the transcription of the fluorescent reporter. **(B)** A cartoon of the experimental setup in which a confocal laser scanning microscope, operating a 561 nm diode-pumped solid-state laser and a 458 nm and 488 nm argon laser, was used to image neurons expressing ClopHensorN. Electrophysiological data was synchronously acquired via patch-clamp recordings in current-clamp (IC_0) mode. Illustration was modified from Raimondo et al. (2013). **(C)** Confocal image of a brain slice from a CamK2a-cre mouse illustrates the fluorescence pattern of virally-transduced pyramidal neurons expressing ClopHensorN. The continuous white line marks the edge of the hippocampus, and the pyramidal layer is delineated with dashed white lines. **(D)** Confocal images of a pyramidal neuron expressing ClopHensorN. The tdTomato protein was imaged using the 561 nm laser, and the fluorescence emission was collected between 635 and 700 nm (left). The E^2GFP protein was imaged using the 458 nm (middle) and 488 nm (right) lasers, and the fluorescence emission in both cases was collected between 500 and 550 nm. **(E)** Confocal image of a brain slice from a PV-cre mouse illustrates the fluorescence pattern of virally-transduced PV interneurons expressing ClopHensorN. **(F)** Confocal images of a PV interneuron expressing ClopHensorN (as shown in 'D'). **(G)** Confocal image of a brain slice from a SST-cre mouse illustrates the fluorescence pattern of virally-transduced SST interneurons expressing ClopHensorN. **(H)** Confocal images of a SST interneuron expressing ClopHensorN (as shown in 'D'). **(I)** Confocal image of a brain slice from a VIP-cre mouse illustrates the fluorescence pattern of virally-transduced VIP interneurons expressing ClopHensorN. **(J)** Confocal images of a VIP interneuron expressing ClopHensorN (as shown in 'D').

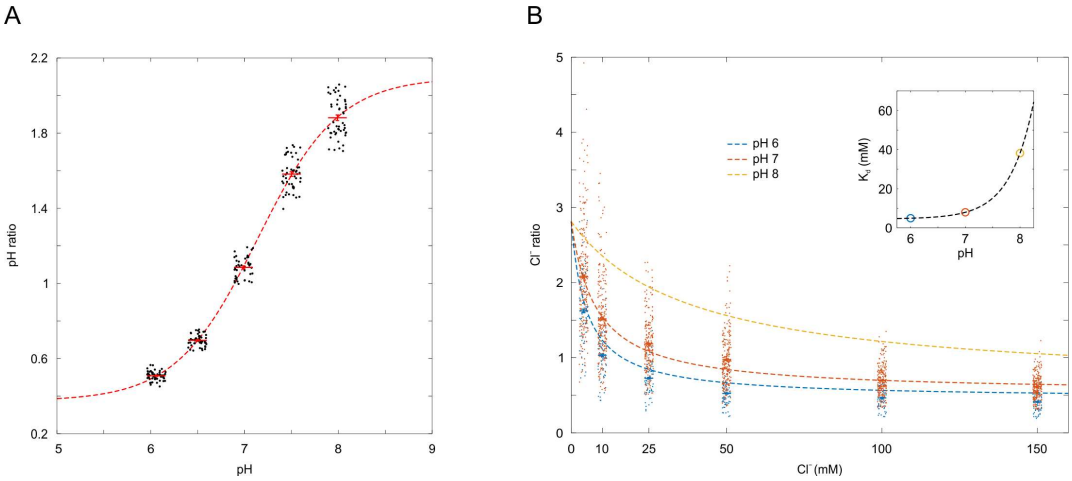

Figure 4.2. ClopHensorN pH and Cl^- calibration. (A) Calibration curve relating the pH sensitive fluorescence ratio (F_{488}/F_{458}) of cells expressing ClopHensorN to their intracellular pH. To measure the pH ratio, ClopHensorN was excited sequentially at two wavelengths (458 nm and 488 nm), and emission was collected in the same 500-550 nm window. Intracellular pH was systematically varied by controlling the extracellular pH in the presence of a proton-permeable ionophore. Data was fit using established equations (Grynkiewicz et al., 1985; Raimondo et al., 2013), and pK_a was found to be 7.14 with a 7.1-7.17 95% confidence interval. **(B)** Calibration curve relating the Cl^- sensitive fluorescence ratio (F_{458}/F_{561}) of cells expressing ClopHensorN to their intracellular Cl^- concentration. To measure the Cl^- ratio, ClopHensorN was excited sequentially at two wavelengths (458 nm and 561 nm), and emission was collected between 500-550 nm and 635-700 nm, respectively. Intracellular Cl^- was manipulated by changing the extracellular Cl^- in the presence of Cl^--permeable ionophores. Data was fit using established equations (as in 'A'), and K_d was found to be 4.95 mM at pH 6, 7.97 mM at pH 7, and 38.21 mM at pH 8.

shown to depend on the intracellular Cl^- concentration with an average K_d of 12.29 mM around the physiological 7.2-7.5 intracellular pH range (**Figure 4.2***B*).

In summary, the pH and Cl^- ratios shown in **Figure 4.2** allowed the independent and simultaneous measurement of absolute intracellular pH and Cl^- concentration, regardless of the amount of expression of the ratiometric probe in different cells. This enabled the quantification of steady-states and temporal dynamics of the intracellular pH and Cl^- concentration in distinct neuronal populations during network events.

4.4 Resting intracellular pH and Cl^- concentration differ between cell types

To investigate the steady-state pH and Cl^- concentration in distinct neuronal populations of the hippocampus, I delivered ClopHensorN to specific cell types by virally transducing brain slices from mice expressing cre recombinase under the control of different promoters (CamK2a, PV, SST and VIP) with AAV8-EF-1α-FLEX-ClopHensorN-WPRE. After 1-4 weeks post transduction, I examined brain slices under a confocal laser scanning microscope and selected individual ClopHensorN-expressing cells for imaging experiments.

Concurrently to imaging the neurons, I performed whole-cell patch-clamp recordings. This was done to confirm that measurements of resting ion concentration were made during periods in which the network was relatively quiescent. My measurements of resting intracellular pH and Cl^- concentration in hippocampal pyramidal neurons are consistent with rat measurements by

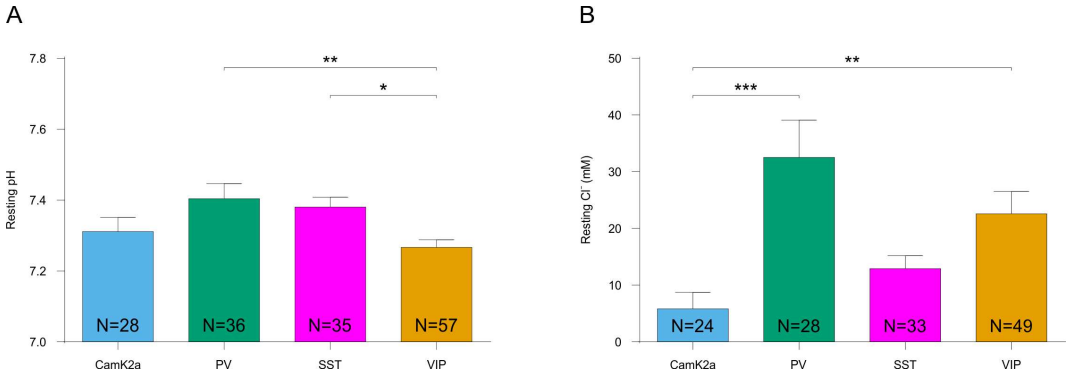

Figure 4.3. Distinct cell types have different intracellular resting pH and Cl^- concentration. (A) VIP interneurons were found to have the most acidic resting intracellular somatic environment compared to other interneuron subtypes ($\chi^2_{(3)}$=13.5, p=0.0037, Kruskal-Wallis test, followed by post-hoc Dunn's multiple comparisons tests; CamK2a vs PV, p=0.8379; CamK2a vs SST, p=0.3609; CamK2a vs VIP, p>0.9999; PV vs SST, p>0.9999; PV vs VIP, p=0.0354; SST vs VIP, p=0.0078). **(B)** PV interneurons were found to have the highest intracellular somatic Cl^- concentration ($\chi^2_{(3)}$=19.56, p=0.0002, Kruskal-Wallis test, followed by post-hoc Dunn's multiple comparisons tests; CamK2a vs PV, p=0.0001; CamK2a vs SST, p=0.1099; CamK2a vs VIP, p=0.0046; PV vs SST, p=0.1817; PV vs VIP, p=0.8356; SST vs VIP, p>0.999). * indicates p<0.05, ** indicates p<0.01, *** indicates p<0.001.

Raimondo et al. (2013). In my experiments, pyramidal cells had an intracellular pH of 7.31±0.04 and a mean resting intracellular Cl^- concentration of 5.8±2.9 mM. In addition to pyramidal neurons, I found that the resting intracellular pH was different between distinct interneuron populations, with VIP interneurons having the lowest somatic pH under baseline conditions (**Figure 4.3***A*). The average resting intracellular pH was 7.4±0.04 for PV interneurons, 7.38±0.03 for SST interneurons, and 7.27±0.02 for VIP interneurons. The intracellular Cl^- concentration was also significantly different across cell types, with PV interneurons having the highest somatic Cl^- concentration (**Figure 4.3***B*). The average resting intracellular Cl^- was 32.5±6.6 mM for PV interneurons, 12.9±2.3 mM for SST interneurons, and 22.6±4 mM for VIP interneurons.

This data demonstrates the ability of the floxed version of ClopHensorN to independently report the intracellular pH and Cl^- concentration in genetically-defined cell types of the hippocampus. The remainder of this chapter will focus on the temporal dynamics of the somatic pH and Cl^- concentration during epileptiform activity.

4.5 Temporal dynamics of intracellular pH and Cl^- concentration during epileptiform events depend on cell type

To investigate if ClopHensorN is able to detect ion dynamics exhibited by different cell types during epileptiform events, I imaged different neuron populations whilst simultaneously acquiring electrophysiological data from pyramidal neurons. I first conducted paired patch-clamp recordings to confirm the prediction that all cell

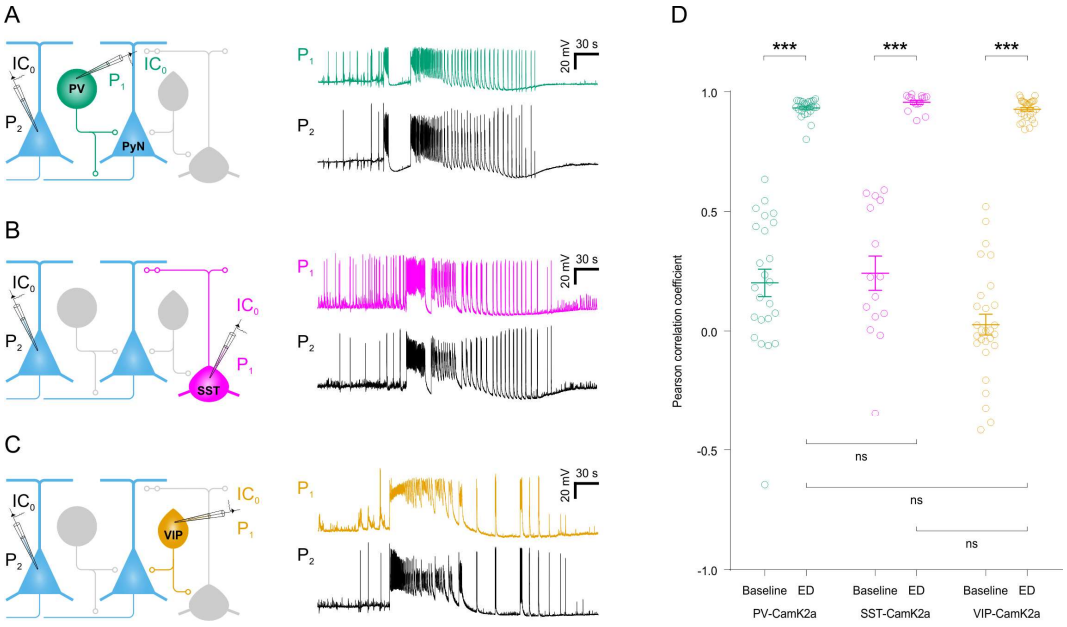

Figure 4.4. The activity of different GABAergic interneuron subtypes and pyramidal neurons is correlated during epileptiform events. (A) Cartoon of the hippocampal circuitry (left), referring to the example traces (right) recorded in current-clamp mode from a PV interneuron (top) and a pyramidal neuron (bottom) pair. **(B)** Cartoon of the hippocampal circuitry (left), referring to the example traces (right) recorded from a SST interneuron (top) and a pyramidal neuron (bottom) pair. **(C)** Cartoon of the hippocampal circuitry (left), referring to the example traces (right) recorded from a VIP interneuron (top) and a pyramidal neuron (bottom) pair. **(D)** During epileptiform events, the electrical activity of PV (N=24 EDs from 8 pairs), SST (N=15 EDs from 8 pairs) and VIP (N=28 EDs from 9 pairs) interneurons was closely related to the activity of nearby pyramidal neurons (interaction between neuron pair type and time window: $F_{(2,64)}=3.771$, $p=0.0283$, repeated measures two-way ANOVA followed by Sidak's post-hoc multiple comparisons of baseline vs ED: PV-CamK2a, $p<0.0001$; SST-CamK2a, $p<0.0001$; VIP-CamK2a, $p<0.0001$). The level of synchrony during EDs was not different across each of the different neuron pair types (Sidak's post-hoc multiple comparisons, $p>0.05$). *** indicates $p<0.001$.

types of interest are highly correlated during epileptiform activity, and that recordings from pyramidal neurons are therefore a good way to monitor the general network activity (**Figure 4.4***A,B,C*). During epileptiform events, pyramidal neurons were highly correlated with PV interneurons (Pearson's coefficient of 0.93±0.01), with SST interneurons (Pearson's coefficient of 0.96±0.01), and with VIP interneurons (Pearson's coefficient of 0.93±0.01), and the degree of synchrony during EDs was not different across the three neuron pair types (**Figure 4.4***D*).

Having confirmed the activity of the different neuron populations is correlated during epileptiform events, I combined confocal imaging of single cells expressing ClopHensorN with whole-cell patch-clamp recordings of pyramidal neurons in brain slices. This allowed me to concurrently acquire pH and Cl^- concentration measurements from the cell body of interest, whilst also closely monitoring the electrical activity of the network without perturbing the physiology of the imaged neuron (**Figure 4.5**). Epileptiform activity occurred spontaneously in the brain slices (Dyhrfjeld-Johnsen et al., 2010; Lillis et al., 2015). To investigate ion dynamics over longer ED durations, magnesium ions were transiently removed from the circulating aCSF (Gutiérrez et al., 1999) in a subset of experiments (23 EDs from pyramidal neurons, 40 EDs from PV cells, 26 EDs from SST cells, and 34 EDs from VIP cells). When analysed separately, data generated using the two models of epileptiform activity showed similar trends. Therefore, to increase statistical power, data from both models were grouped and analysed together. The electrophysiological recordings enabled me to detect the precise onset and duration

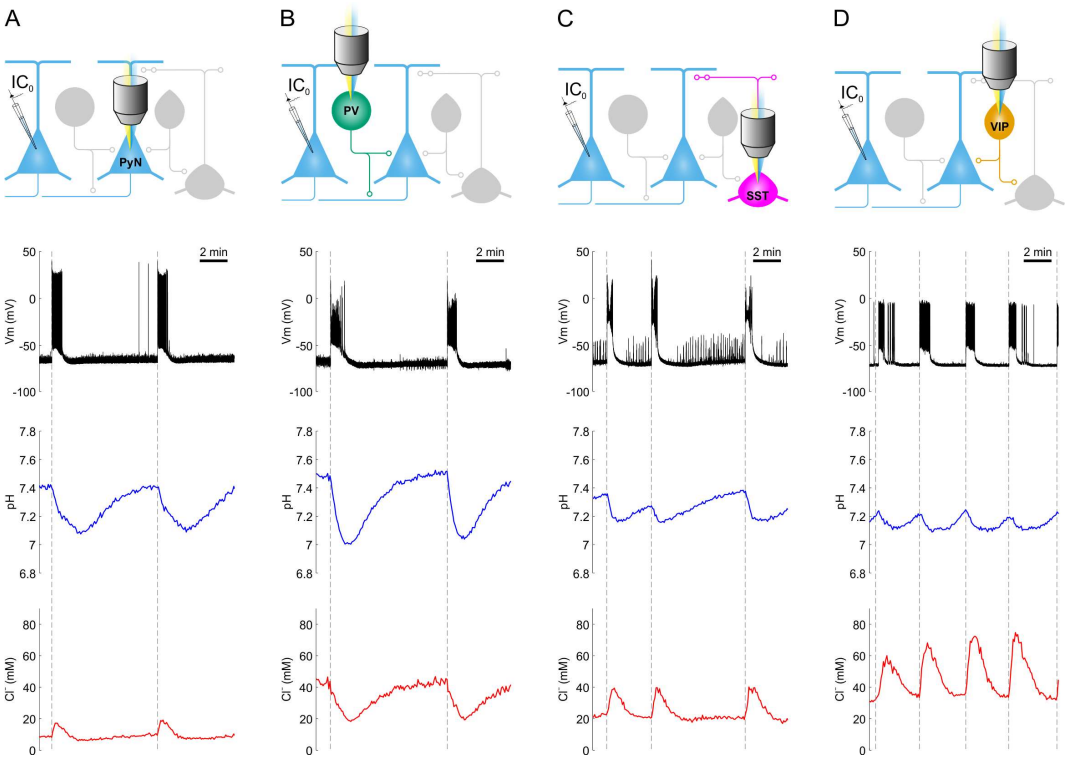

Figure 4.5. Recording intracellular pH and Cl^- dynamics in genetically-defined cell types during epileptiform events. (A) Cartoon (top panel) shows the experimental setup. Network events were monitored by current-clamp recording from a nearby pyramidal cell (black trace, second panel). The intracellular pH (blue trace, third panel) and Cl^- (red trace, bottom panel) are determined by imaging a pyramidal neuron expressing ClopHensorN. Vertical dotted grey lines mark the onset of spontaneous EDs. **(B)** The intracellular pH and Cl^- are determined by imaging a PV interneuron expressing ClopHensorN (as shown in 'A'). **(C)** The intracellular pH and Cl^- are determined by imaging a SST interneuron expressing ClopHensorN (same conventions as in 'A'). **(D)** The intracellular pH and Cl^- are determined by imaging a VIP interneuron expressing ClopHensorN (as shown in 'A').

of the epileptiform events using an automated algorithm (see Materials and Methods, thesis section 2.3), and to correlate the imaging data with the state of the neuronal network (**Figure 4.6**). Following acquisition, the imaging data was processed to correct for differential bleaching of the two fluorophores of the reporter, and to stabilise the fluorescence signal (see Materials and Methods, thesis section 2.10). Using this setup, I found that EDs were associated with marked transients in intracellular pH and Cl^- concentration across all cell types investigated, as shown in the example recordings in **Figure 4.5**. Pyramidal neurons (**Figure 4.5***A*, **Figure 4.6***A*) and GABAergic interneurons (**Figure 4.5***B,C,D*, **Figure 4.6***B,C,D*) experienced different degrees of acidifications during epileptiform events. By contrast, the Cl^- fluxes in PV interneurons (**Figure 4.5***B*, **Figure 4.6***B*) were remarkably different to those experienced by the other cell types (**Figure 4.5***A,C,D*, **Figure 4.6***A,C,D*). Pyramidal cells, as well as SST and VIP interneurons, experienced significant increases in intracellular Cl^- concentration. Interestingly, the PV interneurons showed the opposite, with these cells experiencing an intracellular Cl^- decrease. Superimposed population summary data on intracellular pH and Cl^- concentration transients time-locked to ED onset and end are shown in **Figure 4.6***E*.

4.6 Intracellular pH and Cl^- transients relate to resting state and epileptiform event duration

To quantify the maximum amplitude of the ED-induced intracellular pH and Cl^- concentration transients relative to baseline (i.e. before ED onset), the direction

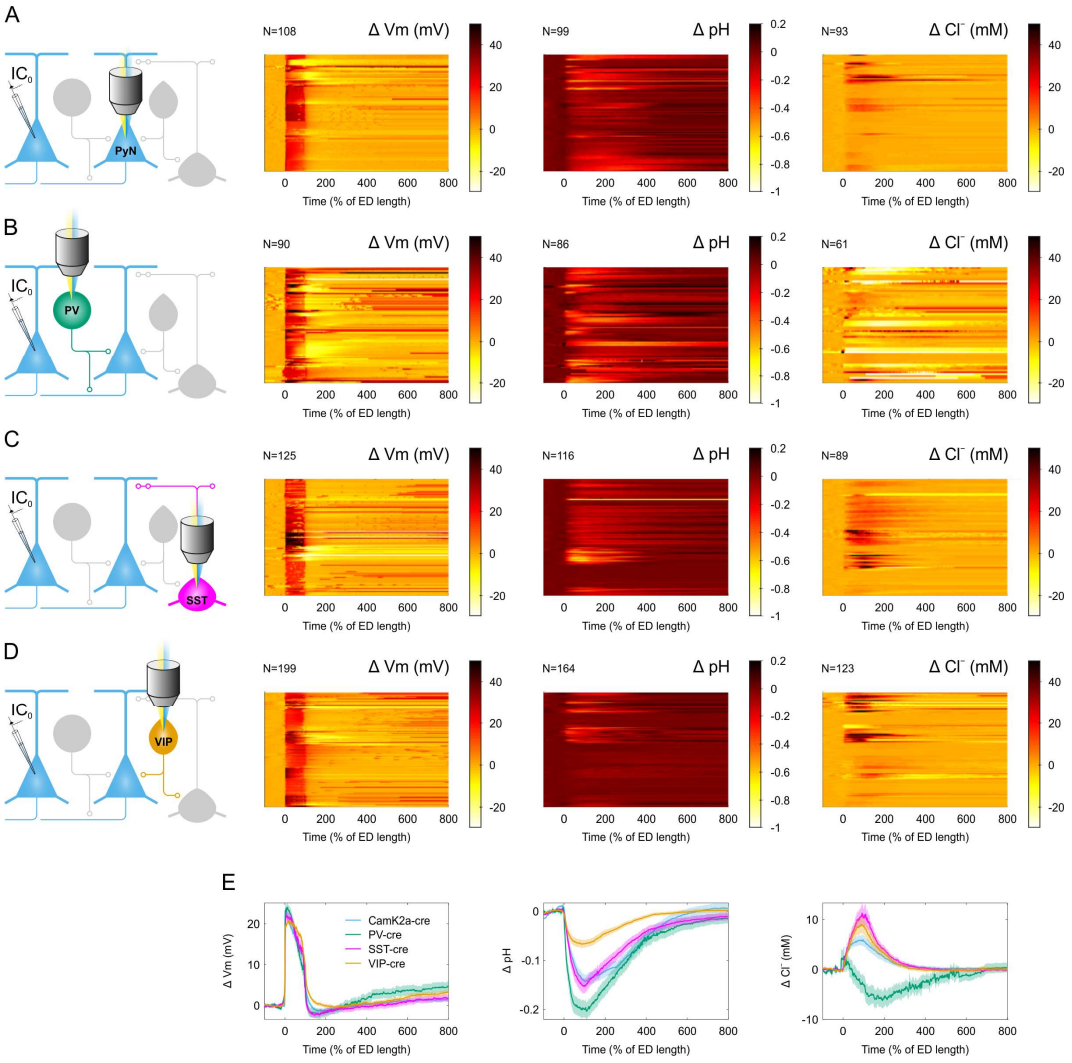

Figure 4.6. Different cell types exhibit distinct intracellular pH and Cl^- dynamics during epileptiform events. (A) Cartoon (left) shows the experimental setup. The relative membrane potential of the pyramidal neuron recorded using patch-clamp (Δ Vm) and the intracellular pH (Δ pH) and Cl^- concentration (Δ Cl^-) determined from imaging pyramidal neurons are shown (right), time-locked to ED onset and end. **(B)** Data resulted from experiments imaging PV interneurons (as shown in 'A'). **(C)** Data resulted from experiments imaging SST interneurons (as shown in 'A'). **(D)** Data resulted from experiments imaging VIP interneurons (as shown in 'A'). **(E)** Population data on Δ Vm (left), Δ pH (middle) and Δ Cl^- (right) for pyramidal neurons and PV, SST and VIP interneurons are shown superimposed.

of each response was first determined by measuring the area under the curve for the time interval between 50-250% of the corresponding ED duration. The peak relative change induced by the epileptiform event was then detected within the same time interval. This eliminated short-lasting artefacts at ED onset, potentially associated with cells briefly shifting focal depth due to tissue movement at the start of epileptiform activity.

All cell types I investigated appeared to acidify during EDs, with the VIP interneurons experiencing the lowest ED-induced change in pH. On average, epileptiform events generated somatic acidic pH shifts that were of similar amplitude in pyramidal neurons and SST interneurons (-0.17±0.01 pH units for pyramidal neurons; -0.17±0.02 pH units for SST interneurons), whereas PV interneurons showed the largest acidic shifts (-0.25±0.02 pH units), and VIP interneurons had the smallest intracellular pH shifts (-0.09±0.01 pH units) (**Figure 4.7***A*).

To further investigate differences in ED-triggered pH shifts between the different cell types, I studied the relationship between the peak amplitude of pH responses, the resting pH and the duration of the corresponding EDs. All four cell types experienced significantly larger acidic shifts in their somatic pH when they started from a more alkaline intracellular resting pH before EDs (**Figure 4.7***B*). However, the gradient of the relationship between resting pH and Δ pH varied between the four cell types. The VIP interneurons showed a significantly lower gradient for this relationship compared to the other cell types. This finding suggests

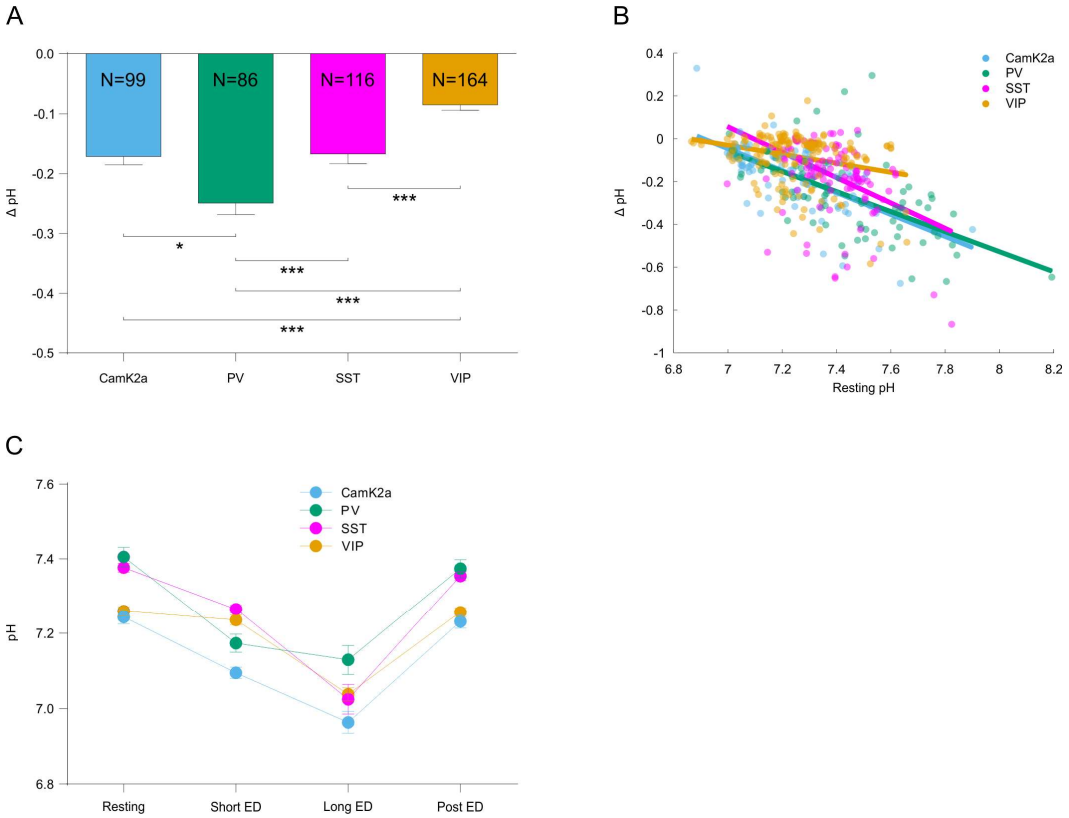

Figure 4.7. Intracellular pH transients during epileptiform events relate to resting state and event duration. (A) Distinct cell types registered different relative amplitudes of pH change during EDs ($\chi^2_{(3)}$=86.74, p<0.0001, Kruskal-Wallis test, followed by post-hoc Dunn's multiple comparisons tests; CamK2a vs PV, p=0.0352; CamK2a vs SST, p>0.9999; CamK2a vs VIP, p<0.0001; PV vs SST, p=0.0002; PV vs VIP, p<0.0001; SST vs VIP, p<0.0001). **(B)** For each cell type, the relative amplitude of intracellular pH change (Δ pH) correlates with the cell's resting pH (interaction between relative pH change and resting pH: $F_{(3)}$=5.2, p=0.0015, one-way ANCOVA followed by Tukey-Kramer post-hoc multiple comparisons for slopes: CamK2a vs PV, p=0.9639; CamK2a vs SST, p=0.9078; CamK2a vs VIP, p=0.0098; PV vs SST, p=0.6904; PV vs VIP, p=0.0186; SST vs VIP, p=0.0061). **(C)** The relative amplitude of intracellular pH change is related to ED length (interaction between cell type and condition: $F_{(9,1379)}$=5.789, p<0.0001, two-way ANOVA followed by Sidak's post-hoc multiple comparisons of resting vs short EDs: CamK2a, p<0.0001; PV, p<0.0001; SST, p<0.0001; VIP, p=0.6409; short vs long EDs: CamK2a, p=0.0136; PV, p=0.6151; SST, p<0.0001; VIP, p<0.0001; resting vs post ED, p>0.05 for all cell types). * indicates p<0.05, *** indicates p<0.001.

that the resting pH of VIP interneurons tended to be less predictive of their ED-associated acidification (**Figure 4.7***B*). The gradient of linear fits were -0.51±0.06 for pyramidal neurons (R^2=0.45), -0.47±0.07 for PV interneurons (R^2=0.38), -0.59±0.12 for SST interneurons (R^2=0.19), and -0.21±0.06 for VIP interneurons (R^2=0.08).

To examine the impact of the duration of epileptiform activity, events with a time span shorter than 60 s were classified as 'short EDs' and events lasting longer than 60 s as 'long EDs'. Short EDs had a mean length of 24.7±0.7 s, whilst long EDs had a mean duration of 199.6±12.6 s. All cell types generally showed a similar monotonic profile, in the sense that long EDs elicited larger acidification compared to short EDs, with the possible exception of PV and VIP interneurons, and intracellular pH recovered to baseline value after EDs (recovery time interval defined between 500-600% of each ED length). While PV interneurons did not show further acidification with longer EDs compared to shorter EDs, VIP interneurons behaved in an opposite manner, only showing a significant change in somatic pH during long EDs (**Figure 4.7***C*). Pyramidal neurons had an intracellular resting pH of 7.24±0.02, reached a pH of 7.1±0.02 during short EDs and a pH of 6.97±0.03 during long EDs, and recovered to a pH of 7.23±0.02 after EDs. SST interneurons started with a resting pH of 7.38±0.01, achieved a pH of 7.26±0.01 during short EDs and a pH of 7.02±0.04 during long EDs, and recovered to a pH of 7.35±0.01 after epileptiform events. By contrast, PV interneurons had a resting pH of 7.41±0.03, reached a pH of 7.17±0.02 during short EDs, which was not

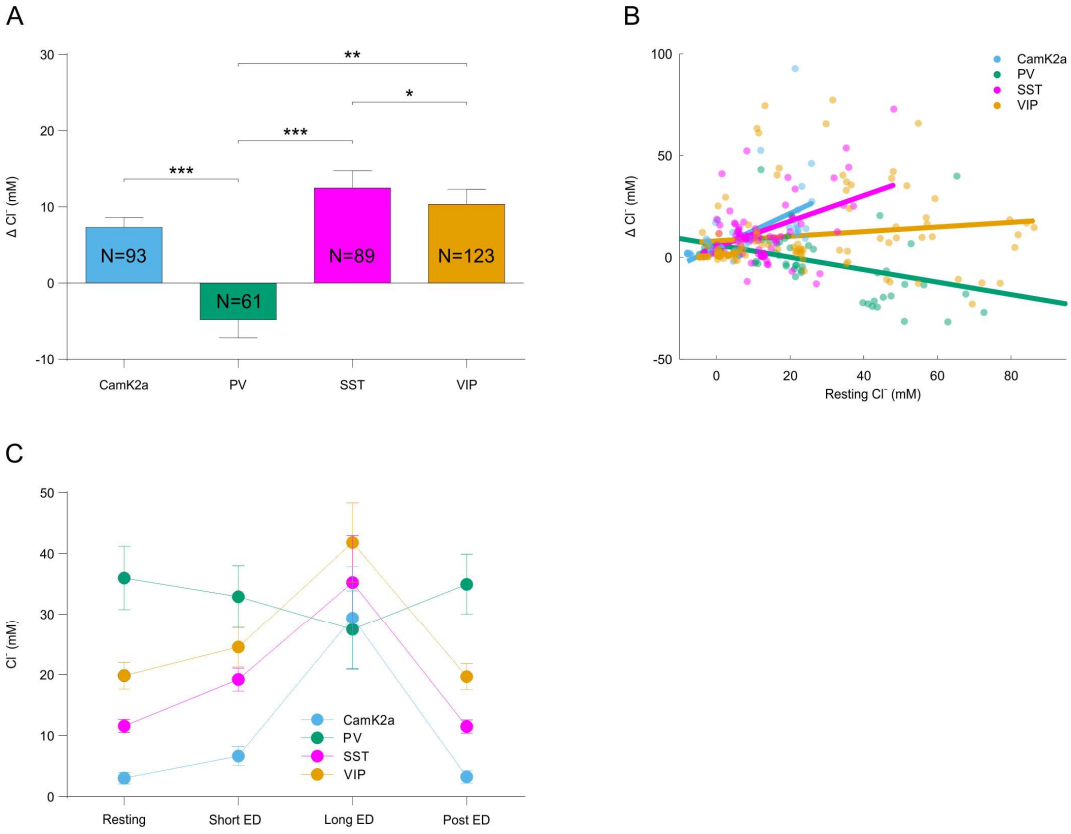

Figure 4.8. Intracellular Cl^- concentration transients during epileptiform events relate to resting state and event duration. (A) Distinct cell types registered different relative amplitudes of intracellular Cl^- change (Δ Cl^-) during EDs ($\chi^2_{(3)}$=33.12, p<0.0001, Kruskal-Wallis test, followed by post-hoc Dunn's multiple comparisons tests; CamK2a vs PV, p=0.0003; CamK2a vs SST, p>0.4125; CamK2a vs VIP, p>0.9999; PV vs SST, p<0.0001; PV vs VIP, p=0.0014; SST vs VIP, p=0.0488). **(B)** The relative amplitude of intracellular Cl^- concentration change is correlated to the resting Cl^- concentration (interaction between relative Cl^- concentration change and resting Cl^- concentration: $F_{(3)}$=19.94, p<0.0001, one-way ANCOVA followed by Tukey-Kramer post-hoc multiple comparisons for slopes: CamK2a vs PV, p<0.0001; CamK2a vs SST, p=0.8628; CamK2a vs VIP, p=0.0027; PV vs SST, p<0.0001; PV vs VIP, p<0.0001; SST vs VIP, p=0.0482). **(C)** The relative amplitude of intracellular Cl^- change correlates to ED length (interaction between cell type and condition: $F_{(9,1082)}$=2.643; p=0.0050, two-way ANOVA followed by Sidak's post-hoc multiple comparisons of resting vs short EDs: CamK2a, p=0.7660; PV, p=0.9220; SST, p=0.2374; VIP, p=0.5246; short vs long EDs: CamK2a, p=0.0057; PV, p=0.8509; SST, p<0.0229; VIP, p<0.0014; resting vs post ED, p>0.05 for all cell types). * indicates p<0.05, ** indicates p<0.01, *** indicates p<0.001.

significantly different during long EDs (pH of 7.13±0.04), and recovered to a pH of 7.37±0.02 after EDs. VIP interneurons started with a pH of 7.26±0.01, which was not significantly different to the pH of 7.24±0.01 during short EDs. However, during the long EDs, the pH of the VIP interneurons became significantly more acidic (7.04±0.02), and then recovered to a pH of 7.26±0.01 after EDs terminated (**Figure 4.7***C*).

In addition to pH transients, the intracellular Cl^- concentration also exhibited ED-induced dynamics that were independently reported by ClopHensorN. On average, all cell types investigated generally loaded Cl^- as a result of epileptiform events, with the exception of PV interneurons that did not load and actually showed a tendency to unload Cl^- during EDs. Pyramidal neurons experienced peak somatic Cl^- concentration shifts of similar amplitude compared to VIP interneurons (7.3±1.3 mM Cl^- change for pyramidal neurons; 10.4±2 mM Cl^- change for VIP interneurons) and SST interneurons loaded Cl^- more compared to the latter (12.5±2.3 mM Cl^- change). Interestingly, the PV interneurons appeared to extrude Cl^- (-4.8±2.4 mM Cl^- change) as shown in **Figure 4.8***A*.

To further investigate the differences in ED-associated Cl^- transients between distinct cell types, I studied the relationship between the peak amplitude of Cl^- transients, the resting Cl^- concentration and the duration of the corresponding EDs. In contrast to the other cell types, PV interneurons experienced a Cl^- unloading effect directly proportional with the resting intracellular Cl^- concentration (**Figure 4.8***B*, $F_{(1,59)}=46.74$, $p<0.0001$). The slopes of linear fits were -0.85±0.11 for pyramidal neurons ($R^2=0.39$), -0.31±0.04 for PV interneurons

(R^2=0.44), 0.63±0.22 for SST interneurons (R^2=0.09), and 0.11±0.08 for VIP interneurons (R^2=0.02).

When accounting for the duration of epileptiform activity, all cell types converged on a similar Cl^- level of 33.5±3.2 mM during long EDs (**Figure 4.8***C*, interaction between cell type and condition: $F_{(9,1082)}$=2.64, p=0.005, two-way ANOVA followed by Tukey's post-hoc multiple comparisons between all cell types during long EDs, p>0.05 for each of the pairwise comparisons). Generally, all neuronal populations followed a similar pattern of Cl^- loading during epileptiform activity, experiencing a higher intracellular Cl^- influx during long events compared to short events. Interestingly, PV interneurons appeared to be an exception to this by showing much less variation in intracellular Cl^- concentration and exhibiting no statistically detectable change during short or long epileptiform events (**Figure 4.8***C*). Pyramidal neurons had an intracellular resting Cl^- concentration of 3.1±1 mM, reached 6.7±1.6 mM Cl^- during short EDs and 29.4±8.5 mM Cl^- during long EDs, and recovered to 3.3±1 mM Cl^- after EDs. SST interneurons started with a resting Cl^- concentration of 11.6±1.1 mM, achieved 19.2±1.9 mM Cl^- during short EDs and 35.3±7.7 mM Cl^- during long EDs, recovering to 11.5±1.1 mM Cl^- after EDs. VIP interneurons had a resting Cl^- concentration of 19.8±2.2 mM, reaching 24.6±3.2 mM Cl^- during short EDs and 41.9±6.5 mM Cl^- during long EDs, and recovering to 19.7±2.1 after EDs. PV interneurons started from a relatively high intracellular resting Cl^- concentration of 36±5.2 mM, reached 32.9±5.1 mM Cl^- during short EDs and 27.5±6.4 mM Cl^- during long EDs, and recovered to 35±4.9 mM Cl^- after EDs (**Figure 4.8***C*). Thus, unlike the other three cell types

investigated, PV intracellular Cl^- appeared to remain more stable throughout epileptiform activity.

4.7 Discussion

In this chapter, I use a novel genetically-encoded H^+ and Cl^- probe to measure the absolute intracellular pH and Cl^- in various neuron populations at baseline and during EDs. The design of the floxed version of ClopHensorN described in this chapter allowed this improved fluorescent reporter to be selectively expressed in specific cell populations. The novel floxed ClopHensorN construct allowed me to be the first to investigate intracellular pH and Cl^- across different interneuron subtypes. To my knowledge, this is the first time the intracellular pH and Cl^- concentration dynamics were reported for specific subtypes of GABAergic interneurons during epileptiform activity using optical methods.

In the mammalian nervous system, hippocampal neurons have been extensively studied with respect to the mechanisms regulating intracellular pH (Chesler, 2003). Protons are considered not to permeate passively through the neuronal membrane (Roos and Boron, 1981), but rather the intracellular pH under baseline conditions is believed to be governed by the balance between acid loading and acid extruding processes (Ruffin et al., 2014). Apart from metabolically-induced intracellular acidification due to anaerobic respiration (Chesler, 2003), it is thought that a Cl^-/HCO_3^- exchanger (Anion Exchanger 3, or AE3) is the principle transport mechanism contributing towards intracellular acidification, by extruding alkali equivalents (Hentschke et al., 2006; Svichar et al., 2009). By contrast, acid extruders that are important for neuronal pH homeostasis include a number of

transmembrane carriers. For example, there are several isoforms of Na^+/H^+ exchangers (NHEs) described, with the isoform most ubiquitously expressed in the CNS being NHE1 (Orlowski and Grinstein, 2004; Luo and Sun, 2007). Raley-Susman et al. (1991) identified that a Na^+/H^+ antiporter was an important mechanism for maintaining the intracellular pH and for recovering from acidic challenges in fetal neurons. However, in mature neurons the main mechanism regulating intracellular pH is the Na^+-dependent Cl^-/HCO_3^- exchanger. This co-transporter is able to perform the coupled influx of one Na^+ and two HCO_3^- equivalents (Schwiening and Boron, 1994; Grichtchenko et al., 2001; Chen et al., 2008). Nevertheless, NHEs are still important regulators of the steady-state of mature neurons (Yao et al., 1999), and are accompanied by other electrogenic or electroneutral Na^+-dependent HCO_3^- transporters (Damkier et al., 2007; Boedtkjer et al., 2008; Cooper et al., 2009). In addition to these mechanisms, Na^+-independent processes have been shown to contribute to pH regulation in mature neurons found within the hippocampus (Bevensee et al., 1996; Yao et al., 1999; Adijanto and Philp, 2012). Apart from transmembrane transport, buffering of acid equivalents also plays a role in establishing pH homeostasis. This can be achieved with using the HCO_3^--dependent carbonic anhydrase system (Supuran, 2008), or through HCO_3^--independent buffers such as phosphate or imidazole moieties (Burton, 1978).

The intracellular pH values that I measured at rest in pyramidal neurons are consistent with data from previous studies (Caspers and Speckmann, 1972; Raimondo et al., 2012a, 2015). In contrast to the wealth of literature on intracellular

pH, I could find no previous reports of intracellular pH in specific subtypes of GABAergic interneurons in the mammalian brain. Overall, I found the intracellular pH of inhibitory neurons to be similar to pyramidal neurons. However, there appear to be specific differences between the different interneuron subtypes. For example, VIP interneurons exhibited the lowest intracellular pH at rest, being ~0.12 pH units below the resting pH of PV or SST interneurons. This is equivalent to an increase of 13 nM (or 31.8%) in H^+ concentration. This leads one to the question: what might be the functional significance of the more acidic resting pH of VIP interneurons?

VIP interneurons are bestowed with certain biophysical traits, which are presumably important for their signalling properties. Higher input resistance and an associated higher excitability have been reported as characteristics of VIP interneurons (Cauli et al., 2000; Lee et al., 2010; Miyoshi et al., 2010; Rudy et al., 2011), consistent with them showing relatively high spontaneous activity across a wide range of behavioural states, including at rest (Jackson et al., 2016). This suggests that the biophysical properties of VIP interneurons mean that they can be more readily excited via afferent input. However, this predisposition to being more excitable comes with the risk of excitotoxicity caused by high levels of transmembrane Ca^{2+} influx (Szydlowska and Tymianski, 2010).

Intracellular acidosis is known to reduce neuronal excitability. Therefore, it could be that the lower intracellular pH within the VIP interneurons is employed to help mitigate the risk of excitotoxicity. Indeed, an increase in intracellular H^+ can reduce cytosolic Ca^{2+} in neurons (Willoughby et al., 2001) and suppress a number of conductances such as the high-voltage-activated Ca^{2+} current (Dixon et al., 1993;

Takahashi and Copenhagen, 1996; Tombaugh and Somjen, 1997). This comes with the consequence of potentially limiting the temporal summation of excitatory postsynaptic potentials, discouraging repetitive firing or reducing neurotransmitter release (Dodge and Rahamimoff, 1967; White et al., 1989; De Schutter and Bower, 1994). Indeed, if the low cytosolic pH of VIP interneurons is part of a neuroprotective mechanism that limits Ca^{2+} conductances, this may be particularly important in the context of ischemic insults that result in neuronal superoxide production (Valentino et al., 1993; Lam et al., 2013). In summary, the differences in steady-state intracellular pH observed across the different interneuron populations could be accounted for at least in part by the differential contribution of distinct buffering systems and/or transport mechanisms. Further studies should investigate the specific mechanism(s) responsible for setting a different resting pH in VIP interneurons.

Having studied the intracellular pH across different cell types at baseline, I then sought to study pH dynamics during periods of elevated neural activity. It is well established that neuronal activity leads to intracellular acidification (Chesler and Kaila, 1992). Consistent with previous observations (Raimondo et al., 2012a, 2013), I found that pyramidal neurons experienced acidic shifts as they are recruited to epileptiform activity. Intracellular pH may lower as a result of neuronal activity for a number of reasons, including the metabolic production of acid equivalents such as CO_2 and lactic acid (Siesjö, 1985; Zhan et al., 1998), the release of protons from intracellular stores triggered by increased cytoplasmic Ca^{2+} levels (Meech and Thomas, 1977), the influx of protons from the Ca^{2+}/H^+ exchange by plasmalemmal

Ca^{2+}-ATPases triggered by activity-induced elevation of the intracellular Ca^{2+} (Schwiening et al., 1993; Makani and Chesler, 2010), and the entry of acid equivalents through voltage- or ligand-gated channels, including HCO_3^- efflux through GABA-activated HCO_3^- conductances (Kaila and Voipio, 1987; Kaila et al., 1992). Although the Ca^{2+}-dependent proton influx is a principal mechanism for activity-induced intracellular acidification (Chesler, 2003), it has been shown to be limited by a depolarisation-triggered alkalisation that is thought to be mediated by H^+ efflux through the voltage-activated H_V1 proton conductance (Cheng et al., 2008). Despite the fact that the likely candidate for activity-induced intracellular acidification is the Ca^{2+}-dependent proton influx, all the phenomena listed above may be happening concurrently during EDs, resulting in the acidic shifts that I and others observed in pyramidal cells (Raimondo et al., 2012a). The extent to which each of these different processes contributes to this effect may be further investigated by pharmacological studies. For example, one could use specific blockers to mechanistically dissect the activity of various transporters or channels during epileptiform activity.

Intracellular pH dynamics during epileptiform activity have not been studied before in interneurons. In this chapter, I showed that, similar to pyramidal neurons, GABAergic interneuron subtypes exhibit a drop in intracellular somatic pH as a result of epileptiform activity. On average, PV interneurons acidified the most, whilst SST interneuron pH shifts were similar to pyramidal neurons, and VIP interneurons acidified the least. Interestingly, this correlated with resting pH. This is demonstrated by the PV interneurons exhibiting a relatively high baseline pH and

large acidic shifts during EDs. By contrast, VIP interneurons were the most acidic at rest and then had a more modest pH shift during EDs. This relationship was least pronounced for VIP interneurons, which may suggest different regulatory mechanisms. Intraneuronal acidification is predicted to reduce both Ca^{2+} inflow and the activity of transmembrane transport processes such as the Ca^{2+}-dependent proton influx (Willoughby et al., 2001). This may potentially be a self-limiting mechanism to prevent the decrease in intracellular pH during EDs. However, in VIP interneurons Ca^{2+}-related proton influx mechanisms could play a less important role. A potential alternative mechanism prevalent in the VIP interneurons could be a depolarisation-triggered alkalisation, which may limit the extent of activity-induced intracellular acidification more than in other interneuron subtypes. This idea is supported by the finding that VIP interneurons acidified only in response to long EDs. By contrast, PV interneurons reached their maximal acidification during short EDs. The high firing rate of PV interneurons may also lead to a relatively faster production of acid equivalents, which could contribute to the fact that short EDs produce maximal pH shifts in PV interneurons.

Overall, my data supports the idea that GABAergic interneurons may employ different pH buffering and/or H^+/HCO_3^- transport mechanisms. Future studies could investigate the differential contribution of pH-regulating processes in PV, SST and VIP interneurons. For example, single-cell transcriptomics could be used to identify likely molecular candidates, such as transporters or ion channels, involved in cell-type-specific pH homeostasis. These could then inform

pharmacological and molecular knockdown experiments to directly test their contribution to controlling intracellular pH dynamics.

Neuronal pH homeostasis is intricately linked to the regulation of intracellular Cl^- at multiple levels, mainly through the coupled transport of HCO_3^- and the activity of carbonic anhydrases promoting the interconversion of CO_2 and H_2O, to HCO_3^- and H^+ (Supuran, 2008). For example, $GABA_A$Rs are permeable to both Cl^- and HCO_3^- (Bormann et al., 1987), and their activation leads to intracellular acidification due to GABA-mediated HCO_3^- efflux, along with a Cl^- flux that is governed by the electrochemical gradient (Kaila and Voipio, 1987). Several of the processes described above represent additional nodes of interaction between the regulation of H^+ and Cl^-, such as the acid loading Cl^-/HCO_3^- exchange that extrudes HCO_3^-, and the Na^+-dependent Cl^-/HCO_3^- transport that accumulates HCO_3^- intracellularly and exports Cl^-. These mechanisms highlight the importance of studying H^+ and Cl^- homeostasis with consideration of their interdependence, as well as the use of tools that make it possible to measure both ions independently.

The main contributors to Cl^- homeostasis are considered to be: (1) the developmentally regulated cation-chloride co-transporters (CCCs), such as KCC2 and NKCC1 (Rivera et al., 1999), (2) a variety of transmembrane ion channels that are permeable to Cl^-, such as synaptic and extra-synaptic ligand-gated $GABA_A$Rs (Jentsch et al., 2002), (3) other transporters, such as the Na^+/Cl^- co-transporter (NCC), and (4) the membrane potential influencing the driving force for Cl^-. Recently, there has been much debate around whether local impermeant anions may influence Cl^- homeostasis (Glykys et al., 2014; Luhmann et al., 2014; Voipio et al.,

2014; Doyon et al., 2016; Düsterwald et al., 2018). The functional balance between all these processes sets the intracellular Cl^- concentration, which has a profound impact on inhibitory neurotransmission in the brain (Doyon et al., 2016).

To directly investigate the intraneuronal Cl^- concentration in specific neuronal populations, I corrected ClopHensorN Cl^- signals for the concurrent pH transients, which allowed independent measurements of absolute intracellular Cl^-. Consistent with previous work (Raimondo et al., 2013; Ellender et al., 2014), I found that pyramidal neurons have a low resting Cl^- concentration. This is equivalent to a chloride reversal of -80.7 mV, or an E_{GABA_A} of -68.9 mV, which are in agreement with previous *in vitro* and *in vivo* studies (Tyzio et al., 2008; Ellender et al., 2014). Interestingly, PV interneurons had the highest resting Cl^- concentration, which is also consistent with previous literature reporting a more depolarised E_{GABA_A} in this population of cells (Vida et al., 2006). This invites the obvious question: why might PV interneurons have a high intracellular resting Cl^- concentration? To answer this, one might consider what are the possible effects of having a more depolarised E_{GABA_A}.

During GABAergic signalling, low postsynaptic intracellular Cl^- sustains a driving force that determines Cl^- ions to enter the cell, causing membrane hyperpolarisation (Kaila, 1994; Glickfeld et al., 2009). However, if Cl^- ions are allowed to accumulate intracellularly, this shifts the E_{GABA_A} closer to the resting membrane potential. When this occurs, the $GABA_A$-mediated conductance is depolarising but remains inhibitory through a shunting mechanism (Staley and

Mody, 1992; Paulus and Rothwell, 2016). If the amount of Cl^- increases further and the E_{GABA_A} is pushed towards the action potential threshold, activation of the GABAergic signalling may be able to trigger action potentials. When this occurs, GABAergic signalling has become excitatory (Ben-Ari et al., 1989; Szabadics et al., 2006).

As PV interneurons have a high resting intracellular Cl^- level, their GABAergic conductances are likely to be shunting or depolarising. Indeed, shunting inhibition has been demonstrated in PV interneurons, which are thought to use this mechanism to promote coherent oscillatory activity in interneuron networks (Vida et al., 2006). In addition to the shunting effects, recent work has revealed that Cl^- loading can result in a lower action potential threshold through Ca^{2+}-dependent Cl^- channels (CaCCs) that are able to couple excitatory postsynaptic potentials and action potential generation with intracellular Cl^- (Huang et al., 2012; Sørensen et al., 2018). Thus, controlling intraneuronal Cl^- levels is expected to have a significant impact on cellular and network excitability. With specific relevance to PV interneurons, the enhanced excitability endowed by increased Cl^- levels places this population of cells in a good position to mediate feedforward inhibition (Hu et al., 2014).

To explain the higher resting intracellular Cl^- concentration observed in the PV interneurons, one needs to consider alternative mechanisms that either promote Cl^- influx or reduce Cl^- efflux. These can include membrane transporters or channels, such as NKCC1 (Payne et al., 2003), Cl^- channels (Rungta et al., 2015), or lower levels of KCC2 (Woodin et al., 2003). This is an exciting area of research

and future studies could investigate the precise mechanisms by which such discrepancies in resting intracellular Cl^- concentration arise between different cell types and the functional implications of these differences. For example, blocking NKCC1 activity with bumetanide while monitoring E_{GABA_A} in PV interneurons could establish whether NKCC1 has a significant role in setting the higher resting intracellular Cl^- levels in this cell type.

Previous work has established that intense GABAergic activity, particularly when coupled with membrane depolarisation, can lead to rapid intracellular Cl^- accumulation in pyramidal neurons (Kaila and Voipio, 1987; Kaila et al., 1989; Thompson and Gähwiler, 1989; Staley et al., 1995; Staley and Proctor, 1999; Ellender et al., 2014). In this chapter, I have been able to reproduce these findings by demonstrating that pyramidal neurons experience a significant Cl^- loading effect during epileptiform events. I then extend this by showing that activity-dependent Cl^- dynamics differ among the various GABAergic interneuron subtypes during EDs.

My data shows that SST and VIP interneurons as well as pyramidal neurons tend to load with Cl^- during EDs. By contrast, PV interneurons did not load but instead showed a tendency to extrude Cl^- during epileptiform activity. Furthermore, I was then able to show that a neuron's resting Cl^- acts as a good predictor of how Cl^- changes during the EDs. This suggests that the Cl^- driving force through $GABA_A$Rs during EDs was likely the most important factor involved in ED-associated Cl^- shifts. Cells that load with Cl^- like the pyramidal and SST cells had lower intracellular Cl^- during baseline conditions, consistent with an increased

contribution of Cl^- extruders such as KCC2 transporters in setting the resting Cl^- level. Therefore, in these neuron populations the driving force for Cl^- appears to have promoted a net Cl^- influx. PV interneurons by contrast, which unloaded Cl^- during EDs, had the highest resting intracellular Cl^- concentration. This is consistent with this interneuron subtype relying less upon Cl^- extruders such as KCC2. Hence, in PV interneurons the driving force for Cl^- was more likely to lead to net Cl^- efflux. In addition, PV interneurons with lower Cl^- levels at rest showed the least evidence of Cl^- unloading.

Interestingly, during the long EDs, intracellular Cl^- concentration tended to converge to a similar level across all cell types. This again suggests that the driving force for Cl^- was indeed the most likely contributor to the observed Cl^- dynamics during epileptiform activity. Given EDs generated by removing Mg^{2+} from the aCSF were on average longer than spontaneous EDs, data segregated by ED length inherently biased measurements towards a specific ED model. Spontaneous EDs consistently represented >80% of all short EDs across cell types. EDs triggered by removing Mg^{2+} from the aCSF consistently represented >60% of all long EDs across cell types. Since data from different models did not appear to show different trends for either short of long EDs, data were combined to increase statistical power. Pyramidal neurons, SST and VIP interneurons required sustained epileptiform activity to significantly change their intracellular Cl^- levels. By contrast, PV interneurons were less volatile in terms of their intracellular Cl^- across a range of epileptiform event durations. This feature of PV interneurons suggests that they may be more likely to maintain an excitation-inhibition balance, even when

challenged with strong GABAergic synaptic currents such as those experienced during epileptiform activity. Maintaining the stability of inputs to PV interneurons may be an important contributor to limiting epileptiform activity. For example, if PV interneurons collapsed their Cl^- gradients, they would become more excitable and may contribute to a more pronounced Cl^- loading in pyramidal neurons, which could aggravate epileptiform activity due to the resulting elevated excitability of pyramidal neurons.

In conclusion, the data I have presented in this chapter has shown that a novel floxed ClopHensorN can be used to independently report the intracellular pH and Cl^- dynamics across different cell types. This has revealed important differences in pH and Cl^- between cell types, which may prove to be relevant for the different functions of these neuron populations both physiologically and during seizure activity. At the same time, my results underly the importance of the reporter's capacity to distinguish between H^+ and Cl^-.

Chapter 5: Preventing seizure recruitment by optogenetic removal of depolarisation block in parvalbumin-expressing interneurons

5.1 Introduction

In the previous chapter, I show that the intracellular Cl^- levels in PV interneurons are maintained during periods of epileptiform activity. This suggests that PV interneurons may be able to sustain a steady excitation-inhibition balance, making this interneuron subtype a reasonable target for potential anti-seizure therapies (see chapter 3).

PV interneurons detect rising excitatory drive in the network, and react pre-emptively by utilising a feedforward mechanism of inhibition to prevent the spread of hyperexcitable activity (Trevelyan et al., 2006, 2007; Schevon et al., 2012; Sessolo et al., 2015). The ability of PV interneurons to constrain this aberrant electrical activity is known as 'inhibitory restraint' (Trevelyan et al., 2006). However, when this inhibitory restraint fails, spatially-clustered pyramidal neurons are recruited to the epileptiform event, allowing the activity to propagate freely (Trevelyan et al., 2006; Cammarota et al., 2013). Immediately prior to their recruitment into EDs, PV interneurons have been shown to transition from a hyperactive state associated with increased network excitation, to a 'block phase', which is characterised by impaired action potential firing (Cammarota et al., 2013). The underlying source for this DB is thought to be the depolarisation-induced inactivation of the voltage-gated cation channels required for spiking.

In this chapter, I use optogenetic techniques to investigate the DB mechanism by which PV interneurons are incapacitated. I also sought to test whether rescuing PV function by preventing DB could enhance the potential for these cells to counteract epileptiform activity.

The first aim of this chapter was to establish and describe a reliable seizure model in which to investigate the phenomenon of inhibitory restraint against epileptiform activity. It was key that the model afforded sufficient time resolution to allow the study and manipulation of inhibitory restraint. Here, I confirm the prediction that PV interneurons contribute to inhibitory restraint via feedforward recruitment prior to the onset of EDs. I then demonstrate that the PV interneuron-mediated inhibitory restraint diminishes prior to ED onset as a result of impaired action potential firing caused by a synaptically-induced DB.

The second aim of this chapter was to test the hypothesis that pulsed activation of a hyperpolarising opsin, archaerhodopsin (Arch), can be used to attenuate the effect of DB on PV interneuron spiking. I will show that employing this strategy reliably re-enables PV interneuron firing both during current-induced DB and during synaptically-induced DB prior to ED onset.

The third and final aim of this chapter was to investigate whether pulsed activation of Arch has the potential to impact epileptiform activity by reversing DB across the population of PV interneurons. Experiments testing the network effect of pulsed activation of Arch in PV interneurons showed a decreased probability of triggering epileptiform events. Moreover, I found that the pronounced change in

membrane properties at the onset of epileptiform activity significantly limited the potential to attenuate DB using light-induced currents.

5.2 NMDA-evoked epileptiform events are a reliable model to study inhibitory restraint *in vitro*

To study inhibitory restraint, I setup an NMDA-evoked seizure model based on previous work by Losi et al. (2010, 2016). NMDA was delivered extracellularly via a picospritzer and patch pipette to the CA3 area of the hippocampus in brain slices, with the aim of promoting local excitability and consequently generating epileptiform events. EDs evoked by delivering NMDA in CA3 occurred with a delay and simultaneously across the network. This is illustrated by dual whole-cell recordings of pyramidal neurons in the CA3 and CA1 regions showing synchronous onset of EDs across these two areas (**Figure 5.1***A*). This demonstrated that the NMDA-evoked EDs generalise across the entire hippocampal preparation.

For this seizure model to be adequate for investigating inhibitory restraint, it would need to show evidence of recruitment of inhibition immediately prior to ED onset. In the period between when NMDA was puffed on to the start of an ED, current-clamp recordings revealed high frequency, low amplitude oscillations in the membrane potential of pyramidal neurons (**Figure 5.1***A*, oblique arrows). To further investigate the synaptic currents during this period, I performed voltage-clamp recordings. Clamping the neuron at -60 mV and using a low Cl^- internal solution allowed me to detect both excitatory and inhibitory synaptic currents, since the -60 mV membrane potential lies between the reversal potential for glutamate

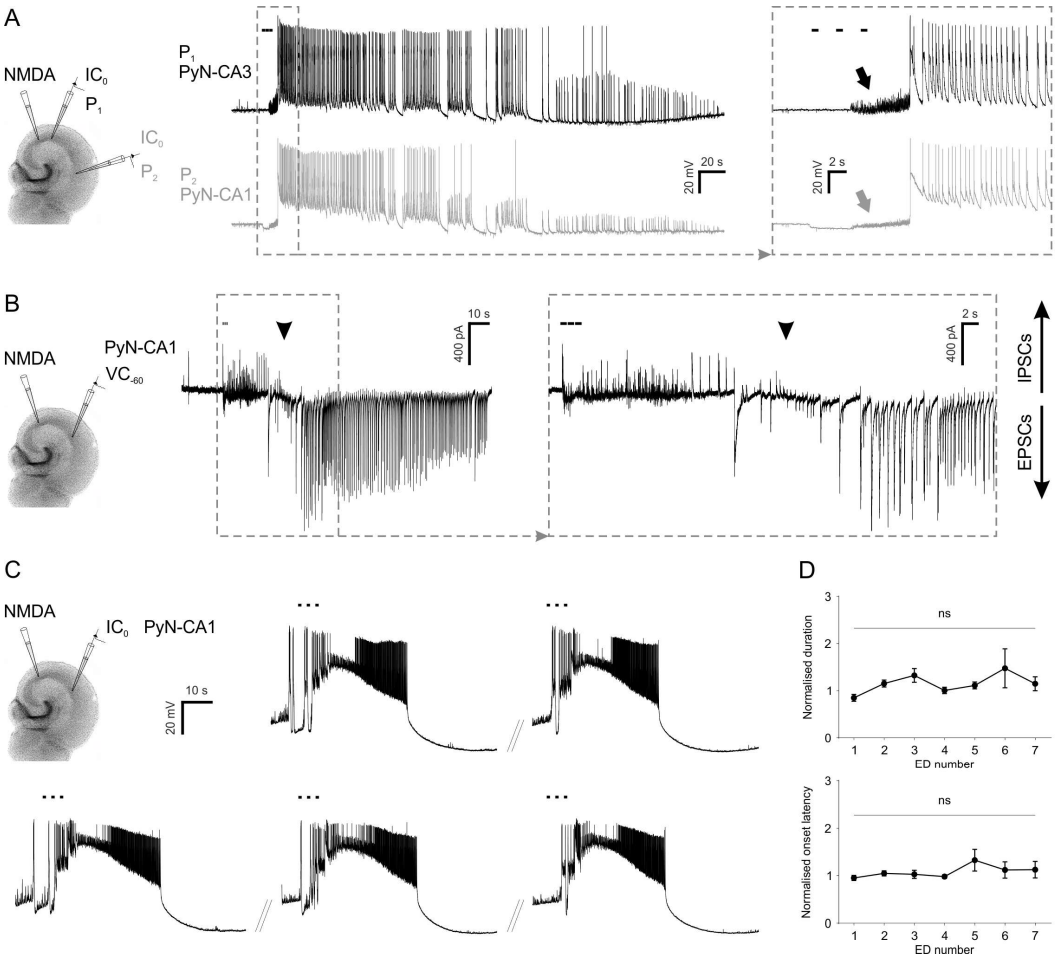

Figure 5.1. Reproducible epileptiform events triggered by NMDA enable the study of inhibitory restraint.(A) Cartoon of the experimental setup (left) shows the NMDA pressure pulses are delivered in the CA3 region of the hippocampus while two pyramidal neurons are simultaneously recorded in CA3 and CA1 in current-clamp mode (right). Note the synchronous ED onset (expanded traces on the right) and electrical activity of the two pyramidal neurons over the course of the event. Arrows point to the high frequency membrane oscillations prior to ED onset. The black bars above traces represent the timing of the NMDA puffs and their horizontal extension represents the puff duration. **(B)** An example of a voltage-clamp recording from a CA1 pyramidal neuron shows the transition from intense inhibitory synaptic inputs to net excitatory currents at seizure onset (black arrow head). Upward deflections represent inhibitory postsynaptic currents (IPSCs), and negative deflections represent excitatory postsynaptic currents (EPSCs). The significant amount of IPSCs occurring immediately after NMDA stimulation and before ED onset is consistent with previous findings of feedforward GABA-mediated inhibition, representing an inhibitory restraint against epileptiform activity (Trevelyan et al., 2006). **(C)** Focal NMDA stimulation evoked highly consistent epileptiform events. An example recording from a CA1 pyramidal

(figure legend continued on facing page) ——————→

responses (approximately 0 mV) and the reversal potential for $GABA_A$ responses (approximately -70 mV), under these recording conditions. These voltage-clamp recordings demonstrated that pyramidal neurons receive intense barrages of synaptic inhibition immediately prior to ED onset (**Figure 5.1***B*), which is consistent with the previously well-described phenomenon of feedforward inhibition (Trevelyan et al., 2006, 2007). This confirms that the seizure model involves feedforward inhibition, therefore validating it as a useful *in vitro* model to study inhibitory restraint.

To find the threshold for triggering EDs, the NMDA pulse duration, pressure and/or number were gradually increased until an ED was evoked. Once the parameters of the pressure pulse were established, EDs were triggered at 4-5 min intervals to study the reproducibility of the epileptiform events. The NMDA stimulations regularly evoked an ED and no failures were observed, even when stimulations were applied repetitively to the same slice (up to 30) over a long period of time (see example in **Figure 5.1***C*). Quantitative analysis of 50 evoked EDs from 9 experiments revealed a mean duration of 36.4±4.8 s (range 8.6 to 209.3 s) and a mean delay of 13.2±1 s (range 1.8 to 28 s) from the delivery of the first NMDA pressure pulse. Although ED length and latency varied across experiments, the parameters of the repeatedly evoked EDs were highly consistent within the same

---

neuron illustrates five consecutive triggered EDs. **(D)** Triggered EDs were reproducible in terms of relative duration (top, $F_{(6,43)}$=1.997, p=0.0871, one-way ANOVA) and relative onset latency (bottom, $F_{(6,43)}$=1.268, p=0.2921, one-way ANOVA). The mean relative duration and latency of EDs are shown with respect to the mean of the first two events (N≥4, from 9 slices).

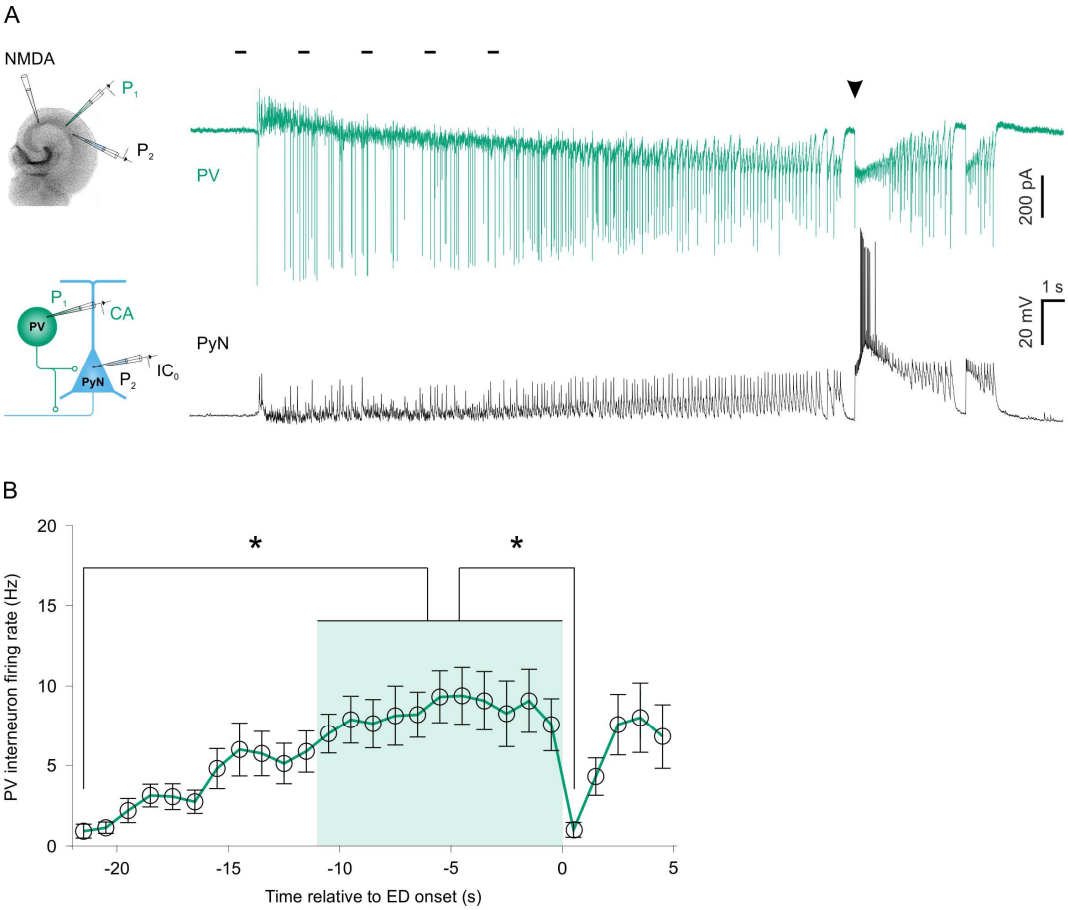

Figure 5.2. PV interneuron-mediated inhibitory restraint fails at ED onset. (A) An example synchronous recording of a PV interneuron (top) in cell-attached mode (CA) and a pyramidal neuron (bottom) in whole-cell current-clamp mode shows that the PV interneuron is recruited early during the pre-ictal time window, but enters a state of depolarising block at the beginning of the ED (black arrow head). **(B)** Population data (N=16 EDs) on PV interneuron firing rate during the pre-ED recruitment time window shows increased spiking output during the first 11 s before ED onset and an abrupt drop in firing rate at ED onset ($\chi^2_{(26)}$=84.27, p<0.0001, Kruskal-Wallis test, followed by post-hoc Dunn's multiple comparisons tests). * indicates p<0.05.

slice/experiment (**Figure 5.1***D*). Statistical analysis did not show any significant variation for ED length or latency, indicating that EDs are triggered with high temporal fidelity (**Figure 5.1***D*), which allows one to control when EDs are generated.

5.3 PV interneuron-mediated inhibitory restraint fails at ED onset

Having determined that the established seizure model involves inhibitory restraint, I then investigated whether the PV interneurons are recruited following NMDA stimulation. To target PV interneurons for electrophysiology recordings, I transduced brain slices prepared from PV-cre mice with AAV vectors containing floxed green fluorescent protein (GFP). After 1-3 weeks post-transduction, GFP-positive PV interneurons were visualised and targeted at the same time as a nearby pyramidal neuron for dual-patch recordings (**Figure 5.2***A*). PV interneurons were recorded in cell-attached mode, which allowed me to leave the physiology and the intracellular environment unperturbed. These experiments confirmed that PV interneurons are recruited during the so-called 'inhibitory restraint' activity. During this period, PV interneurons increased their spiking rate, reaching a peak frequency of 9.4±1.8 Hz at 4-to-5 s before ED onset. However, at the onset of epileptiform events, the firing rate of PV interneurons abruptly fell to 1±0.5 Hz (**Figure 5.2***B*), which was reminiscent of the DB reported by previous work (Cammarota et al., 2013). This would indicate that DB limits the capacity of PV interneurons to contribute towards inhibitory restraint, which ultimately fails at ED onset.

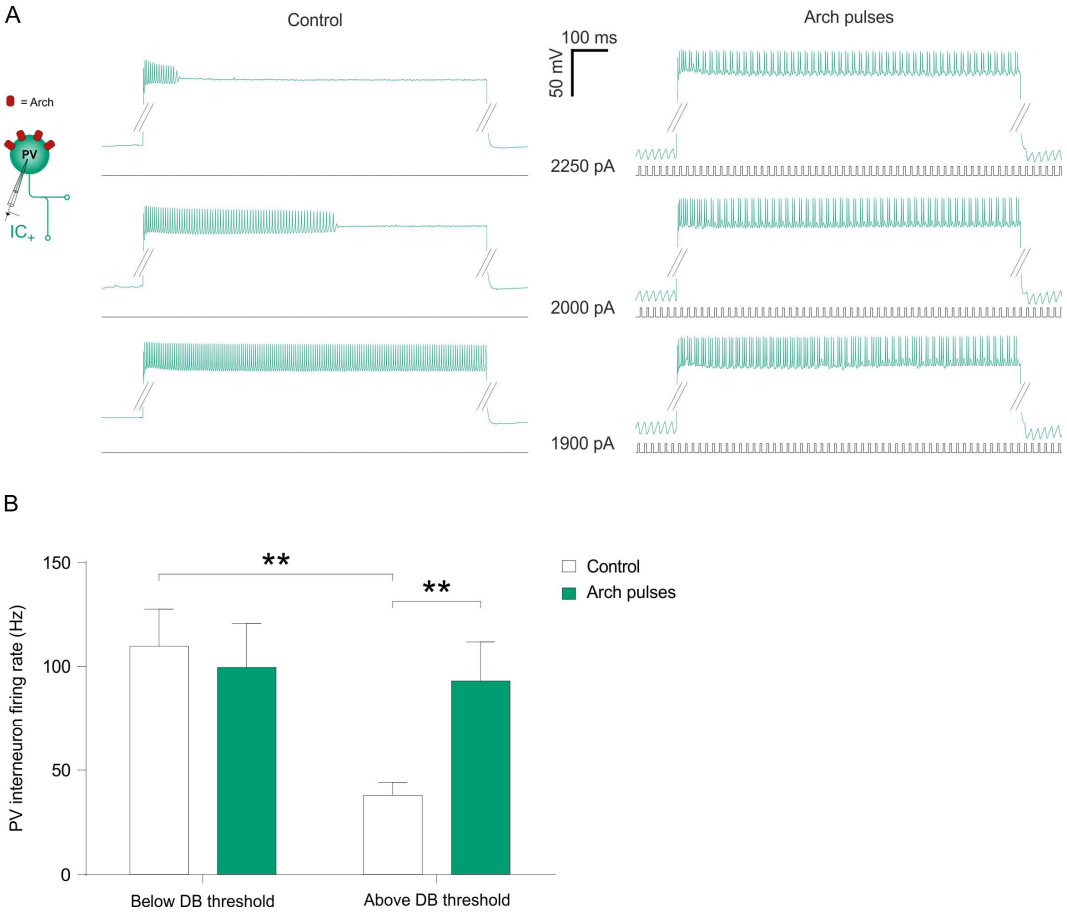

Figure 5.3. Pulsed activation of Arch re-enables spiking in PV interneurons experiencing depolarising block. (A) Cartoon (left) shows that PV interneurons were targeted with the light-driven outward proton pump archaerhodopsin (Arch) and recorded in current-clamp mode. Each of the six recordings (right) consists of a pair of traces representing the LED activation trace (bottom) and the voltage response to somatic current injection (top). The level of injected current is stated on the side of each recording. Arch was activated with 5 ms LED pulses at 50 Hz. **(B)** Arch stimulation was sufficient to reliably re-enable spiking at current injection levels above the threshold for depolarising block (DB) (interaction between current injection level and condition: N=8 cells; $F_{(1,7)}$=12.7; p=0.0092, repeated measures two-way ANOVA matching both factors, followed by Sidak's post-hoc multiple comparisons of firing output between conditions: below DB threshold, p=0.7091; above DB threshold, p=0.0075; and of firing output between the different current levels: control, p=0.0017; pulsed Arch, p=0.8644). ** indicates p<0.01.

5.4 An optogenetic strategy can recover action potential firing in PV interneurons undergoing depolarising block

To test the hypothesis that DB disables PV interneuron spiking, I then tested whether manipulating the membrane voltage of PV interneurons could modify this. I started by injecting positive current into a PV cell during targeted patch-clamp whole-cell recordings. I then used an optogenetic manipulation to modify the membrane potential of the PV cell. Here I utilised the light-activated proton pump Arch that can be used to elicit membrane hyperpolarisations (Chow et al., 2010). This technique allowed me to examine whether brief light-triggered hyperpolarisations could reactivate sufficient voltage-sensitive cation channels to re-enable firing of PV interneurons. To this end, I selectively expressed Arch in PV interneurons by transducing brain slices from PV-cre mice with AAVs delivering the floxed Arch construct. Brain slices were incubated for 3-4 weeks to allow expression of Arch in PV interneurons.

First, I performed current-clamp recordings of Arch-expressing PV interneurons in whole-cell mode, which enabled me to control the membrane voltage through current injections, and allowed me to find the DB threshold, defined as the current step during which spiking seized before the end of the step (**Figure 5.3***A*, middle control trace). Once the DB threshold was identified, several current steps were injected below and above DB threshold, during no activation or pulsed activation of Arch (**Figure 5.3***A*). To test the effect of Arch activation during DB, a widefield, ultrabright green LED was used to deliver 5-ms-long light pulses

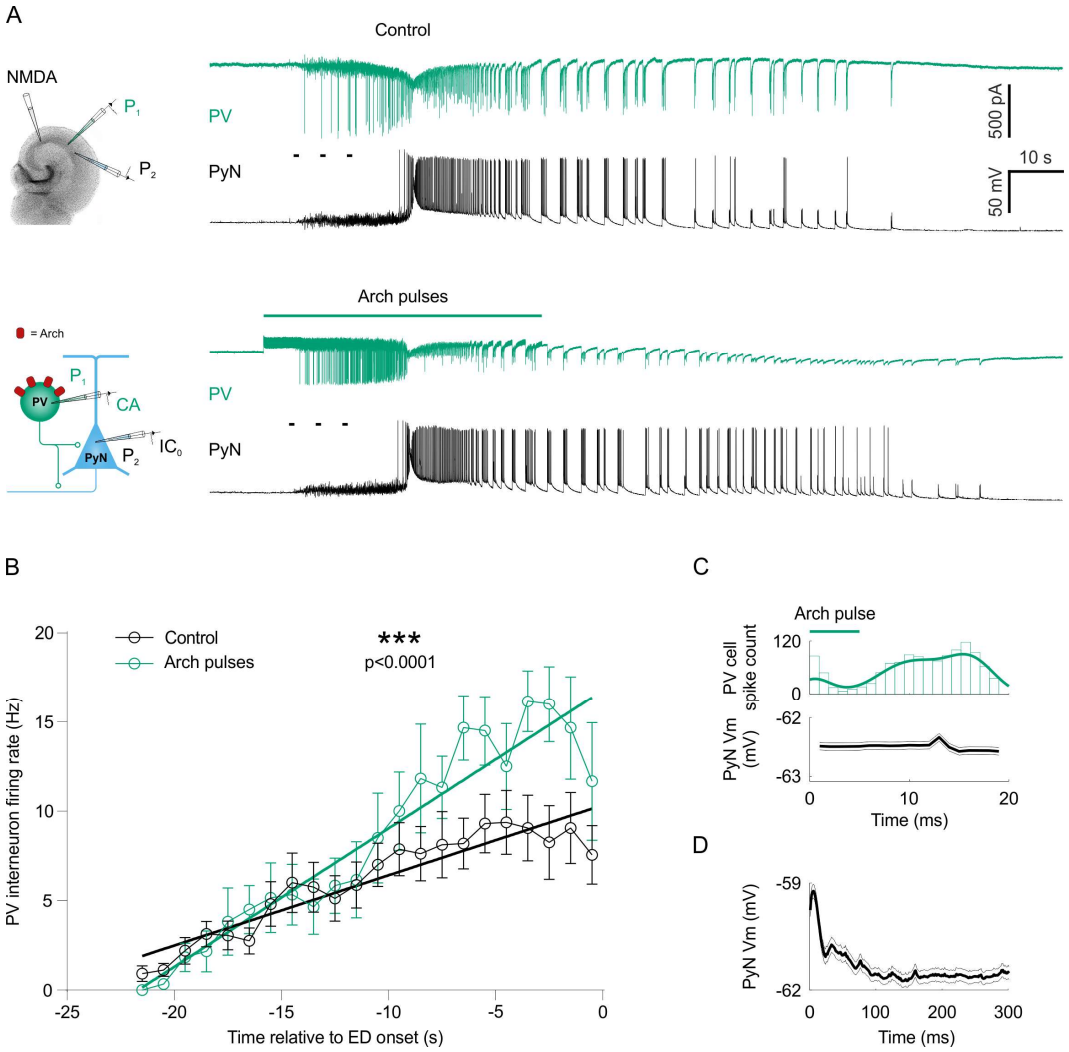

Figure 5.4. Pulsed activation of Arch boosts PV interneuron firing before the onset of epileptiform events. (A) Cartoons (left) showing that PV interneurons were targeted with Arch and recorded simultaneously with a pyramidal neuron during NMDA-triggered EDs. Traces (right) show an example dual patch recording of a PV interneuron (cell-attached, green) and a pyramidal neuron (current-clamp, black). Traces are shown for the two cells under control conditions (top) and during Arch pulses (bottom). Note the increase of firing of the PV interneuron when Arch is pulsed before the ED onset. The black bars above traces represent the timing of the NMDA puffs and their horizontal extension represents the puff duration. **(B)** Population data (N=16 EDs for the control condition and N=6 EDs for the pulsed Arch condition) shows an increase in PV interneuron firing prior to ED onset when Arch was activated (interaction between time relative to ED onset and condition: $F_{(1)}=18.97$; $p<0.0001$, one-way ANCOVA followed by Tukey-Kramer post-hoc comparison for slopes: control vs pulsed Arch, $p<0.0001$). (**C**) The histogram of PV cell firing, time-locked to the delivery of Arch pulses, shows increased firing

(figure legend continued on facing page) ——————————►

at 50 Hz to the entire brain slice. For somatic current injections that did not elicit DB, PV interneurons were able to fire action potentials at 109.8±17.9 Hz. At these levels of current injection, pulsed Arch activation had no significant effect on firing rate (99.7±21.2 Hz). By contrast, for current injections that evoked DB, current-induced depolarisation significantly decreased the firing rate to 38±6.1 Hz under control conditions. This confirmed that DB reduces PV interneuron spiking. When Arch was pulsed under these conditions, PV interneurons were able to fire action potentials at similar rates to when the neurons were below DB threshold (93.2±18.7 Hz). This confirmed that brief hyperpolarising pulses can recover the capacity of PV interneurons to fire action potentials (**Figure 5.3***B*).

To investigate whether the same Arch activation strategy can be used to boost PV interneuron firing before epileptiform events, I performed paired recordings from a pyramidal neuron and an Arch-expressing PV interneuron during NMDA-triggered EDs (**Figure 5.4***A*). The timing of evoked EDs was determined from the activity of pyramidal neurons recorded in current-clamp mode (**Figure 5.4***A*, black traces). As described in the previous section (**Figure 5.2**), under control conditions (no activation of Arch in PV interneurons) and before epileptiform events were triggered, NMDA stimulation recruited PV interneurons (example

---

following the light pulse offset (top). The thick green line superimposed to the histogram represents the fit of a kernel probability distribution. There was no evident entrainment of the pyramidal neuron membrane voltage (below) to the delivery of the Arch pulses. (**D**) Averaged membrane voltage from pyramidal neurons, time-locked to PV cell firing, confirmed that PV interneuron action potentials elicited postsynaptic inhibitory potentials onto pyramidal neurons. *** indicates $p<0.001$.

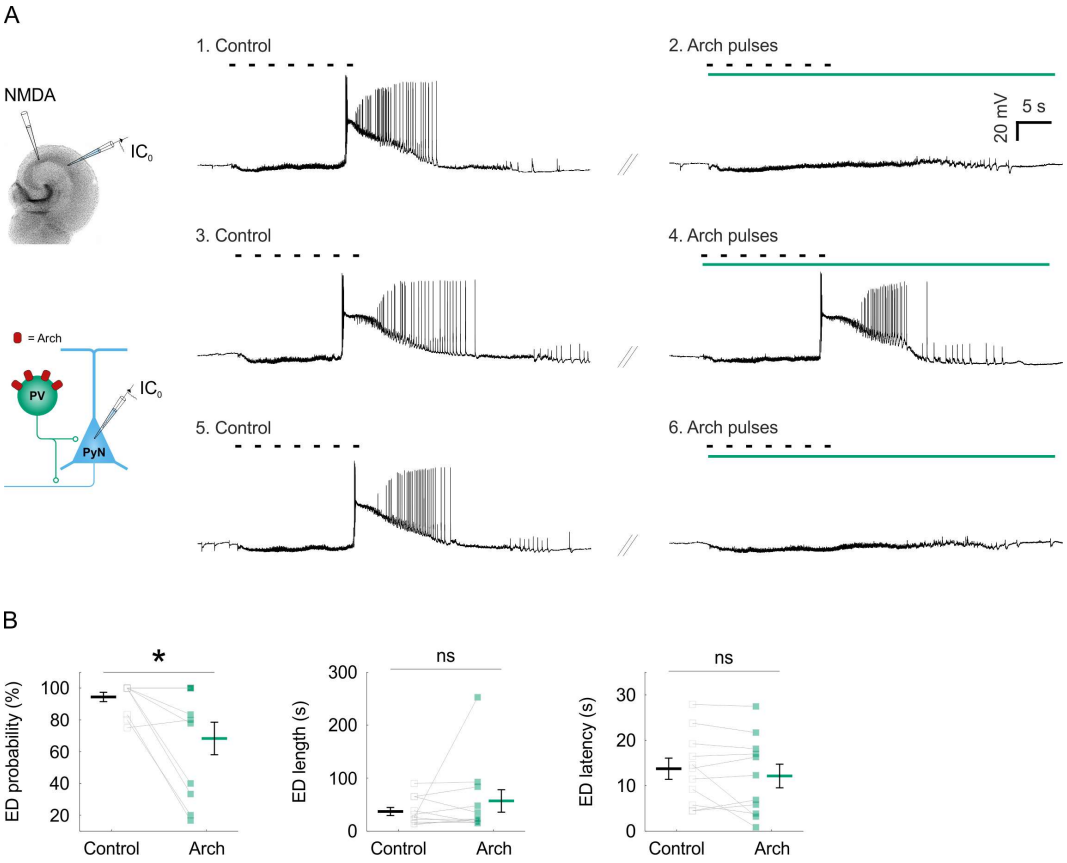

Figure 5.5. Pulsed activation of Arch in PV interneurons decreases the probability of epileptiform events. (A) Cartoons (left) showing that PV interneurons were transduced with Arch and activated optically while current-clamp recordings from pyramidal neurons were used as a readout of the network-wide NMDA-triggered EDs. Traces (right) show six (1→6) NMDA stimulations from the same slice in which EDs were initiated every 5 min and alternated between control and pulsed Arch conditions. In control conditions each NMDA stimulation evoked an ED. However, when NMDA stimulation was initiated at the same time with the train of LED pulses (5 ms pulses at 50 Hz, green bar), the probability of eliciting EDs was significantly lower. NMDA pressure pulses are indicated with black bars above the traces. **(B)** Population data (N=11 experiments) showing the impact of pulsed Arch activation on EDs. The ED probability dropped by 26.1% (top, $W_{(7)}=1$, p=0.0313, two-tailed matched-pairs Wilcoxon signed-rank test). No effect was observed on ED length (middle, $W_{(11)}=25$, p=0.5195, two-tailed matched-pairs Wilcoxon signed-rank test) or latency (bottom, $W_{(11)}=27$, p=0.6377, two-tailed matched-pairs Wilcoxon signed-rank test).

shown in **Figure 5.4***A*, top green trace), which increased their firing frequency until ED onset at a rate of 0.39±0.05 Hz/s (**Figure 5.4***B*, black trend line). Interestingly, pulsed Arch activation appeared to improve the NMDA-evoked recruitment of PV interneurons before ED onset (example shown in **Figure 5.4***A*, bottom green trace). Under these conditions, the speed at which PV interneurons raised their spiking frequency in response to NMDA stimulation increased to 0.77±0.07 Hz/s, leading to a peak firing rate of 16.2±1.7 Hz at 3-to-4 s before ED onset (**Figure 5.4***B*). This suggests that PV interneuron firing actually becomes impaired before the onset of epileptiform events, but can be rescued by brief periods of hyperpolarisation. Interestingly, Arch pulses did not appear to entrain the membrane voltage of pyramidal neurons, although PV interneuron spiking was confirmed to elicit postsynaptic inhibitory potentials onto pyramidal neurons (**Figure 5.4***C,D*).

5.5 Removing PV interneurons from depolarising block reduces the probability of evoking epileptiform events

Having shown that light-induced hyperpolarisation of PV cells rescues their firing capacity, I then investigated the impact of this improved PV interneuron spiking on epileptiform events. To this end, EDs were evoked by NMDA stimulation, and monitored via patch-clamp recordings from pyramidal neurons in the CA region. Epileptiform events were triggered every 4-5 min, alternating between control events and events where Arch was pulsed (**Figure 5.5***A*). Under control conditions (**Figure 5.5***A*, events 1, 3 and 5), the probability of triggering an epileptiform events was high, with an average of 94.4±3%. By contrast, when Arch was pulsed in PV

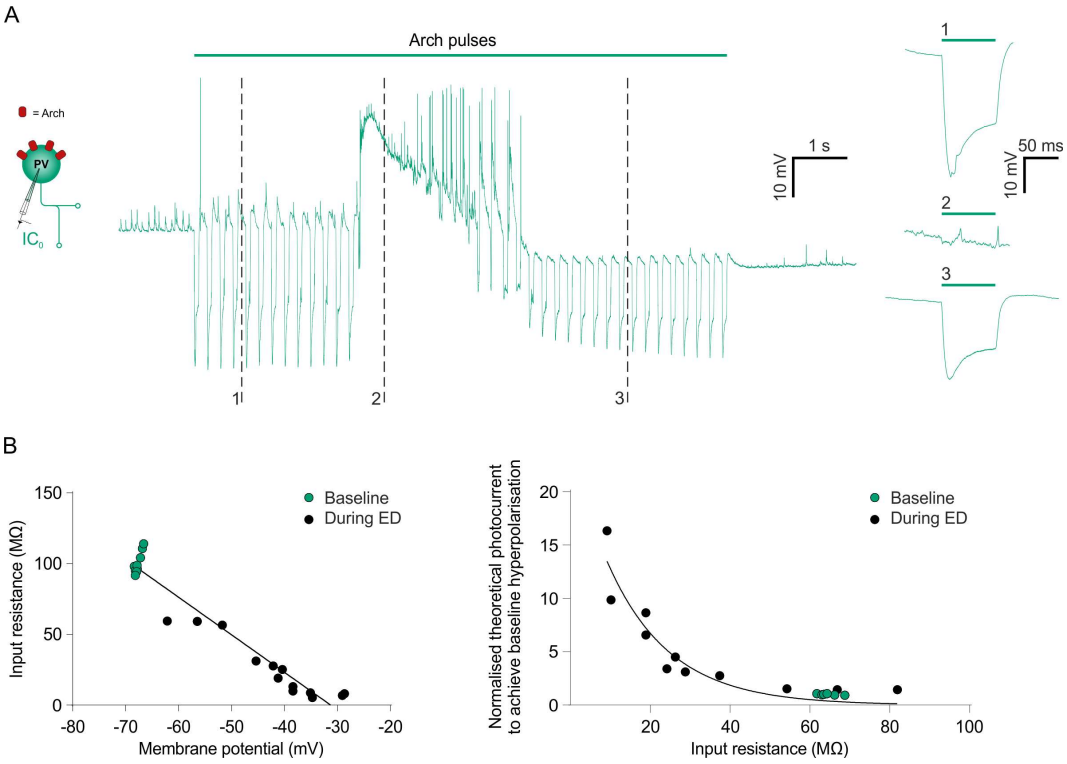

Figure 5.6. After ED onset pulsed activation of Arch cannot affect membrane potential due to changes in input resistance. (A) Cartoon (left) shows that PV interneurons were transduced with Arch and recorded in current-clamp mode. The ED trace (top, right) represents an example whole-cell recording of a PV interneuron during a spontaneous ED. Pulsed Arch activation (green bar) was initiated before the ED and continued for the entire duration of the ED. Note the lack of hyperpolarisation in response to Arch activation during the ED, particularly immediately following the onset of the ED (expanded traces below). **(B)** Data from two EDs showing the measured input resistance of a PV interneuron during baseline, and inferred input resistances during the EDs, plotted as a function of the cell's membrane potential. This was calculated by assuming a stable pulsed photocurrent across time. The input resistance (top) decreased monotonically with the membrane voltage (linear regression, $p<0.0001$, $R^2=0.95$, slope -2.66±0.14). The bottom panel illustrates the calculated photocurrent measured before ED, and the theoretical photocurrent required to obtain the same amount of hyperpolarisation over the range of input resistances inferred during ED (exponential growth model, standard deviation of residuals is 608.6 pA).

interneurons starting with the first NMDA stimulus, the chance of successfully evoking EDs was significantly reduced (**Figure 5.5***A*, events 2, 4 and 6). The probability of triggering EDs dropped by more than a quarter, to 68.3±10.2% during the pulsed Arch condition (**Figure 5.5***B*). When an ED was initiated, no change was detected as a result of Arch activation in terms of ED duration (37±7.7 s during control; 56.9±21.2 s during pulsed Arch) or ED latency (13.7±2.3 s during control; 12.1±2.6 s during pulsed Arch). This suggested that by maintaining the spiking output of PV interneurons during the period of inhibitory restraint, it is possible to reduce the probability of initiating an ED. In other words, increasing feedforward inhibitory strength can oppose epileptiform events.

5.6 Pulsed activation of Arch is limited by changes in the intrinsic properties of PV interneurons during epileptiform events

To investigate the effect of pulsed Arch activation on the membrane potential of PV interneurons, I targeted Arch-expressing PV interneurons for whole-cell recordings in current-clamp mode (**Figure 5.6***A*). Arch activation induced an average hyperpolarising step of 21.9±0.5 mV during baseline (i.e. before EDs). By contrast, at the onset of and during EDs, the hyperpolarising effect was markedly reduced, to the extent that it generated negligible effects on the membrane voltage. (**Figure 5.6***A*). I hypothesised that this was the result of a dramatic change in the cells' input resistance. Indeed, assuming a stable photocurrent was generated by each Arch pulse, I estimated that the input resistance dropped from 100.1±2.3 MΩ during baseline to levels below 10 MΩ around ED onset. The input resistance subsequently recovered in parallel to the membrane potential hyperpolarisation at

a rate of 2.66±0.14 MΩ/mV (**Figure 5.6***B*, top). To illustrate the impact of input resistance changes on the optogenetic manipulation, I inferred the theoretical photocurrent required to sustain the same amount of baseline membrane hyperpolarisation during epileptiform events (**Figure 5.6***B*, bottom). The inferred photocurrent followed a non-linear relationship with the input resistance (time constant τ=-15.58), and reached values above 3 nA around ED onset. This contrasts the calculated Arch-induced photocurrent of 218.6±5.4 pA during baseline (**Figure 5.6***B*, bottom). These results indicate that the Arch strategy of removing PV interneurons from DB, although successful when applied before the onset of EDs, is rendered ineffective once EDs have been initiated due to the associated shifts in input resistance.

5.7 Discussion

In this chapter, I investigated how DB affects PV interneuron function and the role this plays in the generation of EDs. Having established a reliable model of evoked seizure activity, I confirmed that PV interneurons initiate a mechanism of inhibitory restraint in response to surrounding hyperexcitability. However, these cells ultimately fall victim to DB that renders them ineffective when EDs are initiated. Making use of the optogenetic tool Arch, I was able to attenuate the current- or synaptically-induced DB prior to ED onset. Employing this strategy at the network level resulted in a lower probability of triggering epileptiform events, consistent with enhancing PV interneuron-mediated inhibitory restraint.

To investigate the cellular mechanisms that regulate the spread of epileptiform activity through the ‘penumbra’ region, I used an NMDA-evoked

seizure model (Losi et al., 2010, 2016), which I successfully established in mouse hippocampus. A reason for which I chose this model is that it provides good temporal control over the generation of EDs, and the elicited EDs were consistent in terms of latency and duration. Furthermore, using voltage-clamp recordings from pyramidal neurons allowed me to confirm the recruitment of inhibitory synaptic circuits in the period prior to ED initiation. By providing a temporal delay between the delivery of the NMDA stimulus and the onset of the epileptiform event, this model afforded the opportunity to study the mechanisms underlying inhibitory restraint. Cell-attached recordings confirmed the prediction that the PV interneuron population contributes to the stimulus-evoked inhibitory restraint, but that this interneuron population progressively enters DB prior to EDs.

The observed DB prior to EDs rendered PV interneurons incapable of sustaining their inhibitory activity to counteract excitation. Interneurons have been previously identified to enter a state of DB at the onset of epileptiform events (Ziburkus et al., 2006). This can occur as a result of constant inflow of positive somatic current of increasing strength and could be explained by the incomplete return of the voltage-gated Na^+ channels to a fully deinactivated state between action potentials (Bianchi et al., 2012). If delayed-rectifier K^+ currents are unable to counteract this effect and repolarise the membrane, spiking is impaired because the availability of voltage-gated Na^+ channels is progressively reduced. According to this model of DB, it should be possible to reverse this process by invoking negative somatic currents that generate membrane hyperpolarisations, de-inactivate the voltage-dependent Na^+ channels and re-enable spiking. The light-activated

proton pump Arch was identified as an optogenetic tool that could serve this purpose by extruding protons and hyperpolarising the neuronal membrane (Chow et al., 2010). By virtue of its precise temporal manipulation, rapid activation of Arch in PV interneurons generated tightly controlled light-induced hyperpolarisations. This strategy was effective in reversing both current- and synaptically-induced DB. The cell-attached recordings of PV interneurons expressing Arch revealed that pulsed Arch activation progressively enhanced action potential firing before the onset of epileptiform events. This supports the idea that PV interneurons experience some degree of DB prior to the onset of EDs.

Several factors may contribute to the extent of DB and the enhancement of spiking mediated by pulsed Arch activation. Firstly, as described above, the pulsed activation of Arch generates brief hyperpolarisations that are expected to facilitate de-inactivation of the voltage-gated Na^+ channels. Such Arch-induced hyperpolarisation is likely to be spatially non-uniform across neuronal compartments, since fine structures such as axonal processes and dendrites have a lower diameter and hence higher resistance (Magee, 2000). Consequently, the amplitude of the Arch-induced hyperpolarisations (**Figure 5.6**) may be underestimated by somatic recordings. Indeed, depending upon the subcellular expression pattern of the Arch protein, the extent of the membrane potential change may be greater in the axon or axonal terminals, where the effect of the membrane potential on voltage-gated Na^+ channels may be most important.

Secondly, both the amount and the kinetics of membrane depolarisation are thought to contribute to DB (Mickus et al., 1999). Larger depolarisations are

expected to exacerbate DB, as observed during my experiments investigating the current-induced DB. However, a degree of DB can also occur during smaller but more prolongued depolarisations, such as in the case of the synaptically-induced DB prior to ED onset. Indeed, two forms of inactivation of voltage-gated Na^+ channels have been distinguished, which have been linked to distinct channel properties, and operate over different time scales. These have been referred to as fast and slow inactivation, although both forms are reversed by hyperpolarisation (Rudy, 1978; Vilin and Ruben, 2001). Whilst fast inactivation occurs rapidly over the course of an action potential, slow inactivation is elicited by prolonged depolarisation over several seconds (Mickus et al., 1999). In my experiments, the DB induced by somatic current injection was more likely to incorporate fast inactivation, and was evident when PV interneurons fired action potentials at high frequency. By contrast, the synaptically-induced DB was more likely to involve slow inactivation during the relatively long time window of pre-ED inhibitory restraint, and was evident at lower spiking frequencies. Therefore, these two types of voltage-gated Na^+ channel inactivation could explain why DB was observed at different PV interneuron firing rates. The time scale of inhibitory restraint fits with that of the slow inactivation of voltage-gated Na^+ channels. This suggests that slow inactivation of voltage-gated Na^+ channels may play a more important role in limiting the output of PV interneurons during inhibitory restraint. One could imagine experiments to test this by pharmacologically manipulating voltage-gated Na^+ channel inactivation. An example of such an experiment would be using the δ opioid receptor agonist SNC80 (Remy et al., 2004) that has been shown to

preferentially enhance slow but not fast inactivation processes. If PV interneuron firing during the pre-ED phase is limited mainly by slow inactivation of voltage-gated Na^+ channels, the SNC80 drug could potentially promote the collapse of inhibitory restraint. Indeed, SNC80 has been shown to have proconvulsant properties when administered systemically in rats (Bausch et al., 2005). Therefore, the development of drugs that preferentially remove the slow inactivation of voltage-gated Na^+ channels may be useful, although a targeted approach for PV interneurons is more desirable than a non-specific manipulation that can have multiple side effects. This could include modifying voltage-gated Na^+ channels with impaired slow inactivation, which could be specifically delivered to PV interneurons via viral vectors. These hypothetical channels could potentially sustain firing in this interneuron population, even when the endogenous voltage-gated Na^+ channels have undergone slow inactivation.

Thirdly, brief hyperpolarisations may also promote spiking through rebound excitation following the offset of optogenetic stimulation. The underlying cause of the potential rebound excitation could be recruitment of the hyperpolarisation-activated, cyclic nucleotide-gated (HCN) ion channels. These channels are predominantly permeable to Na^+, and have been shown to be expressed in PV interneurons (Aponte et al., 2006). Whereas only a fraction of the HCN channels are open at 'normal' resting membrane potentials, additional channels are recruited by more hyperpolarised states (Poolos, 2012). Thus, Arch-induced hyperpolarisations could theoretically trigger greater Na^+ fluxes through HCN channels, which may generate a rebound depolarisation and action potentials

immediately following the offset of Arch activation. Moreover, HCN channels appear to be predominantly distributed in the soma of hippocampal interneurons (Brennan et al., 2016). Therefore, it may mean that this mechanism is particularly relevant for the PV interneuron (Chen et al., 2001; Lupica et al., 2001). However, HCN channels are open at membrane potentials more negative to -50 mV (Shah, 2018) and neuronal depolarisation appears to deactivate them (Brennan et al., 2016). Taken together, this suggests that although HCN channels may influence PV interneuron excitability under baseline conditions, it seems unlikely that HCN channels contributed to the action potential firing that occurs at more depolarised membrane voltages during epileptiform events. Consistent with this, PV interneuron firing following the offset of Arch pulses did not appear to be entrained by the light activation (**Figure 5.4***C*), but showed a rather wide distribution of spike timing between Arch pulses.

Having considered these additional factors, the network effects observed by optogenetically manipulating PV interneurons seem very likely to have been primarily mediated by the successful reversal of a progressive DB during the pre-ED period. An additional possibility is that Arch pulses resulted in entrainment of the network, which might have also increased the recruitment of PV interneurons. However, I could not detect any entrainment of the pyramidal neuron membrane voltage by the Arch pulses, although PV interneurons did elicit postsynaptic inhibitory effects (**Figure 5.4***C,D*). This suggests that, rather than through network synchronisation, the recovery from inactivation of PV interneuron firing was the main contributor to increasing PV cell spiking. Pulsed Arch activation reduced the

probability of triggering EDs by 31.7%, without affecting ED length or latency. The fact that I did not detect an effect on ED latency could be explained by me not monitoring the position of the recorded neurons relative to the location of the NMDA puff. This may have introduced heterogeneity in ED latency measurements. Another explanation could be that a small change in ED latency may be masked by the variability of latencies to epileptiform events under control conditions. Meanwhile, although recruiting PV interneurons can maintain afterdischarge activity during later phases of EDs (Ellender et al., 2014), the fact that pulsed Arch activation did not significantly affect ED length suggests that this optogenetic strategy may be limited to promoting action potential firing in the pre-ED phase.

PV interneurons could be more susceptible to undergoing DB compared to other cell types. This may occur as a result of the fact that PV interneuron function relies on K^+ channels of the Kv3 type. These ion channels are selectively expressed in PV cells, and are essential for determining their fast spiking phenotype (Du et al., 1996). Given PV cells rely more on K^+ channels, they could be particularly sensitive to increases in extracellular K^+ during intense network activity. Future experiments testing how changes in extracellular K^+ concentration alters action potential generation in different cell types. If PV cells are revealed to be specifically sensitive to extracellular K^+ ions, identifying and targeting K^+ channels with potentially different properties or activation/inactivation kinetics might be useful for preventing DB in PV interneurons.

It is commonly considered that the onset of seizure activity occurs when the excitatory neurons are recruited to the depolarising shifts. Consistent with my data,

PV interneurons are recruited early by surges in excitation in the network, but excitatory neuron activity is limited by a powerful inhibitory restraint to which PV cells rapidly contribute (Parrish et al., 2019). It is possible that the increased inhibitory input to pyramidal neurons during this phase leads to intracellular Cl^- loading, which may cause excitatory neuron burst firing, precipitating the ED and causing the DB in PV interneurons. To test this, monitoring Cl^- levels in pyramidal neurons using optical or electrophysiological methods during the pre-ED phase can confirm whether excitatory neurons do indeed accummulate Cl^- intracelluarly. If this is the case, manipulating the intracellular Cl^- level in pyramidal neurons should impact the network's progression to EDs. Tools such as Cl-out (Alfonsa et al., 2016) or overexpressing KCC2 (Magloire et al., 2018) could help extrude Cl^-, while tools such as halorhodopsin may be used to investigate if Cl^- loading precipitates EDs.

Drugs that operate on the inactivation of Na^+ channels, such as carbamazepine, are commonly used as therapy in epilepsy. It is remarkable that these drugs do not actually promote DB in PV cells and facilitate seizures, especially since PV interneurons can sustain a very high action potential firing rate. Interestingly, carbamazepine and other anticonvulsants with Na^+ channel blocking activity, appear to preferentially affect spiking in pyramidal neurons (Pothmann et al., 2014). Therefore, the anticonvulsant action of this class of drugs results from sparing feedback and feedforward mechanisms.

My data has revealed that the Arch-induced hyperpolarisations in PV cells became drastically attenuated at the same point that the membrane became rapidly depolarised at the start of an ED. Assuming a constant photocurrent is generated by

the proton pump, this observation suggests that the input resistance of neurons also shows a pronounced drop at the onset of EDs. The sudden drop in input resistance is likely explained by the rapid increase in transmembrane channel opening probability, given the intense release of neurotransmitters caused by recruitment of large numbers of neurons to the epileptiform activity. The observed changes in membrane properties ultimately constitute a major limitation for the optogenetic strategy that I employed, rendering Arch activation ineffective at the moment of ED onset. The estimated amount of photocurrent necessary to maintain Arch-induced hyperpolarisations immediately after the start of EDs cannot be delivered by Arch (Chow et al., 2010). Other optogenetic strategies may be more effective. For example, the enhanced chloride pump Jaws (Chuong et al., 2014) may be sufficiently powerful to generate such photocurrents. However, pumping Cl^- into a cell type identified to have high levels of resting Cl^- may result in unwanted depolarising effects (Raimondo et al., 2012b). Therefore, the 'full' DB observed at the onset of EDs could not be rescued by Arch pulses. However, Arch activation successfully recovered PV firing before the onset of EDs, consistent with the possibility that PV cells may progressively enter a 'partial' DB prior to the onset of EDs. This could support the hypothesis that DB in PV interneurons causes EDs, which is supported by my results from network experiments demonstrating reduced probability of EDs when Arch pulses are used to modulate PV interneuron activity. Alternatively, it could be possible that, for example, K^+ accummulation in the extracellular space may be the principle cause, pushing both PV cells to enter DB and the pyramidal neurons to become hyperexcitable and generate EDs. If this is

the case, manipulating extracellular K^+ dynamics during the pre-ED phase, for example by promoting the astrocytic uptake, could prevent EDs.

The effects of pulsing Arch in interneurons should be further explored, since Arch acts as a proton pump and may change intracellular pH. Activation of Arch in excitatory neurons leads to a limited change in their intracellular pH, which stabilises rapidly by reaching a plateau (Chow et al., 2010). Still, it will be interesting to study what the pH dynamics are in the different subtypes of interneurons. To this end, optical probes such as ClopHensorN may be useful in reading intracellular pH during activation of Arch. However, Arch should not be fused with a fluorophore, as this can contaminate the fluorescence emmited by ClopHensorN.

More generally, the data presented in this chapter represents a proof of principle that an optogenetic strategy can counteract DB and enable PV interneurons to maintain inhibitory restraint of epileptiform events.

Chapter 6: General Discussion

In this last chapter I summarise my results and I consider potentially associated methodological shortcomings. Then I discuss how my results could be relevant in understanding the pathophysiology of seizures and I propose areas where this research can be extended in the future.

6.1 Experimental findings

In chapter 3 of my thesis I made use of a combination of *in vitro* and *in vivo* animal models to demonstrate that chemogenetically boosting synaptic output from specific GABAergic interneuron subtypes can suppress seizure activity. To achieve this, I coupled promoter-specific cre recombinase mice with viral-mediated delivery of chemogenetic constructs that I expressed in an *in vitro* model of drug-resistant temporal lobe epilepsy. This approach enabled me to manipulate the activity of three major interneuron lineages of the hippocampus, namely the PV, SST and VIP populations. Targeted electrophysiological recordings from both presynaptic interneurons and postsynaptic principal neurons revealed that each of the three interneuron populations increased their firing rate and synaptic output following CNO-mediated activation of hM_3D_q DREADD receptors. Whilst recruiting VIP interneurons did not change the total duration of the EDs, boosting PV and SST interneuron output robustly reduced epileptiform activity by decreasing event frequency. PV interneurons were able to generate the strongest effect per cell, exhibiting a five-fold greater ability to suppress EDs compared to their SST or VIP counterparts. Consistent with this, recruiting PV interneurons in

an *in vivo* model of acute temporal lobe seizures attenuated convulsive behaviours by more than 80%. This confirmed the potential of this chemogenetic strategy to suppress seizure activity by boosting endogenous inhibitory mechanisms in a cell-type-specific manner.

In chapter 4 I set out to investigate the intracellular pH and Cl^- concentration dynamics experienced by pyramidal neurons and PV, SST and VIP interneurons during EDs. To this end, a floxed version of the pH and Cl^- reporter ClopHensorN was designed. This allowed me to express the fluorescent probe separately in pyramidal cells as well as in all three interneuron subtypes. I combined whole-cell patch-clamp recordings of pyramidal neurons with confocal imaging to allow me to correlate epileptiform activity with the ion concentration transients reported by ClopHensorN. Using this approach, I found that, under baseline conditions, VIP interneurons had a more acidic intracellular somatic environment compared to the other interneuron subtypes. However, during epileptiform activity, all cell types exhibited acidification in a manner that reflected their resting pH. The PV interneurons acidified the most and their pH transients were maximal even for short epileptiform events. By contrast, the VIP interneurons experienced the lowest increase in H^+ concentration, reaching their maximal pH response only during longer epileptiform events. In terms of Cl^- differences, I found that the PV interneurons had the highest resting intracellular Cl^- concentration. Epileptiform activity induced intracellular Cl^- loading in pyramidal neurons, SST and VIP interneurons. By contrast, PV interneurons did not load Cl^-, but in fact appeared to unload Cl^-. This unloading effect was negatively correlated with the resting Cl^-

concentration. Moreover, the PV cells were associated with less pronounced changes of their intracellular Cl^- concentration during EDs compared to the other cell types. Taken together, these findings indicate that distinct subtypes of hippocampal GABAergic interneuron establish their pH and Cl^- homeostasis differently. The fact that interneuron subtypes can exhibit different ion transients is likely to impact how these cell populations contribute to network activity in health and disease.

In chapter 5 I investigated the DB mechanism that is thought to limit how PV interneurons provide inhibitory restraint against epileptiform events. To achieve this, I used optogenetics to prevent PV interneurons from entering into DB, in order to allow them to enhance the inhibitory restraint and help avert the initiation of EDs. I first established an *in vitro* model of seizure recruitment, in which I confirmed that PV interneurons contribute to inhibitory restraint. Combining PV-cre mice with viral-mediated delivery of the inhibitory opsin, Arch, allowed me to selectively manipulate the membrane potential of PV interneurons. I then demonstrate that brief Arch-mediated hyperpolarisations are capable of recovering PV interneuron firing both during current- and synaptically-induced DB. When employed at a population level, this optogenetic strategy resulted in a reduction in the occurrence of epileptiform discharges. This provides a proof of principle that it may be possible to enhance PV interneuron-mediated inhibitory restraint within the epileptic penumbra, in order to disrupt seizure propagation.

6.2 Methodological considerations

6.2.1 Seizure models

All of my *in vitro* experiments were performed in mouse organotypic hippocampal brain slices. This system is practical as it lends itself to a wide range of experimental methods and procedures, while providing the opportunity to examine spontaneously generated epileptiform events. For example, by using organotypic brain slices, I was able to perform targeted patch-clamp recordings, to deliver molecular-genetic tools and to perform optical measurements in parallel with electrophysiological measurements. Organotypic hippocampal slices retain a high degree of similarity to the hippocampus *in vivo*, preserving the tissue organisation and electrophysiological properties of the mossy fibre pathway (Gutiérrez and Heinemann, 1999). At the same time, at a cellular level, neurons in organotypic hippocampal slices develop equivalently and maintain the morphological and signalling characteristics of age-matched neurons in the intact hippocampus (De Simoni et al., 2003).

However, under culture conditions, the tissue suffers a loss of afferent connections from other brain structures following the explant of hippocampal slices, most notably the contralateral hippocampus, the septum and the entorhinal cortex. This in turn favours mossy fibre sprouting and the generation of aberrant synapses and recurrent excitatory connections between the DG and CA1 areas (Gutiérrez and Heinemann, 1999). This pattern of hippocampal circuit reorganisation is thought to be a feature of temporal lobe epilepsy, as suggested by evidence from several animal models of established epilepsy (Frotscher and

Zimmer, 1983; Ben-Ari et al., 1984; Tauck and Nadler, 1985; Cavazos and Sutula, 1990; Shibley and Smith, 2002) and from hippocampal tissue from patients who underwent resective epilepsy surgery (Babb et al., 1991; Isokawa et al., 1993). Consistent with this rearrangement of the excitatory circuit, organotypic hippocampal slices exhibit increased glutamatergic neurotransmission (De Simoni et al., 2003), and appear to undergo a process of post-traumatic epileptogenesis allowing them to develop spontaneous epileptiform activity (Dyhrfjeld-Johnsen et al., 2010; Lillis et al., 2015). Thus, properties that distinguish organotypic slices from the intact hippocampus, such as denervation and synaptic reorganisation, are considered hallmarks of temporal lobe epilepsy (Bausch and McNamara, 2000). Nonetheless, it is not entirely clear if the organotypic hippocampal slices recapitulate aspects pertaining to sclerosis, or to what degree the early bursting activity reflects the fact that the tissue is collected at a young age when axonal growth is facilitated. Axonal sprouting of mossy fibres may trigger spiking similar to a developmental process required to guide the maturation of the newly formed synapses (Dyhrfjeld-Johnsen et al., 2010).

Several regions of the hippocampus may be important in seizure generation. Given that mossy fibre sprouting originates in the DG, and if we consider the possible contribution of this process to increasing network excitability, the DG plays an important part in seizure generation. At the same time, the CA3 area contains mutually connected pyramidal neurons, which could also participate in producing runaway excitation. Several studies also demonstrated that epileptiform activity can be readily triggered by tetanic stimulation and sustained in isolated

hippocampal CA1 regions (Fujiwara-Tsukamoto et al., 2004; Isomura et al., 2008). Although each of these regions individually are important in generating/sustaining epileptiform activity, they contribute cooperatively to support spontaneous synchronous activity through aberrant recurrent connections within the trisynaptic circuit (Gutiérrez and Heinemann, 1999).

In my experiments, I was able to exploit this capacity of organotypic hippocampal slices to generate spontaneous epileptiform activity. This enabled me to both monitor and manipulate the activity and ion dynamics of specific interneuron populations of the hippocampus during epileptiform events. Of particular relevance to my work on inhibitory interneurons, is the observation that GABAergic transmission remains intact in the organotypic hippocampal preparation, probably because the axons of local inhibitory circuits are less likely to be severed during the slicing procedure (De Simoni et al., 2003). Moreover, to validate the fact that GABAergic interneurons retain their specific morphological patterns in this preparation, I showed that the distribution profiles of neuronal processes from distinct interneuron populations is consistent with that found in the intact hippocampus (Léránth et al., 1984; Acsády et al., 1996; Katona et al., 1999; Pawelzik et al., 2002; Chamberland et al., 2010; Bartos and Elgueta, 2012; Lovett-Barron et al., 2012; Tyan et al., 2014) (**Figure 3.1**, **Figure 3.3**). Taken together, these findings support the conclusion that GABAergic interneurons preserve their morphological and functional characteristics in organotypic hippocampal slices. Therefore, using this tissue preparation allows for the study of the inhibitory system of the hippocampus in the context of EDs.

An alternative to organotypic slices would be the use of acute slices, which offer the advantage that the brain tissue is left to develop under normal conditions in the intact animal up to the point of the explant. This method is thought to preserve more of the anatomy and function of the neuronal network as found *in vivo*. However, acute slices do not exhibit spontaneous epileptiform activity, and therefore do not represent a model of temporal lobe epilepsy. Epileptiform events are not readily triggered in acute hippocampal slices, and the resulting EDs are generally short-lived. Furthermore, acute hippocampal slices do not lend themselves to imaging studies. This is due to the accumulation of surface debris that results from neuronal death induced by the slicing procedure. By contrast, organotypic preparations are characterised by a clear tissue surface and afford good optical access for imaging experiments using genetically encoded reporters (Raimondo et al., 2016).

In addition to using spontaneous EDs in organotypic slices as a model of seizure activity in temporal lobe epilepsy, I also used NMDA *in vitro* and 4-AP *in vivo*. Local application of NMDA in brain slices has been established as a model of focal seizure activity and has been previously used to investigate the initiation and spread of epileptiform events with high spatial and temporal fidelity in cortex (Losi et al., 2010; Sessolo et al., 2015; Losi et al., 2016). In my experiments, local application of NMDA in the hippocampus resulted in epileptiform activity that was generalised across the whole preparation, without evidence of gradual propagation. This could be explained by the fact that the hippocampus has a different architecture compared to the neocortex, and the relatively simpler trisynaptic hippocampal

circuitry may allow much faster propagation speeds of epileptiform activity. In addition to the different tissue organisation, the organotypic hippocampal slices are known to become hyperexcitable as a result of the recurrent excitatory connections that form *in vitro* (Gutiérrez and Heinemann, 1999). A disadvantage of the NMDA model is the fact that it is not a model of epilepsy, but rather a model of evoked seizures. This model therefore cannot be used to study features of chronic epilepsy. However, a major advantage of this model is that by extending the pre-ED time window, one is afforded the important opportunity to study the mechanisms underlying inhibitory restraint. This 'restraint' phenomenon is thought to represent a barrage of inhibition in the area surrounding the seizure focus (the so-called 'penumbra') (Trevelyan et al., 2006). In conclusion, although the NMDA model does not lend itself to studying chronic epilepsy, it provides a valuable opportunity to investigate the critical factors and mechanisms pertaining to inhibitory restraint.

The *in vivo* 4-AP model was chosen to confirm the anticonvulsant potential of chemogenetically boosting PV interneuron output, because it allows for a controlled focal induction of seizure activity (Salam et al., 2017). An alternative to this acute model would be a chronic *in vivo* model of epilepsy, such as the pilocarpine or kainic acid models. These models of epilepsy capture the process of epileptogenesis underlying the development of spontaneous seizures, which is thought to provide a more accurate reproduction of the pathophysiology in epileptic patients. However, these chronic models require the animals to undergo a more complex protocol, with significant mortality rates. These models consist of inducing a single acute prolonged seizure (or status epilepticus) by injecting a

proconvulsant drug, such as kainic acid or pilocarpine, either in the brain of the animal or intraperitoneally (Reddy and Kuruba, 2013). This is followed by a latent period after which animals start to spontaneously exhibit seizures (Kandratavicius et al., 2014). The variability in frequency and severity of the spontaneous seizures, and the fact that epileptic events may be triggered from outside of the hippocampus, are reasons why a more controlled and rapid methodological approach was preferred. Moreover, models of acutely triggered focal seizures proved to be instrumental in the development of anti-seizure drugs (Kupferberg, 2001).

When combining cellular manipulations with seizure models, it is important to consider how these processes may interact with one another at the cellular level. For example, using the K^+ channel blocker 4-AP is known to induce recurrent epileptiform discharges both *in vitro* and *in vivo* (Szente and Baranyi, 1987; Armand et al., 1999). It has been shown that 4-AP blocks channels in the Kv1 and Kv3 family, as well as D-type currents. This causes a considerable increase in neuronal excitability (Gustafsson et al., 1982; Storm, 1988). At the same time, blocking K^+ channels with 4-AP leads to enhanced presynaptic Ca^{2+} influx at the level of synaptic terminals, by prolonging the duration of presynaptic action potentials (Jones and Heinemann, 1987). Interneuron excitability seems to be preferentially affected by low doses of 4-AP, perhaps because their generally fast-spiking phenotype relies more on K^+ channels of the Kv3 family (Segal, 1987; Martina et al., 1998). Indeed, hippocampal GABAergic interneuron activity was shown to be promoted by 4-AP, which can then encourage synchronised activity in pyramidal neurons by eliciting postsynaptic hyperpolarising potentials (Segal,

1987; Perreault and Avoli, 1992; Sinha and Saggau, 2001). This synchronising effect on the network can initiate epileptiform discharges. Furthermore, the synchronous release of GABA, coupled with the activity-induced extracellular K^+ accumulation, are implicated in allowing hyperexcitability to develop (Segal, 1987; Perreault and Avoli, 1992). The fact that the 4-AP model may have specific effects on interneuron excitability could be a caveat of the current work, since GABAergic interneurons were also the target for the chemogenetic manipulation. However, whereas the 4-AP was applied focally into the hippocampus, DREADDs expression was widespread across the rostro-caudal extent of the hippocampus and the CNO was delivered systemically. Therefore, the chemogenetic effects would be expected to involve PV interneurons throughout hippocampal regions around the seizure focus. Moreover, the fact that convulsive behaviours were preferentially suppressed is consistent with preventing seizure spread.

6.2.2 Estimating the intracellular pH and Cl^- concentration

A floxed version of the ClopHensorN reporter was designed to measure the intracellular pH and Cl^- concentration in genetically defined neuronal populations (chapter 4). Although this fluorescence indicator affords simultaneous and independent quantification of pH and Cl^- concentration, there are challenges associated with using this technique. This is largely due to the relatively complex inference process required to translate optical signals into absolute concentrations of the two ion species. For example, the requirement to alternate between different excitation wavelengths may pose optical challenges related to their differential scattering in brain tissue (Sato et al., 2017). Moreover, fluorescence indicators like

ClopHensorN require calibration, which is inevitably performed in a different set of cells than the one that is ultimately investigated. Furthermore, the need for optical signals to be translated into ion concentrations by inference against a population average may introduce measurement noise. However, despite these limitations, ClopHensorN holds many advantages in measuring intracellular pH and Cl^-, which is why I chose to employ this technique. Next, I consider potential alternatives to using this reporter, and their associated strengths and weaknesses, which ultimately explain why ClopHensorN was selected as an appropriate indicator for H^+ and Cl^-.

The first measurements of intracellular pH used pH-sensitive microelectrodes (Rose and Deitmer, 1995). However, this technique was limited by the size of these microelectrodes and by the damage they inflicted to the cells being recorded. An alternative approach is to use pH-sensitive dyes, such as fluorescein analogues (Boyarsky et al., 1988). However, these have been shown to block the Ca^{2+}/H^+ ATPase (Gatto and Milanick, 1993; Chesler, 2003), an important mechanism contributing to activity-dependent intracellular acidification (Schwiening et al., 1993; Svichar et al., 2011). Genetically encoded GFP-based pH indicators, such as ClopHensorN, do not suffer from these limitations. In addition, these genetic biosensors have a number of advantages such as the capability for cell-specific and subcellular targeting, higher signal-to-noise ratio and spatial resolution, no interaction with the intracellular pH regulatory processes and no fluorophore leakage (Bizzarri et al., 2009).

As with pH techniques, measurements of intracellular Cl^- concentration were first made possible by Cl^--sensitive electrodes (Mauro, 1954). However, this

technique had slow kinetics for detection and the damage it introduced to the recorded cells led to electrophysiology techniques, namely perforated patch-clamp recordings, being preferred. This allowed Cl^- levels to be indirectly inferred by estimating E_{GABA_A}. The gramicidin perforated patch method was shown not to perturb intracellular Cl^-, since gramicidin pores are not permeable to Cl^- (Kyrozis and Reichling, 1995). However, these pores are permeable to small cations such as Na^+, K^+ and H^+, which could potentially influence E_{GABA_A} and therefore the inferred Cl^- concentration. An additional electrophysiological method for estimating Cl^- involves a dual cell-attached configuration in which $GABA_A$ and NMDA receptor currents are recorded (Tyzio et al., 2008). Measuring the reversal of NMDA receptors permits the estimation of the resting membrane potential, while determining E_{GABA_A} subsequently allows Cl^- levels to be inferred. This approach has the advantage of being less invasive and enables a more accurate measurement of the resting membrane voltage and therefore of the Cl^- driving force, virtue of the fact that shunting conductances induced by the whole-cell patch-clamp configuration are absent (Tyzio et al., 2008). Nonetheless, the cell-attached method is suitable for estimating resting states rather than ion dynamics, and generally electrophysiological methods sample relatively slowly. Furthermore, the electrophysiological methods rely on $GABA_AR$ activation in order to calculate E_{GABA_A}. This poses a significant challenge when trying to estimate intracellular Cl^- during epileptiform events, particularly given the significant drop in input resistance induced by epileptiform activity (**Figure 5.6**).

The alternative to electrophysiological methods is live cell imaging. Cl^--sensitive quinolinium-based dyes were used initially as they were easily loaded into neurons and they were suitable for two-photon imaging. However, these techniques were limited by low signal-to-noise, toxicity, leakage and bleaching (Bregestovski et al., 2009). Next came the development of ratiometric genetically encoded Cl^- indicators such as Clomeleon and Cl-sensor (Kuner and Augustine, 2000; Markova et al., 2008; Grimley et al., 2013). These reporters were not plagued by artefacts related to reporter concentration, but were influenced by changes in intracellular pH. The approach was later improved, which led to the development of ClopHensor and ClopHensorN (Arosio et al., 2010; Raimondo et al., 2013). The main advantage of these probes is their ability to accommodate for changes in intracellular pH. A related molecule to ClopHensorN is a new reporter called LSSmClopHensor, which has been shown to be compatible with *in vivo* imaging if the effects of brain tissue on the sensor's spectrometry are accounted for (Sato et al., 2017). As ClopHensor-based reporters use multiple wavelengths, they are vulnerable to the effects of tissue scattering. Correcting for spectral alteration caused by brain structures is most important when imaging deep in tissue, which is needed when imaging *in vivo*. It is unlikely that my measurements were affected by this phenomenon given that the neurons I recorded were superficial in the tissue, and organotypic slices are thin. One particularity of optically interpreting Cl^- is that the calibration curve of ClopHensor-based reporters has better resolution for inferring changes in ratio values for lower Cl^- concentrations. Therefore, high values of inferred Cl^- may be associated with an increased estimation error, compared to low values of inferred

Cl^-. This is particularly relevant for Cl^- levels estimated in PV interneurons. Therefore, the intracellular Cl^- concentration in PV interneurons might be slightly overestimated. Another limitation of ClopHensorN or LSSmClopHensor is that the fitted time constant for Cl^- interaction at pH 7 is ~175 ms, which restricts the temporal resolution at which Cl^- dynamics can be measured. Finally, all ratiometric reporters critically depend on the stoichiometry between the two fluorophores from which they are constructed. Alterations in intracellular production or degradation of proteins may potentially affect the coupling of the two fluorophores. Fortunately, I found no evidence of separation and/or aggregation of fluorophores in my expression of ClopHensorN in the organotypic slices.

In summary, whilst electrophysiological methods may have greater sensitivity and perhaps accuracy, imaging methods offer the chance to monitor ion dynamics throughout the entire course of epileptiform events. Furthermore, once the imaging technique is established, it allows for more rapid data collection. Amongst imaging methods, ClopHensorN brings technical challenges, but solves the important pH sensitivity problem and offers good temporal resolution where significant Cl^- fluxes occur.

Having reflected on the methodological considerations, I will now discuss the wider implications of my findings and how they might be investigated further in future experiments. To structure this wider discussion, I will first reflect on my measurements of ion dynamics in genetically-defined interneuron populations and then on how my findings speak to manipulating these interneuron subtypes.

6.3 Monitoring ion dynamics in GABAergic interneurons during epileptiform events

6.3.1 pH transients during epileptiform activity

In chapter 4 of this thesis I have shown that PV, SST and VIP interneurons, as well as pyramidal neurons, acidify during epileptiform events. Interestingly, these interneuron subtypes have different intracellular pH resting states, and this relates to the extent to which they acidify during epileptiform activity. From this data, there are three questions that arise. First, where do the protons mediating this effect come from? Second, how does this phenomenon impact the pH of the extracellular space? Finally, what are the functional consequences of these differences in pH both at baseline and during epileptiform activity?

One important mediator of pH changes is thought to be the influx of protons resulting from Ca^{2+}/H^{+} exchange by plasmalemmal Ca^{2+}-ATPases. These co-transporters work by removing activity-induced intracellular Ca^{2+} (Schwiening et al., 1993; Makani and Chesler, 2010). As these transporters allow for intracellular H^{+} influx, it is thought that this process would lead to an alkalinisation of the extracellular space. However, it is also important to consider astrocytes, which have been shown to become more alkaline during epileptiform activity (Raimondo et al., 2016). This is a result of the activity of the electrogenic Na^{+}/HCO_3^{-} co-transporter NBCe1, which mediates the influx of one Na^{+} ion and two HCO_3^{-} ions, forcing the extracellular space to become more acidic. These opposing shifts in neuronal and astrocytic pH make the extracellular pH dynamics complex. Furthermore, as astrocytic alkalinisation is faster than neuronal acidification (Raimondo et al.,

2016), one would predict that the extracellular space acidifies transiently at the onset of epileptiform events. As the epileptiform event progresses and neurons become more acidic, the resulting extracellular decrease in H^+ would be predicted to attenuate the initial acidosis and even promote alkalosis. Such biphasic changes in extracellular pH have indeed been reported (Siesjö, 1985; Krishtal et al., 1987; Chesler and Kaila, 1992). However, the dynamics of extracellular pH can vary depending on the relative contribution of the astrocytic and neuronal components, and on the brain structure in which they occur (Chesler and Kaila, 1992). Furthermore, intense network activity and the associated high intracellular metabolic activity that occur during seizures, can lead to the production and diffusion of lactic acid. This can prolong extracellular acidosis, even after seizure activity has terminated (Siesjö, 1985).

As part of a complex interplay between intra- and extracellular compartments, the resulting extracellular changes in pH can themselves have a marked effect on network excitability. For example, extracellular acidification has been postulated to represent a negative feedback against increases in network activity (Ransom, 1992), acting as a form of endogenous anticonvulsant (Lennox, 1928a; Velísek et al., 1994). Extracellular acidosis has been found to decrease the conductance and gating properties of Na^+, K^+ and Ca^{2+} channels (Tombaugh and Somjen, 1996), as well as reducing the current through AMPA and NMDA receptors (Giffard et al., 1990; McDonald et al., 1998). Furthermore, extracellular acidification can enhance GABAergic conductances (Pasternack et al., 1996). Another study identified that acidosis stimulates GABAergic interneurons through

the proton-gated Na^+ channels called ASIC1a, thereby increasing network inhibition and promoting the termination of epileptiform events (Ziemann et al., 2008). At the same time, intracellular acidification of neurons has been shown to counteract epileptiform activity (Xiong et al., 2000). This supports the idea that lowering the cytosolic pH may play an important role in protecting against excessive neuronal activity (Lam et al., 2013). Indeed, as discussed in chapter 4, low intracellular pH has been previously shown to reduce Ca^{2+} conductances (Dixon et al., 1993; Takahashi and Copenhagen, 1996; Tombaugh and Somjen, 1997), which could reduce repetitive firing and neurotransmitter release (Dodge and Rahamimoff, 1967; White et al., 1989; De Schutter and Bower, 1994).

Whilst it is important to consider the separate contribution of both the intra- and extracellular compartments to network excitability, in reality the intracellular and extracellular pH are inextricably linked. For example, metabolic acidosis is known to lower both the extracellular and intracellular pH (Salameh et al., 2014) and this could be the mechanism by which certain anti-seizure therapies exert their effect, as suggested in the ketogenic diet (Lennox, 1928b) or the administration of carbonic anhydrase inhibitors that reduce the production of bicarbonate (Velísek and Velísková, 1994; Leniger et al., 2002; Hamidi and Avoli, 2015). Indeed, valproate, acetazolamide and topiramate are all anti-seizure drugs that are known to inhibit carbonic anhydrases (Supuran, 2008).

GABAergic interneurons may be a potentially interesting target and mediator of acidosis effects. At the same time as experiencing pH dynamics caused by epileptiform events, GABAergic interneurons are likely to play an important

role in mediating the effects of acidosis on network excitability. In addition to these cells being particularly sensitive to extracellular acidosis through acid-sensing channels (Ziemann et al., 2008), fast GABAergic synaptic transmission may itself be affected by intracellular acidification. This could hyperpolarise the reversal potential of HCO_3^- due to consumption of intracellular HCO_3^-. This would be expected to cause a hyperpolarisation of E_{GABA_A} and an enhancement of $GABA_A$R-mediated inhibition. The size of this effect would depend on the relative HCO_3^- consumption caused by acidosis of the extracellular space. The net effect could be an increased presynaptic recruitment of GABAergic interneurons leading to an enhanced postsynaptic $GABA_A$R-mediated hyperpolarisation. Therefore, activity-induced acidosis could promote the GABAergic system's role in seizure termination.

Although lowering of general intracellular pH levels has been shown to promote epileptiform event termination, the extent to which acidification of GABAergic interneurons contributes to this protective effect is not clear. One could imagine experiments in which this could be examined. For example, to investigate the effects of cell-specific intracellular pH changes, the light-activated proton pump Arch (Chow et al., 2010) could be used to alkalinise genetically-defined interneuron population. However, activation of the proton efflux through Arch also generates membrane hyperpolarisation, which may be a significant confounding factor. Manipulating intracellular pH would also be interesting in the context of epileptogenesis, when certain types of GABAergic interneurons are known to be depleted, such as SST interneurons (Robbins et al., 1991). If a low intracellular pH

has a neuroprotective effect, could SST interneurons be rescued from depletion during epileptogenesis? Finding tools to specifically control intracellular pH without altering the membrane potential would be useful in addressing these issues. Transcriptional profiling of genetically-defined interneuron subtypes (Paul et al., 2017; Harris et al., 2018) could also reveal specific isoenzymes that become targets for pharmacological manipulations. For example, the carbonic anhydrase type II has been identified in a subset of GABAergic interneurons in the human hippocampus (Kida et al., 2006). RNA interference could then be used to selectively manipulate these genes in specific cell types.

The study of mechanisms contributing to the resting pH or activity-induced acidification of interneurons would also benefit from the use of existing pharmacological tools. For example, while monitoring pH with ClopHensorN, the contribution of the Ca^{2+}/H^{+} exchange could be assessed by using caloxins to inhibit the plasmalemmal Ca^{2+} ATPase (Pande et al., 2011). Similarly, the contribution of $GABA_A$Rs to acidification could be assessed with selective receptor antagonists such as gabazine or bicuculline methiodide (Ueno et al., 1997). Such pharmacological experiments are likely to provide insights into how distinct interneuron subtypes can exhibit different resting pH (for example VIP interneurons) and could, more generally, help elucidate how they regulate their pH homeostasis.

6.3.2 Cl^- transients during epileptiform activity

In chapter 4 I have discovered that two major interneuron populations of the hippocampus (SST and VIP interneurons), like pyramidal neurons, show

pronounced loading of Cl^- during epileptiform events. Uniquely, PV interneurons do not load, but may actually unload Cl^- during epileptiform activity. These findings led to two pertinent questions. First, why do some neuron populations load Cl^- during epileptiform events, and other do not? Second, what are the implications for this cell-type specific phenomenon?

During $GABA_AR$ activation, Cl^- flows down its electrochemical gradient. In neurons that have low levels of Cl^- under resting conditions, Cl^- tends to enter the cell. Particularly during periods of membrane depolarisation, the increased driving force for Cl^- influx is expected to favour increases in intracellular Cl^-. Indeed, the coupling of intense $GABA_AR$ activation with membrane depolarisation during epileptiform events is known to induce positive shifts in E_{GABA_A} in pyramidal neurons, which changes the subsequent driving force for Cl^- (Kaila and Voipio, 1987; Ilie et al., 2012; Raimondo et al., 2012c). Neurons may accumulate Cl^- to the extent that the transmembrane gradient collapses and the driving force reverses, allowing GABAergic signalling to become depolarising or even excitatory (Raimondo et al., 2017). From all cell types investigated in this thesis, PV interneurons had the highest level of Cl^- under resting conditions. Given a mean resting Cl^- concentration of 32.5 mM, the estimated E_{GABA_A} in PV interneurons is approximately -40 mV. Such a depolarised value for E_{GABA_A} would be expected to be much closer to, or even above, the membrane potential of PV interneurons during epileptiform activity (**Figure 4.4**) (Vida et al., 2006; Cammarota et al., 2013). These conditions would be expected to generate modest Cl^- fluxes and potentially Cl^- effluxes rather than influxes. The resting intracellular level of Cl^- is therefore

critical in determining the direction of transmembrane ion flow during epileptiform events. Consistent with this, I found that the Cl^- unloading effect becomes less pronounced in PV interneurons that have a lower resting intracellular Cl^-.

At seizure onset, the dynamic nature of the driving force for Cl^- during intense $GABA_AR$ activation is likely to impact the way neurons integrate their excitatory and inhibitory inputs. The reduction of the Cl^- gradient in pyramidal, SST and VIP cells is expected to shift the balance of excitatory-to-inhibitory inputs towards excitation. This would occur as a result of the strength of inhibitory conductances being diminished by the depolarised E_{GABA_A}. By contrast, PV interneurons do not collapse their Cl^- gradients, and are therefore well-placed to maintain their E/I balance, despite their recruitment to seizure activity (**Figure 6.1**). Instead of a disruption in the balance of E/I inputs at seizure onset, PV interneurons are instead affected in terms of their output by DB (as shown in chapter 5).

As the seizure progresses, the SST and VIP cells follow a similar pattern to the pyramidal cells and would be predicted to become increasingly affected by the collapse in their transmembrane Cl^- gradients. The result of Cl^- loading in pyramidal neurons during seizure events is that $GABA_A$-mediated inhibition would become ineffective at silencing their activity, as it becomes excitatory (Ellender et al., 2014). The fact that SST and VIP interneurons also reach high intracellular Cl^- levels during seizure activity may act as a positive feedback loop. For example, if the E/I balance in VIP interneurons increases, this interneuron population would become more excitable. VIP interneurons are known to preferentially target other

Figure 6.1. Predicted excitation-inhibition balance of pyramidal neurons and PV interneurons. The cartoon (left) illustrates a pyramidal neuron (blue) and a PV interneuron (green). Chloride dynamics are shown for the two cell types (middle). During a seizure event, Cl^- flows into the pyramidal neuron, whereas the PV interneuron intracellular Cl^- is relatively high at rest and drops slightly as a result of the seizure (middle). The predicted E/I balance is shown for the two cell types (right). Given the Cl^- inflow during the seizure and impact on $GABA_AR$ transmission, the pyramidal neuron's excitation-inhibition (E/I) balance is predicted to increase significantly. However, the more stable Cl^- levels in the PV interneuron are predicted to result in a more stable E/I balance.

interneuron subtypes, particularly SST interneurons, which are themselves experiencing a transmembrane Cl^- collapse and a shift in E/I balance towards excitation. By contrast, PV interneurons are predicted to maintain a more stable E/I balance. The net effect could be that, during a seizure, pyramidal neurons experience a shift in input across their somatodendritic axis, as dendrite-targeting SST interneurons become relatively more excited.

At the same time, pyramidal neurons also load with Cl^-, and this is expected to be more pronounced in smaller subcellular compartments such as dendrites (Qian and Sejnowski, 1990). Interestingly, the opposite has been found, with ED-induced depolarising shifts in E_{GABA_A} appearing to be more pronounced in the somatic rather than the dendritic compartment (Ellender et al., 2014). One explanation for this result could be that the dendritic compartment may contain a relatively high KCC2 expression compared to the somatic compartment. Elevated KCC2 activity would be predicted to keep Cl^- levels low by opposing Cl^- loading. This is consistent with

my result that, during epileptiform activity SST interneurons with a low resting Cl^- concentration (and presumably higher expression of KCC2) loaded Cl^- less than SST interneurons with higher resting Cl^- levels (**Figure 4.8**). Future research could investigate the impact on ED progression of selectively manipulating interneuron subtypes so that their Cl^- levels are more stable. For example, one could imagine selectively overexpressing KCC2 in SST interneurons. If the increased capacity to export Cl^- ions pushes the E/I balance towards inhibition, this could reduce SST interneuron-mediated excitatory effects onto pyramidal neurons.

Once a seizure has been initiated, probably the most obvious cell type to target to break the hypothesised positive feedback loop is the pyramidal neuron. Mature pyramidal neurons are known to express KCC2, and the activity of this transporter is critical in limiting the severity of epileptiform activity (Silayeva et al., 2015). The activity of KCC2 is enhanced by phosphorylation of serine 940 (Lee et al., 2007). However, epileptiform activity has been shown to dephosphorylate KCC2 serine 940 and therefore reduce its activity (Silayeva et al., 2015), which could further compromise the ability of neurons to discard accumulating Cl^- during seizure events. Therefore, effective therapeutic strategies could involve overexpressing KCC2 (Magloire et al., 2018) and/or preventing its dephosphorylation in pyramidal neurons (Moore et al., 2018), in order to boost KCC2-mediated Cl^- extrusion.

Taken together, one should consider that the most appropriate cell type to target in the context of epileptiform activity may depend on the timing of the manipulation. The stability of input matching of PV interneurons compared to other

interneuron subtypes makes them a desirable candidate for manipulations aimed at preventing a network from entering into a seizure. However, at seizure onset, PV interneurons face an output problem (to be discussed further below). Once seizures start, the most rational target for manipulation is likely the pyramidal neuron. Enhanced Cl^- extrusion can be achieved by either overexpressing KCC2 (Magloire et al., 2018) or by using novel cooperative optogenetic tools such as Cl-out (Alfonsa et al., 2016). These could prove to be valuable strategies in suppressing ongoing epileptiform activity.

6.4 Controlling ion dynamics in GABAergic interneurons during seizure events

In this thesis I show that the activity of PV and SST interneurons can be chemogenetically enhanced to suppress epileptiform events (chapter 3). I also demonstrate that the recruitment of PV interneurons driven by network excitation can be increased by removing them from DB with an inhibitory opsin (chapter 5). This leads one to the question: how can two opposing manipulations result in the same type of impact on epileptiform activity? Here, I will attempt to answer this question by incorporating these results into a proposed model of seizure recruitment that may be relevant in the context of focal epilepsy.

6.4.1 A model of seizure recruitment in focal epilepsy

Figure 6.2 illustrates my attempt to integrate the experimental findings from this thesis into a model describing the spatio-temporal excitation-inhibition dynamics in the context of a focal seizure. These ideas draw on previous literature

investigating the spatial spread of epileptiform activity (Trevelyan et al., 2006, 2007).

In this model, the generation of a focal seizure event requires the existence of a pathologic epileptic 'focus', which is able to recruit the surrounding seizure 'core', representing a critical mass of neurons necessary and sufficient to generate a seizure that can then spread into the adjacent healthy tissue called the epileptic 'penumbra' (**Figure 6.2**). A seizure is initiated when excitation generated by the pathologic focus rapidly overcomes inhibition and recruits the core (**Figure 6.2**, left). If inhibition is enhanced within the core region, as in the case of my chemogenetic manipulations (chapter 3), the effect of excitation from the epileptic focus is attenuated and the critical mass of neurons required to generate a seizure is not recruited. The result is that the seizure is not initiated.

However, if inhibition is not strong enough to counteract excitation at this point, a seizure is generated and starts to spread into the adjacent penumbra (**Figure 6.2**, right). This activates an endogenous restraint mechanism in the form of feedforward inhibition, which opposes the seizure front by matching excitation. If the excitation level grows above a critical threshold, the feedforward inhibition may start to fail because of the output limitation imposed by DB in key interneuron populations. At this point, excitation can overcome inhibition and precipitate the recruitment of the local network to the seizure front. If, however, the effects of DB are experimentally mitigated, the inhibitory mechanisms have greater capacity to overcome excitation, preventing further network recruitment and seizure spread.

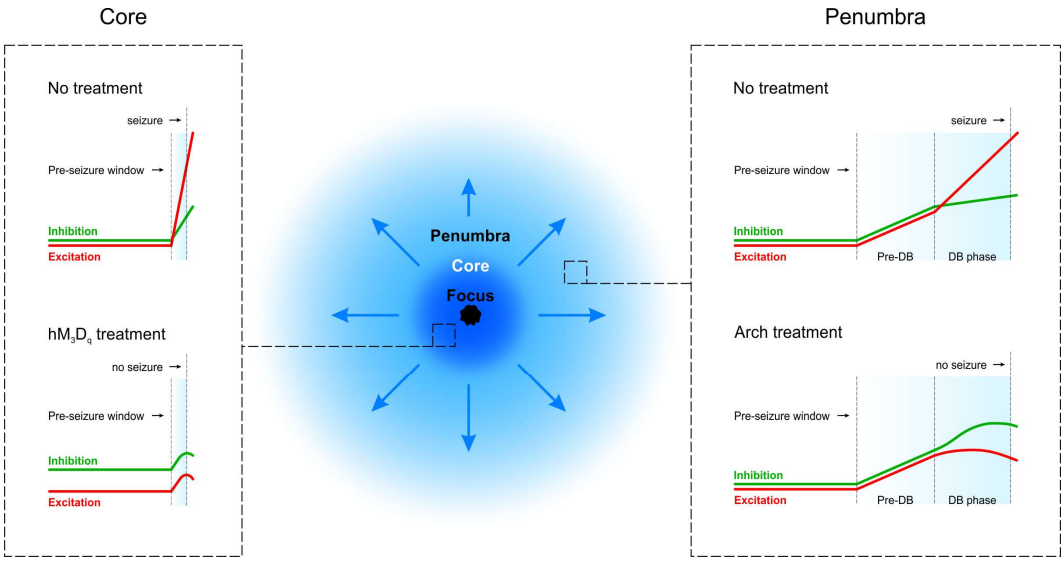

Figure 6.2. A proposed model of spatio-temporal excitation-inhibition dynamics during recruitment to a seizure event. A schematic illustration of a seizure initiated from a focus of damaged tissue (black area in the centre) and the dynamic events occurring in the core (dark blue area around the focus) and surrounding penumbra (light blue area around the core). Events at the core (left box) are characterised by a brief pre-seizure phase in which excitation rapidly overcomes inhibition. Boosting synaptic inhibition during baseline can prevent epileptiform events by dominating excitation pre-emptively. The seizure front spreads by recruiting more neurons in the adjacent penumbra, which opposes the propagating wave via feedforward inhibition (right box). The activity in the penumbra before seizure recruitment comprises two distinct phases, separated by the point at which PV interneuron firing starts to be impaired by DB. During the DB phase, the capacity of feedforward inhibition to oppose excitation is compromised and this leads to seizure spread. Arch pulsed stimulation of PV interneurons may prevent seizure events by boosting inhibition during the period that DB would normally interfere with the capacity of PV interneurons to generate action potentials.

The abrupt onset of spontaneous EDs observed in my experiments is consistent with what one would expect to occur with a rapidly recruited epileptic core. Furthermore, the inhibitory restraint revealed experimentally in this thesis is consistent with my findings and previous studies that have described how the GABAergic system within the penumbra can oppose the spread of epileptiform activity (Trevelyan and Schevon, 2013).

Since this is a working model of focal seizures, it presents opportunities for further testing. First, the validity of the model would need to be tested. This could be done by monitoring distinct populations of cells to investigate how fast and/or synchronously they are recruited around the seizure focus, or even further away in the penumbra. For example, visualising excitatory neuron activity by Ca^{2+} imaging suggests that clusters of pyramidal neurons are recruited to the seizure front once the local GABAergic inhibitory restraint has failed (Trevelyan et al., 2006, 2007).

Selective manipulation of different regions of the network, relative to the seizure focus, could also help to test the model. A prediction of the model is that selective manipulation of the area around the focus preferentially impacts seizure generation, whilst selective manipulation of the penumbra is predicted to disrupt seizure propagation. The findings of my thesis demonstrate that boosting inhibition is capable of preventing seizure generation, whilst enhancing the inhibitory restraint prevented epileptiform recruitment. One could imagine the opposite experiment, where inhibition is attenuated. It has been shown that antagonising the GABAergic system produces seizures (Miles and Wong, 1987; Treiman, 2001). Moreover,

collapsing the inhibitory restraint results in much faster spread of seizures compared to when inhibition is intact (Chervin et al., 1988; Trevelyan et al., 2006).

Neither strategy that I used to enhance inhibition was 100% effective, in the sense that neither completely abolished epileptiform activity. Why was this the case and what could one do to improve the efficacy of these strategies? If the model is correct, it would be useful to understand the limitations of the manipulations that I have employed and to try to refine them by increasing their strength and specificity. Further validating the model using these more powered and targeted manipulations may help improve intervention options.

The chemogenetic strategy, for example, relies on G proteins and on their intracellular signalling cascade (Alexander et al., 2009). An obvious limitation for this type of manipulation is the amount of G proteins that the target cells produce. Overexpressing the specific G_q protein that is required for signal transduction of excitatory DREADDs could be a method to boost their efficacy in promoting neuronal activity. However, a potential problem of increasing the excitatory effect of the chemogenetic manipulation is that too much excitation could result in DB and the subsequent collapse of inhibition. The pulsed Arch strategy for reducing DB also has limitations. Most notably, the photocurrent produced by Arch is rendered ineffective in generating hyperpolarisations when the neuronal membrane resistance decreases due to intense neurotransmitter release.

DB may not be the only mechanism by which inhibitory restraint fails. Several alternative presynaptic mechanisms have been proposed, such as synaptic

depression (Kraushaar and Jonas, 2000), the reduction of release probability caused by $GABA_BR$ and metabotropic glutamate receptor activation (Giustizieri et al., 2005), or the depletion of the releasable pool of synaptic vesicles (Zhang et al., 2012). However, my data shows that removing DB allows for an increased firing rate of PV interneurons, which reduced the probability of epileptiform events. Therefore, the fact that an increase of firing had an effect on epileptiform activity argues against the presynaptic vesicular depletion hypothesis.

The optogenetic manipulation for removing DB represents only a proof of concept. This provides the opportunity to refine the strategy of removing DB, potentially by using non-optical approaches. For example, K^+ channels of the Kv3.1 type could be selectively overexpressed in PV interneurons of the penumbra. This K^+ channel has useful properties such as fast activation at depolarised potentials and rapid deactivation, which facilitate the sustained fast spiking pattern of PV interneurons (Chow et al., 1999). Overexpression of the channel could promote higher frequency firing during inhibitory restraint, and may help to prevent DB by opposing depolarisation. Gene therapies based on K^+ channel have been previously proposed, but for the purpose of transducing and inhibiting excitatory neurons (Wykes et al., 2012; Snowball et al., 2018). This could be a useful approach, especially after neurons are recruited to the seizure event. Another recently published study makes use of a glutamate-gated Cl^- channel expressed in excitatory neurons (Lieb et al., 2018). One could imagine this may be useful for targeting the healthy tissue around the pathologic focus, where Cl^- levels in pyramidal neurons are presumably low before seizure recruitment. However, this approach may

precipitate the collapse of GABAergic inhibition if intracellular Cl^- accumulates more rapidly in excitatory neurons. One could imagine making use of glutamate-sensing moieties to design K^+ channels that are activated by pathologic levels of extracellular glutamate. Arguably, a combination of glutamate-gated K^+ (Chen et al., 1999; Janovjak et al., 2010) and Cl^- channels could work synergistically: K^+ conductances would oppose membrane depolarisation, hence preventing Cl^- accumulation in excitatory neurons. This strategy could be selectively employed at the seizure core, whilst methods to boost inhibitory restraint could be used in the penumbra, such as, a K^+-selective, light-gated ion channel that could be used as an alternative optogenetic strategy to remove DB in PV interneurons (Cosentino et al., 2015).

Having discussed my results and possible future experiments in the context of a model of focal epilepsy, I will use the next section to discuss the strengths and weaknesses of adopting optogenetic and chemogenetic strategies in interneurons.

6.4.2 Optogenetic versus chemogenetic recruitment of specific interneurons

A series of studies using rodent models have successfully applied optogenetic approaches for disrupting epileptiform networks. Like chemogenetic approaches, optogenetics lends itself to cell-type targeting and this work has helped define the role of different interneuron types. For example, it has been shown that when combined with real-time seizure detection methods, temporally controlled optogenetic activation of interneuron populations can provide effective disruption of epileptic activity (Krook-Magnuson et al., 2013; Ledri et al., 2014; Sessolo et al., 2015). However, this work has also revealed that optogenetic activation of

interneurons can actually initiate epileptiform activity, in a manner that may depend on the network state (Sessolo et al., 2015; Yekhlef et al., 2015; Assaf and Schiller, 2016; Chang et al., 2018a). This phenomenon seems to be associated with the pulsed light-activation and enforced synchronisation of interneuron activity, which can then synchronise the network by inducing time-locked post-inhibitory rebound spiking (Sessolo et al., 2015; Chang et al., 2018a). In addition to these temporal aspects, optogenetic strategies face other challenges for disrupting seizures. These include the delivery of light to structures that may be deep within the brain, or to cells that may be distributed over large regions (Wykes et al., 2016).

Chemogenetic intervention strategies may mitigate these issues, as they offer the potential to modulate cellular activity on larger spatial and temporal scales. Effects from chemogenetics can be coordinated across large areas of tissue, due to the systemic delivery of the activating drug (Alexander et al., 2009). Furthermore, the fact that DREADDs are G-protein coupled receptors and act through endogenous cellular mechanisms, may avoid unwanted effects associated with artificial synchronisation of the network (Wang et al., 2017). However, their reliance upon the cell's own intracellular machinery may limit the potential for chemogenetics. Whereas optogenetic strategies have the power to use light energy to move ions against concentration gradients, chemogenetic strategies must rely upon endogenous mechanisms, at least in their current form. Nonetheless, chemogenetics lends itself to translational approaches more readily than optogenetics. I found that the activation of G_q-coupled receptors in PV and SST interneurons is sufficient to considerably reduce the probability of initiation of

epileptic network activity. As well as supporting chemogenetic strategies, this has implications for drug discovery. As more single-cell RNA sequencing studies are published, the identification of G_q-coupled receptors that are enriched in PV or SST cells, but not in VIP interneurons and excitatory cells, becomes a possibility. The present study suggests that such G protein-coupled receptors would represent potential drug targets for temporal lobe epilepsy.

Despite the success of my experiments and of previous work (Kätzel et al., 2014; Wang et al., 2018), there remain questions about how inert the designed drugs are for the selective activation of the DREADDs, and whether these need to be refined further (Gomez et al., 2017). Any cell-targeted strategy must also consider how the contributions of particular cell types may change in epilepsy. Cell types may be lost or change their signalling at different stages of the disease (Robbins et al., 1991; Cohen et al., 2002; Wang et al., 2017). Furthermore, the contribution of a cell type may also depend on their location relative to the epileptic focus (Sessolo et al., 2015), their position in the epileptic circuit (Paz and Huguenard, 2015a), and their effects may change dynamically during an individual epileptiform events (Ellender et al., 2014). For these reasons, multiple anti-seizure strategies may be required, perhaps using one strategy for pathologically affected cells within the epileptic focus and another strategy for surrounding healthier circuits.

Finally, there are challenges associated with translation to humans. For example, there are currently no interneuron subtype-specific gene promoters that are small enough for AAV-vector-based gene therapy (Nathanson et al., 2009). Future progress in this direction is necessary if we hope to capitalise on the direct

translational value of gene-based strategies, and the use of cell-targeted clinical therapies.

6.5 Concluding remarks

My findings support the conclusion that ion dynamics in GABAergic interneurons are important in the context of epileptiform activity. Monitoring and controlling these ion dynamics can provide insight into the development of new therapies. An understanding of the behaviour of different interneuron subtypes during seizure activity is likely to allow one to target the most appropriate cell population. Given the spatio-temporal dynamics of seizure recruitment in focal epilepsy, it may be beneficial to employ different complementary strategies for manipulating the GABAergic system. Moreover, my work supports the use of selective chemogenetic targeting of the inhibitory system as an approach to disrupt epileptiform synchronisation of the epileptic core. At the same time, strengthening inhibitory restraint within the surrounding penumbra, may be key to preventing seizure spread. Such cell-specific strategies have the attraction of being controllable and yet avoiding the system-wide effects of drugs that enhance GABA-mediated inhibition in a non-cell-selective fashion.

References

Abad, M. F. C., Di Benedetto, G., Magalhães, P. J., Filippin, L., and Pozzan, T. (2004). Mitochondrial pH monitored by a new engineered green fluorescent protein mutant. *J. Biol. Chem.* 279, 11521–11529. doi:10.1074/jbc.M306766200.

Acsády, L., Görcs, T. J., and Freund, T. F. (1996). Different populations of vasoactive intestinal polypeptide-immunoreactive interneurons are specialized to control pyramidal cells or interneurons in the hippocampus. *Neuroscience* 73, 317–334. doi:10.1016/0306-4522(95)00609-5.

Adijanto, J., and Philp, N. J. (2012). The SLC16A family of monocarboxylate transporters (MCTs)--physiology and function in cellular metabolism, pH homeostasis, and fluid transport. *Curr. Top. Membr.* 70, 275–311. doi:10.1016/B978-0-12-394316-3.00009-0.

Albus, K., Wahab, A., and Heinemann, U. (2008). Standard antiepileptic drugs fail to block epileptiform activity in rat organotypic hippocampal slice cultures. *Br. J. Pharmacol.* 154, 709–724. doi:10.1038/bjp.2008.112.

Alexander, G. M., Rogan, S. C., Abbas, A. I., Armbruster, B. N., Pei, Y., Allen, J. A., et al. (2009). Remote control of neuronal activity in transgenic mice expressing evolved G protein-coupled receptors. *Neuron* 63, 27–39. doi:10.1016/j.neuron.2009.06.014.

Alfonsa, H., Lakey, J. H., Lightowlers, R. N., and Trevelyan, A. J. (2016). Cl-out is a novel cooperative optogenetic tool for extruding chloride from neurons. *Nat. Commun.* 7, 13495. doi:10.1038/ncomms13495.

Alfonsa, H., Merricks, E. M., Codadu, N. K., Cunningham, M. O., Deisseroth, K., Racca, C., et al. (2015). The Contribution of Raised Intraneuronal Chloride to Epileptic Network Activity. *J. Neurosci.* 35, 7715–7726. doi:10.1523/JNEUROSCI.4105-14.2015.

Alger, B. E., and Nicoll, R. A. (1982). Feed-forward dendritic inhibition in rat hippocampal pyramidal cells studied in vitro. *J. Physiol.* 328, 105–123.

Alonso, A., and Köhler, C. (1982). Evidence for separate projections of hippocampal pyramidal and non-pyramidal neurons to different parts of the septum in the rat brain. *Neurosci. Lett.* 31, 209–214.

Amzica, F., Massimini, M., and Manfridi, A. (2002). Spatial buffering during slow and paroxysmal sleep oscillations in cortical networks of glial cells in vivo. *J. Neurosci. Off. J. Soc. Neurosci.* 22, 1042–1053.

Amzica, F., and Steriade, M. (2000). Neuronal and glial membrane potentials during sleep and paroxysmal oscillations in the neocortex. *J. Neurosci. Off. J. Soc. Neurosci.* 20, 6648–6665.

Anderson, S. A., Eisenstat, D. D., Shi, L., and Rubenstein, J. L. R. (1997). Interneuron Migration from Basal Forebrain to Neocortex: Dependence on Dlx Genes. *Science* 278, 474–476. doi:10.1126/science.278.5337.474.

Andrioli, A., Alonso-Nanclares, L., Arellano, J. I., and DeFelipe, J. (2007). Quantitative analysis of parvalbumin-immunoreactive cells in the human epileptic hippocampus. *Neuroscience* 149, 131–143. doi:10.1016/j.neuroscience.2007.07.029.

Aponte, Y., Lien, C.-C., Reisinger, E., and Jonas, P. (2006). Hyperpolarization-activated cation channels in fast-spiking interneurons of rat hippocampus. *J. Physiol.* 574, 229–243. doi:10.1113/jphysiol.2005.104042.

Aravanis, A. M., Wang, L.-P., Zhang, F., Meltzer, L. A., Mogri, M. Z., Schneider, M. B., et al. (2007). An optical neural interface: in vivo control of rodent motor cortex with integrated fiberoptic and optogenetic technology. *J. Neural Eng.* 4, S143-156. doi:10.1088/1741-2560/4/3/S02.

Armand, V., Hoffmann, P., Vergnes, M., and Heinemann, U. (1999). Epileptiform activity induced by 4-aminopyridine in entorhinal cortex hippocampal slices of rats with a genetically determined absence epilepsy (GAERS). *Brain Res.* 841, 62–69.

Armbruster, B. N., Li, X., Pausch, M. H., Herlitze, S., and Roth, B. L. (2007). Evolving the lock to fit the key to create a family of G protein-coupled receptors potently activated by an inert ligand. *Proc. Natl. Acad. Sci.* 104, 5163–5168. doi:10.1073/pnas.0700293104.

Armstrong, C., Krook-Magnuson, E., Oijala, M., and Soltesz, I. (2013). Closed-loop optogenetic intervention in mice. *Nat. Protoc.* 8, 1475–1493. doi:10.1038/nprot.2013.080.

Arosio, D., Ricci, F., Marchetti, L., Gualdani, R., Albertazzi, L., and Beltram, F. (2010). Simultaneous intracellular chloride and pH measurements using a GFP-based sensor. *Nat. Methods* 7, 516–518. doi:10.1038/nmeth.1471.

Assaf, F., and Schiller, Y. (2016). The antiepileptic and ictogenic effects of optogenetic neurostimulation of PV-expressing interneurons. *J. Neurophysiol.* 116, 1694–1704. doi:10.1152/jn.00744.2015.

Atallah, B. V., Bruns, W., Carandini, M., and Scanziani, M. (2012). Parvalbumin-expressing interneurons linearly transform cortical responses to visual stimuli. *Neuron* 73, 159–170. doi:10.1016/j.neuron.2011.12.013.

Avaliani, N., Andersson, M., Runegaard, A. H., Woldbye, D., and Kokaia, M. (2016). DREADDs suppress seizure-like activity in a mouse model of pharmacoresistant epileptic brain tissue. *Gene Ther.* 23, 760–766. doi:10.1038/gt.2016.56.

Avoli, M., Louvel, J., Pumain, R., and Olivier, A. (1987). Seizure-like discharges induced by lowering [Mg2+]o in the human epileptogenic neocortex maintained in vitro. *Brain Res.* 417, 199–203.

Babb, T. L., Kupfer, W. R., Pretorius, J. K., Crandall, P. H., and Levesque, M. F. (1991). Synaptic reorganization by mossy fibers in human epileptic fascia dentata. *Neuroscience* 42, 351–363. doi:10.1016/0306-4522(91)90380-7.

Banghart, M., Borges, K., Isacoff, E., Trauner, D., and Kramer, R. H. (2004). Light-activated ion channels for remote control of neuronal firing. *Nat. Neurosci.* 7, 1381–1386. doi:10.1038/nn1356.

Banke, T. G., and McBain, C. J. (2006). GABAergic input onto CA3 hippocampal interneurons remains shunting throughout development. *J. Neurosci. Off. J. Soc. Neurosci.* 26, 11720–11725. doi:10.1523/JNEUROSCI.2887-06.2006.

Bartos, M., and Elgueta, C. (2012). Functional characteristics of parvalbumin- and cholecystokinin-expressing basket cells. *J. Physiol.* 590, 669–681. doi:10.1113/jphysiol.2011.226175.

Bausch, S. B., Garland, J. P., and Yamada, J. (2005). The delta opioid receptor agonist, SNC80, has complex, dose-dependent effects on pilocarpine-induced seizures in Sprague-Dawley rats. *Brain Res.* 1045, 38–44. doi:10.1016/j.brainres.2005.03.008.

Bausch, S. B., and McNamara, J. O. (2000). Synaptic connections from multiple subfields contribute to granule cell hyperexcitability in hippocampal slice cultures. *J. Neurophysiol.* 84, 2918–2932. doi:10.1152/jn.2000.84.6.2918.

Ben-Ari, Y., Cherubini, E., Corradetti, R., and Gaiarsa, J. L. (1989). Giant synaptic potentials in immature rat CA3 hippocampal neurones. *J. Physiol.* 416, 303–325.

Ben-Ari, Y., and Lagowska, J. (1978). [Epileptogenic action of intra-amygdaloid injection of kainic acid]. *Comptes Rendus Hebd. Seances Acad. Sci. Ser. Sci. Nat.* 287, 813–816.

Ben-Ari, Y., Lagowska, J., Tremblay, E., and Le Gal La Salle, G. (1979). A new model of focal status epilepticus: intra-amygdaloid application of kainic acid elicits repetitive secondarily generalized convulsive seizures. *Brain Res.* 163, 176–179.

Ben-Ari, Y., Tremblay, E., Berger, M., and Nitecka, L. (1984). Kainic acid seizure syndrome and binding sites in developing rats. *Dev. Brain Res.* 14, 284–288. doi:10.1016/0165-3806(84)90314-6.

Ben-Ari, Y., Tremblay, E., and Ottersen, O. P. (1980). Injections of kainic acid into the amygdaloid complex of the rat: an electrographic, clinical and histological study in relation to the pathology of epilepsy. *Neuroscience* 5, 515–528.

Bennett, M. R., Gibson, W. G., and Robinson, J. (1994). Dynamics of the CA3 pyramidal neuron autoassociative memory network in the hippocampus. *Philos. Trans. R. Soc. Lond. B. Biol. Sci.* 343, 167–187. doi:10.1098/rstb.1994.0019.

Bergstrom, R. A., Choi, J. H., Manduca, A., Shin, H.-S., Worrell, G. A., and Howe, C. L. (2013). Automated identification of multiple seizure-related and interictal epileptiform event types in the EEG of mice. *Sci. Rep.* 3. doi:10.1038/srep01483.

Bevensee, M. O., Cummins, T. R., Haddad, G. G., Boron, W. F., and Boyarsky, G. (1996). pH regulation in single CA1 neurons acutely isolated from the hippocampi of immature and mature rats. *J. Physiol.* 494, 315–328. doi:10.1113/jphysiol.1996.sp021494.

Bianchi, D., Marasco, A., Limongiello, A., Marchetti, C., Marie, H., Tirozzi, B., et al. (2012). On the mechanisms underlying the depolarization block in the spiking dynamics of CA1 pyramidal neurons. *J. Comput. Neurosci.* 33, 207–225. doi:10.1007/s10827-012-0383-y.

Bizzarri, R., Serresi, M., Luin, S., and Beltram, F. (2009). Green fluorescent protein based pH indicators for in vivo use: a review. *Anal. Bioanal. Chem.* 393, 1107–1122. doi:10.1007/s00216-008-2515-9.

Bliss, T. V., and Gardner-Medwin, A. R. (1973). Long-lasting potentiation of synaptic transmission in the dentate area of the unanaestetized rabbit following stimulation of the perforant path. *J. Physiol.* 232, 357–374.

Bliss, T. V., and Lomo, T. (1973). Long-lasting potentiation of synaptic transmission in the dentate area of the anaesthetized rabbit following stimulation of the perforant path. *J. Physiol.* 232, 331–356.

Blomfield, S. (1974). Arithmetical operations performed by nerve cells. *Brain Res.* 69, 115–124.

Boedtkjer, E., Praetorius, J., Füchtbauer, E.-M., and Aalkjaer, C. (2008). Antibody-independent localization of the electroneutral Na+-HCO3- cotransporter

NBCn1 (slc4a7) in mice. *Am. J. Physiol. Cell Physiol.* 294, C591-603. doi:10.1152/ajpcell.00281.2007.

Boesmans, W., Hao, M. M., and Berghe, P. V. (2018). Optogenetic and chemogenetic techniques for neurogastroenterology. *Nat. Rev. Gastroenterol. Hepatol.* 15, 21–38. doi:10.1038/nrgastro.2017.151.

Bolam, J. P., Hanley, J. J., Booth, P. A., and Bevan, M. D. (2000). Synaptic organisation of the basal ganglia. *J. Anat.* 196 (Pt 4), 527–542.

Bormann, J. (2000). The 'ABC' of GABA receptors. *Trends Pharmacol. Sci.* 21, 16–19. doi:10.1016/S0165-6147(99)01413-3.

Bormann, J., and Feigenspan, A. (1995). GABAc receptors. *Trends Neurosci.* 18, 515–519. doi:10.1016/0166-2236(95)98370-E.

Bormann, J., Hamill, O. P., and Sakmann, B. (1987). Mechanism of anion permeation through channels gated by glycine and gamma-aminobutyric acid in mouse cultured spinal neurones. *J. Physiol.* 385, 243–286.

Bouchet, C., and Cazauvieilh, J.-B. (1825). *De l'épilepsie considérée dans ses rapports avec l'aliénation mentale.: Recherches sur la nature et le siège de ces deux maladies; mémoire qui a remporté le prix au concours établi par M. Esquirol (2 septembre 1825),*.

Boyarsky, G., Ganz, M. B., Sterzel, R. B., and Boron, W. F. (1988). pH regulation in single glomerular mesangial cells. I. Acid extrusion in absence and presence of HCO3-. *Am. J. Physiol.* 255, C844-856. doi:10.1152/ajpcell.1988.255.6.C844.

Boyden, E. S., Zhang, F., Bamberg, E., Nagel, G., and Deisseroth, K. (2005). Millisecond-timescale, genetically targeted optical control of neural activity. *Nat. Neurosci.* 8, 1263–1268. doi:10.1038/nn1525.

Bregestovski, P., Waseem, T., and Mukhtarov, M. (2009). Genetically encoded optical sensors for monitoring of intracellular chloride and chloride-selective channel activity. *Front. Mol. Neurosci.* 2. doi:10.3389/neuro.02.015.2009.

Brennan, G. P., Baram, T. Z., and Poolos, N. P. (2016). Hyperpolarization-Activated Cyclic Nucleotide-Gated (HCN) Channels in Epilepsy. *Cold Spring Harb. Perspect. Med.* 6. doi:10.1101/cshperspect.a022384.

Buckmaster, P. S. (2012). "Mossy Fiber Sprouting in the Dentate Gyrus," in *Jasper's Basic Mechanisms of the Epilepsies*, eds. J. L. Noebels, M. Avoli, M. A. Rogawski, R. W. Olsen, and A. V. Delgado-Escueta (Bethesda (MD): National Center for Biotechnology Information (US)). Available at:

http://www.ncbi.nlm.nih.gov/books/NBK98174/ [Accessed September 23, 2018].

Buckmaster, P. S., and Lew, F. H. (2011). Rapamycin Suppresses Mossy Fiber Sprouting But Not Seizure Frequency in a Mouse Model of Temporal Lobe Epilepsy. *J. Neurosci.* 31, 2337–2347. doi:10.1523/JNEUROSCI.4852-10.2011.

Burn, J., Dennis, M., Bamford, J., Sandercock, P., Wade, D., and Warlow, C. (1997). Epileptic seizures after a first stroke: the Oxfordshire Community Stroke Project. *BMJ* 315, 1582–1587.

Burnham, W. M. (2002). "Why are Complex Partial Seizures Intractable?," in *Intractable Seizures: Diagnosis, Treatment, and Prevention* Advances in Experimental Medicine and Biology., eds. W. M. Burnham, P. L. Carlen, and P. A. Hwang (Boston, MA: Springer US), 107–110. doi:10.1007/978-1-4615-1335-3_12.

Burton, R. F. (1978). Intracellular buffering. *Respir. Physiol.* 33, 51–58.

Butt, A. M., and Kalsi, A. (2006). Inwardly rectifying potassium channels (Kir) in central nervous system glia: a special role for Kir4.1 in glial functions. *J. Cell. Mol. Med.* 10, 33–44.

Buzsáki, G. (1984). Feed-forward inhibition in the hippocampal formation. *Prog. Neurobiol.* 22, 131–153.

Cajal, S. R. y (1893). *Estructura del asta de ammon y fascia dentata*. tip. de Fortanet.

Cajal, S. R. y (2002). *Texture of the Nervous System of Man and the Vertebrates: Volume III An annotated and edited translation of the original Spanish text with the additions of the French version by Pedro Pasik and Tauba Pasik.* , eds. P. Pasik and T. Pasik Wien: Springer-Verlag Available at: //www.springer.com/gb/book/9783211832028 [Accessed September 27, 2018].

Cammarota, M., Losi, G., Chiavegato, A., Zonta, M., and Carmignoto, G. (2013). Fast spiking interneuron control of seizure propagation in a cortical slice model of focal epilepsy. *J. Physiol.* 591, 807–822. doi:10.1113/jphysiol.2012.238154.

Cardin, J. A., Palmer, L. A., and Contreras, D. (2008). Cellular mechanisms underlying stimulus-dependent gain modulation in primary visual cortex neurons in vivo. *Neuron* 59, 150–160. doi:10.1016/j.neuron.2008.05.002.

Caspers, H., and Speckmann, E.-J. (1972). Cerebral pO2, pCO2 and pH: Changes During Convulsive Activity and their Significance for Spontaneous Arrest

of Seizures. *Epilepsia* 13, 699–725. doi:10.1111/j.1528-1157.1972.tb04403.x.

Cauli, B., Porter, J. T., Tsuzuki, K., Lambolez, B., Rossier, J., Quenet, B., et al. (2000). Classification of fusiform neocortical interneurons based on unsupervised clustering. *Proc. Natl. Acad. Sci. U. S. A.* 97, 6144–6149.

Cavazos, J., and Sutula, T. P. (1990). Progressive neuronal loss induced by kindling: a possible mechanism for mossy fiber synaptic reorganization and hippocampal sclerosis. *Brain Res.* 527, 1–6. doi:10.1016/0006-8993(90)91054-K.

Chamberland, S., Salesse, C., Topolnik, D., and Topolnik, L. (2010). Synapse-Specific Inhibitory Control of Hippocampal Feedback Inhibitory Circuit. *Front. Cell. Neurosci.* 4. doi:10.3389/fncel.2010.00130.

Chamberland, S., and Topolnik, L. (2012). Inhibitory control of hippocampal inhibitory neurons. *Front. Neurosci.* 6. doi:10.3389/fnins.2012.00165.

Chang, M., Dian, J. A., Dufour, S., Wang, L., Moradi Chameh, H., Ramani, M., et al. (2018a). Brief activation of GABAergic interneurons initiates the transition to ictal events through post-inhibitory rebound excitation. *Neurobiol. Dis.* 109, 102–116. doi:10.1016/j.nbd.2017.10.007.

Chang, R., Eriksen, J., and Edwards, R. H. (2018b). The dual role of chloride in synaptic vesicle glutamate transport. *eLife* 7. doi:10.7554/eLife.34896.

Chen, C.-C., Lu, J., Yang, R., Ding, J. B., and Zuo, Y. (2017). Selective activation of parvalbumin interneurons prevents stress-induced synapse loss and perceptual defects. *Mol. Psychiatry*. doi:10.1038/mp.2017.159.

Chen, G. Q., Cui, C., Mayer, M. L., and Gouaux, E. (1999). Functional characterization of a potassium-selective prokaryotic glutamate receptor. *Nature* 402, 817–821. doi:10.1038/45568.

Chen, K., Aradi, I., Thon, N., Eghbal-Ahmadi, M., Baram, T. Z., and Soltesz, I. (2001). Persistently modified h-channels after complex febrile seizures convert the seizure-induced enhancement of inhibition to hyperexcitability. *Nat. Med.* 7, 331–337. doi:10.1038/85480.

Chen, L.-M., Kelly, M. L., Parker, M. D., Bouyer, P., Gill, H. S., Felie, J. M., et al. (2008). Expression and localization of Na-driven Cl-HCO(3)(-) exchanger (SLC4A8) in rodent CNS. *Neuroscience* 153, 162–174. doi:10.1016/j.neuroscience.2008.02.018.

Chen, N.-H., Reith, M. E. A., and Quick, M. W. (2004). Synaptic uptake and beyond: the sodium- and chloride-dependent neurotransmitter transporter family SLC6. *Pflüg. Arch.* 447, 519–531. doi:10.1007/s00424-003-1064-5.

Cheng, Y. M., Kelly, T., and Church, J. (2008). Potential contribution of a voltage-activated proton conductance to acid extrusion from rat hippocampal neurons. *Neuroscience* 151, 1084–1098. doi:10.1016/j.neuroscience.2007.12.007.

Chervin, R. D., Pierce, P. A., and Connors, B. W. (1988). Periodicity and directionality in the propagation of epileptiform discharges across neocortex. *J. Neurophysiol.* 60, 1695–1713. doi:10.1152/jn.1988.60.5.1695.

Chesler, M. (2003). Regulation and Modulation of pH in the Brain. *Physiol. Rev.* 83, 1183–1221. doi:10.1152/physrev.00010.2003.

Chesler, M., and Kaila, K. (1992). Modulation of pH by neuronal activity. *Trends Neurosci.* 15, 396–402.

Chow, A., Erisir, A., Farb, C., Nadal, M. S., Ozaita, A., Lau, D., et al. (1999). K(+) channel expression distinguishes subpopulations of parvalbumin- and somatostatin-containing neocortical interneurons. *J. Neurosci. Off. J. Soc. Neurosci.* 19, 9332–9345.

Chow, B. Y., Han, X., Dobry, A. S., Qian, X., Chuong, A. S., Li, M., et al. (2010). High-performance genetically targetable optical neural silencing by light-driven proton pumps. *Nature* 463, 98–102. doi:10.1038/nature08652.

Chuong, A. S., Miri, M. L., Busskamp, V., Matthews, G. A. C., Acker, L. C., Sørensen, A. T., et al. (2014). Noninvasive optical inhibition with a red-shifted microbial rhodopsin. *Nat. Neurosci.* 17, 1123–1129. doi:10.1038/nn.3752.

Cobb, S. R., Buhl, E. H., Halasy, K., Paulsen, O., and Somogyi, P. (1995). Synchronization of neuronal activity in hippocampus by individual GABAergic interneurons. *Nature* 378, 75–78. doi:10.1038/378075a0.

Cobos, I., Calcagnotto, M. E., Vilaythong, A. J., Thwin, M. T., Noebels, J. L., Baraban, S. C., et al. (2005). Mice lacking *Dlx1* show subtype-specific loss of interneurons, reduced inhibition and epilepsy. *Nat. Neurosci.* 8, 1059–1068. doi:10.1038/nn1499.

Cohen, I., Navarro, V., Clemenceau, S., Baulac, M., and Miles, R. (2002). On the Origin of Interictal Activity in Human Temporal Lobe Epilepsy in Vitro. *Science* 298, 1418–1421. doi:10.1126/science.1076510.

Cooper, D. S., Yang, H. S., He, P., Kim, E., Rajbhandari, I., Yun, C. C., et al. (2009). Sodium/bicarbonate cotransporter NBCn1/slc4a7 increases cytotoxicity in magnesium depletion in primary cultures of hippocampal

neurons. *Eur. J. Neurosci.* 29, 437–446. doi:10.1111/j.1460-9568.2008.06611.x.

Cope, D. W., Maccaferri, G., Márton, L. F., Roberts, J. D. B., Cobden, P. M., and Somogyi, P. (2002). Cholecystokinin-immunopositive basket and Schaffer collateral-associated interneurones target different domains of pyramidal cells in the CA1 area of the rat hippocampus. *Neuroscience* 109, 63–80. doi:10.1016/S0306-4522(01)00440-7.

Cosentino, C., Alberio, L., Gazzarrini, S., Aquila, M., Romano, E., Cermenati, S., et al. (2015). Optogenetics. Engineering of a light-gated potassium channel. *Science* 348, 707–710. doi:10.1126/science.aaa2787.

Cossart, R., Dinocourt, C., Hirsch, J. C., Merchan-Perez, A., De Felipe, J., Ben-Ari, Y., et al. (2001). Dendritic but not somatic GABAergic inhibition is decreased in experimental epilepsy. *Nat. Neurosci.* 4, 52–62. doi:10.1038/82900.

Cristo, G. D., Wu, C., Chattopadhyaya, B., Ango, F., Knott, G., Welker, E., et al. (2004). Subcellular domain-restricted GABAergic innervation in primary visual cortex in the absence of sensory and thalamic inputs. *Nat. Neurosci.* 7, 1184–1186. doi:10.1038/nn1334.

Csicsvari, J., Hirase, H., Czurko, A., and Buzsáki, G. (1998). Reliability and state dependence of pyramidal cell-interneuron synapses in the hippocampus: an ensemble approach in the behaving rat. *Neuron* 21, 179–189.

Cunha-Reis, D., Ribeiro, J. A., and Sebastião, A. M. (2005). VIP enhances synaptic transmission to hippocampal CA1 pyramidal cells through activation of both VPAC1 and VPAC2 receptors. *Brain Res.* 1049, 52–60. doi:10.1016/j.brainres.2005.04.077.

Czapiński, P., Blaszczyk, B., and Czuczwar, S. J. (2005). Mechanisms of action of antiepileptic drugs. *Curr. Top. Med. Chem.* 5, 3–14. doi:https://doi.org/10.2174/1568026053386962.

Damkier, H. H., Nielsen, S., and Praetorius, J. (2007). Molecular expression of SLC4-derived Na+-dependent anion transporters in selected human tissues. *Am. J. Physiol. Regul. Integr. Comp. Physiol.* 293, R2136-2146. doi:10.1152/ajpregu.00356.2007.

de Lanerolle, N. C., Kim, J. H., Robbins, R. J., and Spencer, D. D. (1989). Hippocampal interneuron loss and plasticity in human temporal lobe epilepsy. *Brain Res.* 495, 387–395. doi:10.1016/0006-8993(89)90234-5.

De Schutter, E., and Bower, J. M. (1994). An active membrane model of the cerebellar Purkinje cell. I. Simulation of current clamps in slice. *J. Neurophysiol.* 71, 375–400. doi:10.1152/jn.1994.71.1.375.

De Simoni, A., Griesinger, C. B., and Edwards, F. A. (2003). Development of rat CA1 neurones in acute versus organotypic slices: role of experience in synaptic morphology and activity. *J. Physiol.* 550, 135–147. doi:10.1113/jphysiol.2003.039099.

DeFelipe, J. (1993). Neocortical Neuronal Diversity: Chemical Heterogeneity Revealed by Colocalization Studies of Classic Neurotransmitters, Neuropeptides, Calcium-binding Proteins, and Cell Surface Molecules. *Cereb. Cortex* 3, 273–289. doi:10.1093/cercor/3.4.273.

Deisseroth, K. (2010). Optogenetics. *Nat. Methods*. doi:10.1038/nmeth.f.324.

Denker, S. P., and Barber, D. L. (2002). Cell migration requires both ion translocation and cytoskeletal anchoring by the Na-H exchanger NHE1. *J. Cell Biol.* 159, 1087–1096. doi:10.1083/jcb.200208050.

Derchansky, M., Jahromi, S. S., Mamani, M., Shin, D. S., Sik, A., and Carlen, P. L. (2008). Transition to seizures in the isolated immature mouse hippocampus: a switch from dominant phasic inhibition to dominant phasic excitation. *J. Physiol.* 586, 477–494. doi:10.1113/jphysiol.2007.143065.

Devinsky, O., Hesdorffer, D. C., Thurman, D. J., Lhatoo, S., and Richerson, G. (2016). Sudden unexpected death in epilepsy: epidemiology, mechanisms, and prevention. *Lancet Neurol.* 15, 1075–1088. doi:10.1016/S1474-4422(16)30158-2.

Devinsky, O., Vezzani, A., O'Brien, T. J., Jette, N., Scheffer, I. E., Curtis, M. de, et al. (2018). Epilepsy. *Nat. Rev. Dis. Primer* 4, 18024. doi:10.1038/nrdp.2018.24.

Dichter, M. A., and Ayala, G. F. (1987). Cellular mechanisms of epilepsy: a status report. *Science* 237, 157–164.

Dixon, D. B., Takahashi, K., and Copenhagen, D. R. (1993). L-glutamate suppresses HVA calcium current in catfish horizontal cells by raising intracellular proton concentration. *Neuron* 11, 267–277.

Dodge, F. A., and Rahamimoff, R. (1967). Co-operative action of calcium ions in transmitter release at the neuromuscular junction. *J. Physiol.* 193, 419–432.

Doyon, N., Vinay, L., Prescott, S. A., and De Koninck, Y. (2016). Chloride Regulation: A Dynamic Equilibrium Crucial for Synaptic Inhibition. *Neuron* 89, 1157–1172. doi:10.1016/j.neuron.2016.02.030.

Drapeau, P., and Nachshen, D. A. (1988). Effects of lowering extracellular and cytosolic pH on calcium fluxes, cytosolic calcium levels, and transmitter release in presynaptic nerve terminals isolated from rat brain. *J. Gen. Physiol.* 91, 305–315.

Du, J., Zhang, L., Weiser, M., Rudy, B., and McBain, C. J. (1996). Developmental expression and functional characterization of the potassium-channel subunit Kv3.1b in parvalbumin-containing interneurons of the rat hippocampus. *J. Neurosci. Off. J. Soc. Neurosci.* 16, 506–518.

Düsterwald, K. M., Currin, C. B., Burman, R. J., Akerman, C. J., Kay, A. R., and Raimondo, J. V. (2018). Biophysical models reveal the relative importance of transporter proteins and impermeant anions in chloride homeostasis. *eLife* 7, e39575. doi:10.7554/eLife.39575.

Dyhrfjeld-Johnsen, J., Berdichevsky, Y., Swiercz, W., Sabolek, H., and Staley, K. J. (2010). Interictal Spikes Precede Ictal Discharges in an Organotypic Hippocampal Slice Culture Model of Epileptogenesis. *J. Clin. Neurophysiol.* 27, 418–424. doi:10.1097/WNP.0b013e3181fe0709.

Dzhala, V. I., Kuchibhotla, K. V., Glykys, J. C., Kahle, K. T., Swiercz, W. B., Feng, G., et al. (2010). Progressive NKCC1-Dependent Neuronal Chloride Accumulation during Neonatal Seizures. *J. Neurosci.* 30, 11745–11761. doi:10.1523/JNEUROSCI.1769-10.2010.

Ellender, T. J., Raimondo, J. V., Irkle, A., Lamsa, K. P., and Akerman, C. J. (2014). Excitatory Effects of Parvalbumin-Expressing Interneurons Maintain Hippocampal Epileptiform Activity via Synchronous Afterdischarges. *J. Neurosci.* 34, 15208–15222. doi:10.1523/JNEUROSCI.1747-14.2014.

Faber, E. S. L., and Sah, P. (2003). Calcium-activated potassium channels: multiple contributions to neuronal function. *Neurosci. Rev. J. Bringing Neurobiol. Neurol. Psychiatry* 9, 181–194. doi:10.1177/1073858403009003011.

Faundez, V., and Hartzell, H. C. (2004). Intracellular Chloride Channels: Determinants of Function in the Endosomal Pathway. *Sci. Signal.* 2004, re8–re8. doi:10.1126/stke.2332004re8.

Fazel, S., Wolf, A., Långström, N., Newton, C. R., and Lichtenstein, P. (2013). Premature mortality in epilepsy and the role of psychiatric comorbidity: a total population study. *The Lancet* 382, 1646–1654. doi:10.1016/S0140-6736(13)60899-5.

Feldberg, W., and Sherwood, S. L. (1957). Effects of calcium and potassium injected into the cerebral ventricles of the cat. *J. Physiol.* 139, 408–416.

Fisher, R. E., Gray, R., and Johnston, D. (1990). Properties and distribution of single voltage-gated calcium channels in adult hippocampal neurons. *J. Neurophysiol.* 64, 91–104. doi:10.1152/jn.1990.64.1.91.

Fisher, R. S., Acevedo, C., Arzimanoglou, A., Bogacz, A., Cross, J. H., Elger, C. E., et al. (2014). ILAE official report: a practical clinical definition of epilepsy. *Epilepsia* 55, 475–482. doi:10.1111/epi.12550.

Forcelli, P. A. (2017). Applications of optogenetic and chemogenetic methods to seizure circuits: Where to go next? *J. Neurosci. Res.* 95, 2345–2356. doi:10.1002/jnr.24135.

Forgac, M. (2007). Vacuolar ATPases: rotary proton pumps in physiology and pathophysiology. *Nat. Rev. Mol. Cell Biol.* 8, 917–929. doi:10.1038/nrm2272.

Freund, T. F., and Buzsáki, G. (1996). Interneurons of the hippocampus. *Hippocampus* 6, 347–470. doi:10.1002/(SICI)1098-1063(1996)6:4<347::AID-HIPO1>3.0.CO;2-I.

Fritschy, J.-M. (2008). Epilepsy, E/I balance and GABAA receptor plasticity. *Front. Mol. Neurosci.* 1. doi:10.3389/neuro.02.005.2008.

Fröhlich, F., Bazhenov, M., Iragui-Madoz, V., and Sejnowski, T. J. (2008). Potassium dynamics in the epileptic cortex: new insights on an old topic. *Neurosci. Rev. J. Bringing Neurobiol. Neurol. Psychiatry* 14, 422–433. doi:10.1177/1073858408317955.

Frotscher, M., and Zimmer, J. (1983). Lesion-induced mossy fibers to the molecular layer of the rat fascia dentata: identification of postsynaptic granule cells by the Golgi-EM technique. *J. Comp. Neurol.* 215, 299–311. doi:10.1002/cne.902150306.

Fuentealba, P., Begum, R., Capogna, M., Jinno, S., Márton, L. F., Csicsvari, J., et al. (2008). Ivy Cells: A Population of Nitric-Oxide-Producing, Slow-Spiking GABAergic Neurons and Their Involvement in Hippocampal Network Activity. *Neuron* 57, 917–929. doi:10.1016/j.neuron.2008.01.034.

Fuentealba, P., Klausberger, T., Karayannis, T., Suen, W. Y., Huck, J., Tomioka, R., et al. (2010). Expression of COUP-TFII Nuclear Receptor in Restricted GABAergic Neuronal Populations in the Adult Rat Hippocampus. *J. Neurosci.* 30, 1595–1609. doi:10.1523/JNEUROSCI.4199-09.2010.

Fujiwara-Tsukamoto, Y., Isomura, Y., Kaneda, K., and Takada, M. (2004). Synaptic interactions between pyramidal cells and interneurone subtypes during seizure-like activity in the rat hippocampus. *J. Physiol.* 557, 961–979. doi:10.1113/jphysiol.2003.059915.

Gale, K. (1992). GABA and epilepsy: basic concepts from preclinical research. *Epilepsia* 33 Suppl 5, S3-12.

Gatto, C., and Milanick, M. A. (1993). Inhibition of the red blood cell calcium pump by eosin and other fluorescein analogues. *Am. J. Physiol.* 264, C1577-1586. doi:10.1152/ajpcell.1993.264.6.C1577.

Giffard, R. G., Monyer, H., Christine, C. W., and Choi, D. W. (1990). Acidosis reduces NMDA receptor activation, glutamate neurotoxicity, and oxygen-glucose deprivation neuronal injury in cortical cultures. *Brain Res.* 506, 339–342.

Giustizieri, M., Bernardi, G., Mercuri, N. B., and Berretta, N. (2005). Distinct Mechanisms of Presynaptic Inhibition at GABAergic Synapses of the Rat Substantia Nigra Pars Compacta. *J. Neurophysiol.* 94, 1992–2003. doi:10.1152/jn.00171.2005.

Glickfeld, L. L., Roberts, J. D., Somogyi, P., and Scanziani, M. (2009). Interneurons hyperpolarize pyramidal cells along their entire somatodendritic axis. *Nat. Neurosci.* 12, 21–23. doi:10.1038/nn.2230.

Glykys, J., Dzhala, V., Egawa, K., Balena, T., Saponjian, Y., Kuchibhotla, K. V., et al. (2014). Local impermeant anions establish the neuronal chloride concentration. *Science* 343, 670–675. doi:10.1126/science.1245423.

Goddard, G. V. (1967). Development of Epileptic Seizures through Brain Stimulation at Low Intensity. *Nature* 214, 1020–1021. doi:10.1038/2141020a0.

Gomez, J. L., Bonaventura, J., Lesniak, W., Mathews, W. B., Sysa-Shah, P., Rodriguez, L. A., et al. (2017). Chemogenetics revealed: DREADD occupancy and activation via converted clozapine. *Science* 357, 503–507. doi:10.1126/science.aan2475.

Grichtchenko, I. I., Choi, I., Zhong, X., Bray-Ward, P., Russell, J. M., and Boron, W. F. (2001). Cloning, characterization, and chromosomal mapping of a human electroneutral Na(+)-driven Cl-HCO3 exchanger. *J. Biol. Chem.* 276, 8358–8363. doi:10.1074/jbc.C000716200.

Grimley, J. S., Li, L., Wang, W., Wen, L., Beese, L. S., Hellinga, H. W., et al. (2013). Visualization of Synaptic Inhibition with an Optogenetic Sensor Developed by Cell-Free Protein Engineering Automation. *J. Neurosci.* 33, 16297–16309. doi:10.1523/JNEUROSCI.4616-11.2013.

Grynkiewicz, G., Poenie, M., and Tsien, R. Y. (1985). A new generation of Ca2+ indicators with greatly improved fluorescence properties. *J. Biol. Chem.* 260, 3440–3450.

Guerrini, R., and Dobyns, W. B. (2014). Malformations of cortical development: clinical features and genetic causes. *Lancet Neurol.* 13, 710–726. doi:10.1016/S1474-4422(14)70040-7.

Gulyás, A. I., Hájos, N., and Freund, T. F. (1996). Interneurons containing calretinin are specialized to control other interneurons in the rat hippocampus. *J. Neurosci. Off. J. Soc. Neurosci.* 16, 3397–3411.

Gustafsson, B., Galvan, M., Grafe, P., and Wigström, H. (1982). A transient outward current in a mammalian central neurone blocked by 4-aminopyridine. *Nature* 299, 252–254. doi:10.1038/299252a0.

Gutiérrez, R., Armand, V., Schuchmann, S., and Heinemann, U. (1999). Epileptiform activity induced by low Mg2+ in cultured rat hippocampal slices. *Brain Res.* 815, 294–303.

Gutiérrez, R., and Heinemann, U. (1999). Synaptic reorganization in explanted cultures of rat hippocampus. *Brain Res.* 815, 304–316.

Haider, B., Duque, A., Hasenstaub, A. R., and McCormick, D. A. (2006). Neocortical network activity in vivo is generated through a dynamic balance of excitation and inhibition. *J. Neurosci. Off. J. Soc. Neurosci.* 26, 4535–4545. doi:10.1523/JNEUROSCI.5297-05.2006.

Halasy, K., Buhl, E. H., Lörinczi, Z., Tamás, G., and Somogyi, P. (1996). Synaptic target selectivity and input of GABAergic basket and bistratified interneurons in the CA1 area of the rat hippocampus. *Hippocampus* 6, 306–329. doi:10.1002/(SICI)1098-1063(1996)6:3<306::AID-HIPO8>3.0.CO;2-K.

Hamidi, S., and Avoli, M. (2015). Carbonic anhydrase inhibition by acetazolamide reduces in vitro epileptiform synchronization. *Neuropharmacology* 95, 377–387. doi:10.1016/j.neuropharm.2015.04.015.

Hamm, J. P., and Yuste, R. (2016). Somatostatin interneurons control a key component of mismatch negativity in the mouse visual cortex. *Cell Rep.* 16, 597–604. doi:10.1016/j.celrep.2016.06.037.

Han, X., and Boyden, E. S. (2007). Multiple-color optical activation, silencing, and desynchronization of neural activity, with single-spike temporal resolution. *PloS One* 2, e299. doi:10.1371/journal.pone.0000299.

Han, X., Chow, B. Y., Zhou, H., Klapoetke, N. C., Chuong, A., Rajimehr, R., et al. (2011). A high-light sensitivity optical neural silencer: development and application to optogenetic control of non-human primate cortex. *Front. Syst. Neurosci.* 5, 18. doi:10.3389/fnsys.2011.00018.

Harris, K. D., Hochgerner, H., Skene, N. G., Magno, L., Katona, L., Bengtsson Gonzales, C., et al. (2018). Classes and continua of hippocampal CA1 inhibitory neurons revealed by single-cell transcriptomics. *PLoS Biol.* 16, e2006387. doi:10.1371/journal.pbio.2006387.

Hartline, H. K., Wagner, H. G., and Ratliff, F. (1956). Inhibition in the eye of Limulus. *J. Gen. Physiol.* 39, 651–673.

Hauser, W. A., and Beghi, E. (2008). First seizure definitions and worldwide incidence and mortality. *Epilepsia* 49 Suppl 1, 8–12. doi:10.1111/j.1528-1167.2008.01443.x.

Heinemann, U., Beck, H., Dreier, J. P., Ficker, E., Stabel, J., and Zhang, C. L. (1992). The dentate gyrus as a regulated gate for the propagation of epileptiform activity. *Epilepsy Res. Suppl.* 7, 273–280.

Hentschke, M., Wiemann, M., Hentschke, S., Kurth, I., Hermans-Borgmeyer, I., Seidenbecher, T., et al. (2006). Mice with a Targeted Disruption of the Cl−/HCO3− Exchanger AE3 Display a Reduced Seizure Threshold. *Mol. Cell. Biol.* 26, 182–191. doi:10.1128/MCB.26.1.182-191.2006.

Higo, S., Udaka, N., and Tamamaki, N. (2007). Long-range GABAergic projection neurons in the cat neocortex. *J. Comp. Neurol.* 503, 421–431. doi:10.1002/cne.21395.

Hill, D. R., and Bowery, N. G. (1981). 3H-baclofen and 3H-GABA bind to bicuculline-insensitive GABA B sites in rat brain. *Nature* 290, 149–152.

Hille, B. (1978). Ionic channels in excitable membranes. Current problems and biophysical approaches. *Biophys. J.* 22, 283–294.

Hinterkeuser, S., Schröder, W., Hager, G., Seifert, G., Blümcke, I., Elger, C. E., et al. (2000). Astrocytes in the hippocampus of patients with temporal lobe epilepsy display changes in potassium conductances. *Eur. J. Neurosci.* 12, 2087–2096.

Howard, M. A., Rubenstein, J. L. R., and Baraban, S. C. (2014). Bidirectional homeostatic plasticity induced by interneuron cell death and transplantation in vivo. *Proc. Natl. Acad. Sci.* 111, 492–497. doi:10.1073/pnas.1307784111.

Hu, H., Gan, J., and Jonas, P. (2014). Fast-spiking, parvalbumin+ GABAergic interneurons: From cellular design to microcircuit function. *Science* 345, 1255263. doi:10.1126/science.1255263.

Huang, W. C., Xiao, S., Huang, F., Harfe, B. D., Jan, Y. N., and Jan, L. Y. (2012). Calcium-Activated Chloride Channels (CaCCs) Regulate Action Potential

and Synaptic Response in Hippocampal Neurons. *Neuron* 74, 179–192. doi:10.1016/j.neuron.2012.01.033.

Huber, D., Petreanu, L., Ghitani, N., Ranade, S., Hromádka, T., Mainen, Z., et al. (2008). Sparse optical microstimulation in barrel cortex drives learned behaviour in freely moving mice. *Nature* 451, 61–64. doi:10.1038/nature06445.

Huberfeld, G., Wittner, L., Clemenceau, S., Baulac, M., Kaila, K., Miles, R., et al. (2007). Perturbed Chloride Homeostasis and GABAergic Signaling in Human Temporal Lobe Epilepsy. *J. Neurosci.* 27, 9866–9873. doi:10.1523/JNEUROSCI.2761-07.2007.

Hunt, R. F., and Baraban, S. C. (2015). Interneuron Transplantation as a Treatment for Epilepsy. *Cold Spring Harb. Perspect. Med.* 5, a022376. doi:10.1101/cshperspect.a022376.

Ilg, A.-K., Enkel, T., Bartsch, D., and Bähner, F. (2018). Behavioral Effects of Acute Systemic Low-Dose Clozapine in Wild-Type Rats: Implications for the Use of DREADDs in Behavioral Neuroscience. *Front. Behav. Neurosci.* 12. doi:10.3389/fnbeh.2018.00173.

Ilie, A., Raimondo, J. V., and Akerman, C. J. (2012). Adenosine Release during Seizures Attenuates GABAA Receptor-Mediated Depolarization. *J. Neurosci.* 32, 5321–5332. doi:10.1523/JNEUROSCI.5412-11.2012.

Isaacson, J. S., and Scanziani, M. (2011). How inhibition shapes cortical activity. *Neuron* 72, 231–243. doi:10.1016/j.neuron.2011.09.027.

Isokawa, M., Levesque, M. F., Babb, T. L., and Engel, J. (1993). Single mossy fiber axonal systems of human dentate granule cells studied in hippocampal slices from patients with temporal lobe epilepsy. *J. Neurosci. Off. J. Soc. Neurosci.* 13, 1511–1522.

Isomura, Y., Fujiwara-Tsukamoto, Y., and Takada, M. (2008). A network mechanism underlying hippocampal seizure-like synchronous oscillations. *Neurosci. Res.* 61, 227–233. doi:10.1016/j.neures.2008.04.002.

Jackson, J., Ayzenshtat, I., Karnani, M. M., and Yuste, R. (2016). VIP+ interneurons control neocortical activity across brain states. *J. Neurophysiol.* 115, 3008–3017. doi:10.1152/jn.01124.2015.

Janovjak, H., Szobota, S., Wyart, C., Trauner, D., and Isacoff, E. Y. (2010). A light-gated, potassium-selective glutamate receptor for the optical inhibition of neuronal firing. *Nat. Neurosci.* 13, 1027–1032. doi:10.1038/nn.2589.

Jefferys, J. G. (1990). Basic mechanisms of focal epilepsies. *Exp. Physiol.* 75, 127–162. doi:10.1113/expphysiol.1990.sp003390.

Jentsch, T. J., Stein, V., Weinreich, F., and Zdebik, A. A. (2002). Molecular structure and physiological function of chloride channels. *Physiol. Rev.* 82, 503–568. doi:10.1152/physrev.00029.2001.

Jobe, P. C., Picchioni, A. L., and Chin, L. (1973). Role of brain norepinephrine in audiogenic seizure in the rat. *J. Pharmacol. Exp. Ther.* 184, 1–10.

Johnson, J. L. (1978). The excitant amino acids glutamic and aspartic acid as transmitter candidates in the vertebrate central nervous system. *Prog. Neurobiol.* 10, 155–202.

Jones, R. S. G., and Heinemann, U. (1987). Pre and postsynaptic K+ and Ca2+ fluxes in area CA1 of the rat hippocampus in vitro: effects of Ni2+, TEA and 4-AP. *Exp. Brain Res.* 68, 205–209. doi:10.1007/BF00255246.

Kaila, K. (1994). Ionic basis of GABAA receptor channel function in the nervous system. *Prog. Neurobiol.* 42, 489–537.

Kaila, K., Paalasmaa, P., Taira, T., and Voipio, J. (1992). pH transients due to monosynaptic activation of GABAA receptors in rat hippocampal slices. *Neuroreport* 3, 105–108.

Kaila, K., Pasternack, M., Saarikoski, J., and Voipio, J. (1989). Influence of GABA-gated bicarbonate conductance on potential, current and intracellular chloride in crayfish muscle fibres. *J. Physiol.* 416, 161–181.

Kaila, K., Ruusuvuori, E., Seja, P., Voipio, J., and Puskarjov, M. (2014). GABA actions and ionic plasticity in epilepsy. *Curr. Opin. Neurobiol.* 26, 34–41. doi:10.1016/j.conb.2013.11.004.

Kaila, K., and Voipio, J. (1987). Postsynaptic fall in intracellular pH induced by GABA-activated bicarbonate conductance. *Nature* 330, 163–165. doi:10.1038/330163a0.

Kampa, B. M., Clements, J., Jonas, P., and Stuart, G. J. (2004). Kinetics of Mg2+ unblock of NMDA receptors: implications for spike-timing dependent synaptic plasticity. *J. Physiol.* 556, 337–345. doi:10.1113/jphysiol.2003.058842.

Kandratavicius, L., Balista, P. A., Lopes-Aguiar, C., Ruggiero, R. N., Umeoka, E. H., Garcia-Cairasco, N., et al. (2014). Animal models of epilepsy: use and limitations. *Neuropsychiatr. Dis. Treat.* 10, 1693–1705. doi:10.2147/NDT.S50371.

Katona, I., Acsády, L., and Freund, T. F. (1999). Postsynaptic targets of somatostatin-immunoreactive interneurons in the rat hippocampus. *Neuroscience* 88, 37–55. doi:10.1016/S0306-4522(98)00302-9.

Kätzel, D., Nicholson, E., Schorge, S., Walker, M. C., and Kullmann, D. M. (2014). Chemical–genetic attenuation of focal neocortical seizures. *Nat. Commun.* 5, 3847. doi:10.1038/ncomms4847.

Kawaguchi, Y., Katsumaru, H., Kosaka, T., Heizmann, C. W., and Hama, K. (1987). Fast spiking cells in rat hippocampus (CA1 region) contain the calcium-binding protein parvalbumin. *Brain Res.* 416, 369–374. doi:10.1016/0006-8993(87)90921-8.

Keezer, M. R., Sisodiya, S. M., and Sander, J. W. (2016). Comorbidities of epilepsy: current concepts and future perspectives. *Lancet Neurol.* 15, 106–115. doi:10.1016/S1474-4422(15)00225-2.

Khoshkhoo, S., Vogt, D., and Sohal, V. S. (2017). Dynamic, Cell-Type-Specific Roles for GABAergic Interneurons in a Mouse Model of Optogenetically Inducible Seizures. *Neuron* 93, 291–298. doi:10.1016/j.neuron.2016.11.043.

Kida, E., Palminiello, S., Golabek, A. A., Walus, M., Wierzba-Bobrowicz, T., Rabe, A., et al. (2006). Carbonic anhydrase II in the developing and adult human brain. *J. Neuropathol. Exp. Neurol.* 65, 664–674. doi:10.1097/01.jnen.0000225905.52002.3e.

Klausberger, T. (2009). GABAergic interneurons targeting dendrites of pyramidal cells in the CA1 area of the hippocampus. *Eur. J. Neurosci.* 30, 947–957. doi:10.1111/j.1460-9568.2009.06913.x.

Klausberger, T., Magill, P. J., Márton, L. F., Roberts, J. D. B., Cobden, P. M., Buzsáki, G., et al. (2003). Brain-state- and cell-type-specific firing of hippocampal interneurons in vivo. *Nature* 421, 844–848. doi:10.1038/nature01374.

Klausberger, T., Márton, L. F., Baude, A., Roberts, J. D. B., Magill, P. J., and Somogyi, P. (2004). Spike timing of dendrite-targeting bistratified cells during hippocampal network oscillations *in vivo*. *Nat. Neurosci.* 7, 41–47. doi:10.1038/nn1159.

Klausberger, T., Marton, L. F., O'Neill, J., Huck, J. H. J., Dalezios, Y., Fuentealba, P., et al. (2005). Complementary Roles of Cholecystokinin- and Parvalbumin-Expressing GABAergic Neurons in Hippocampal Network Oscillations. *J. Neurosci.* 25, 9782–9793. doi:10.1523/JNEUROSCI.3269-05.2005.

Klausberger, T., and Somogyi, P. (2008). Neuronal Diversity and Temporal Dynamics: The Unity of Hippocampal Circuit Operations. *Science* 321, 53–57. doi:10.1126/science.1149381.

Knierim, J. J. (2015). The hippocampus. *Curr. Biol.* 25, R1116–R1121. doi:10.1016/j.cub.2015.10.049.

Ko, H., Hofer, S. B., Pichler, B., Buchanan, K. A., Sjöström, P. J., and Mrsic-Flogel, T. D. (2011). Functional specificity of local synaptic connections in neocortical networks. *Nature* 473, 87–91. doi:10.1038/nature09880.

Kofuji, P., and Newman, E. A. (2004). Potassium buffering in the central nervous system. *Neuroscience* 129, 1045–1056. doi:10.1016/j.neuroscience.2004.06.008.

Köhler, C. (1982). Distribution and morphology of vasoactive intestinal polypeptide-like immunoreactive neurons in regio superior of the rat hippocampal formation. *Neurosci. Lett.* 33, 265–270. doi:10.1016/0304-3940(82)90382-2.

Kraushaar, U., and Jonas, P. (2000). Efficacy and Stability of Quantal GABA Release at a Hippocampal Interneuron–Principal Neuron Synapse. *J. Neurosci.* 20, 5594–5607. doi:10.1523/JNEUROSCI.20-15-05594.2000.

Krishtal, O. A., Osipchuk, Y. V., Shelest, T. N., and Smirnoff, S. V. (1987). Rapid extracellular pH transients related to synaptic transmission in rat hippocampal slices. *Brain Res.* 436, 352–356.

Krook-Magnuson, E., Armstrong, C., Oijala, M., and Soltesz, I. (2013). On-demand optogenetic control of spontaneous seizures in temporal lobe epilepsy. *Nat. Commun.* 4, 1376. doi:10.1038/ncomms2376.

Kumar, S. S., and Buckmaster, P. S. (2006). Hyperexcitability, Interneurons, and Loss of GABAergic Synapses in Entorhinal Cortex in a Model of Temporal Lobe Epilepsy. *J. Neurosci.* 26, 4613–4623. doi:10.1523/JNEUROSCI.0064-06.2006.

Kuner, T., and Augustine, G. J. (2000). A Genetically Encoded Ratiometric Indicator for Chloride: Capturing Chloride Transients in Cultured Hippocampal Neurons. *Neuron* 27, 447–459. doi:10.1016/S0896-6273(00)00056-8.

Kupferberg, H. (2001). Animal Models Used in the Screening of Antiepileptic Drugs. *Epilepsia* 42, 7–12. doi:10.1111/j.1528-1167.2001.00002.x.

Kwan, P., and Brodie, M. J. (2009). Early Identification of Refractory Epilepsy. *http://dx.doi.org/10.1056/NEJM200002033420503*. doi:10.1056/NEJM200002033420503.

Kyrozis, A., and Reichling, D. B. (1995). Perforated-patch recording with gramicidin avoids artifactual changes in intracellular chloride concentration. *J. Neurosci. Methods* 57, 27–35.

Lam, T. I., Brennan-Minnella, A. M., Won, S. J., Shen, Y., Hefner, C., Shi, Y., et al. (2013). Intracellular pH reduction prevents excitotoxic and ischemic neuronal death by inhibiting NADPH oxidase. *Proc. Natl. Acad. Sci.* 110, E4362–E4368. doi:10.1073/pnas.1313029110.

Lancaster, E., and Dalmau, J. (2012). Neuronal autoantigens—pathogenesis, associated disorders and antibody testing. *Nat. Rev. Neurol.* 8, 380–390. doi:10.1038/nrneurol.2012.99.

Lancaster, E., Lai, M., Peng, X., Hughes, E., Constantinescu, R., Raizer, J., et al. (2010). Antibodies to the GABA(B) receptor in limbic encephalitis with seizures: case series and characterisation of the antigen. *Lancet Neurol.* 9, 67–76. doi:10.1016/S1474-4422(09)70324-2.

Ledri, M., Madsen, M. G., Nikitidou, L., Kirik, D., and Kokaia, M. (2014). Global Optogenetic Activation of Inhibitory Interneurons during Epileptiform Activity. *J. Neurosci.* 34, 3364–3377. doi:10.1523/JNEUROSCI.2734-13.2014.

Lee, H. H. C., Walker, J. A., Williams, J. R., Goodier, R. J., Payne, J. A., and Moss, S. J. (2007). Direct protein kinase C-dependent phosphorylation regulates the cell surface stability and activity of the potassium chloride cotransporter KCC2. *J. Biol. Chem.* 282, 29777–29784. doi:10.1074/jbc.M705053200.

Lee, S., Hjerling-Leffler, J., Zagha, E., Fishell, G., and Rudy, B. (2010). The Largest Group of Superficial Neocortical GABAergic Interneurons Expresses Ionotropic Serotonin Receptors. *J. Neurosci.* 30, 16796–16808. doi:10.1523/JNEUROSCI.1869-10.2010.

Lee, S., Kruglikov, I., Huang, Z. J., Fishell, G., and Rudy, B. (2013). A disinhibitory circuit mediates motor integration in the somatosensory cortex. *Nat. Neurosci.* 16, 1662–1670. doi:10.1038/nn.3544.

Leestma, J. E., Annegers, J. F., Brodie, M. J., Brown, S., Schraeder, P., Siscovick, D., et al. (1997). Sudden unexplained death in epilepsy: observations from a large clinical development program. *Epilepsia* 38, 47–55.

Lehmann, T. N., Gabriel, S., Eilers, A., Njunting, M., Kovacs, R., Schulze, K., et al. (2001). Fluorescent tracer in pilocarpine-treated rats shows widespread aberrant hippocampal neuronal connectivity. *Eur. J. Neurosci.* 14, 83–95.

Leniger, T., Wiemann, M., Bingmann, D., Widman, G., Hufnagel, A., and Bonnet, U. (2002). Carbonic anhydrase inhibitor sulthiame reduces intracellular pH and epileptiform activity of hippocampal CA3 neurons. *Epilepsia* 43, 469–474.

Lennox, W. (1928a). The effect on epileptic seizures of varying the composition of the respired air. *J Clin Invest* 6, 23–24.

Lennox, W. G. (1928b). Ketogenic Diet in the Treatment of Epilepsy. *N. Engl. J. Med.* 199, 74–75. doi:10.1056/NEJM192807121990206.

Léránth, Cs., Frotscher, M., Tömböl, T., and Palkovits, M. (1984). Ultrastructure and synaptic connections of vasoactive intestinal polypeptide-like immunoreactive non-pyramidal neurons and axon terminals in the rat hippocampus. *Neuroscience* 12, 531–542. doi:10.1016/0306-4522(84)90071-X.

Lesage, F. (2003). Pharmacology of neuronal background potassium channels. *Neuropharmacology* 44, 1–7.

Letzkus, J. J., Wolff, S. B. E., Meyer, E. M. M., Tovote, P., Courtin, J., Herry, C., et al. (2011). A disinhibitory microcircuit for associative fear learning in the auditory cortex. *Nature* 480, 331–335. doi:10.1038/nature10674.

Lieb, A., Qiu, Y., Dixon, C. L., Heller, J. P., Walker, M. C., Schorge, S., et al. (2018). Biochemical autoregulatory gene therapy for focal epilepsy. *Nat. Med.* 24, 1324–1329. doi:10.1038/s41591-018-0103-x.

Lillis, K. P., Wang, Z., Mail, M., Zhao, G. Q., Berdichevsky, Y., Bacskai, B., et al. (2015). Evolution of Network Synchronization during Early Epileptogenesis Parallels Synaptic Circuit Alterations. *J. Neurosci.* 35, 9920–9934. doi:10.1523/JNEUROSCI.4007-14.2015.

Lodish, H., Berk, A., Zipursky, S. L., Matsudaira, P., Baltimore, D., and Darnell, J. (2000). The Action Potential and Conduction of Electric Impulses. *Mol. Cell Biol. 4th Ed.* Available at: https://www.ncbi.nlm.nih.gov/books/NBK21668/ [Accessed September 24, 2018].

Lopes, G., Bonacchi, N., Frazão, J., Neto, J. P., Atallah, B. V., Soares, S., et al. (2015). Bonsai: an event-based framework for processing and controlling data streams. *Front. Neuroinformatics* 9. doi:10.3389/fninf.2015.00007.

Löscher, W. (2017). Animal Models of Seizures and Epilepsy: Past, Present, and Future Role for the Discovery of Antiseizure Drugs. *Neurochem. Res.* 42, 1873–1888. doi:10.1007/s11064-017-2222-z.

Losi, G., Cammarota, M., Chiavegato, A., Gomez-Gonzalo, M., and Carmignoto, G. (2010). A new experimental model of focal seizures in the entorhinal cortex. *Epilepsia* 51, 1493–1502. doi:10.1111/j.1528-1167.2009.02472.x.

Losi, G., Marcon, I., Mariotti, L., Sessolo, M., Chiavegato, A., and Carmignoto, G. (2016). A brain slice experimental model to study the generation and the

propagation of focally-induced epileptiform activity. *J. Neurosci. Methods* 260, 125–131. doi:10.1016/j.jneumeth.2015.04.001.

Lothman, E. W., Bertram, E. H., Kapur, J., and Stringer, J. L. (1990). Recurrent spontaneous hippocampal seizures in the rat as a chronic sequela to limbic status epilepticus. *Epilepsy Res.* 6, 110–118. doi:10.1016/0920-1211(90)90085-A.

Lothman, E. W., Stringer, J. L., and Bertram, E. H. (1992). The dentate gyrus as a control point for seizures in the hippocampus and beyond. *Epilepsy Res. Suppl.* 7, 301–313.

Lovett-Barron, M., Turi, G. F., Kaifosh, P., Lee, P. H., Bolze, F., Sun, X.-H., et al. (2012). Regulation of neuronal input transformations by tunable dendritic inhibition. *Nat. Neurosci.* 15, 423–430. doi:10.1038/nn.3024.

Lowenstein, D. H. (2009). Epilepsy after head injury: an overview. *Epilepsia* 50 Suppl 2, 4–9. doi:10.1111/j.1528-1167.2008.02004.x.

Luhmann, H. J., Kirischuk, S., and Kilb, W. (2014). Comment on "Local impermeant anions establish the neuronal chloride concentration." *Science* 345, 1130. doi:10.1126/science.1255337.

Luo, J., and Sun, D. (2007). Physiology and pathophysiology of Na(+)/H(+) exchange isoform 1 in the central nervous system. *Curr. Neurovasc. Res.* 4, 205–215.

Lupica, C. R., Bell, J. A., Hoffman, A. F., and Watson, P. L. (2001). Contribution of the hyperpolarization-activated current (I(h)) to membrane potential and GABA release in hippocampal interneurons. *J. Neurophysiol.* 86, 261–268. doi:10.1152/jn.2001.86.1.261.

Lüscher, H. R., and Shiner, J. S. (1990). Computation of action potential propagation and presynaptic bouton activation in terminal arborizations of different geometries. *Biophys. J.* 58, 1377–1388. doi:10.1016/S0006-3495(90)82484-X.

Magee, J. C. (2000). Dendritic integration of excitatory synaptic input. *Nat. Rev. Neurosci.* 1, 181–190. doi:10.1038/35044552.

Maglóczky, Z., and Freund, T. F. (2005). Impaired and repaired inhibitory circuits in the epileptic human hippocampus. *Trends Neurosci.* 28, 334–340. doi:10.1016/j.tins.2005.04.002.

Magloire, V., Cornford, J. H., Lieb, A., Kullmann, D. M., and Pavlov, I. (2018). KCC2 overexpression prevents the paradoxical seizure-promoting action of somatic inhibition. *bioRxiv*, 279539. doi:10.1101/279539.

Makani, S., and Chesler, M. (2010). Rapid rise of extracellular pH evoked by neural activity is generated by the plasma membrane calcium ATPase. *J. Neurophysiol.* 103, 667–676. doi:10.1152/jn.00948.2009.

Manvich, D. F., Webster, K. A., Foster, S. L., Farrell, M. S., Ritchie, J. C., Porter, J. H., et al. (2018). The DREADD agonist clozapine N -oxide (CNO) is reverse-metabolized to clozapine and produces clozapine-like interoceptive stimulus effects in rats and mice. *Sci. Rep.* 8, 3840. doi:10.1038/s41598-018-22116-z.

Markova, O., Mukhtarov, M., Real, E., Jacob, Y., and Bregestovski, P. (2008). Genetically encoded chloride indicator with improved sensitivity. *J. Neurosci. Methods* 170, 67–76. doi:10.1016/j.jneumeth.2007.12.016.

Markram, H., Toledo-Rodriguez, M., Wang, Y., Gupta, A., Silberberg, G., and Wu, C. (2004). Interneurons of the neocortical inhibitory system. *Nat. Rev. Neurosci.* 5, 793–807. doi:10.1038/nrn1519.

Martina, M., Schultz, J. H., Ehmke, H., Monyer, H., and Jonas, P. (1998). Functional and Molecular Differences between Voltage-Gated K+ Channels of Fast-Spiking Interneurons and Pyramidal Neurons of Rat Hippocampus. *J. Neurosci.* 18, 8111–8125. doi:10.1523/JNEUROSCI.18-20-08111.1998.

Martineau, M., Guzman, R. E., Fahlke, C., and Klingauf, J. (2017). VGLUT1 functions as a glutamate/proton exchanger with chloride channel activity in hippocampal glutamatergic synapses. *Nat. Commun.* 8, 2279. doi:10.1038/s41467-017-02367-6.

Marx, M., Haas, C. A., and Häussler, U. (2013). Differential vulnerability of interneurons in the epileptic hippocampus. *Front. Cell. Neurosci.* 7. doi:10.3389/fncel.2013.00167.

Matas, J., Chum, O., Urban, M., and Pajdla, T. (2004). Robust wide-baseline stereo from maximally stable extremal regions. *Image Vis. Comput.* 22, 761–767. doi:10.1016/j.imavis.2004.02.006.

Mathern, G. W., Babb, T. L., Pretorius, J. K., and Leite, J. P. (1995). Reactive synaptogenesis and neuron densities for neuropeptide Y, somatostatin, and glutamate decarboxylase immunoreactivity in the epileptogenic human fascia dentata. *J. Neurosci.* 15, 3990–4004. doi:10.1523/JNEUROSCI.15-05-03990.1995.

Mathern, G. W., Cifuentes, F., Leite, J. P., Pretorius, J. K., and Babb, T. L. (1993). Hippocampal EEG excitability and chronic spontaneous seizures are associated with aberrant synaptic reorganization in the rat intrahippocampal kainate model. *Electroencephalogr. Clin. Neurophysiol.* 87, 326–339. doi:10.1016/0013-4694(93)90186-Y.

Mauro, A. (1954). Electrochemical potential difference of chloride ion in the giant squid axon-sea water system. *Fed Proc* 13.

McBain, C. J., DiChiara, T. J., and Kauer, J. A. (1994). Activation of metabotropic glutamate receptors differentially affects two classes of hippocampal interneurons and potentiates excitatory synaptic transmission. *J. Neurosci.* 14, 4433–4445. doi:10.1523/JNEUROSCI.14-07-04433.1994.

McDonald, J. W., Bhattacharyya, T., Sensi, S. L., Lobner, D., Ying, H. S., Canzoniero, L. M., et al. (1998). Extracellular acidity potentiates AMPA receptor-mediated cortical neuronal death. *J. Neurosci. Off. J. Soc. Neurosci.* 18, 6290–6299.

McKinney, R. A., Debanne, D., Gähwiler, B. H., and Thompson, S. M. (1997). Lesion-induced axonal sprouting and hyperexcitability in the hippocampus in vitro: implications for the genesis of posttraumatic epilepsy. *Nat. Med.* 3, 990–996.

McOmish, C. E., Lira, A., Hanks, J. B., and Gingrich, J. A. (2012). Clozapine-Induced Locomotor Suppression is Mediated by 5-HT2A Receptors in the Forebrain. *Neuropsychopharmacology* 37, 2747–2755. doi:10.1038/npp.2012.139.

Meech, R. W., and Thomas, R. C. (1977). The effect of calcium injection on the intracellular sodium and pH of snail neurones. *J. Physiol.* 265, 867–879.

Mellanby, J., George, G., Robinson, A., and Thompson, P. (1977). Epileptiform syndrome in rats produced by injecting tetanus toxin into the hippocampus. *J. Neurol. Neurosurg. Psychiatry* 40, 404–414. doi:10.1136/jnnp.40.4.404.

Merritt, H. H., and Putnam, T. J. (1938). Sodium diphenyl hydantoinate in the treatment of convulsive disorders. *J. Am. Med. Assoc.* 111, 1068–1073. doi:10.1001/jama.1938.02790380010004.

Meyer, J. S., Gotoh, F., and Tazaki, Y. (1961). Inhibitory action of carbon dioxide and acetazoleamide in seizure activity. *Electroencephalogr. Clin. Neurophysiol.* 13, 762–775.

Mickus, T., Jung, H.-Y., and Spruston, N. (1999). Slow Sodium Channel Inactivation in CA1 Pyramidal Cells. *Ann. N. Y. Acad. Sci.* 868, 97–101. doi:10.1111/j.1749-6632.1999.tb11280.x.

Miles, R. (1990). Synaptic excitation of inhibitory cells by single CA3 hippocampal pyramidal cells of the guinea-pig in vitro. *J. Physiol.* 428, 61–77.

Miles, R., Blaesse, P., Huberfeld, G., Wittner, L., and Kaila, K. (2012). "Chloride homeostasis and GABA signaling in temporal lobe epilepsy," in *Jasper's Basic Mechanisms of the Epilepsies*, eds. J. L. Noebels, M. Avoli, M. A.

Rogawski, R. W. Olsen, and A. V. Delgado-Escueta (Bethesda (MD): National Center for Biotechnology Information (US)). Available at: http://www.ncbi.nlm.nih.gov/books/NBK98162/ [Accessed October 1, 2018].

Miles, R., Tóth, K., Gulyás, A. I., Hájos, N., and Freund, T. F. (1996). Differences between Somatic and Dendritic Inhibition in the Hippocampus. *Neuron* 16, 815–823. doi:10.1016/S0896-6273(00)80101-4.

Miles, R., and Wong, R. K. (1987). Latent synaptic pathways revealed after tetanic stimulation in the hippocampus. *Nature* 329, 724–726. doi:10.1038/329724a0.

Miyoshi, G., Hjerling-Leffler, J., Karayannis, T., Sousa, V. H., Butt, S. J. B., Battiste, J., et al. (2010). Genetic Fate Mapping Reveals That the Caudal Ganglionic Eminence Produces a Large and Diverse Population of Superficial Cortical Interneurons. *J. Neurosci.* 30, 1582–1594. doi:10.1523/JNEUROSCI.4515-09.2010.

Moore, Y. E., Deeb, T. Z., Chadchankar, H., Brandon, N. J., and Moss, S. J. (2018). Potentiating KCC2 activity is sufficient to limit the onset and severity of seizures. *Proc. Natl. Acad. Sci.*, 201810134. doi:10.1073/pnas.1810134115.

Morimoto, K., Fahnestock, M., and Racine, R. J. (2004). Kindling and status epilepticus models of epilepsy: rewiring the brain. *Prog. Neurobiol.* 73, 1–60. doi:10.1016/j.pneurobio.2004.03.009.

Mula, M. (2011). GABAergic drugs in the treatment of epilepsy: modern or outmoded? *Future Med. Chem.* 3, 177–182. doi:10.4155/fmc.10.296.

Muñoz, A., Méndez, P., DeFelipe, J., and Alvarez-Leefmans, F. J. (2007). Cation-chloride cotransporters and GABA-ergic innervation in the human epileptic hippocampus. *Epilepsia* 48, 663–673. doi:10.1111/j.1528-1167.2007.00986.x.

Nagel, G., Szellas, T., Huhn, W., Kateriya, S., Adeishvili, N., Berthold, P., et al. (2003). Channelrhodopsin-2, a directly light-gated cation-selective membrane channel. *Proc. Natl. Acad. Sci. U. S. A.* 100, 13940–13945. doi:10.1073/pnas.1936192100.

Nakajima, K., and Marunaka, Y. (2016). Intracellular chloride ion concentration in differentiating neuronal cell and its role in growing neurite. *Biochem. Biophys. Res. Commun.* 479, 338–342. doi:10.1016/j.bbrc.2016.09.075.

Nakanishi, S. (1994). Metabotropic glutamate receptors: Synaptic transmission, modulation, and plasticity. *Neuron* 13, 1031–1037. doi:10.1016/0896-6273(94)90043-4.

Nakanishi, S., and Masu, M. (1994). Molecular diversity and functions of glutamate receptors. *Annu. Rev. Biophys. Biomol. Struct.* 23, 319–348. doi:10.1146/annurev.bb.23.060194.001535.

Nathanson, J. L., Jappelli, R., Scheeff, E. D., Manning, G., Obata, K., Brenner, S., et al. (2009). Short Promoters in Viral Vectors Drive Selective Expression in Mammalian Inhibitory Neurons, but do not Restrict Activity to Specific Inhibitory Cell-Types. *Front. Neural Circuits* 3. doi:10.3389/neuro.04.019.2009.

Ngugi, A. K., Bottomley, C., Kleinschmidt, I., Sander, J. W., and Newton, C. R. (2010). Estimation of the burden of active and life-time epilepsy: a meta-analytic approach. *Epilepsia* 51, 883–890. doi:10.1111/j.1528-1167.2009.02481.x.

Nistér, D., and Stewénius, H. (2008). Linear Time Maximally Stable Extremal Regions. in *Computer Vision – ECCV 2008* Lecture Notes in Computer Science. (Springer, Berlin, Heidelberg), 183–196. doi:10.1007/978-3-540-88688-4_14.

O'Brien, D. (1998). Toxic and metabolic causes of seizures. *Clin. Tech. Small Anim. Pract.* 13, 159–166. doi:10.1016/S1096-2867(98)80037-6.

Okun, M., and Lampl, I. (2008). Instantaneous correlation of excitation and inhibition during ongoing and sensory-evoked activities. *Nat. Neurosci.* 11, 535–537. doi:10.1038/nn.2105.

Olsen, R. W., and Avoli, M. (1997). GABA and epileptogenesis. *Epilepsia* 38, 399–407.

Olsen, R. W., and Sieghart, W. (2008). International Union of Pharmacology. LXX. Subtypes of gamma-aminobutyric acid(A) receptors: classification on the basis of subunit composition, pharmacology, and function. Update. *Pharmacol. Rev.* 60, 243–260. doi:10.1124/pr.108.00505.

Orkand, R. K. (1980). Extracellular potassium accumulation in the nervous system. *Fed. Proc.* 39, 1515–1518.

Orlowski, J., and Grinstein, S. (2004). Diversity of the mammalian sodium/proton exchanger SLC9 gene family. *Pflüg. Arch.* 447, 549–565. doi:10.1007/s00424-003-1110-3.

Palma, E., Amici, M., Sobrero, F., Spinelli, G., Di Angelantonio, S., Ragozzino, D., et al. (2006). Anomalous levels of Cl- transporters in the hippocampal subiculum from temporal lobe epilepsy patients make GABA excitatory. *Proc. Natl. Acad. Sci. U. S. A.* 103, 8465–8468. doi:10.1073/pnas.0602979103.

Pan, Z., Kao, T., Horvath, Z., Lemos, J., Sul, J.-Y., Cranstoun, S. D., et al. (2006). A Common Ankyrin-G-Based Mechanism Retains KCNQ and NaV Channels at Electrically Active Domains of the Axon. *J. Neurosci.* 26, 2599–2613. doi:10.1523/JNEUROSCI.4314-05.2006.

Pande, J., Szewczyk, M. M., and Grover, A. K. (2011). Allosteric inhibitors of plasma membrane Ca2+ pumps: Invention and applications of caloxins. *World J. Biol. Chem.* 2, 39–47. doi:10.4331/wjbc.v2.i3.39.

Parrish, R. R., Codadu, N. K., Scott, C. M.-G., and Trevelyan, A. J. (2019). Feedforward inhibition ahead of ictal wavefronts is provided by both parvalbumin and somatostatin expressing interneurons. *J. Physiol.* doi:10.1113/JP277749.

Pasternack, M., Smirnov, S., and Kaila, K. (1996). Proton modulation of functionally distinct GABAA receptors in acutely isolated pyramidal neurons of rat hippocampus. *Neuropharmacology* 35, 1279–1288.

Patil, P. G., Brody, D. L., and Yue, D. T. (1998). Preferential Closed-State Inactivation of Neuronal Calcium Channels. *Neuron* 20, 1027–1038. doi:10.1016/S0896-6273(00)80483-3.

Paul, A., Crow, M., Raudales, R., He, M., Gillis, J., and Huang, Z. J. (2017). Transcriptional Architecture of Synaptic Communication Delineates GABAergic Neuron Identity. *Cell* 171, 522-539.e20. doi:10.1016/j.cell.2017.08.032.

Paulus, W., and Rothwell, J. C. (2016). Membrane resistance and shunting inhibition: where biophysics meets state-dependent human neurophysiology. *J. Physiol.* 594, 2719–2728. doi:10.1113/JP271452.

Pawelzik, H., Hughes, D. I., and Thomson, A. M. (2002). Physiological and morphological diversity of immunocytochemically defined parvalbumin- and cholecystokinin-positive interneurones in CA1 of the adult rat hippocampus. *J. Comp. Neurol.* 443, 346–367. doi:10.1002/cne.10118.

Payne, J. A., Rivera, C., Voipio, J., and Kaila, K. (2003). Cation–chloride co-transporters in neuronal communication, development and trauma. *Trends Neurosci.* 26, 199–206. doi:10.1016/S0166-2236(03)00068-7.

Paz, J. T., Davidson, T. J., Frechette, E. S., Delord, B., Parada, I., Peng, K., et al. (2013). Closed-loop optogenetic control of thalamus as a new tool to interrupt seizures after cortical injury. *Nat. Neurosci.* 16, 64–70. doi:10.1038/nn.3269.

Paz, J. T., and Huguenard, J. R. (2015a). Microcircuits and their interactions in epilepsy: is the focus out of focus? *Nat. Neurosci.* 18, 351–359. doi:10.1038/nn.3950.

Paz, J. T., and Huguenard, J. R. (2015b). Optogenetics and Epilepsy: Past, Present and Future. *Epilepsy Curr.* 15, 34–38. doi:10.5698/1535-7597-15.1.34.

Perez, Y., Morin, F., Beaulieu, C., and Lacaille, J. C. (1996). Axonal sprouting of CA1 pyramidal cells in hyperexcitable hippocampal slices of kainate-treated rats. *Eur. J. Neurosci.* 8, 736–748.

Perreault, P., and Avoli, M. (1992). 4-aminopyridine-induced epileptiform activity and a GABA-mediated long-lasting depolarization in the rat hippocampus. *J. Neurosci. Off. J. Soc. Neurosci.* 12, 104–115.

Pi, H.-J., Hangya, B., Kvitsiani, D., Sanders, J. I., Huang, Z. J., and Kepecs, A. (2013). Cortical interneurons that specialize in disinhibitory control. *Nature* 503, 521–524. doi:10.1038/nature12676.

Poolos, N. P. (2012). "Hyperpolarization-Activated Cyclic Nucleotide-Gated (HCN) Ion Channelopathy in Epilepsy," in *Jasper's Basic Mechanisms of the Epilepsies*, eds. J. L. Noebels, M. Avoli, M. A. Rogawski, R. W. Olsen, and A. V. Delgado-Escueta (Bethesda (MD): National Center for Biotechnology Information (US)). Available at: http://www.ncbi.nlm.nih.gov/books/NBK98137/ [Accessed August 28, 2018].

Pothmann, L., Müller, C., Averkin, R. G., Bellistri, E., Miklitz, C., Uebachs, M., et al. (2014). Function of Inhibitory Micronetworks Is Spared by Na+ Channel-Acting Anticonvulsant Drugs. *J. Neurosci.* 34, 9720–9735. doi:10.1523/JNEUROSCI.2395-13.2014.

Pouille, F., and Scanziani, M. (2001). Enforcement of temporal fidelity in pyramidal cells by somatic feed-forward inhibition. *Science* 293, 1159–1163. doi:10.1126/science.1060342.

Pouille, F., Watkinson, O., Scanziani, M., and Trevelyan, A. J. (2013). The contribution of synaptic location to inhibitory gain control in pyramidal cells. *Physiol. Rep.* 1. doi:10.1002/phy2.67.

Powell, E. M., Campbell, D. B., Stanwood, G. D., Davis, C., Noebels, J. L., and Levitt, P. (2003). Genetic Disruption of Cortical Interneuron Development Causes Region- and GABA Cell Type-Specific Deficits, Epilepsy, and Behavioral Dysfunction. *J. Neurosci.* 23, 622–631. doi:10.1523/JNEUROSCI.23-02-00622.2003.

Price, C. J., Cauli, B., Kovacs, E. R., Kulik, A., Lambolez, B., Shigemoto, R., et al. (2005). Neurogliaform neurons form a novel inhibitory network in the hippocampal CA1 area. *J. Neurosci. Off. J. Soc. Neurosci.* 25, 6775–6786. doi:10.1523/JNEUROSCI.1135-05.2005.

Pumain, R., Menini, C., Heinemann, U., Louvel, J., and Silva-Barrat, C. (1985). Chemical synaptic transmission is not necessary for epileptic seizures to persist in the baboon Papio papio. *Exp. Neurol.* 89, 250–258.

Putney, L. K., and Barber, D. L. (2003). Na-H exchange-dependent increase in intracellular pH times G2/M entry and transition. *J. Biol. Chem.* 278, 44645–44649. doi:10.1074/jbc.M308099200.

Qian, H. (1995). "GABAC Receptors in the Vertebrate Retina," in *Webvision: The Organization of the Retina and Visual System*, eds. H. Kolb, E. Fernandez, and R. Nelson (Salt Lake City (UT): University of Utah Health Sciences Center). Available at: http://www.ncbi.nlm.nih.gov/books/NBK11540/ [Accessed October 3, 2018].

Qian, N., and Sejnowski, T. J. (1990). When is an inhibitory synapse effective? *Proc. Natl. Acad. Sci. U. S. A.* 87, 8145–8149.

Raimondo, J. V., Burman, R. J., Katz, A. A., and Akerman, C. J. (2015). Ion dynamics during seizures. *Front. Cell. Neurosci.* 9. doi:10.3389/fncel.2015.00419.

Raimondo, J. V., Irkle, A., Wefelmeyer, W., Newey, S. E., and Akerman, C. J. (2012a). Genetically encoded proton sensors reveal activity-dependent pH changes in neurons. *Front. Mol. Neurosci.* 5. doi:10.3389/fnmol.2012.00068.

Raimondo, J. V., Joyce, B., Kay, L., Schlagheck, T., Newey, S. E., Srinivas, S., et al. (2013). A genetically-encoded chloride and pH sensor for dissociating ion dynamics in the nervous system. *Front. Cell. Neurosci.* 7. doi:10.3389/fncel.2013.00202.

Raimondo, J. V., Kay, L., Ellender, T. J., and Akerman, C. J. (2012b). Optogenetic silencing strategies differ in their effects on inhibitory synaptic transmission. *Nat. Neurosci.* 15, 1102–1104. doi:10.1038/nn.3143.

Raimondo, J. V., Markram, H., and Akerman, C. J. (2012c). Short-term ionic plasticity at GABAergic synapses. *Front. Synaptic Neurosci.* 4, 5. doi:10.3389/fnsyn.2012.00005.

Raimondo, J. V., Richards, B. A., and Woodin, M. A. (2017). Neuronal chloride and excitability — the big impact of small changes. *Curr. Opin. Neurobiol.* 43, 35–42. doi:10.1016/j.conb.2016.11.012.

Raimondo, J. V., Tomes, H., Irkle, A., Kay, L., Kellaway, L., Markram, H., et al. (2016). Tight Coupling of Astrocyte pH Dynamics to Epileptiform Activity Revealed by Genetically Encoded pH Sensors. *J. Neurosci.* 36, 7002–7013. doi:10.1523/JNEUROSCI.0664-16.2016.

Raley-Susman, K. M., Cragoe, E. J., Sapolsky, R. M., and Kopito, R. R. (1991). Regulation of intracellular pH in cultured hippocampal neurons by an amiloride-insensitive Na+/H+ exchanger. *J. Biol. Chem.* 266, 2739–2745.

Ransom, B. R. (1992). "Chapter 3: Glial modulation of neural excitability mediated by extracellular pH: a hypothesis," in *Progress in Brain Research* Neuronal-Astrocytic Interactions., eds. A. C. H. Yu, L. Hertz, M. D. Norenberg, E. Syková, and S. G. Waxman (Elsevier), 37–46. doi:10.1016/S0079-6123(08)61737-9.

Reddy, D. S., and Kuruba, R. (2013). Experimental Models of Status Epilepticus and Neuronal Injury for Evaluation of Therapeutic Interventions. *Int. J. Mol. Sci.* 14, 18284–18318. doi:10.3390/ijms140918284.

Remy, C., Remy, S., Beck, H., Swandulla, D., and Hans, M. (2004). Modulation of voltage-dependent sodium channels by the delta-agonist SNC80 in acutely isolated rat hippocampal neurons. *Neuropharmacology* 47, 1102–1112. doi:10.1016/j.neuropharm.2004.06.034.

Rivera, C., Voipio, J., Payne, J. A., Ruusuvuori, E., Lahtinen, H., Lamsa, K., et al. (1999). The K+/Cl- co-transporter KCC2 renders GABA hyperpolarizing during neuronal maturation. *Nature* 397, 251–255. doi:10.1038/16697.

Rivera, C., Voipio, J., Thomas-Crusells, J., Li, H., Emri, Z., Sipilä, S., et al. (2004). Mechanism of activity-dependent downregulation of the neuron-specific K-Cl cotransporter KCC2. *J. Neurosci. Off. J. Soc. Neurosci.* 24, 4683–4691. doi:10.1523/JNEUROSCI.5265-03.2004.

Robbins, R. J., Brines, M. L., Kim, J. H., Adrian, T., De Lanerolle, N., Welsh, S., et al. (1991). A selective loss of somatostatin in the hippocampus of patients with temporal lobe epilepsy. *Ann. Neurol.* 29, 325–332. doi:10.1002/ana.410290316.

Roos, A., and Boron, W. F. (1981). Intracellular pH. *Physiol. Rev.* 61, 296–434. doi:10.1152/physrev.1981.61.2.296.

Rose, C. R., and Deitmer, J. W. (1995). Stimulus-evoked changes of extra- and intracellular pH in the leech central nervous system. II. Mechanisms and maintenance of pH homeostasis. *J. Neurophysiol.* 73, 132–140. doi:10.1152/jn.1995.73.1.132.

Roux, L., and Buzsáki, G. (2015). Tasks for inhibitory interneurons in intact brain circuits. *Neuropharmacology* 0, 10–23. doi:10.1016/j.neuropharm.2014.09.011.

Rudy, B. (1978). Slow inactivation of the sodium conductance in squid giant axons. Pronase resistance. *J. Physiol.* 283, 1–21.

Rudy, B., Fishell, G., Lee, S., and Hjerling-Leffler, J. (2011). Three Groups of Interneurons Account for Nearly 100% of Neocortical GABAergic Neurons. *Dev. Neurobiol.* 71, 45–61. doi:10.1002/dneu.20853.

Ruffin, V. A., Salameh, A. I., Boron, W. F., and Parker, M. D. (2014). Intracellular pH regulation by acid-base transporters in mammalian neurons. *Front. Physiol.* 5. doi:10.3389/fphys.2014.00043.

Rungta, R. L., Choi, H. B., Tyson, J. R., Malik, A., Dissing-Olesen, L., Lin, P. J. C., et al. (2015). The Cellular Mechanisms of Neuronal Swelling Underlying Cytotoxic Edema. *Cell* 161, 610–621. doi:10.1016/j.cell.2015.03.029.

Salam, M. T., Montandon, G., Genov, R., Devinsky, O., Campo, M. D., and Carlen, P. L. (2017). Mortality with brainstem seizures from focal 4-aminopyridine–induced recurrent hippocampal seizures. *Epilepsia* 58, 1637–1644. doi:10.1111/epi.13846.

Salameh, A. I., Ruffin, V. A., and Boron, W. F. (2014). Effects of metabolic acidosis on intracellular pH responses in multiple cell types. *Am. J. Physiol. - Regul. Integr. Comp. Physiol.* 307, R1413–R1427. doi:10.1152/ajpregu.00154.2014.

Salin, P., Tseng, G. F., Hoffman, S., Parada, I., and Prince, D. A. (1995). Axonal sprouting in layer V pyramidal neurons of chronically injured cerebral cortex. *J. Neurosci. Off. J. Soc. Neurosci.* 15, 8234–8245.

Sato, S. S., Artoni, P., Landi, S., Cozzolino, O., Parra, R., Pracucci, E., et al. (2017). Simultaneous two-photon imaging of intracellular chloride concentration and pH in mouse pyramidal neurons in vivo. *Proc. Natl. Acad. Sci.*, 201702861. doi:10.1073/pnas.1702861114.

Scheffer, I. E., Berkovic, S., Capovilla, G., Connolly, M. B., French, J., Guilhoto, L., et al. (2017). ILAE classification of the epilepsies: Position paper of the ILAE Commission for Classification and Terminology. *Epilepsia* 58, 512–521. doi:10.1111/epi.13709.

Scheffer, I. E., Bhatia, K. P., Lopes-Cendes, I., Fish, D. R., Marsden, C. D., Andermann, E., et al. (1995). Autosomal dominant nocturnal frontal lobe epilepsy. A distinctive clinical disorder. *Brain J. Neurol.* 118 (Pt 1), 61–73.

Scheibel, M. E., Crandall, P. H., and Scheibel, A. B. (1974). The hippocampal-dentate complex in temporal lobe epilepsy. A Golgi study. *Epilepsia* 15, 55–80.

Schevon, C. A., Weiss, S. A., McKhann Jr, G., Goodman, R. R., Yuste, R., Emerson, R. G., et al. (2012). Evidence of an inhibitory restraint of seizure activity in humans. *Nat. Commun.* 3, 1060. doi:10.1038/ncomms2056.

Schuchmann, S., Schmitz, D., Rivera, C., Vanhatalo, S., Salmen, B., Mackie, K., et al. (2006). Experimental febrile seizures are precipitated by a hyperthermia-induced respiratory alkalosis. *Nat. Med.* 12, 817–823. doi:10.1038/nm1422.

Schultz, C., and Engelhardt, M. (2014). Anatomy of the hippocampal formation. *Front. Neurol. Neurosci.* 34, 6–17. doi:10.1159/000360925.

Schwartzkroin, P. A. (1994). Role of the hippocampus in epilepsy. *Hippocampus* 4, 239–242. doi:10.1002/hipo.450040302.

Schwiening, C. J., and Boron, W. F. (1994). Regulation of intracellular pH in pyramidal neurones from the rat hippocampus by Na(+)-dependent Cl(-)-HCO3- exchange. *J. Physiol.* 475, 59–67. doi:10.1113/jphysiol.1994.sp020049.

Schwiening, C. J., Kennedy, H. J., and Thomas, R. C. (1993). Calcium-hydrogen exchange by the plasma membrane Ca-ATPase of voltage-clamped snail neurons. *Proc. Biol. Sci.* 253, 285–289.

Scoville, W. B., and Milner, B. (1957). Loss of recent memory after bilateral hippocampal lesions. *J. Neurol. Neurosurg. Psychiatry* 20, 11–21.

Segal, M. (1987). Repetitive inhibitory postsynaptic potentials evoked by 4-aminopyridine in hippocampal neurons in vitro. *Brain Res.* 414, 285–293. doi:10.1016/0006-8993(87)90008-4.

Sessolo, M., Marcon, I., Bovetti, S., Losi, G., Cammarota, M., Ratto, G. M., et al. (2015). Parvalbumin-Positive Inhibitory Interneurons Oppose Propagation But Favor Generation of Focal Epileptiform Activity. *J. Neurosci.* 35, 9544–9557. doi:10.1523/JNEUROSCI.5117-14.2015.

Shah, M. M. (2018). Neuronal HCN channel function and plasticity. *Curr. Opin. Physiol.* 2, 92–97. doi:10.1016/j.cophys.2018.01.001.

Sharma, S., Puttachary, S., Thippeswamy, A., Kanthasamy, A. G., and Thippeswamy, T. (2018). Status Epilepticus: Behavioral and Electroencephalography Seizure Correlates in Kainate Experimental Models. *Front. Neurol.* 9. doi:10.3389/fneur.2018.00007.

Shibley, H., and Smith, B. N. (2002). Pilocarpine-induced status epilepticus results in mossy fiber sprouting and spontaneous seizures in C57BL/6 and CD-1 mice. *Epilepsy Res.* 49, 109–120.

Shih, P.-Y., Savtchenko, L. P., Kamasawa, N., Dembitskaya, Y., McHugh, T. J., Rusakov, D. A., et al. (2013). Retrograde Synaptic Signaling Mediated by K+ Efflux through Postsynaptic NMDA Receptors. *Cell Rep.* 5, 941–951. doi:10.1016/j.celrep.2013.10.026.

Siesjö, B. K. (1985). Acid-base homeostasis in the brain: physiology, chemistry, and neurochemical pathology. *Prog. Brain Res.* 63, 121–154. doi:10.1016/S0079-6123(08)61980-9.

Sigel, E., Mamalaki, C., and Barnard, E. A. (1982). Isolation of a GABA receptor from bovine brain using a benzodiazepine affinity column. *FEBS Lett.* 147, 45–48.

Sik, A., Penttonen, M., Ylinen, A., and Buzsáki, G. (1995). Hippocampal CA1 interneurons: an in vivo intracellular labeling study. *J. Neurosci. Off. J. Soc. Neurosci.* 15, 6651–6665.

Silayeva, L., Deeb, T. Z., Hines, R. M., Kelley, M. R., Munoz, M. B., Lee, H. H. C., et al. (2015). KCC2 activity is critical in limiting the onset and severity of status epilepticus. *Proc. Natl. Acad. Sci.* 112, 3523–3528. doi:10.1073/pnas.1415126112.

Silver, R. A. (2010). Neuronal arithmetic. *Nat. Rev. Neurosci.* 11, 474–489. doi:10.1038/nrn2864.

Singhi, P., Ray, M., Singhi, S., and Khandelwal, N. (2000). Clinical spectrum of 500 children with neurocysticercosis and response to albendazole therapy. *J. Child Neurol.* 15, 207–213. doi:10.1177/088307380001500401.

Sinha, S. R., and Saggau, P. (2001). Imaging of 4-AP-induced, GABA(A)-dependent spontaneous synchronized activity mediated by the hippocampal interneuron network. *J. Neurophysiol.* 86, 381–391. doi:10.1152/jn.2001.86.1.381.

Sinning, A., and Hübner, C. A. (2013). Minireview: pH and synaptic transmission. *FEBS Lett.* 587, 1923–1928. doi:10.1016/j.febslet.2013.04.045.

Skou, J. C., and Esmann, M. (1992). The Na,K-ATPase. *J. Bioenerg. Biomembr.* 24, 249–261.

Sladeczek, F., Pin, J.-P., Récasens, M., Bockaert, J., and Weiss, S. (1985). Glutamate stimulates inositol phosphate formation in striatal neurones. *Nature* 317, 717–719. doi:10.1038/317717a0.

Sloviter, R. S. (1987). Decreased hippocampal inhibition and a selective loss of interneurons in experimental epilepsy. *Science* 235, 73–76. doi:10.1126/science.2879352.

Sloviter, R. S. (1991). Permanently altered hippocampal structure, excitability, and inhibition after experimental status epilepticus in the rat: The "dormant basket cell" hypothesis and its possible relevance to temporal lobe epilepsy. *Hippocampus* 1, 41–66. doi:10.1002/hipo.450010106.

Sloviter, R. S., and Bumanglag, A. V. (2013). Defining "epileptogenesis" and identifying "antiepileptogenic targets" in animal models of acquired temporal lobe epilepsy is not as simple as it might seem. *Neuropharmacology* 69, 3–15. doi:10.1016/j.neuropharm.2012.01.022.

Sloviter, R. S., Sollas, A. L., Barbaro, N. M., and Laxer, K. D. (1991). Calcium-binding protein (calbindin-D28K) and parvalbumin immunocytochemistry in the normal and epileptic human hippocampus. *J. Comp. Neurol.* 308, 381–396. doi:10.1002/cne.903080306.

Sloviter, R. S., Zappone, C. A., Harvey, B. D., Bumanglag, A. V., Bender, R. A., and Frotscher, M. (2003). "Dormant basket cell" hypothesis revisited: Relative vulnerabilities of dentate gyrus mossy cells and inhibitory interneurons after hippocampal status epilepticus in the rat. *J. Comp. Neurol.* 459, 44–76. doi:10.1002/cne.10630.

Sloviter, R. S., Zappone, C. A., Harvey, B. D., and Frotscher, M. (2006). Kainic acid-induced recurrent mossy fiber innervation of dentate gyrus inhibitory interneurons: possible anatomical substrate of granule cell hyper-inhibition in chronically epileptic rats. *J. Comp. Neurol.* 494, 944–960. doi:10.1002/cne.20850.

Snodgrass, S. R. (1992). GABA and epilepsy: their complex relationship and the evolution of our understanding. *J. Child Neurol.* 7, 77–86. doi:10.1177/088307389200700114.

Snowball, A., Chabrol, E., Wykes, R. C., Lieb, A., Hashemi, K. S., Kullmann, D. M., et al. (2018). Epilepsy gene therapy using non-integrating lentiviral delivery of an engineered potassium channel gene. *bioRxiv*, 298588. doi:10.1101/298588.

Somjen, G. G. (2002). Ion regulation in the brain: implications for pathophysiology. *Neurosci. Rev. J. Bringing Neurobiol. Neurol. Psychiatry* 8, 254–267. doi:10.1177/1073858402008003011.

Sommer, W. (1880). Erkrankung des Ammonshorns als aetiologisches Moment der Epilepsie. *Arch. Für Psychiatr. Nervenkrankh.* 10, 631–675.

Somogyi, P. (1977). A specific ‘axo-axonal’ interneuron in the visual cortex of the rat. *Brain Res.* 136, 345–350. doi:10.1016/0006-8993(77)90808-3.

Somogyi, P., Freund, T. F., and Cowey, A. (1982). The axo-axonic interneuron in the cerebral cortex of the rat, cat and monkey. *Neuroscience* 7, 2577–2607. doi:10.1016/0306-4522(82)90086-0.

Somogyi, P., Hodgson, A. J., Smith, A. D., Nunzi, M. G., Gorio, A., and Wu, J. Y. (1984). Different populations of GABAergic neurons in the visual cortex and hippocampus of cat contain somatostatin- or cholecystokinin-immunoreactive material. *J. Neurosci.* 4, 2590–2603. doi:10.1523/JNEUROSCI.04-10-02590.1984.

Somogyi, P., Katona, L., Klausberger, T., Lasztóczi, B., and Viney, T. J. (2014). Temporal redistribution of inhibition over neuronal subcellular domains underlies state-dependent rhythmic change of excitability in the hippocampus. *Phil Trans R Soc B* 369, 20120518. doi:10.1098/rstb.2012.0518.

Sørensen, A. T., Ledri, M., Melis, M., Nikitidou Ledri, L., Andersson, M., and Kokaia, M. (2018). Altered Chloride Homeostasis Decreases the Action Potential Threshold and Increases Hyperexcitability in Hippocampal Neurons. *eNeuro* 4. doi:10.1523/ENEURO.0172-17.2017.

Srivastava, J., Barber, D. L., and Jacobson, M. P. (2007). Intracellular pH sensors: design principles and functional significance. *Physiol. Bethesda Md* 22, 30–39. doi:10.1152/physiol.00035.2006.

Stackman, J., Robert W. (2005). The Synaptic Organization of the Brain. Fifth Edition. Edited by Gordon M Shepherd. *Q. Rev. Biol.* 80, 502–502. doi:10.1086/501315.

Staley, K. J., and Mody, I. (1992). Shunting of excitatory input to dentate gyrus granule cells by a depolarizing GABAA receptor-mediated postsynaptic conductance. *J. Neurophysiol.* 68, 197–212. doi:10.1152/jn.1992.68.1.197.

Staley, K. J., and Proctor, W. R. (1999). Modulation of mammalian dendritic GABA(A) receptor function by the kinetics of Cl- and HCO3- transport. *J. Physiol.* 519 Pt 3, 693–712.

Staley, K. J., Soldo, B. L., and Proctor, W. R. (1995). Ionic mechanisms of neuronal excitation by inhibitory GABAA receptors. *Science* 269, 977–981.

Stoppini, L., Buchs, P.-A., and Muller, D. (1991). A simple method for organotypic cultures of nervous tissue. *J. Neurosci. Methods* 37, 173–182. doi:10.1016/0165-0270(91)90128-M.

Storm, J. F. (1988). Temporal integration by a slowly inactivating K+ current in hippocampal neurons. *Nature* 336, 379–381. doi:10.1038/336379a0.

Streit, P., Thompson, S. M., and Gähwiler, B. H. (1989). Anatomical and Physiological Properties of GABAergic Neurotransmission in Organotypic Slice Cultures of Rat Hippocampus. *Eur. J. Neurosci.* 1, 603–615. doi:10.1111/j.1460-9568.1989.tb00366.x.

Su, H., Sochivko, D., Becker, A., Chen, J., Jiang, Y., Yaari, Y., et al. (2002). Upregulation of a T-type Ca2+ channel causes a long-lasting modification of neuronal firing mode after status epilepticus. *J. Neurosci. Off. J. Soc. Neurosci.* 22, 3645–3655. doi:20026339.

Südhof, T. C. (2012). Calcium Control of Neurotransmitter Release. *Cold Spring Harb. Perspect. Biol.* 4. doi:10.1101/cshperspect.a011353.

Sukhotinsky, I., Chan, A. M., Ahmed, O. J., Rao, V. R., Gradinaru, V., Ramakrishnan, C., et al. (2013). Optogenetic delay of status epilepticus onset in an in vivo rodent epilepsy model. *PloS One* 8, e62013. doi:10.1371/journal.pone.0062013.

Sundstrom, L. E., Brana, C., Gatherer, M., Mepham, J., and Rougier, A. (2001). Somatostatin- and neuropeptide Y-synthesizing neurones in the fascia dentata of humans with temporal lobe epilepsy. *Brain J. Neurol.* 124, 688–697.

Supuran, C. T. (2008). Carbonic anhydrases--an overview. *Curr. Pharm. Des.* 14, 603–614.

Sutula, T. P., and Dudek, F. E. (2007). Unmasking recurrent excitation generated by mossy fiber sprouting in the epileptic dentate gyrus: an emergent property of a complex system. *Prog. Brain Res.* 163, 541–563. doi:10.1016/S0079-6123(07)63029-5.

Svichar, N., Esquenazi, S., Chen, H.-Y., and Chesler, M. (2011). Preemptive regulation of intracellular pH in hippocampal neurons by a dual mechanism of depolarization-induced alkalinization. *J. Neurosci. Off. J. Soc. Neurosci.* 31, 6997–7004. doi:10.1523/JNEUROSCI.6088-10.2011.

Svichar, N., Waheed, A., Sly, W. S., Hennings, J. C., Hübner, C. A., and Chesler, M. (2009). Carbonic Anhydrases CA4 and CA14 Both Enhance AE3-Mediated Cl−–HCO3− Exchange in Hippocampal Neurons. *J. Neurosci.* 29, 3252–3258. doi:10.1523/JNEUROSCI.0036-09.2009.

Szabadics, J., Varga, C., Molnár, G., Oláh, S., Barzó, P., and Tamás, G. (2006). Excitatory effect of GABAergic axo-axonic cells in cortical microcircuits. *Science* 311, 233–235. doi:10.1126/science.1121325.

Szente, M., and Baranyi, A. (1987). Mechanism of aminopyridine-induced ictal seizure activity in the cat neocortex. *Brain Res.* 413, 368–373.

Szydlowska, K., and Tymianski, M. (2010). Calcium, ischemia and excitotoxicity. *Cell Calcium* 47, 122–129. doi:10.1016/j.ceca.2010.01.003.

Tabb, J. S., Kish, P. E., Van Dyke, R., and Ueda, T. (1992). Glutamate transport into synaptic vesicles. Roles of membrane potential, pH gradient, and intravesicular pH. *J. Biol. Chem.* 267, 15412–15418.

Takahashi, K.-I., and Copenhagen, D. R. (1996). Modulation of neuronal function by intracellular pH. *Neurosci. Res.* 24, 109–116. doi:10.1016/0168-0102(95)00989-2.

Tallent, M. K., and Qiu, C. (2008). Somatostatin: An endogenous antiepileptic. *Mol. Cell. Endocrinol.* 286, 96–103. doi:10.1016/j.mce.2007.12.004.

Tamás, G., Szabadics, J., and Somogyi, P. (2002). Cell type- and subcellular position-dependent summation of unitary postsynaptic potentials in neocortical neurons. *J. Neurosci. Off. J. Soc. Neurosci.* 22, 740–747.

Tanaka, T., Tanaka, S., Fujita, T., Takano, K., Fukuda, H., Sako, K., et al. (1992). Experimental complex partial seizures induced by a microinjection of kainic acid into limbic structures. *Prog. Neurobiol.* 38, 317–334. doi:10.1016/0301-0082(92)90023-8.

Taniguchi, H., He, M., Wu, P., Kim, S., Paik, R., Sugino, K., et al. (2011). A Resource of Cre Driver Lines for Genetic Targeting of GABAergic Neurons in Cerebral Cortex. *Neuron* 71, 995–1013. doi:10.1016/j.neuron.2011.07.026.

Tardy, B., Lafond, P., Convers, P., Page, Y., Zeni, F., Viallon, A., et al. (1995). Adult first generalized seizure: Etiology, biological tests, EEG, CT scan, in an ED. *Am. J. Emerg. Med.* 13, 1–5. doi:10.1016/0735-6757(95)90229-5.

Tauck, D. L., and Nadler, J. V. (1985). Evidence of functional mossy fiber sprouting in hippocampal formation of kainic acid-treated rats. *J. Neurosci. Off. J. Soc. Neurosci.* 5, 1016–1022.

Temkin, O. (1994). *The Falling Sickness: A History of Epilepsy from the Greeks to the Beginnings of Modern Neurology*. JHU Press.

Teyler, T. J., and DiScenna, P. (1985). The role of hippocampus in memory: A hypothesis. *Neurosci. Biobehav. Rev.* 9, 377–389. doi:10.1016/0149-7634(85)90016-8.

Thompson, S. M., and Gähwiler, B. H. (1989). Activity-dependent disinhibition. I. Repetitive stimulation reduces IPSP driving force and conductance in the

hippocampus in vitro. *J. Neurophysiol.* 61, 501–511. doi:10.1152/jn.1989.61.3.501.

Thomson, A. M., West, D. C., Wang, Y., and Bannister, A. P. (2002). Synaptic connections and small circuits involving excitatory and inhibitory neurons in layers 2-5 of adult rat and cat neocortex: triple intracellular recordings and biocytin labelling in vitro. *Cereb. Cortex N. Y. N 1991* 12, 936–953.

Toman, J. E. P., Swinyard, E. A., and Goodman, L. S. (1946). Properties of maximal seizures, and their alteration by anticonvulsant drugs and other agents. *J. Neurophysiol.* 9, 231–239. doi:10.1152/jn.1946.9.3.231.

Tombaugh, G. C., and Somjen, G. G. (1996). Effects of extracellular pH on voltage-gated Na+, K+ and Ca2+ currents in isolated rat CA1 neurons. *J. Physiol.* 493 (Pt 3), 719–732.

Tombaugh, G. C., and Somjen, G. G. (1997). Differential sensitivity to intracellular pH among high- and low-threshold Ca2+ currents in isolated rat CA1 neurons. *J. Neurophysiol.* 77, 639–653. doi:10.1152/jn.1997.77.2.639.

Tønnesen, J., Sørensen, A. T., Deisseroth, K., Lundberg, C., and Kokaia, M. (2009). Optogenetic control of epileptiform activity. *Proc. Natl. Acad. Sci. U. S. A.* 106, 12162–12167. doi:10.1073/pnas.0901915106.

Tóth, K., and Maglóczky, Z. (2014). The vulnerability of calretinin-containing hippocampal interneurons to temporal lobe epilepsy. *Front. Neuroanat.* 8. doi:10.3389/fnana.2014.00100.

Traub, R. D., and Wong, R. K. (1982). Cellular mechanism of neuronal synchronization in epilepsy. *Science* 216, 745–747.

Treiman, D. M. (2001). GABAergic Mechanisms in Epilepsy. *Epilepsia* 42, 8–12. doi:10.1046/j.1528-1157.2001.042suppl.3008.x.

Trevelyan, A. J. (2016). Do Cortical Circuits Need Protecting from Themselves? *Trends Neurosci.* 39, 502–511. doi:10.1016/j.tins.2016.06.002.

Trevelyan, A. J., and Schevon, C. A. (2013). How inhibition influences seizure propagation. *Neuropharmacology* 69, 45–54. doi:10.1016/j.neuropharm.2012.06.015.

Trevelyan, A. J., Sussillo, D., Watson, B. O., and Yuste, R. (2006). Modular Propagation of Epileptiform Activity: Evidence for an Inhibitory Veto in Neocortex. *J. Neurosci.* 26, 12447–12455. doi:10.1523/JNEUROSCI.2787-06.2006.

Trevelyan, A. J., Sussillo, D., and Yuste, R. (2007). Feedforward inhibition contributes to the control of epileptiform propagation speed. *J. Neurosci.* 27, 3383–3387. doi:10.1523/JNEUROSCI.0145-07.2007.

Tse, K., Puttachary, S., Beamer, E., Sills, G. J., and Thippeswamy, T. (2014). Advantages of Repeated Low Dose against Single High Dose of Kainate in C57BL/6J Mouse Model of Status Epilepticus: Behavioral and Electroencephalographic Studies. *PLoS ONE* 9. doi:10.1371/journal.pone.0096622.

Turski, W. A., Cavalheiro, E. A., Schwarz, M., Czuczwar, S. J., Kleinrok, Z., and Turski, L. (1983). Limbic seizures produced by pilocarpine in rats: Behavioural, electroencephalographic and neuropathological study. *Behav. Brain Res.* 9, 315–335. doi:10.1016/0166-4328(83)90136-5.

Tyan, L., Chamberland, S., Magnin, E., Camiré, O., Francavilla, R., David, L. S., et al. (2014). Dendritic Inhibition Provided by Interneuron-Specific Cells Controls the Firing Rate and Timing of the Hippocampal Feedback Inhibitory Circuitry. *J. Neurosci.* 34, 4534–4547. doi:10.1523/JNEUROSCI.3813-13.2014.

Tyzio, R., Minlebaev, M., Rheims, S., Ivanov, A., Jorquera, I., Holmes, G. L., et al. (2008). Postnatal changes in somatic γ-aminobutyric acid signalling in the rat hippocampus. *Eur. J. Neurosci.* 27, 2515–2528. doi:10.1111/j.1460-9568.2008.06234.x.

Ueno, S., Bracamontes, J., Zorumski, C., Weiss, D. S., and Steinbach, J. H. (1997). Bicuculline and gabazine are allosteric inhibitors of channel opening of the GABAA receptor. *J. Neurosci. Off. J. Soc. Neurosci.* 17, 625–634.

Valentino, K., Newcomb, R., Gadbois, T., Singh, T., Bowersox, S., Bitner, S., et al. (1993). A selective N-type calcium channel antagonist protects against neuronal loss after global cerebral ischemia. *Proc. Natl. Acad. Sci. U. S. A.* 90, 7894–7897.

van Luijtelaar, E. L., and Coenen, A. M. (1986). Two types of electrocortical paroxysms in an inbred strain of rats. *Neurosci. Lett.* 70, 393–397.

Van Vreeswijk, C., Abbott, L. F., and Ermentrout, G. B. (1994). When inhibition not excitation synchronizes neural firing. *J. Comput. Neurosci.* 1, 313–321.

Vardy, E., Robinson, J. E., Li, C., Olsen, R. H. J., DiBerto, J. F., Giguere, P. M., et al. (2015). A New DREADD Facilitates the Multiplexed Chemogenetic Interrogation of Behavior. *Neuron* 86, 936–946. doi:10.1016/j.neuron.2015.03.065.

Varga, C., Golshani, P., and Soltesz, I. (2012). Frequency-invariant temporal ordering of interneuronal discharges during hippocampal oscillations in awake mice. *Proc. Natl. Acad. Sci.* 109, E2726–E2734. doi:10.1073/pnas.1210929109.

Velísek, L., Dreier, J. P., Stanton, P. K., Heinemann, U., and Moshé, S. L. (1994). Lowering of extracellular pH suppresses low-Mg(2+)-induces seizures in combined entorhinal cortex-hippocampal slices. *Exp. Brain Res.* 101, 44–52.

Velísek, L., and Velísková, J. (1994). Anticonvulsant action of carbonic anhydrase inhibition. *Sb. Lek.* 95, 161–171.

Vida, I., Bartos, M., and Jonas, P. (2006). Shunting Inhibition Improves Robustness of Gamma Oscillations in Hippocampal Interneuron Networks by Homogenizing Firing Rates. *Neuron* 49, 107–117. doi:10.1016/j.neuron.2005.11.036.

Vilin, Y. Y., and Ruben, P. C. (2001). Slow inactivation in voltage-gated sodium channels. *Cell Biochem. Biophys.* 35, 171–190. doi:10.1385/CBB:35:2:171.

Vliet, V., A, E., da Costa Araújo, S., Redeker, S., van Schaik, R., Aronica, E., et al. (2007). Blood–brain barrier leakage may lead to progression of temporal lobe epilepsy. *Brain* 130, 521–534. doi:10.1093/brain/awl318.

Voipio, J., Boron, W. F., Jones, S. W., Hopfer, U., Payne, J. A., and Kaila, K. (2014). Comment on "Local impermeant anions establish the neuronal chloride concentration." *Science* 345, 1130–1130. doi:10.1126/science.1252978.

Vos, T., Allen, C., Arora, M., Barber, R. M., Bhutta, Z. A., Brown, A., et al. (2016). Global, regional, and national incidence, prevalence, and years lived with disability for 310 diseases and injuries, 1990–2015: a systematic analysis for the Global Burden of Disease Study 2015. *The Lancet* 388, 1545–1602. doi:10.1016/S0140-6736(16)31678-6.

Wahab, A., Heinemann, U., and Albus, K. (2009). Effects of γ-aminobutyric acid (GABA) agonists and a GABA uptake inhibitor on pharmacoresistant seizure like events in organotypic hippocampal slice cultures. *Epilepsy Res.* 86, 113–123. doi:10.1016/j.eplepsyres.2009.05.008.

Walker, M. C., Ruiz, A., and Kullmann, D. M. (2002). Do Mossy Fibers Release GABA? *Epilepsia* 43, 196–202. doi:10.1046/j.1528-1157.43.s.5.6.x.

Wang, K.-W., Chang, W.-N., Chang, H.-W., Chuang, Y.-C., Tsai, N.-W., Wang, H.-C., et al. (2005). The significance of seizures and other predictive factors

during the acute illness for the long-term outcome after bacterial meningitis. *Seizure* 14, 586–592. doi:10.1016/j.seizure.2005.09.004.

Wang, Q., Shen, F.-Y., Zou, R., Zheng, J.-J., Yu, X., and Wang, Y.-W. (2017). Ketamine-induced apoptosis in the mouse cerebral cortex follows similar characteristic of physiological apoptosis and can be regulated by neuronal activity. *Mol. Brain* 10, 24. doi:10.1186/s13041-017-0302-2.

Wang, Y., Liang, J., Chen, L., Shen, Y., Zhao, J., Xu, C., et al. (2018). Pharmaco-genetic therapeutics targeting parvalbumin neurons attenuate temporal lobe epilepsy. *Neurobiol. Dis.* 117, 149–160. doi:10.1016/j.nbd.2018.06.006.

Watkins, J. C., and Evans, R. H. (1981). Excitatory amino acid transmitters. *Annu. Rev. Pharmacol. Toxicol.* 21, 165–204. doi:10.1146/annurev.pa.21.040181.001121.

Well, G. T. J. van, Paes, B. F., Terwee, C. B., Springer, P., Roord, J. J., Donald, P. R., et al. (2009). Twenty Years of Pediatric Tuberculous Meningitis: A Retrospective Cohort Study in the Western Cape of South Africa. *Pediatrics* 123, e1–e8. doi:10.1542/peds.2008-1353.

White, E. J., Juchniewicz, H. J., and Clark, J. B. (1989). Effects of Lactic Acidosis on the Function of Cerebral Cortical Synaptosomes. *J. Neurochem.* 52, 154–161. doi:10.1111/j.1471-4159.1989.tb10910.x.

Wietek, J., Wiegert, J. S., Adeishvili, N., Schneider, F., Watanabe, H., Tsunoda, S. P., et al. (2014). Conversion of Channelrhodopsin into a Light-Gated Chloride Channel. *Science* 344, 409–412. doi:10.1126/science.1249375.

Wilent, W. B., and Contreras, D. (2004). Synaptic Responses to Whisker Deflections in Rat Barrel Cortex as a Function of Cortical Layer and Stimulus Intensity. *J. Neurosci.* 24, 3985–3998. doi:10.1523/JNEUROSCI.5782-03.2004.

Williams, J. C., and Denison, T. (2013). From Optogenetic Technologies to Neuromodulation Therapies. *Sci. Transl. Med.* 5, 177ps6-177ps6. doi:10.1126/scitranslmed.3003100.

Willoughby, D., Thomas, R. C., and Schwiening, C. J. (2001). The effects of intracellular pH changes on resting cytosolic calcium in voltage-clamped snail neurones. *J. Physiol.* 530, 405–416. doi:10.1111/j.1469-7793.2001.0405k.x.

Wilson, N. R., Runyan, C. A., Wang, F. L., and Sur, M. (2012). Division and subtraction by distinct cortical inhibitory networks in vivo. *Nature* 488, 343–348. doi:10.1038/nature11347.

Wittner, L., Maglóczky, Z., Borhegyi, Z., Halász, P., Tóth, S., Eross, L., et al. (2001). Preservation of perisomatic inhibitory input of granule cells in the epileptic human dentate gyrus. *Neuroscience* 108, 587–600.

Wong, R. K. S., Prince, D. A., and Basbaum, A. I. (1979). Intradendritic recordings from hippocampal neurons. *Proc. Natl. Acad. Sci. U. S. A.* 76, 986–990.

Woodin, M. A., Ganguly, K., and Poo, M. (2003). Coincident pre- and postsynaptic activity modifies GABAergic synapses by postsynaptic changes in Cl- transporter activity. *Neuron* 39, 807–820.

Wuarin, J. P., and Dudek, F. E. (2001). Excitatory synaptic input to granule cells increases with time after kainate treatment. *J. Neurophysiol.* 85, 1067–1077. doi:10.1152/jn.2001.85.3.1067.

Wykes, R. C., Heeroma, J. H., Mantoan, L., Zheng, K., MacDonald, D. C., Deisseroth, K., et al. (2012). Optogenetic and Potassium Channel Gene Therapy in a Rodent Model of Focal Neocortical Epilepsy. *Sci. Transl. Med.* 4, 161ra152. doi:10.1126/scitranslmed.3004190.

Wykes, R. C., Kullmann, D. M., Pavlov, I., and Magloire, V. (2016). Optogenetic approaches to treat epilepsy. *J. Neurosci. Methods* 260, 215–220. doi:10.1016/j.jneumeth.2015.06.004.

Xiong, Z.-Q., Saggau, P., and Stringer, J. L. (2000). Activity-Dependent Intracellular Acidification Correlates with the Duration of Seizure Activity. *J. Neurosci.* 20, 1290–1296. doi:10.1523/JNEUROSCI.20-04-01290.2000.

Yaari, Y., Konnerth, A., and Heinemann, U. (1986). Nonsynaptic epileptogenesis in the mammalian hippocampus in vitro. II. Role of extracellular potassium. *J. Neurophysiol.* 56, 424–438. doi:10.1152/jn.1986.56.2.424.

Yang, K., Trepanier, C. H., Li, H., Beazely, M. A., Lerner, E. A., Jackson, M. F., et al. (2009). Vasoactive intestinal peptide acts via multiple signal pathways to regulate hippocampal NMDA receptors and synaptic transmission. *Hippocampus* 19, 779–789. doi:10.1002/hipo.20559.

Yao, H., Ma, E., Gu, X.-Q., and Haddad, G. G. (1999). Intracellular pH regulation of CA1 neurons in Na^+/H^+ isoform 1 mutant mice. *J. Clin. Invest.* 104, 637–645. doi:10.1172/JCI6785.

Yekhlef, L., Breschi, G. L., Lagostena, L., Russo, G., and Taverna, S. (2015). Selective activation of parvalbumin- or somatostatin-expressing interneurons triggers epileptic seizurelike activity in mouse medial entorhinal cortex. *J. Neurophysiol.* 113, 1616–1630. doi:10.1152/jn.00841.2014.

Yizhar, O., Fenno, L. E., Davidson, T. J., Mogri, M., and Deisseroth, K. (2011). Optogenetics in Neural Systems. *Neuron* 71, 9–34. doi:10.1016/j.neuron.2011.06.004.

Yuste, R. (2005). Origin and Classification of Neocortical Interneurons. *Neuron* 48, 524–527. doi:10.1016/j.neuron.2005.11.012.

Zemelman, B. V., Lee, G. A., Ng, M., and Miesenböck, G. (2002). Selective photostimulation of genetically chARGed neurons. *Neuron* 33, 15–22.

Zhan, R. Z., Fujiwara, N., Tanaka, E., and Shimoji, K. (1998). Intracellular acidification induced by membrane depolarization in rat hippocampal slices: roles of intracellular Ca2+ and glycolysis. *Brain Res.* 780, 86–94. doi:10.1016/S0006-8993(97)01149-9.

Zhang, F., Wang, L.-P., Brauner, M., Liewald, J. F., Kay, K., Watzke, N., et al. (2007). Multimodal fast optical interrogation of neural circuitry. *Nature* 446, 633–639. doi:10.1038/nature05744.

Zhang, Z. J., Koifman, J., Shin, D. S., Ye, H., Florez, C. M., Zhang, L., et al. (2012). Transition to seizure: ictal discharge is preceded by exhausted presynaptic GABA release in the hippocampal CA3 region. *J. Neurosci. Off. J. Soc. Neurosci.* 32, 2499–2512. doi:10.1523/JNEUROSCI.4247-11.2012.

Zhao, M., Alleva, R., Ma, H., Daniel, A. G. S., and Schwartz, T. H. (2015). Optogenetic tools for modulating and probing the epileptic network. *Epilepsy Res.* 116, 15–26. doi:10.1016/j.eplepsyres.2015.06.010.

Ziburkus, J., Cressman, J. R., Barreto, E., and Schiff, S. J. (2006). Interneuron and Pyramidal Cell Interplay During In Vitro Seizure-Like Events. *J. Neurophysiol.* 95, 3948–3954. doi:10.1152/jn.01378.2005.

Ziemann, A. E., Schnizler, M. K., Albert, G. W., Severson, M. A., Howard, M. A., Welsh, M. J., et al. (2008). Seizure termination by acidosis depends on ASIC1a. *Nat. Neurosci.* 11, 816–822. doi:10.1038/nn.2132.